

Institut für Strukturmechanik
Institute of Structural Mechanics

Bauhaus-

Bauhaus-Universität Weimar

Weimar

ISM-Bericht 1/2018
Thi Mai Hoa Luong

Identification of the State of Stress in Iron and Steel Truss
Structures by Vibration-based Experimental Investigations

Tom Lahmer

Herausgeber
Timon Rabczuk

Carsten Könke

ISM-Bericht 1/2018
Institut für Strukturmechanik
Fakultät Bauingenieurwesen
Bauhaus-Universität Weimar
Marienstraße 15
D-99423 Weimar
Germany

ISSN: 1610-7381

Tel. +49 (0)3643/584504
Fax. +49(0)3643/584514

<http://www.uni-weimar.de/Bauing/ism>

Identification of the State of Stress in Iron and Steel Truss Structures by Vibration–based Experimental Investigations

Von der
Fakultät für Architektur, Bauingenieurwesen und Stadtplanung
der Brandenburgischen Technischen Universität Cottbus–Senftenberg
zur Erlangung des akademischen Grades eines
Doktor–Ingenieurs (Dr.–Ing.)
genehmigte

Dissertation

vorgelegt von
Ing., M.Sc.

Thi Mai Hoa Luong
aus Hanoi, Vietnam

Gutachter: Prof. Dr.–Ing. Werner Lorenz
Gutachter: Prof. Dr. ir. Guido De Roeck
Gutachter: Dr.–Ing. Volkmar Zabel
Tag der Disputation: 22. Juni 2017

ABSTRACT

Safety evaluation of truss structures depends upon the determination of the axial forces and corresponding stresses in axially loaded members. Due to presence of damages, change in intended use, increase in service loads or accidental actions, structural assessment of existing truss structures is necessary. This applies particularly to iron and steel trusses that are still in use, including historic and heritage monuments. Precise identification of the stresses plays a crucial role for the preservation of historic trusses. The assessment measures require non-destructiveness, minimum intervention and practical applicability.

The axial forces in truss structures can be estimated by static calculations using the method of joints, method of sections or finite element method, if accurate information about parameters such as external loads, geometrical characteristics, mechanical properties, boundary conditions and joint connections are known. However, precise information about these parameters is difficult to be obtained in practice. Especially in the cases of historic constructions, reasonable assumptions about the uncertain parameters may not be acquired.

Motivated by the preservation of existing truss-type constructions composed of axially loaded slender members, the present work aims to develop a non-destructive methodology to identify the axial forces or corresponding stress states in iron and steel truss structures. The approach is based on vibration measurements and the finite element method combined with optimization techniques.

After a state of the art review, numerical and experimental studies were carried out on three partial systems of truss-type structures. The investigated systems included single bars, a two-bar truss-like system and a five-bar truss. They were developed step-by-step as built-up truss-type constructions that are constituted of individual members connecting at joints. The examined aspects included the effects of structural loading on the dynamic performance of truss structures, modelling of joint connections, mode pairing criteria, selection of updating parameters and definition of an objective function, as well as the use of different optimization techniques.

Concerning the axial force effects on the structural dynamic responses, the effects of the stress stiffening become more complicated for multiple-member truss systems with increasing complexity. The coexistence of both compressive and tensile forces in trusses has counteracting effects on the modal parameters. These effects cause variation of natural frequencies and interchange of modes when the loads or corresponding member forces are changed. To examine the axial force effects on the structures at different stress states, in the numerical study and laboratory experiments, loads were applied progressively to the investigated truss-like systems.

Regarding the modelling of joints for truss-type structures, the joint flexibility affects the structural dynamic responses. Therefore, the numerical models of truss-type structures include joint models with variable rotational springs to represent semi-rigid connections.

Considering the mode pairing criterion, the mode pairing is performed by adapting an enhanced modal assurance criterion with the calculation of the modal strain energy. The criterion allows the selection of desired clusters of degrees of freedom related to specific modes. With respect to the model updating strategies, the selection of updating parameters and the choice of an appropriate objective function are identified to be significantly important. In addition, three different optimization techniques were applied to compare their suitability for the inverse axial force identification and estimation of joint flexibility of truss structures. The results of the numerical study and laboratory tests show that nature-inspired optimization methods are considered as promising techniques.

A methodology consisted of a two-stage model updating procedure using optimization techniques was proposed for the determination of multiple member axial forces and estimation of the joint flexibility of truss-type structures. In the first stage optimization, the validation criterion is based on the experimentally identified global natural frequencies and mode shapes of the truss. Additionally, the axial forces in selected individual members of the truss are used. They are estimated from the natural frequencies and five amplitudes of the corresponding local mode shapes of the members using an analytically-based algorithm. Based on the results of the identified axial forces in the first stage, a second optimization procedure for the joint stiffnesses is performed. In this stage, the modal parameters of the global natural frequencies and mode shapes are used as validation criterion.

From the results of the laboratory experiments, the identified axial forces by the proposed methodology agree well with the experimentally measured axial forces of the investigated systems at different stress states. Moreover, based on the numerical verification, the identified joint stiffnesses indicate reasonably the joint flexibility in relation to the pinned or rigid conditions.

To assess the relevance of the proposed methodology on existing structures in real-life conditions, an in-situ experiment was carried out on a historic Wiegmann-Polonceau truss in the city of Potsdam. The in-situ experiment shows that uncertainties relating the mechanical and geometrical properties of historic trusses as well as the experimental sensor setup can influence the accuracy of the axial force identification. In the present work, recommendations are given for the development of a guideline of measuring concepts and assessment strategies applied to existing truss structures. The intention is to integrate the proposed methodology as part of the Structural Health Monitoring for historic truss-type constructions.

KURZFASSUNG

Die Bewertung der Tragfähigkeit von Fachwerkkonstruktionen ist wesentlich von den vorhandenen Stabnormalkräften und den daraus resultierenden Spannungen abhängig. Eine Zustands- und Tragfähigkeitsbewertung der bestehenden Konstruktion ist besonders dann erforderlich, wenn aufgrund von Nutzungsänderungen bzw. Umbaumaßnahmen höhere Lasten auf das Tragwerk aufgebracht werden sollen, oder sich Schäden an der Konstruktion bzw. dem Material zeigen. Dies gilt vor allem für eiserne und stählerne Fachwerkkonstruktionen, welche beispielsweise in historischen Gebäuden zu finden sind. Für die Identifizierung des Normalkraft- bzw. Spannungszustands und die darauf aufbauende Tragfähigkeitsbewertung der Konstruktion ist ein zerstörungsfreies und praktikables Verfahren erforderlich, welches zudem nur minimal in die bestehende Struktur eingreift.

Liegen ausreichend Informationen hinsichtlich der äußeren Beanspruchung, der Geometrie, der Materialeigenschaften, der Auflagersituation sowie der Freiheitsgrade in den Knotenverbindungen vor, können die Stabnormalkräfte in der Fachwerkkonstruktion in Form einer statischen Berechnung ermittelt werden. Allerdings ist es in der Praxis oftmals schwierig für bestehende Tragwerke, insbesondere historische Fachwerkkonstruktionen, präzise Informationen für die genannten Parameter zu erhalten oder adäquate Annahmen zu treffen.

Die vorliegende Arbeit zielt darauf ab ein zerstörungsfreies Verfahren zu entwickeln, welches in der Lage ist die Spannungszustände in fachwerkartigen Eisen- und Stahltragwerken mit filigranen Stäben zu identifizieren. Das Verfahren basiert auf Schwingungsmessungen und der Finite-Elemente-Methode in Verbindung mit Optimierungsstrategien.

Nach einer ausführlichen Recherche zum Stand der Technik wurden im Rahmen der Arbeit numerische und experimentelle Untersuchungen an Teilsystemen von fachwerkartigen Tragstrukturen durchgeführt. Bei den untersuchten Konstruktionen handelt es sich um ein Einzelstabsystem, ein Zweistabsystem sowie ein aus fünf Stäben bestehendes Fachwerksystem. Die Entwicklung vom Einzelstabsystem zum komplexen Fachwerksystem erfolgt durch schrittweises Hinzufügen von Einzelstäben sowie deren Verbindungen in den Knoten. In den Untersuchungen wurden mehrere Aspekte betrachtet. Neben dem Einfluss der äußeren Belastung auf das dynamische Verhalten der Konstruktion werden in dem Analyseverfahren die Modellierung der Knotenverbindungen, die Zuordnung der Eigenschwingformen, die Auswahl und Festlegung von Kalibrierungsparametern, die Definition von Zielfunktionen, sowie die verschiedenen Optimierungsmethoden untersucht.

Mit zunehmender Komplexität des Tragwerkes wird der Einfluss der Stabnormalkräfte auf das dynamische Verhalten komplizierter. Das heißt, das gleichzeitige Vorliegen von Druck- und Zugkräften, welche jeweils eine entgegengesetzte Wirkung auf die modalen Parameter besitzen, führt bei einer Variation der Belastung zu einer Veränderung der Eigenfrequenzen und einer vergleichsweise schwierigeren Zuordnung der jeweiligen Eigenschwingformen. Um ein geeignetes Evaluierungsverfahren zu entwickeln, wurden in den Laborversuchen verschiedene Belastungszustände an den Tragwerkssystemen

berücksichtigt. Die auf die Konstruktion wirkende äußere Belastung wurde hierfür schrittweise gesteigert. Außerdem wurde sowohl das dynamische Verhalten des globalen Systems als auch das der Einzelstäbe durch die Modellierung der Knotenverbindungen und die dafür angesetzte Rotationssteifigkeit beeinflusst. Im numerischen Modell wurden die Knotenverbindungen als streuende Größen behandelt und daher als teilweise eingespannte (*semi-rigid*) Rotationsfedern modelliert.

Bezüglich der Zuordnung der Eigenschwingformen wurde ein alternatives Kriterium zur Berechnung der modalen Formänderungsarbeiten angewendet. Dieses Kriterium ermöglicht es, den gewünschten Bereich (*Cluster*) von Freiheitsgraden in Bezug auf bestimmte Eigenformen auszuwählen. Im Hinblick auf die Kalibrierungsstrategien sind besonders die Auswahl der Kalibrierungsparameter und die Verwendung passender Zielfunktionen von großer Bedeutung. Unter Berücksichtigung der unbekanntenen Stabnormalkräfte und unsicheren Rotationsfedersteifigkeiten in den Knotenverbindungen wurden verschiedene Optimierungsstrategien untersucht und miteinander verglichen. Anhand des Vergleichs wurde ein entsprechendes Verfahren zur Bestimmung der Stabnormalkräfte entwickelt. Die Verwendung von naturinspirierten Optimierungsverfahren hat sich dabei als geeignet herausgestellt.

Für die Bestimmung der Stabnormalkräfte in fachwerkartigen Tragwerken und zur Abschätzung der Rotationsfedersteifigkeit in den Knotenverbindungen wird ein zweistufiges Modelloptimierungsverfahren vorgeschlagen. Im ersten Schritt werden als Validierungskriterium die experimentell ermittelten globalen Eigenfrequenzen und Eigenformen der Fachwerkstruktur verwendet. Ergänzend können die Stabnormalkräfte in ausgewählten Zuggliedern aus Einzelstabuntersuchungen als zusätzliche Informationen herangezogen werden. Die Stabkräfte der Zugglieder lassen sich mit Hilfe eines analytisch basierten Algorithmus anhand der lokalen Eigenfrequenzen eines Stabes und fünf Amplituden der dazugehörigen Eigenformen berechnen. Basierend auf den Ergebnissen der identifizierten Stabnormalkräfte kann ein zweiter Optimierungsprozess zur Bestimmung der Rotationsfedersteifigkeit in den Knotenverbindungen durchgeführt werden. Hierzu werden ausschließlich die modalen Parameter der globalen Eigenfrequenzen und -formen der gesamten Fachwerkstruktur herangezogen.

Die Ergebnisse der im Labor getesteten Tragsysteme weisen für verschieden hohe Beanspruchungen eine sehr gute Übereinstimmung zwischen den im Versuch aufgebrachten und den mit Hilfe des entwickelten Verfahrens identifizierten Stabnormalkräften auf. Hinsichtlich der Rotationsfedersteifigkeit in den Knotenverbindungen konnte ebenfalls eine gute Übereinstimmung zwischen den identifizierten Werten und den angenommenen Randbedingungen des numerisch modellierten Tragwerkes in Bezug auf die gelenkige oder biegesteife Bedingung erzielt werden.

Um das entwickelte und durch Laborversuche validierte Verfahren auch auf bestehende Tragwerke übertragen zu können, wurde eine in-situ Untersuchung an einem historischen Wiegmann-Polonceau-Fachwerk in Potsdam durchgeführt. Die in-situ Untersuchung hat gezeigt, dass die Genauigkeit bei der Bestimmung der Stabnormalkräfte von den vorhandenen Unsicherheiten hinsichtlich der mechanischen und geometrischen Eigenschaften des historischen Fachwerkes sowie der experimentellen Sensoranordnung beeinflusst wird. Für die in-situ Untersuchung von historischen Fachwerkstrukturen wurden in der Arbeit Empfehlungen zur Erarbeitung einer Leitlinie für die Erstellung von Messkonzepten sowie Hilfestellungen bei der Entwicklung von Bemessungsstrategien entwickelt. Darüber hinaus ist beabsichtigt das Verfahren für das *Structural Health Monitoring* von historischen fachwerkartigen Tragwerken einzusetzen.

DANKSAGUNG

Die vorliegende Dissertation „Bestimmung des Beanspruchungszustands in fachwerkartigen Eisen- und Stahltragwerken mit Hilfe schwingungsbasierter experimenteller Untersuchungen“ entstand während meiner Tätigkeit als wissenschaftliche Mitarbeiterin am Lehrstuhl Bautechnikgeschichte und Tragwerkserhaltung der Brandenburgischen Technischen Universität (BTU) Cottbus–Senftenberg. Neben meiner Tätigkeit an der BTU war ich Doktorandin im Fachbereich 7.2 Ingenieurbau der Bundesanstalt für Materialforschung und –prüfung (BAM) sowie Gastwissenschaftlerin am Institut für Strukturmechanik (ISM) der Bauhaus–Universität Weimar.

Mein besonderer Dank richtet sich an meinen Doktorvater, Herrn Prof. Dr.–Ing. Werner Lorenz, der das Thema meiner Dissertation initiiert sowie mich während der Promotionsarbeit intensiv gefördert hat.

Weiterhin möchte ich mich bei Herrn Dr.–Ing. Volkmar Zabel vom ISM für die ausführlichen wissenschaftlichen Diskussionen und die fachliche Hilfestellung sowie die Möglichkeit zur Durchführung von Laborversuchen an der Bauhaus–Universität Weimar herzlich bedanken.

Ein Dankeschön gilt Herrn Prof. Dr. ir. Guido De Roeck von der KU Leuven für die wertvollen Hinweise und die Begutachtung der Doktorarbeit. Ferner danke ich Herrn Prof. Dr.–Ing. Achim Bleicher und Frau Dr.–Ing. Yvonne Ciupack von der BTU für die Übernahme des Vorsitzes sowie die Teilnahme an dem Prüfungsausschuss.

Des Weiteren möchte ich mich bei den Kollegen des Fachbereiches 7.2 der BAM, vor allem bei Herrn Rolf Günter Rohrman und Herrn Samir Said, für die Unterstützung bei der Planung und Durchführung der in–situ–Schwingungsmessungen in Potsdam bedanken.

Für die fachkundige Hilfe und die Umsetzung der Laborversuche danke ich dem Leiter Herrn Wolf–Dieter Vogler sowie allen weiteren Kollegen der versuchstechnischen Einrichtung der Bauhaus–Universität Weimar. Zudem möchte ich mich bei Herrn Dr.–Ing. Lữ Mai, Herrn Dr. phil. Cosmin Anitescu und Herrn Albrecht Schmidt vom ISM für die anregenden Diskussionen sowie die vielfältige Unterstützung bedanken.

Den Kollegen des Lehrstuhls Bautechnikgeschichte und Tragwerkserhaltung der BTU Cottbus–Senftenberg, insbesondere Herrn Dr.–Ing. Volker Wetzke, Herrn Dr.–Ing. Roland May und Herrn Bernhard Heres, danke ich für die konstruktiven Anmerkungen und Hinweise.

Weiterhin gilt mein Dank dem Deutschen Akademischen Austauschdienst (DAAD) für die finanzielle Förderung, welche mir die Promotion erst ermöglicht hat.

Abschließend möchte ich meiner Familie, die mich stets unterstützt und motiviert hat, herzlich danken. Darüber hinaus danke ich besonders Herrn Dr.–Ing. Dustin Häbler und seiner Familie für den Rückhalt während der Promotionszeit.

Berlin, Mai 2017

Thị Mai Hoa Lương

NOMENCLATURE

Abbreviations

AB	Analytical-based
ANPSD	Average Normalized Power Spectral Densities
ARSM	Adaptive Response Surface Method
CE	Civil Engineering
CM	Component Method
CSS	Circular solid cross-section
DFG	Deutsche Forschungsgemeinschaft
Dyn.	Dynamic
EF	Empirical formula
EFDD	Enhanced Frequency Domain Decomposition
EMA	Experimental Modal Analysis
EMAC	Energy-based Modal Assurance Criterion
EX	Excitation point
FDD	Frequency Domain Decomposition
FEM	Finite Element Method
FFT	Fast Fourier Transform
FRF	Frequency Response Function
GA	Genetic Algorithm
HPBM	Half Power Bandwidth Method
ICOMOS	International Council of Monuments and Sites
ISCARSAH	International Scientific Committee on the Analysis and Restoration of Structures of Architectural Heritage
MAC	Modal Assurance Criterion
MDOF	Multiple Degree of Freedom
MU	Model updating
NLPQL	Nonlinear Programming by Quadratic Lagrangian
OMA	Operational Modal Analysis
OMAX	Operational Modal Analysis with exogenous inputs
PP	Peak Picking
PSO	Particle Swarm Optimization
SDOF	Singular Degree of Freedom
SG	Strain gauge
SHM	Structural Health Monitoring
SPR	Updating the parameter(s) of the rotational spring stiffness only
SSI	Stochastic Subspace Identification
SSI-cov/ref	Reference-based Covariance-driven Stochastic Subspace Identification
SSI-data/ref	Reference-based Data-driven Stochastic Subspace Identification

SSI/ref	Reference-based Stochastic Subspace Identification
Stat.	Static
Stat.–Dyn.	Mixed static–dynamic
SVD	Singular Value Decomposition
TB	Turnbuckle

List of Symbols

A	Cross-sectional area
a_1, a_2, a_3	Designate constants depending on axial force
a, b, c	Weighting factor for the terms of the objective function
B	Coefficient matrix
C_k	Coefficients of spring constants representing boundary conditions
d_{bar}	Diameter of solid circular bar
E	Elastic modulus
EI	Bending stiffness
f	Frequency [Hz]
Δf	Variation of frequency
f_{obj}	Objective function
$f_{p0.01}$	Technical proportional limit
$f_{p0.2}$	0.2% strain limit
f_u	Tensile strength
g	Designated complex number depending on axial force
G	Shear modulus
I	Moment of inertia
k_r	Rotational spring stiffness
k_t	Translational spring stiffness
k_y	Shear deformation coefficient
K	Stiffness matrix
K_G	Geometric stiffness matrix
L	Length
m	Vector containing values of displacements at sensor positions
m_s	Mass of sensor
M	Mass matrix
n	Mode number
N	Member axial force
N^a	Identified force by analytical-based algorithm
N_{Euler}	Buckling force
N^{ref}	Axial force corresponding to a reference stress
p_1, p_2	Real constants as expression of η and \mathcal{G}
P	Applied load / force
ΔP	Variation of force
q_1, q_2	Real constants as expressions of α and g

s_{kr}	Stiffness index
S	Characteristic matrix
t	Time
v	Displacement
x	Position along the span / position of sensor / coordinate
x_s	Position of sensor
y	Coordinate
Y	Time-dependent amplitude of free-vibration motion
z	Coordinate

Greek Letters

α	Designated constant depending on material properties of structural member, its natural frequency and mode shape
β	Designated constant as expression of a_1 , a_2 and a_3
γ_{kr}	Fixity factor
Δ	Difference / variation
Δ_n	Normalized error norm
ε	Strain
η	Designated constant depending on axial force
θ	Rotational displacement
λ_{ij}	Ratio of modal displacements in two among five points of a mode
λ_n	Variable representing different boundary conditions
λ_s	Slenderness
ξ	Bending stiffness parameter
Π	Relative modal strain energy
ρ	Mass density
σ	Axial stress
σ^{ref}	Reference stress
\mathcal{G}	Designated constant depending on material properties of structural member
ϕ	Modal vector / mode shape
$\hat{\phi}$	Eigenvectors
ω	Circular frequency [rad/s]

Mathematical Notations

$\{ \bullet \}$	Vector
$[\bullet]$	Matrix
$[\bullet]_{ij}$	Row i , column j of a matrix
$\{ \bullet \}^T$	Transpose of a vector
$[\bullet]^T$	Transpose of a matrix
$[\bullet]^\dagger$	Pseudo matrix
$\ \bullet \ _2$	Euclidean vector norm

Subscripts

<i>i</i>	member number (in the notation of rotational spring stiffness)
<i>I</i>	joint number (in the notation of rotational spring stiffness)
<i>n</i>	<i>n</i> th mode
<i>r</i>	rotational
<i>t</i>	translational

Superscripts

<i>exp</i>	experimentally identified
<i>id</i>	numerically identified by the proposed methodology
<i>num</i>	numerically calculated
<i>true</i>	numerically calculated to simulate experimental data

CONTENTS

ABSTRACT	v
KURZFASSUNG	vii
DANKSAGUNG	ix
NOMENCLATURE	xi
CONTENTS	xv
1 INTRODUCTION	1
1.1 Axial Force Identification for Civil Engineering Structures	2
1.2 Historic Truss Structures as Study Context.....	2
1.2.1 Historical Emergence	3
1.2.2 Iron as Structural Material	3
1.2.3 Wiegmann–Polonceau Truss.....	5
1.2.4 Iron Roof Trusses of the State Hermitage Museum, Saint Petersburg.....	9
1.2.5 Safety Assessment of Existing Iron and Steel Structures.....	11
1.3 Motivation of Structural Assessment for Existing Truss Structures.....	13
1.4 General State of Research.....	14
1.5 Objectives and Focus of the Research.....	17
1.6 Outline of the Thesis.....	18
2 STATE OF RESEARCH AND PROPOSED METHODOLOGY	19
2.1 Theoretical Background.....	20
2.1.1 Stress Stiffening.....	20
2.1.2 Stress Stiffening in Isolated Bar and Truss Structures	23
2.1.3 State of the Art Axial Force Identification Methods	24
2.1.4 Analytical–based Algorithms for Axial Force Identification	26
2.2 Modelling and Analysis of Semi–Rigid Connections.....	33
2.3 Finite Element Model Updating for Civil Engineering Structures.....	37
2.3.1 Background of Selected Optimization Techniques.....	38
2.3.2 Background of Experimental Modal Identification	40
2.3.3 Model Updating Framework	43
2.4 Proposed Methodology	44
2.4.1 Sensitivity Analysis.....	45
2.4.2 Proposed Two–Stage Model Updating Procedure	45
2.4.3 Definition of Objective Functions.....	47
2.4.4 Mode Pairing Criteria	47
2.4.5 Optimization Process.....	48
2.5 Discussions.....	50
	xv

3	VERIFICATION OF METHODOLOGY BY NUMERICAL STUDY	51
3.1	Overview of Investigated Systems	52
3.2	Single–Bar Systems	52
3.2.1	Effects of Stress Stiffening and Joint Flexibility	54
3.2.2	Selection of Modes to use Analytical–based Algorithm	59
3.2.3	Sensitivity Analysis	59
3.2.4	Identification of Axial Forces and Joint Stiffness	62
3.2.5	Computational Efficiency of Optimization Techniques	66
3.2.6	Error Analysis	67
3.2.7	Estimation of Joint Stiffness at Symmetric Locations of Structures	69
3.3	Two–Bar System	71
3.3.1	Global and Local Analyses of Truss Structures	74
3.3.2	Sensitivity Analysis	75
3.3.3	Identification of Axial Force and Joint Stiffness	76
3.3.4	Error Analysis	77
3.3.5	Estimation of Joint Stiffness at Symmetric Locations of Structures	78
3.4	Five–Bar Truss System	81
3.4.1	Mode Pairing Criteria	85
3.4.2	Selection of Modes to use Analytical–based Algorithm	87
3.4.3	Sensitivity Analysis	89
3.4.4	Identification of Axial Forces and Joint Stiffness	89
3.5	Discussions	90
4	VALIDATION OF METHODOLOGY BY LABORATORY EXPERIMENTS	93
4.1	Overview of Laboratory Experiments	94
4.2	Single–Bar Systems	94
4.2.1	Modal Parameter Identification	96
4.2.2	Identification of Axial Force and Estimation of Joint Stiffness	98
4.3	Two–bar System	99
4.3.1	Material Tests to Determine Stress–Strain Characteristics	103
4.3.2	Modal Parameter Identification	104
4.3.3	Identification of Axial Force and Joint Stiffness	105
4.4	Five–Bar Truss System	110
4.4.1	Modal Parameter Identification	113
4.4.2	Identification of Axial Force and Joint Stiffness	114
4.5	Discussions	116
5	RECOMMENDATIONS FOR IN–SITU EXPERIMENTS	117
5.1	Purpose and Scope of In–situ Experiment	118
5.2	Description of Historic Truss Structure	118
5.3	Finite Element Modelling	120
5.3.1	Static Analysis of Axial Force and Axial Stress Distribution	123
5.3.2	Dynamic Analysis and Stress Stiffening	125

5.4 In-situ Experiment	125
5.4.1 Modal Parameter Identification	126
5.5 Analysis Strategies and Results	127
5.5.1 Identification of Axial Force for Single Truss Member	128
5.5.2 Preliminary Calibration of the Numerical Model.....	130
5.6 Recommended Scheme for Future In-situ Experiments	131
5.7 Discussions.....	138
6 CONCLUSIONS AND FUTURE RESEARCH	139
6.1 Conclusions	140
6.2 Future Research	145
REFERENCES	147
LIST OF FIGURES	159
LIST OF TABLES	163
APPENDIX	167

1

INTRODUCTION



An overview of historic iron and steel truss structures is given in this chapter as study context for the research work; followed by a statement of motivation. After that, the general state of research will be discussed. Finally, the objectives, scope of the research and the outline of the thesis will be presented.

1.1 Axial Force Identification for Civil Engineering Structures

Axial force identification is of importance in the field of structural restoration and safety assessment. It is also useful for the verification of models and design assumptions for civil engineering structures composed of axially loaded members, such as roof trusses, truss girders and space trusses.

Due to accumulation of inherent degradation and damages, service loads and accidental actions, existing structures require maintenance over time. For historic constructions in cases of the presence of damages or change in the intended use, their safety evaluation is even more essential. During the past decades, preservation of monuments and cultural heritage structures has gained increasing appreciation in modern societies. The conservation of historic constructions is not only a cultural requirement but also to satisfy economic and sustainable development demands.

In the context of existing structures, iron and steel trusses supporting the roof of buildings are of interest. Many of those structures are still in use today in historic and heritage monuments, for example the iron roof trusses of the State Hermitage Museum in Saint Petersburg, which are of enormous significance thanks to a variety of constructive prototypes and richness of details from the early days of the European iron construction [LORENZ (2005, 2010)]. The assessment methods require respect of the original structure.

The study in this section aims to draw a general picture of the historical emergence, material and structural characteristics of iron and steel truss structures to understand their design in the past and condition in present time, as well as to emphasize the importance of the structural evaluation for historic trusses.

1.2 Historic Truss Structures as Study Context

Since the end of the 18th century, first cast iron, then wrought iron and finally steel has been increasingly used as a structural material. In the 19th century, engineering design rules became more scientific¹. Developments in materials science and the theory of statics² allowed major improvements in structural design. Truss systems were developed

¹ Work and energy principles that govern the behavior of structures were already defined in the 18th century [KURRER (2008)]. John Bernoulli in 1717 defined the principle of virtual work. By 1744, Leonard Euler developed mathematical techniques to derive equilibrium equations. Bélidor published *L'architecture hydraulique* from 1737–1753, in which integral calculus was used for the first time in solving technical problems. The advanced state of mechanics was exemplified by Joseph Lagrange's work *Mécanique Analytique* published in 1787. Yet the principles of mechanics were not proved to be applied to the rational design of trusses before the 19th century.

² According to HOLZER (2012) and KURRER (2008), the early attempts at computational modeling of real-life building structures are due to Johann Albert Eytelwein (*Handbuch der Statik*, 1808) and Claude Louis Marie Henri Navier (*Résumé des Leçons*, 1826). Based on the theory of bending of elastic rods, they suggested – independently of each other – an approach of “decomposing” a structure into simple parts such as continuous beams and simple struts. In Germany, increasing indications of a departure from the “decomposition” approach was from the early 1840s onwards. Karl Culmann and Johann Wilhelm Schwedler realized the striking effects of “making everything isostatic” by the assumption that all the joints of a trussed structure are “pinned-jointed”, i.e. the statically determinate truss, in their journal publications of 1851. Furthermore, the remarkable publications of John Macquorn Rankine's *Manual of Applied Mechanics* and August Ritter's *Elementare Theorie und Berechnung eiserner Dach- und Brücken-Constructionen* (1863) lead to the triumph of truss theory in Germany, Great Britain, and Italy in the second half of the 19th century.

in the progress of practicing new types of structures and being driven towards analytical understanding. Trusses have been built as structural systems of bridges; truss roofs appeared as a prominent form in various constructions such as railway stations, market halls, and industrial buildings. Nowadays, historic trusses can still be found in use in many existing constructions, and a number of them play an important load-supporting role. Truss-type structural systems remain in present-day in wide application for civil engineering structures, for example roof trusses of buildings, truss girders of suspension bridges, space trusses of steel offshore or aerospace structures.

1.2.1 Historical Emergence

The truss construction principles as known today are rooted back to the early timber roof structures. Because of the limitations of timber to meet the requirements for larger roof spans, demand for reduction in dimensions of structural elements as well as simplification of connections, iron was gradually used to replace traditional timber material. For iron, the length available was not as limited as for timber, the jointing was much simpler, and a greater variety of forms could be created. In addition, the high stiffness and strength of iron allowed the design of filigree structures that were preferred in construction for visual appearance reasons, for example slender iron columns offered a less obstructed view. Furthermore, iron was thought of as having much better resistance to fire compared to timber. As more and more theatres were built throughout Europe in the 18th century during the Age of Enlightenment, the number of terrible fires was growing. Iron was used as structural elements with the assumption of being fire-proof³.

Only until the 19th century, the potential of the truss has been explored and experimented systematically by the bridge builders to meet the demands of rapidly expanding transportation systems of the time [LORENZ (1990), RINKE and KOTNIK (2010)]. The development of railroads in the 1820s created an urgent need for bridges to be able to carry heavy moving loads as well as for new large buildings for terminals and maintenance facilities [GASPARINI and PROVOST (1989)]. The rush to satisfy those needs accelerated the application of the scientific principles of mechanics in structural design process and fostered advances in the production and fabrication of the material *iron*.

1.2.2 Iron as Structural Material

Iron was referred to as material of modern engineering. The new building materials *cast iron* as well as early forms of what is nowadays called *steel*, stand in close connection with the fundamental change of human culture and life in the 18th and 19th century [LORENZ (2012)], which is nowadays referred to as industrial revolution⁴.

Cast iron was produced in blast furnaces by using three basic raw materials – ore, a fuel, and chalk⁵ to tie up the molten slag. Up to the beginning of the 18th century, generally,

³ For example, wrought-iron columns and brackets were used for the Théâtre Français by the architect Victor Louis (1731–1807) [ADDIS (2012)]. The new building of the Théâtre Français was opened in 1790 after a terrible fire in 1781. Here a wrought iron roof truss was built with a clear span of about 28 m.

⁴ The new designs developed from iron were classified as characteristic for the industrial age. According to Society for Industrial Archeology (1984): “There is nothing more fundamental to the man-made physical world than the materials of which its elements are composed; likewise, nothing more basic to the smaller industrial world than the ferrous metals.”

⁵ or something comparable.

charcoal was used as the fuel. In 1709, Abraham Darby at Coalbrookdale started using coal and then coke as the fuel. Coke made the furnaces much more efficient so that they could melt much larger quantities of iron ore to produce pig iron used for casting. This allowed for the first time in history the mass production of an iron building material – characterized by high carbon content that has good compression strength but is brittle.

In 1784, the British Henry Cort got a patent to re-smelt Darby’s pig iron to be able to produce a material rather different and especially far less brittle than cast iron. It was made in a puddling process where the carbon was burned out of the iron by heating with an oxygen-rich flame. The additional oxygen burned away the carbon while the iron was worked on by workmen. *Wrought iron*, or *puddle iron*, or *weld-iron* became the main iron material in the 19th century, which was already quite similar to nowadays steel.

In the second half of the 19th century, first Henry Bessemer, i.e. *Bessemer converter*, acid lining in 1855, then the Martin brothers together with the Siemens brothers, i.e. *Siemens–Martin process* in 1864–65, and Sidney G. Thomas with Percy C. Gilchrist, i.e. *Thomas converter*, basic lining in 1878, opened the way to the second generation of steel as a building material, characterized by a new dimension of quality and mass production, i.e. the so-called *Ingot Iron*, or *mild/soft steel*, or *low carbon steel*.

The properties of different alloys of iron are shown in Table 1.1, which are given with further details in ADDIS (2012). The main characteristics are that cast iron is highly strong in compression and relatively weak in tension, but brittle. Wrought iron is ductile and equally strong in compression and tension, but can only be shaped by rolling or forging, thus limiting its structural and decorative forms. Mild steel has similar properties to those of wrought iron, but it is generally stronger, and can be cast as well as rolled. However, mild steel has a lower resistance to corrosion than wrought iron.

Since the development of industrial production of iron, loadbearing members using iron were used for a variety of structures⁶, such as mills, railway stations, market halls, and so on. Concerning iron roof trusses, there was no sudden replacement of the timber with iron trusses, but rather a mixture of different types of roofs that were combinations of timber and iron, and of entirely iron with different mixes of cast and wrought iron.

Table 1.1 – Key properties of the alloys of iron [adapted from ADDIS (2012)].

		Wrought iron	Cast iron	Mild steel
Proportion of carbon	%	0.02 – 0.05	2.5 – 4.0	0.2 – 1.0
Temperature to manufacture	°C	1000	1130 – 1200	1500
Fracture behaviour		Ductile	Brittle	Ductile
Tensile strength	N/mm ²	280 – 370	120	350 – 450
Compressive strength	N/mm ²	240 – 310	600 – 800	350 – 450
Modulus of elasticity	N/mm ²	155 000 – 220 000 ⁷	85 000 – 90 000 ⁸	210 000
Corrosion resistance		Good	Very good	Poor

⁶ The evolution of the manufacture and use of iron loadbearing members in the building industry can be found for instance in SUTHERLAND (1963–64), SUTHERLAND (1997).

⁷ The modulus of elasticity of approximately 165 000 N/mm² for wrought iron was given as an example in BATES (1984); DE BOUW (2010) mentioned a range from 163 000 – 215 000 N/mm² by historic books as well as 171 000 – 190 000 N/mm² by tensile tests; a value of 160 000 N/mm² was derived for the structural survey in the New Hermitage in Saint Petersburg by HERES (2006); a value of 169 000 N/mm² was used for the structural analysis of the elliptical beams in the Winter Palace of the State Hermitage Museum by HÄBLER (2011); O’SULLIVAN and SWALES (2008) concluded a mean value of 197 000 N/mm² based on a histogram of values that was compiled from tensile tests on various American, British and Norwegian wrought irons.

⁸ A value of approximately 83 000 N/mm² was given as an example in BATES (1984).

Some examples of iron roof trusses that still exist today are shown in Figure 1.1. The tented roof over the Hall of Liberation in Kelheim [LORENZ (2001)] witnessed for instance the early development of compound construction in cast and wrought iron.

With the search for adequate construction methods and forms, the 19th century was a time of experimentation and discovery. New structural forms triggered the development of structural engineering, when engineers were orienting themselves increasingly towards the natural sciences, i.e. a comprehensive degree of control and a redefinition of the load-bearing structure. The increasing efforts to make the understanding of the load-bearing structure more scientific, together with new building materials had a radical influence on construction [RINKE and SCHWARTZ (2010)]. New load-bearing systems came about, including Wiegmann–Polonceau trusses, lattice trusses, diverse trussed girders, also barrel roofs and domes. The Wiegmann–Polonceau truss, proposed by the German engineer, Rudolf Wiegmann (1804–1865), and the Frenchman, Jean–Barthélémy Camille Polonceau (1813–1859)⁹, has become familiar in railway stations throughout the world.

1.2.3 Wiegmann–Polonceau Truss

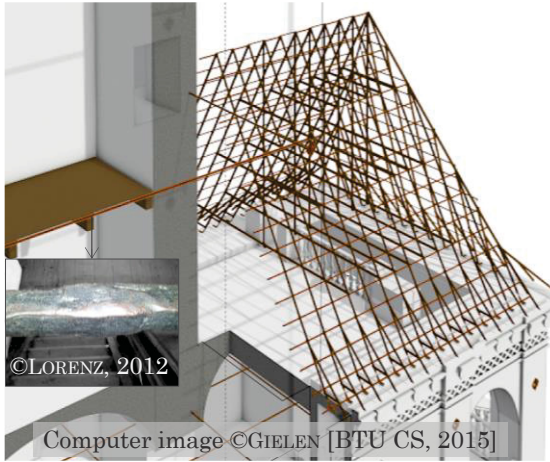
The evolution and history of the Wiegmann–Polonceau trusses have been described for instance in KURRER (2008) and HOLZER (2006). They are popular support system of the iron building constructions since the second half of the 19th century, particularly in the form of in–plane girders. The emergence of the Wiegmann–Polonceau truss in the first half of the 19th century was from the idea of a non–displaceable three–pin–jointed system for the construction of beam and frame structures [LORENZ (1990)]. Figure 1.2 illustrates the principle of the Wiegmann–Polonceau truss based on the theory of trussed beam. Originally, the principal rafters were made of timber and the tension ties of wrought iron to use optimally each material. Once iron was more established as structural components and its production was improved, the components had evolved from timber to iron.

Regarding the static calculations, for simplification, mainly compressive and tensile forces were assumed in the individual members of the statically indeterminate Wiegmann–Polonceau trusses. The construction system was easier than those that were known until then. These trusses were also easy to assemble and accounted for the resulting side thrust in arched and vaulted constructions. The concise and efficient forms of the Wiegmann–Polonceau truss were widely used to shelter large halls, for example the train station Gare d’Austerlitz in Paris (see Figure 1.3). The station is about 280 m long; the truss has a span length of about 51 m and height of approximately 28 m from the ground by the engineer Leonce Reynaud (1803–1880) [SCHULTZ et al. (2001)].

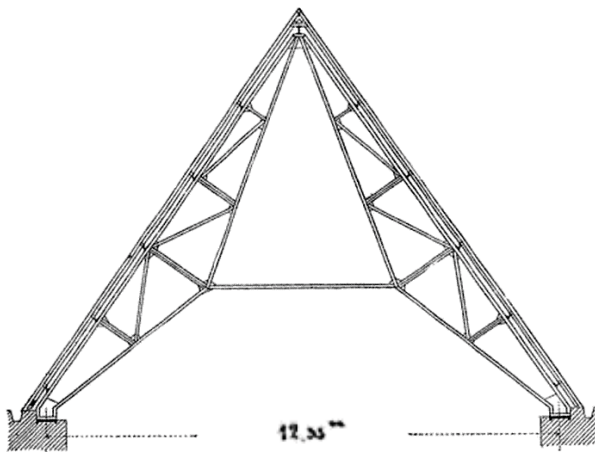
Concerning the fabrication, the forming of truss structure as an addition of structural members with similar elements allowed reduction of fabrication and simplification of design [YEOMANS (1992)]. Trusses were not built in one piece, because those would have been heavy, having little resistance to out of plane bending, and vulnerable to problems in the handling process between casting and erection. As a result, a truss was most often

⁹ The Wiegmann–Polonceau truss was almost simultaneously published by independent work in 1839 by the architect and professor at the Royal Academy of Arts in Dusseldorf, Rudolf Wiegmann, in the brochure *Construction von Kettenbrücken nach dem Dreieckssysteme* (1839) and Jean–Barthélémy Camille Polonceau in *Revue générale de l’Architecture et des Travaux Publics* (1840) [HOLZER (2006)].

(a) Nevyansk, Russia
[LORENZ and HERES (2015)]



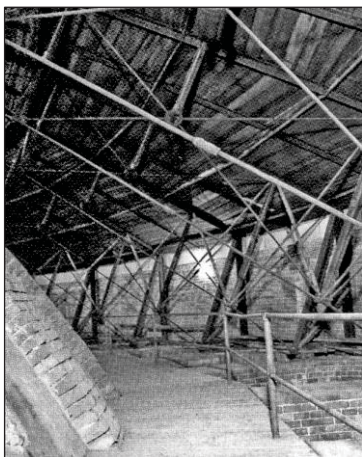
(a) Sachsenhausen, Germany
[SCHMITT and LANDSBERG (1897)]



(b) Ulm, Germany
[WOUTERS and COOMANS (2015)]



(c) Kelheim, Germany
[Archive BTU CS (2001)]



(d) Brugge, Belgium
[WOUTERS and COOMANS (2015)]



(e) Cologne, Germany
[BORGER (1980)]



Figure 1.1 – Examples of historic iron roof trusses that exist in present–time.

constructed in a number of pieces to be joined together. It was therefore necessary to provide some means of fitting them together and allowing compensate for manufacture. For instance, turnbuckles were used, such that member dimensions could be adjusted during erection as well as preloading could be provided to achieve a desired deformation or prestresse state of the truss. An example of trusses with turnbuckle elements at a historic building called *Reithalle* in Potsdam is given in Figure 1.4.

In addition, as seen by the strut members of the truss at *Reithalle* (see Figure 1.5), the shape of the strut member¹⁰ in compression is referred to as *bulged crucifix* [DE BOUW (2010)]. The thickening of the members in the middle was to avoid buckling. Crucifix cast iron strut was assumed to be the most optimal and economical form for small cast iron compression members such as those of the Wiegmann–Polonceau trusses.

The aspects related to optimally shaped beams in combination with single spans to permit substantial savings in material seemed to have been particularly relevant for example in Germany around the middle of the 19th century [HOLZER (2012)]. The experimentation on shape included fish–belly beams and under–spanned beams in the first half of the 19th century as well as parabolic girders, Schwedler girders, half–parabolic girders, and other systems in the second half of the century.

Some remarks about the Wiegmann–Polonceau trusses can be briefly summarized as follows. The trusses were invented in about 1839 to meet the demand of larger spans and a desire of optimal use of the material and components. The simplified design of the trusses assumed all hinged joints. The individual elements of the truss are assumed to have mainly compressive and tensile forces.

The advantages of these types of trusses are the structural efficiency, which had been proven over the years. The Wiegmann–Polonceau trusses are characterized as light–weight structures with impressive weight–to–span ratio and slender tension members. The drawback of the hinged trusses at that time was possibly the high cost to produce members with special shapes such as the compression struts and the connection parts to assemble all components together. The development of iron and steel production and selected examples of Wiegmann–Polonceau roof trusses are highlighted in Appendix A.

About the material properties of historic structures, the need for a better understanding of the properties of iron became increasingly important as engineers and architects designed structures of greater span and complexity at the time of the development of trusses [O'SULLIVAN and SWALES (2008)]. Historic iron exists in various forms, each of which might be manufactured in its own way and having its own properties. DE BOUW and WOUTERS (2011) stressed that to determine exactly which material was used in a certain case, one should take some samples and bring together the results of different material tests such as chemical analyses, metallographies, tensile tests, hardness measurements¹¹, and so on. However, it is often not the cases that samples of historic structures can be available for material tests. In any cases, an in–depth research of the construction history of the structures is recommended to make reasonable assumptions of the material properties.

¹⁰ An extensive study in Netherlands by NIEUWMEIJER (2001) showed evolution of the Wiegmann–Polonceau trusses' components. The use of the crucifix cast iron for the compression struts were around 1856–1904.

¹¹ Metallography and Vickers hardness tester can be used to determine the type of metal in historic metal structures, e.g. wrought iron or Ingot iron, and to predict the ultimate tensile strength [WOUTERS et al. (2011)].

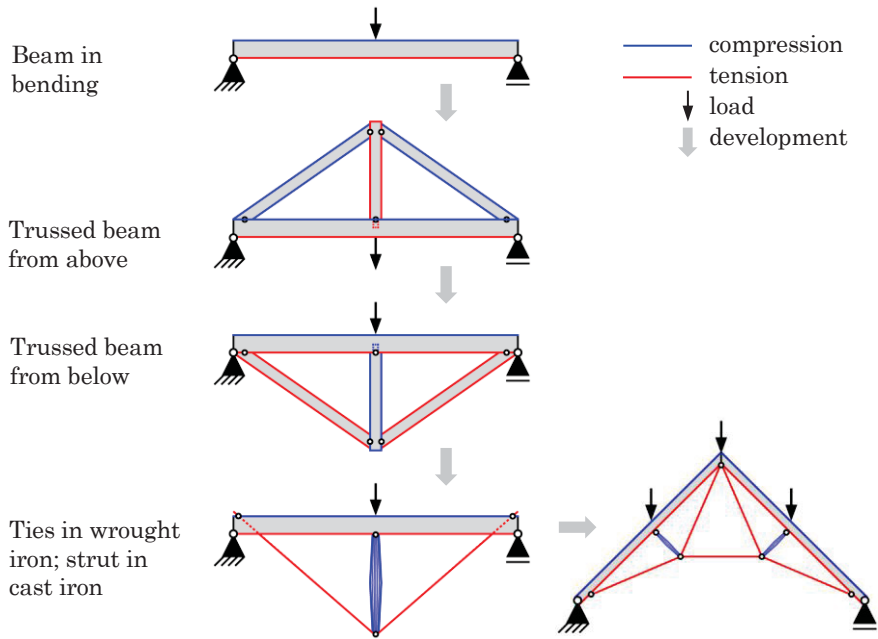
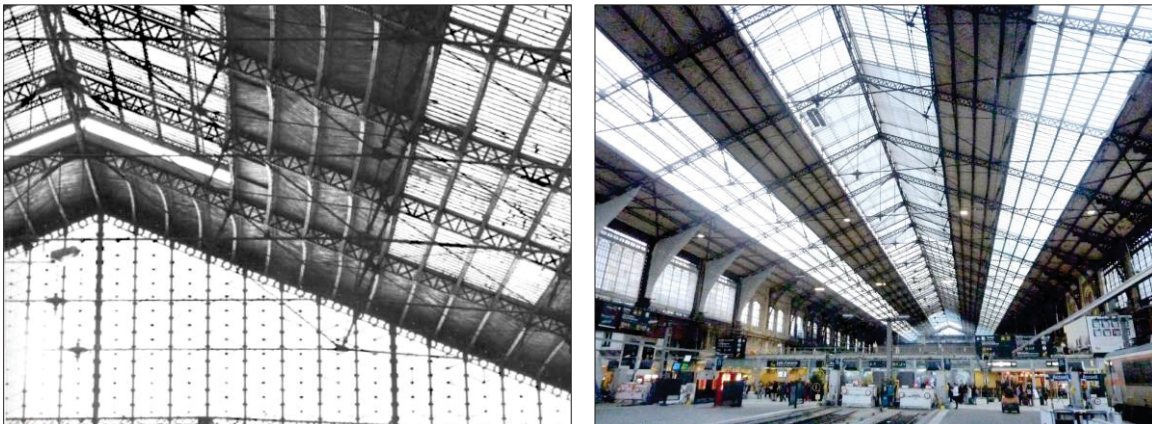


Figure 1.2 – Historico-logical development of Wiegmann–Polonceau truss [adapted from KURRER (2008)].

(a) Gare d'Austerlitz, Paris (1869)
[from HARTUNG (1983)]

(b) Gare d'Austerlitz in present time
(photo taken in 2015)



(c) Similar form of the Wiegmann–Polonceau truss to the one at Gare d'Austerlitz, Paris.

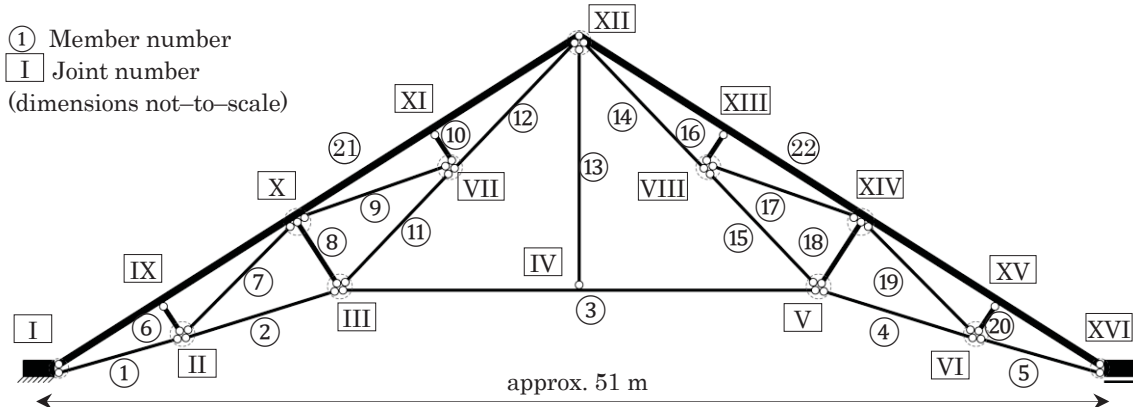


Figure 1.3 – Example of historic iron Wiegmann–Polonceau trusses: Gare d'Austerlitz, Paris (1869), span length of approximately 51 m and height of about 28 m from the ground.

1.2.4 Iron Roof Trusses of the State Hermitage Museum, Saint Petersburg

In the particular case, the State Hermitage Museum in Saint Petersburg is known as one of the world's most important museums. The impressive buildings around the former Winter Palace of the Russian Tsar are protected as a World Heritage Site. They are home to not only the famous art collection but also have an enormous historical significance in the construction history, since the roofs and ceilings are crisscrossed by a dense network of iron structures. Starting in 1838 after a devastating fire¹², iron structures were supplied for almost all roofs and floors of the buildings. These structures were put up by four different manufacturers within a period of thirteen years. In terms of volume, variety of application and richness of details, they are “outstanding evidence of early European structural steelwork and a greatly revealing ensemble from the early days of the European iron construction” [HERES (2006)]. An example of the iron roof trusses in the Old Hermitage is given in Figure 1.6.

The roof and ceiling structures are in large areas still preserved in the original state. They were surveyed, systematically documented and structurally evaluated within the framework of a research project¹³ carried out by the Chair of Construction History and Structural Preservation, Brandenburg University of Technology (BTU) Cottbus–Senftenberg [LORENZ and HERES (2006), HERES (2006)]. The analysis aims at understanding the mindsets and strategies of designers in dealing with the new building material iron at the time, reconstructing the design processes and stages of construction, as well as analysing the load bearing behaviour and quality of the engineering design.

To determine the mechanical properties of the iron, material tests were carried out for samples from the New Hermitage. All elements of the load-bearing structures were determined to be made of wrought iron. The material samples subjected to tensile tests showed the characteristic layered breaking structure of puddel iron. The material used in construction was ductile, with a failure strain of about 15 %. The characteristics derived for the structural assessment by HERES (2006) were as follows: an yield strength of 170 N/mm², a tensile strength of 300 N/mm² and the modulus of elasticity of 160 000 N/mm².

Considering the connections and bearings of iron trusses, mostly a cast iron shoe was used for bearings, which is confirmed by a literature study [DE BOUW (2010)] (see Figure 1.7). The connection between the tension ties, central tension tie and compression strut was often formed by one or two parallel gusset plates creating a hinged connection. In the case of one gusset plate, the tension ties, central tension tie and compression strut end with a fork to connect to the gusset plate. When two parallel plates were used, the members end with an eye-bar that was connected in-between the plates. The components were built in the way that allowed hinged connections to assure optimal use of materials, as well as for calculation purposes.

¹² Highly extensive use of iron was due to the devastating fire which destroyed a large part of the Winter Palace in the winter of 1837. In the process of the immediate reconstruction of the Imperial Palace that followed, iron load-bearing structures were used which were thought to be fire-proof. From 1840, iron structures were built with great variety and different constructive prototypes.

¹³ The research project *Die Eisenkonstruktionen in den Gebäuden der Staatlichen Eremitage St. Petersburg – Erfassung, Analyse und Bewertung im Kontext des frühen europäischen Stahlbaus* was funded by the Deutsche Forschungsgemeinschaft (DFG) (2008 – 2015) [LORENZ and HERES (2006)].

(a) *Reithalle* Potsdam in present-day



(b) Connection of compression strut to tension ties



(c) Similar form of the Wiegmann–Polonceau truss to the one at *Reithalle* Potsdam

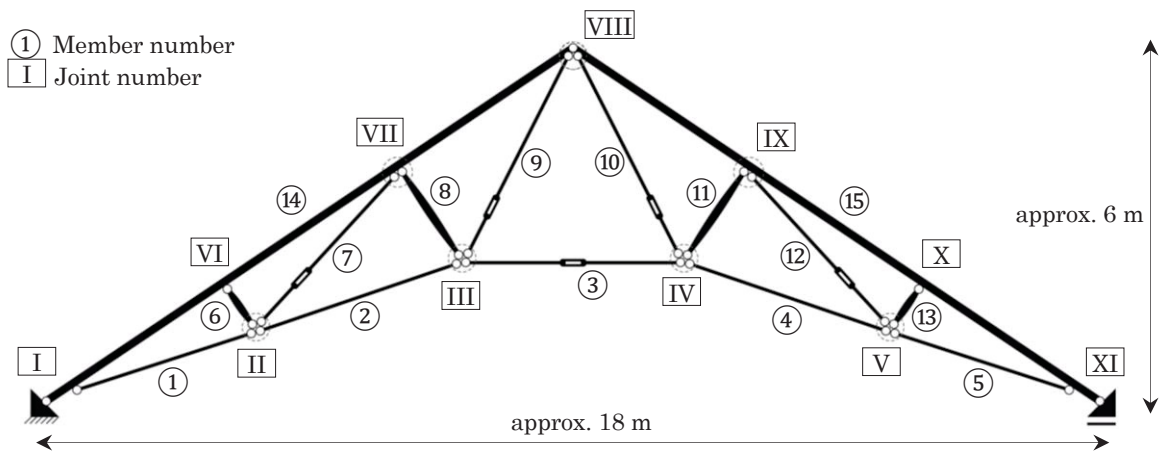
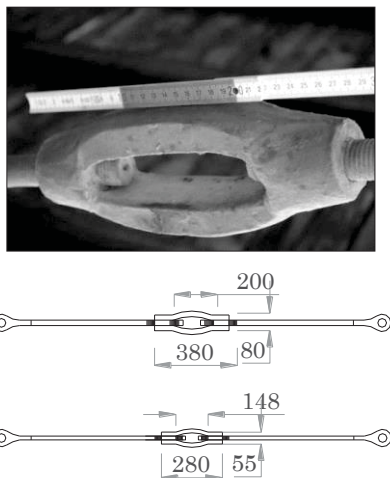


Figure 1.4 – Historic iron Wiegmann–Polonceau trusses at *Reithalle* Potsdam (1885–1891) with span length of approximately 18 m, height of approximately 6 m and several members with turnbuckles to adjust lengths and apply preload.

(a) Turnbuckle element



(b) Compression strut in optimal shape

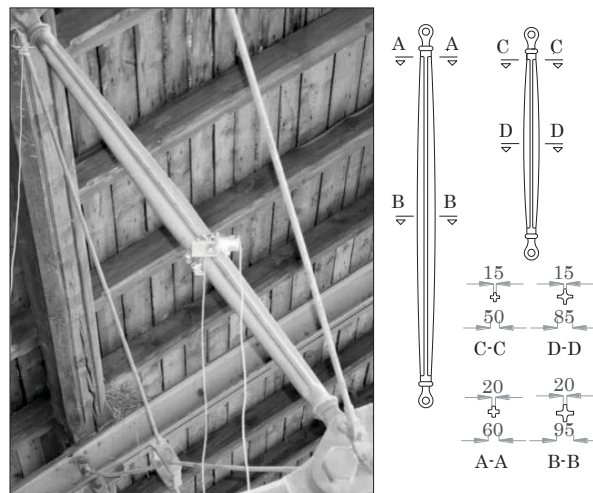


Figure 1.5 – Turnbuckle elements and optimally–shaped compressive struts of the historic iron Wiegmann–Polonceau trusses at *Reithalle* Potsdam (1885–1891).

1.2.5 Safety Assessment of Existing Iron and Steel Structures

Assessment, maintenance and restoration of existing buildings have become one of the most important tasks of civil engineering in research, teaching and practice [LORENZ (2011)]. The preservation of monuments is regarded as an important theme for iron and steel structures since the 1970s. Its relevance has grown steadily ever since. It took time, however, to understand monument protection as an engineering task. A milestone in this direction was the Deutsche Forschungsgemeinschaft (DFG)'s special research area 315: *Preserving historically significant buildings*, which explored for the first time systematically historic iron materials and steel structures between 1985 and 1999. At the international level, the International Scientific Committee on the Analysis and Restoration of Structures of Architectural Heritage (ISCARSAH) and the International Council of Monuments and Sites (ICOMOS) are to be emphasized. In 2003, the guideline *Principles for the Analysis, Conservation and Structural Restoration of Architectural Heritage* was adopted as an official ICOMOS Charter for engineers.

The conservation of historic structures and monuments as required by the ICOMOS Charter is seen in three phases: (i) diagnosis; (ii) safety evaluation; and (iii) design of intervention. Without the first and second phases, the necessity and type of an intervention cannot be assessed. The intervention itself is to act in the best care for the monuments, i.e. *best intervention is no intervention*. Lessons learnt from the unnecessary demolition of great structures or the deficient performance of strengthening measures of some old constructions bring engineers closer to achieving a better understanding of the behaviour of existing structures as well as better assessment methods.

Concerning the case study of the iron roof trusses in the State Hermitage Museum, the static analyses were performed based on the modelling assumptions resulting from different interpretations of the effects of joints and elements, e.g. turnbuckles, threads and nuts at the connections [HERES (2006), KEIL (2009)¹⁴]. Model calculations in-plane and three-dimensional were carried out, according to the present-day standards. While the condition of the trusses remained below the material's set limit, several rectangular rafters in compression demonstrated buckling. It is, however, relevant to note that flat rectangular top-chord rafters commonly experience stability issues resulting in deformations. While the rafters lay above the limit in the stress verification, they lay significantly below the tensile strength. The static calculations were unable, or with great difficulty, to take into account the relevance of the planned load-bearing ability as well as the stabilizing effects of the neighbouring construction components such as the roof lathing. In the end, the condition of the existing trusses was decisive. No signs of failure such as noticeable deformation in the areas of critical rafters were found.

Another example is the present-day structural analysis of the Brussels model schools that were built between 1875 and 1920 [DE BOUW and WOUTERS (2011)]. At the time of the model schools, no compulsory calculation methods and design rules existed; as a result, the design was mostly made by the experience of the designer himself. Based on the findings of the building techniques and the material properties, finite element models were set up to evaluate and compare the structural behaviour of the Wiegmann-Polonceau and Ardant trusses using the Eurocodes of today's practice [DE BOUW (2010)].

¹⁴ A complete list of the related theses, publications and presentations to the research project of the Hermitage Museum is available on the webpage of the Chair of Construction History and Structural Preservation: www.b-tu.de/fg-bautechnikgeschichte/forschung/laufende-projekte/eremitage-st-petersburg.

(a) Historic iron roof trusses in in the Old Hermitage, State Hermitage Museum



(b) Truss form in the Old Hermitage, State Hermitage Museum

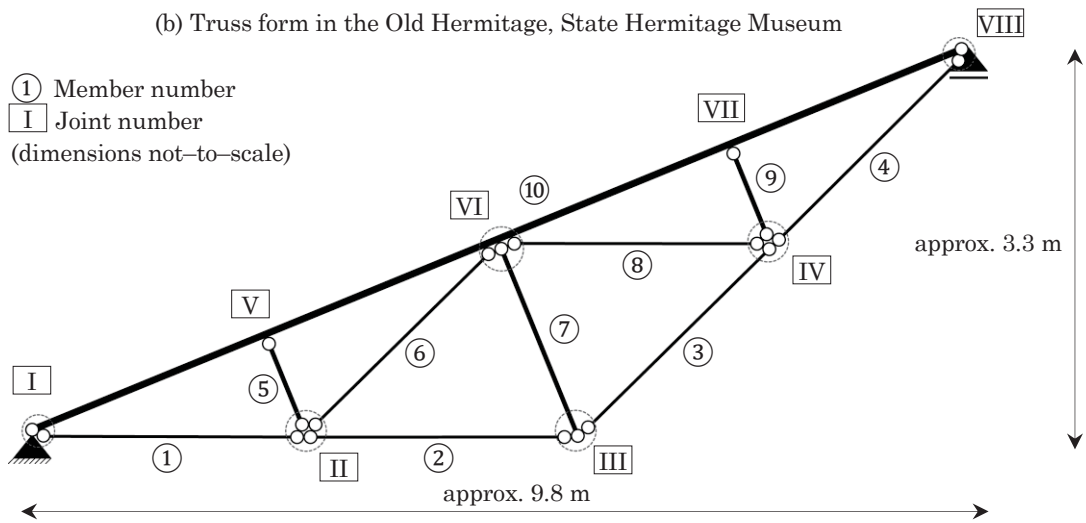


Figure 1.6 – Iron trusses in the State Hermitage Museum, Saint Petersburg [BTU CS (2011)].

(a) Detail of bearings and connections



(b) Detail of connections



Figure 1.7 – Details of bearings and connections for the case–study of iron roof trusses in the State Hermitage Museum in Saint Petersburg [BTU CS (2011)].

The results of the local stability checks showed that all the Wiegmann–Polonceau trusses meet the requirements of the Eurocode’s stability checks. However, the calculation models of the Ardant trusses predict several local stability problems. Still, the trusses stand for over 90 years, and recent visual inspections did not reveal stability problems. DE BOUW (2010) recommended the search for historic calculation notes and broadening of the typologies. Another important factor to be investigated further is the behaviour of the historic (rivet) connections and the modelling of these connections.

The case studies illustrate that for historic iron truss structures, static calculations of an assumed model cannot give accurate estimation of the axial forces and stress states, due to difficulty to acquire precise information about the parameters such as loading condition and joint connections, as well as uncertainties related to corrosion damages or presence of prestress in turnbuckles, etc. A non–destructive reliable method is needed to allow accurate identification and verification of the stress states of existing trusses.

1.3 Motivation of Structural Assessment for Existing Truss Structures

From the brief study of historic truss structures, the potential problems and challenges for the static estimation of the existing axial forces in iron and steel trusses are summarized as follows.

- The axial forces in truss members can be estimated by forward methods such as method of joints, method of sections or the finite element method [KRENK and HØGSBERG (2013)], provided information about parameters such as external loads, prestress of turnbuckles, support conditions and joint connections are known. However, an accurate estimation of the axial forces can only be achieved when the parameter inputs are given precisely, which is difficult to obtain in practice.
- The idealization of trusses with basic assumptions such as pinned joints makes these types of structures seem to be simple to analyse using static calculations. In practice, trusses are not ideally pin–jointed but are constructed by bolting or riveting the ends of the members to gusset plates, in which friction is present. For historic trusses, uncertainties due to damage risks such as corrosion make an appropriate assumption for joint conditions even more difficult.
- Beside joint and boundary conditions, there exist challenges relating to uncertainties in material properties of historic structures. The mechanical characteristics of iron and steel obtained through non–industrial processes in the past are difficult to determine through non–destructive tests.
- In addition, although the sectional properties of a truss might appear as known parameters, geometrical and mechanical properties of the cross–section may be altered due to corrosion.
- Moreover, another important uncertainty in the static estimation of the existing forces in truss structures is related to the initial tensions caused by pre–stressing turnbuckles, as well as the fitting–temperature of those iron structures.
- Furthermore, environmental factors such as temperature, humidity, etc., may cause seasonal variation of the load state and damages such as corrosion.
- Local damages can cause re–distribution of the axial forces in truss members, thus analysis assuming the truss at design state may be no longer valid.
- Loads and safety factors according to present–day standards cannot be directly applicable to historic structures. Thus, conservative results about the efficiency of existing trusses as defined today might require strengthening for the structures.

- Direct force measurement using strain gauges inconveniently requires that the forces be known at the instant of gauge application. This is not possible unless the structure is known to be in a zero-load state. Destructive or partially-destructive methods to identify the axial forces are not desired for historic structures.

Motivated by the importance of the preservation of historic truss structures and considering the challenges when working with historic constructions, a practical non-destructive method is required to verify the axial forces and stress states in existing truss structures.

1.4 General State of Research

As mentioned, forward methods¹⁵ can be used to calculate the axial forces in truss structures. However, due to difficulty or limitation to obtain precise information of the input parameters for manual calculations or numerical models in the forward methods, inverse methods have therefore been applied. In inverse methods, the unknown input parameters, particularly the loads, are determined based on the output parameters such as static deformations or modal parameters of natural frequencies and mode shapes.

The non-destructive inverse identification of the axial forces in axially loaded structural members has been studied by many researchers. The identification techniques can be classified according to static, static-dynamic or purely dynamic, as well as depending on the types of applications on different civil engineering structures, for instance columns, cables, tie-rods or space frames. A timeline overview of the existing axial force identification methods is given in Table 1.2.

Early works have been associated with the determination of critical buckling load in axially loaded columns. Tension force identification for cables has been intensively studied. Considering axially loaded single beam such as tie-rods supporting arches and vaults, a number of methods have been proposed. Dynamic methods have been taking advantages over static methods thanks to advances in testing equipment, convenient testing procedure and reliable measurements.

Relating axially loaded members as part of a structure, two approaches for the axial force identification can be considered as: (i) methods making use of the finite element formulations coupled with model updating techniques, which concerns the multiple axial force estimation for all members of a truss or framework structure [GREENING and LIEVEN (2003), BAHRA and GREENING (2006), BAHRA and GREENING (2009), BAHRA and GREENING (2011)]; and (ii) analytically-based methods for beams with unknown boundary conditions [LI et al. (2012), REBECCHI et al. (2013), MAES et al. (2013)] that have the generality to be applied to a single beam or beams as part of a structure.

Despite the variety of methods, the following shortcomings are present:

- The methods for cables are not immediately applicable to tie-bars or beam members since they cannot be modelled as cables. Moreover, the identification of

¹⁵ In forward methods, the modal parameters can be calculated when the input structural parameters, e.g. axial force and boundary conditions, are given. The work of BAYCAN et al. (1991), which set forth the theory of prestressing to control the frequencies of frameworks can be thought of as forward problem in the sense of prescribing force for dynamic-based requirements. Inverse problem in the present work is referred to the identification of the axial loading and joint conditions from the experimentally identified modal parameters.

tension forces in cables often concerns with high tension values. Certain methods are therefore only relevant for the cases of such high-tension forces.

- Regarding experimental-based static methods for single bars, they require the measurements of displacements and/or strains at several cross-sections of the bar due to applied static loads. However, these methods are particularly sensitive to the experimental errors due to small values of strains or displacements. Moreover, it may be difficult in practice to apply loads as well as measure vertical deflections for structures that are positioned at considerable heights, such as tie-bars in arched and vaulted structures or roof trusses.
- Mixed static-dynamic approaches require more than one experimental technique. In addition, they are still affected by the drawbacks related to the strain and deflection measurements.
- In many dynamic-based methods, only the information of the natural frequencies is used, in some cases only the frequency of a single mode is adopted. Other useful information, such as the natural frequencies of higher modes or the mode shapes, are discarded. For trusses and space frames compared to single bars, because the vibration behaviour is more complex, closely spaced modes with similar modes of vibration occur. Therefore, the adaptation of only the natural frequencies without the information of the mode shapes for the identification and validation process is insufficient to assure correct and accurate results.
- The majority of the existing methods investigated single structural elements, i.e., beams, those are not as part of a built-up structure. These methods are not directly applicable to truss structures.

Considering the approaches for axially loaded members as part of a structure, the following shortcomings are present:

- The available identification methods using finite element modelling coupled with model updating techniques [GREENING and LIEVEN (2003), BAHRA and GREENING (2006), BAHRA and GREENING (2009), BAHRA and GREENING (2011)] are based on sensitivity or gradient-based searching algorithms, whose success is significantly dependent on the assumptions of the initial values of the target parameters. In addition, the joint connections of the investigated truss structures are all ideally assumed as hinged or rigid, which in reality do not exist. Boundary conditions and joint connections have effects on the dynamic behaviour of a structure. As a result, the accuracy of identified axial forces is affected if the effect of the joint flexibility is not considered.
- The analytical-based methods can be sensitive to small errors on the input parameters [MAES et al. (2013)], the locations of the instrumented sensors and the quality of the mode shape coordinate measurements [REBECCHI et al. (2013)]. Moreover, the analytical-based approaches provide more than one result of the identified force of a member, i.e. one for each mode of vibration, and therefore are subjective to the mode selection [LI et al. (2012), REBECCHI et al. (2013), MAES et al. (2013)]. In the work of MAES et al. (2013), using the frequency domain approach, a single identified force was averaged from a selected range of the identified forces. Nevertheless, the selection of this range is not generalized. Furthermore, as only individual members are considered, a global model of the structure is not available. The axial forces can be only identified for tested members. Although the methods for single beams offer the advantage of simplified analysis procedure, they do not apply in an obvious way to assemblies of members in trusses and frameworks.

Table 1.2 – Overview of axial force identification methods (from 1936 onwards).

Year	Author	Classifi- cation	Method	Application				Modal Identified Info.			
				Column	Cable*	Beam	Truss	ω	ϕ	N	k_r
1936	STEPHENS	Dyn.	AB	•	•			•		•	
1951	LURIE	Dyn.	AB	•				•		•	•
1953	GOLDHAMMER and JOHNSON	Dyn.	AB	•				•		•	
1957	KLEIN	Dyn.	AB	•				•		•	
1967	HORTON et al.	Dyn.	AB	•				•		•	
1968	JACOBSON and WENNER	Dyn.	AB	•				•		•	
1970	HORTON and STRUBLE	Stat.	AB	•						•	
1971	BARUCH	Stat.	AB	•						•	•
1980	SEGALL and BARUCH	Dyn.	AB	•				•	•	•	
1980	SHINKE et al.	Dyn.	AB		•			•		•	
1988	OHLSSON	Dyn.	AB	•				•		•	
1988	CROCI	Stat.	AB		•					•	
1991	PLAUT	Dyn.	AB	•				•		•	•
1991	KYSKA	Dyn.	AB		•			•		•	
1992	BATI et al.	Stat.	AB			•				•	
1994	BLASI and SORACE	Stat.–Dyn.	AB			•		•		•	•
1994	CASAS	Stat.–Dyn.	MU		•			•		•	
1995	LIVINGSTON et al.	Dyn.	MU			•		•	○	•	
1996	SORACE	Stat.–Dyn.	AB			•		•		•	•
1996	HIROSHI et al.	Dyn.	EF		•			•		•	
1996	ZUI et al.	Dyn.	EF		•			•		•	
1998	RUSSELL and LARDNER	Dyn.	AB		•			•		•	
1998	SCHEIBE and DEMELT	Dyn.	MU		•			•		•	
2001	BATI and TONIETTI	Stat.	AB			•				•	
2003	AHN et al.	Dyn.	AB		•			•		•	
2003	GREENING and LIEVEN	Dyn.	MU	○		○	•	•		•	
2004	GO and LIOU	Dyn.	AB	•				•		•	
2005	LAGOMARSINO and CALDERINI	Dyn.	MU			•		•		•	
2005	REN et al.	Dyn.	EF		•			•		•	
2005	HIGGINS et al.	Dyn.	MU		•			•		•	
2005	SIEGERT et al.	Dyn.	MU		•			•		•	
2006	PARK et al.	Dyn.	MU		•	○		•		•	•
2006	HOLST et al.	Stat.	AB		•					•	
2006	GEIER et al.	Dyn.	AB		•			•		•	
2006	MEHRABI	Dyn.	AB		•			•		•	
2006	RIAD	Dyn.	MU		•			•		•	
2006	PARK et al.	Dyn.	MU		•	○		•		•	•
2006	BAHRA and GREENING	Dyn.	MU	○		○	•	•		•	
2007	KIM and PARK	Dyn.	MU		•	○		•		•	
2008	TULLINI and LAUDIERO	Stat.–Dyn.	AB			•		•		•	
2009	BAHRA and GREENING	Dyn.	MU	○		○	•	•		•	
2009	BUDELMANN et al.	Stat.	AB		•					•	
2010	AMABILI et al.	Dyn.	MU			•		•		•	•
2011	LUONG et al.	Dyn.	MU			•		•		•	
2011	BAHRA and GREENING	Dyn.	MU	○		○	•	•		•	
2012	LI et al.	Dyn.	AB	•		•	○	•	•	•	•
2013	WICHMANN et al.	Stat.	AB		•					•	
2013	TULLINI	Stat.	AB	•		•				•	•
2013	GENTILINI et al.	Dyn.	MU			•		•	•	•	•
2013	REBECCHI et al.	Dyn.	AB	•		•	○	•	•	•	
2013	MAES et al.	Dyn.	AB	•		•	○	•	•	•	

○ – Indirect application / Optional; • – Direct application / Required;

ω – Eigenfrequency; ϕ – Mode shapes; N – Axial force / Column buckling force; k_r – Rotational spring stiffness

AB – Analytical-based solution; EF – Empirical formula; MU – Model updating;

Stat. – Static; Stat.–Dyn. – Mixed static–dynamic; Dyn. – Dynamic;

*For cables, due to large amount of research publications, only selected references are listed; a more extended review can be found for instance in MEHRABI (2006), CHEN et al. (2016).

To predict the structural responses under different load scenarios or to design structural health monitoring schemes, a global model of the structure is required.

So far, the studies carried out to identify the static axial forces in iron and steel bars as part of a multiple-member truss structure still impose limitations. A methodology that considers a global truss structure and provides accurate identification of the axial loads as well as estimation of the joint stiffnesses still does not exist. Thus, the development of a practical and reliable methodology to be applied to existing multiple-member trusses is necessary. The advantageous aspects of the approaches for single members can be used for the axial force identification of a global multiple-member truss structure.

1.5 Objectives and Focus of the Research

Based on the state of research relating to the identification of the axial forces of iron and steel truss structures and advances in dynamic testing methods in the past decades, a research project was started at Brandenburg University of Technology (BTU) Cottbus–Senftenberg, in cooperation with Bundesanstalt für Materialforschung und –prüfung (BAM) and Bauhaus–Universität Weimar. The aim is to assess the structural safety of existing iron and steel truss structures in the context of the structural health monitoring (SHM) using a non-destructive vibration-based experimental approach.

Particularly, the two main objectives of the research work are: (i) to identify the multiple axial forces and corresponding stresses of truss structures; (ii) to assess the joint flexibility by examining assumptions for the modelling and analysis of joints of truss-type constructions. From the identified axial forces and joint stiffnesses of trusses, an accurate global model is acquired to approximate the actual behaviour of the structure.

The approach of the work is experimental-based, i.e. to use information that is gained directly on the structures by vibration measurements. Even though there may be errors associated with experimental measurements, the identified axial forces and corresponding stresses are expected to be a better representation of the actual state of stress of the structures than the predictions that are based solely on assumptions and static calculations of an analyzed model.

The characteristics of the systems of interest are light-weight iron and steel truss-type structures composed of slender members. In addition, the structures are primarily subjected to axial forces. Moreover, planar truss structures are of focus, with the possibility to extend to space truss structures. Furthermore, the present work examines the relationship between the axial load in slender truss members assuming that no significant (transverse) deflections exist, because deflections arising as a side effect of the axial loading or initial imperfections of the structure are known to affect the structural dynamic behaviour [GREENING and LIEVEN (2003)].

The research work was carried out in several phases. First, the scientific development in the field and the theoretical background were examined. After that, numerical simulation was carried out for the development of a proposed methodology. In the second phase, an exemplary in-situ experiment was performed on an existing Wiegmann–Polonceau truss structure to examine the possibility of identifying the modal parameters of historic iron truss structures, in cooperation with Bundesanstalt für Materialforschung und –prüfung (BAM). In the third phase, laboratory tests were carried out in cooperation with Bauhaus–Universität Weimar, which allowed the application and validation of the proposed methodology of the present work.

1.6 Outline of the Thesis

The thesis is organized in six chapters; a schematic representation of the outline of the thesis is presented in Figure 1.8.

Chapter 1 gives the introduction to the work, starting with a brief overview of historic iron and steel truss structures as study context, followed by the motivation and general state of the research. After that, the objectives and scope of the work as well as the outline of the thesis are provided;

Chapter 2 addresses the state of the art methodologies and the theoretical background of the analytical-based methods to identify the axial forces in axially loaded structural members. In addition, discussion about semi-rigid connection modelling and analysis is given. The vibration-based model updating using different optimization techniques are reviewed. Furthermore, the proposed methodology in the present work is described;

Chapter 3 presents the numerical study for the application of the proposed methodology to identify multiple axial forces and estimate the joint flexibility of truss structures. Sensitivity analysis and optimization strategies were performed for three partial truss-type systems of single bars, a two-bar truss-like structure and a five-bar truss;

Chapter 4 describes the laboratory experiments for the truss-type systems. Issues such as the distribution of sensors in different setups, the performance of the dynamic tests with increasing load steps and the modal parameter identification at each load step are addressed. The results of the inverse identification of the axial forces and joint stiffnesses of the systems by the proposed methodology are presented;

Chapter 5 presents a case study of an in-situ dynamic test on a representative historic Wiegmann-Polonceau truss structure. Possible challenges of in-situ tests on existing truss structures are discussed. Moreover, a recommended scheme for the experimental-based safety assessment applicable to existing trusses is given;

Chapter 6 summarizes the conclusions of the research work and includes the recommendations for future research.

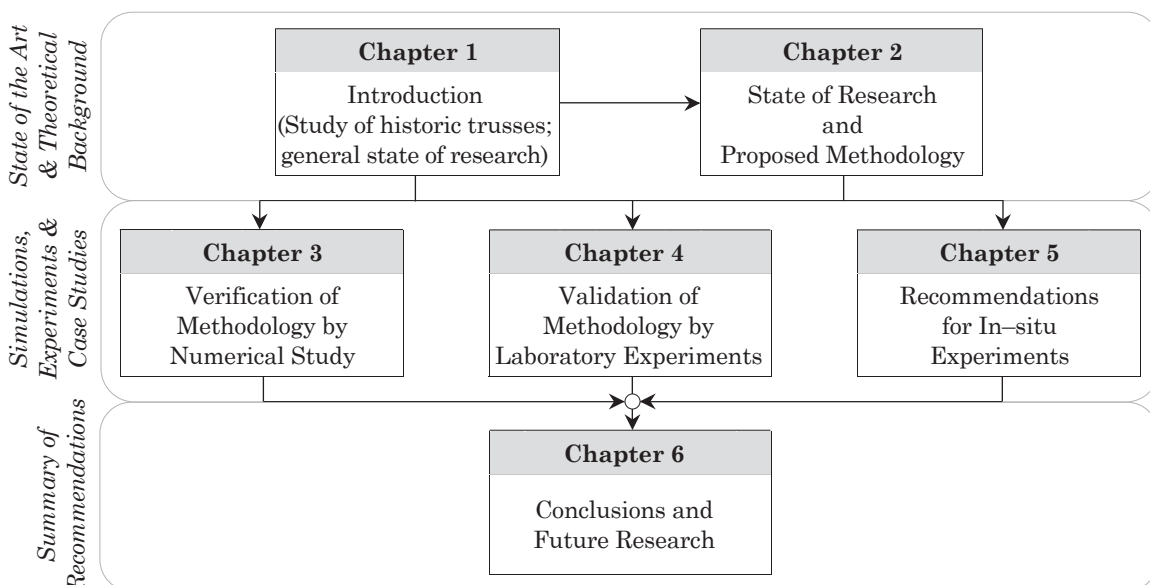
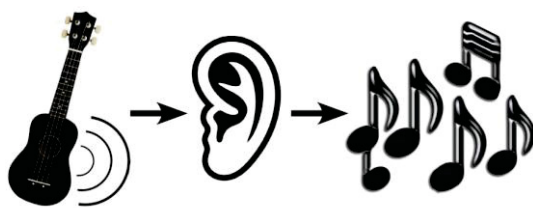


Figure 1.8 – Outline of the thesis.

2

STATE OF RESEARCH AND PROPOSED METHODOLOGY



The theoretical background of selected analytical-based methods is reviewed for a better understanding of the development of the proposed methodology in the present work. In addition, the background of semi-rigid connections in structural analysis and design is provided. Moreover, an overview of the finite element model updating methods and optimization techniques is given. The application of the vibration-based model updating using global search optimization techniques for the inverse identification of axial forces and estimation of joint flexibility of truss structures is discussed.

2.1 Theoretical Background

Analytical– and numerical–based methods have been proposed to identify the axial forces in structural members. Each approach has its advantages and disadvantages. For completeness, the theory relating to the dynamic response of structure members subjected to axial force effects is presented briefly.

2.1.1 Stress Stiffening

Axial forces acting in a flexural element causes change in its stiffness and thus influence the vibration behavior of a member. This phenomenon is referred to as *stress stiffening*¹⁶. For slender structural elements, the axial loads result in a lack of stiffness in the transverse direction, for example buckling of columns, plates or shells. Stress stiffening affects potentially all load–carrying structural elements, although only for slender elements such as strings, beams, thin shells, etc., significant variations to lateral stability and vibration characteristics are noted.

From the partial differential equation of motion of a prismatic member having uniform physical properties with the assumptions of small deflection, based on Euler–Bernoulli beam theory, the free–vibration equation of motion is known as

$$EI \frac{\partial^4 v}{\partial x^4} + \rho A \frac{\partial^2 v}{\partial t^2} = 0 \quad (2.1)$$

where EI is the flexural stiffness of the beam, v the transverse displacement response, x the position along the span, ρ mass density, A the cross–sectional area and t is time.

Applying appropriate boundary conditions, a series of the solution for the frequencies of a beam without the axial–force effects can be expressed as

$$\omega_n = \lambda_n^2 \sqrt{\frac{EI}{\rho AL^4}} \quad (2.2)$$

where ω_n is the circular natural frequency of n th mode [rad/s], λ_n represents different boundary conditions [LUONG (2010)], and L is length of the bar. For a pinned–pinned beam independent from the axial–force effects, the frequency solution is

$$\omega_n = (n\pi)^2 \sqrt{\frac{EI}{\rho AL^4}}, \quad n = 1, 2, 3, \dots \quad (2.3)$$

where n is the mode number. For a rigid–rigid beam excluding the axial force effects, the following frequency expression applies

¹⁶ Stress stiffening phenomenon is understood as an alteration of stiffness leading to a dependence of the modal parameters upon structural loading [GREENING and LIEVEN (2003)].

$$\omega_n = \left(\frac{(2n+1)\pi}{2} \right)^2 \sqrt{\frac{EI}{\rho AL^4}}, \quad n = 1, 2, 3, \dots \quad (2.4)$$

Upon axial loading on strings or cables, because the low bending stiffness of the string is negligible, the transversal strength of a string is therefore only dependent on the axial force. The differential equation of motion from the dynamic equilibrium in the transversal direction is given by

$$-N \frac{\partial^2 v}{\partial x^2} + \rho A \frac{\partial^2 v}{\partial t^2} = 0 \quad (2.5)$$

where a positive value of N implies a tension state of the string, whereas a negative N indicates a compression state. A simply-supported string including the axial force effects has the following frequency expression,

$$\omega_n = n\pi \sqrt{\frac{N}{\rho AL^2}}, \quad n = 1, 2, 3, \dots \quad (2.6)$$

Many vibration methods used for the cable tension estimation are mainly based on the theory of vibrating string, which is considered as simplest method.

When considering free vibrations of a Euler–Bernoulli beam subjected to a time-invariant uniform axial force throughout its length, a term related to the force N is added to the equation of motion of the bar. Eq. (2.1) can be rewritten as

$$EI \frac{\partial^4 v}{\partial x^4} - N \frac{\partial^2 v}{\partial x^2} + \rho A \frac{\partial^2 v}{\partial t^2} = 0 \quad (2.7)$$

For a simply-supported beam, the frequency expression including the axial force effects is given by

$$\omega_n = n\pi \sqrt{\frac{n^2 \pi^2 EI}{\rho AL^4} + \frac{N}{\rho AL^2}}, \quad n = 1, 2, 3, \dots \quad (2.8)$$

If bending stiffness is negligible in the cases of strings or cables, the frequency expression reverts to the natural frequency of a string in Eq. (2.6) respectively. Eq. (2.8) can be rewritten with the same meaning as

$$\omega_n = n^2 \pi^2 \sqrt{\frac{EI}{\rho AL^4} + \frac{1}{n^2 \pi^2} \frac{N}{\rho AL^2}}, \quad n = 1, 2, 3, \dots \quad (2.9)$$

In the above expression, it can be realized that for higher modes, the axial force effects reduce and eventually diminish. Eq. (2.8) can be also expressed in term of the critical buckling load, which is relevant for members under compression

$$\omega_n = n\pi \sqrt{\frac{n^2\pi^2 EI}{\rho A L^4} \left(1 - \frac{N}{N_{Euler}}\right)}, \quad n = 1, 2, 3, \dots \quad (2.10)$$

where the critical buckling load N_{Euler} is given by

$$N_{Euler} = \frac{n^2\pi^2 EI}{L^2} \quad (2.11)$$

It should be noted that the vibration is assumed at low levels where the amplitude is sufficiently small, so that the assumption of a constant axial load in the bar can hold true. For other boundary conditions of the bar, such as semi-rigid or rigid-rigid, and including the axial-force effects, closed-form solutions do not exist [LUONG (2012)]. Approximate solutions were studied, for example PETERSEN (2000) for the boundary conditions of one end rigid and one end hinged, or both ends rigid.

When rotational inertia and shear deformation are taken into account based on Timoshenko beam theory, the differential equation excluding the axial force effects is

$$EI \frac{\partial^4 v}{\partial x^4} + \rho A \frac{\partial^2 v}{\partial t^2} + \rho I \frac{\partial^4 v}{\partial t^2 \partial x^2} - \frac{EI\rho}{k_y G} \frac{\partial^4 v}{\partial t^2 \partial x^2} + \frac{\rho^2 I}{k_y G} \frac{\partial^4 v}{\partial t^4} = 0 \quad (2.12)$$

where G is the shear modulus and k_y is the shear deformation coefficient. If a small impact of the combined effect of the rotational inertia and shear deformation is neglected but their individual effects are considered, an approximate expression for the natural frequency for a simply supported beam is obtained as

$$\omega_n = n^2\pi^2 \frac{\sqrt{\frac{EI}{\rho A L^4}}}{\sqrt{1 + \frac{n^2\pi^2 I}{A L^2} + \frac{n^2\pi^2 EI}{k_y G A L^2}}}, \quad n = 1, 2, 3, \dots \quad (2.13)$$

The influence of the rotational inertia and shear deformation increases for higher modes; but for lower modes the impact can be considered negligible as exemplified by TIMOSHENKO et al. (1974) and ABRAMOVICH and ELISHAKOFF (1990). For Timoshenko beam, the influence of the rotational inertia and shear deformation lead to a lowering of the frequency values in comparison to Euler-Bernoulli beam. The most complete description of a Timoshenko beam element including the axial force effects is governed by

$$\begin{aligned} EI \frac{\partial^4 v}{\partial x^4} + \frac{EIN}{k_y GA} \frac{\partial^2 v}{\partial x^4} - N \frac{\partial^2 v}{\partial x^2} + \rho A \frac{\partial^2 v}{\partial t^2} + \rho I \frac{\partial^4 v}{\partial t^2 \partial x^2} \\ - \frac{EI\rho}{k_y G} \frac{\partial^4 v}{\partial t^2 \partial x^2} - \frac{N\rho I}{k_y GA} \frac{\partial^4 v}{\partial t^2 \partial x^2} + \frac{\rho^2 I}{k_y G} \frac{\partial^4 v}{\partial t^4} = 0 \end{aligned} \quad (2.14)$$

A closed form frequency expression for a Timoshenko beam does not exist, even for a simply supported beam.

When no analytical solutions for single beams exist and for complex structures, the finite element method provides a means for the analysis of a structure under stress stiffening. Consider a Euler–Bernoulli beam segment with uniform cross–section, the mass matrix and the stiffness matrix in general form [CLOUGH and PENZIEN (1995)] are as follows

$$[M] = \frac{\rho AL}{420} \begin{bmatrix} 156 & 22L & 54 & -13L \\ 22L & 4L^2 & 13L & -3L^2 \\ 54 & 13L & 156 & -22L \\ -13L & -3L^2 & -22L & 4L^2 \end{bmatrix} \quad (2.15)$$

$$[K] = \frac{2(EA)}{L^3} \begin{bmatrix} 6 & 3L & -6 & 3L \\ 3L & 2L^2 & -3L & L^2 \\ -6 & -3L & 6 & -3L \\ 3L & L^2 & -3L & 2L^2 \end{bmatrix} \quad (2.16)$$

where M and K represent mass and stiffness matrices. To account for the presence of axial–force effects in the finite element method, a new element called geometric stiffness [CLOUGH and PENZIEN (1995)] is introduced to the stiffness of the whole structure

$$[K_G] = \frac{N}{30L} \begin{bmatrix} 36 & 3L & -36 & 3L \\ 3L & 4L^2 & -3L & -L^2 \\ -36 & -3L & 36 & -3L \\ 3L & -L^2 & -3L & 4L^2 \end{bmatrix} \quad (2.17)$$

where K_G represents geometric–stiffness matrix. The geometric stiffness property depends on the configuration of the structure as well as its loading condition.

2.1.2 Stress Stiffening in Isolated Bar and Truss Structures

From the theoretical study of single members subjected to axial loading, some remarks are as follows. All natural frequencies of a member will experience a modification to their magnitudes when being subjected to axial loading. The magnitude of the modification varies depending on the modes and decreases as the mode increases. The static tensile force increases the natural frequencies of a structural member; whereas static compressive force decreases the member’s natural frequencies. Compressive loading leads eventually to static buckling, at which the fundamental dynamic mode and Euler mode merges and the fundamental frequency vanishes. For a simply supported beam, the fundamental vibration and buckling modes are identical. The relationship between load and frequency is nonlinear. The eigenvalues exhibit significant variations with respect to load, whereas the eigenvectors or mode shapes for an isolated member are stationary or quasi–stationary [BAHRA and GREENING (2006)].

While the effects of the axial load on an isolated bar or beam are well understood, the dynamic behaviour of collective members of a built–up truss structure subjected to the axial force effects have been less investigated. BAHRA and GREENING (2006) discussed the frame fundamental frequencies as global coupled systems of analogous single members.

The higher number of members a system has, the more complicated the effects of the axial forces are. The tensile and compressive forces coexist in a framework and cause contrarious variations of natural frequencies as well as interchanges of modes. Furthermore, a phenomenon that is referred to as *mode veering*¹⁷ occurs, which makes the pairing of modes for a structure at different stress states difficult. This affects for instance the mode pairing between the experimentally identified and numerically computed modes during a model updating process.

2.1.3 State of the Art Axial Force Identification Methods

Over the past decades, many procedures have been proposed for the non-destructive inverse identification of the axial forces in axially loaded structural members. A timeline overview of the methods has been given in Chapter 1. The methods can be categorized according to different types of civil engineering structures, e.g. columns, cables, tie-rods, trusses and frameworks, or depending on whether static, mixed static-dynamic or purely dynamic approaches are applied. Selected methods are discussed next.

OHLSSON (1988) investigated the instability of slender members, whose dynamic characteristics are dependent on the compressive force. The present axial load in a column can be estimated by analytical solution as a fraction of the Euler buckling load based on measurements of two successive eigenfrequencies, or by repeated measurements of one eigenfrequency at the existing unknown axial force and a well-known additional applied force by means of an added mass on top of the column. The estimated compressive force by the analytical equation for a simply supported column was close to the measured experimental force with a difference of approximately 4 %. In JACOBSON and WENNER (1968), after the stiffness of the end constraints of a prismatic column subjected to null axial load were determined, the critical load was analytically derived.

Intensive research has been conducted for the identification of the tension force in cables. With main consideration of prestressed tendons in bridges, several monitoring techniques for steel tensile cables were reported in HOLST et al. (2006). A magnetoelastic measurement technique was described to measure the prestressing force. Magnetoelastic-based techniques were also used by SCHEIBE and DEMELT (1998). The disadvantage of these measurement techniques is that a portion of the cable material has to be kept for calibration. Acoustic-based methods were examined by HIGGINS et al. (2005). The change in the dynamic (acoustic) behavior is recorded when energy is released by failure of a wire or a strand of the tension members. Nevertheless, the high cost and requirement of the testing procedure limit the use of those methods.

SHINKE et al. (1980) proposed dynamical identification of cable tension force using natural frequencies. Although the method is simple and speedy, it is not suitable for members that are not slender or not sufficiently tensioned. RIAD (2006) stressed that generally for short cables, the actual vibration length and the bending stiffness of the cables have a considerable influence on their dynamic properties. AHN et al. (2003) analytically

¹⁷ “A pair of modes exhibit the veering characteristics in a way that they move towards each other in the frequency spectrum as loading varies and then move apart again without meeting”. When plotting frequency variations with respect to load, around the veer, frequency loci are almost nonlinear; mode shapes of the respective modes continuously exchange and become ambiguous. When the veer is passed, the mode shapes have completely switched positions in the spectrum [BAHRA and GREENING (2006)].

investigated the parameters affecting the cable forces to introduce an error correction algorithm that accounted for the errors in the mass, length, bending stiffness, sag extensibility and natural frequency identification. However, compared with measured force values, deviations were up to 10 % for short cables.

The disadvantage of the techniques for the axial force identification in cables is that the simplified theory or closed form solution of vibrating strings is not sufficiently accurate for beam-like members. In addition, the tension forces in cables are considerably higher than that in beams or truss structures.

To distinguish the methods for cables or beam-type structural members, LI et al. (2012) discussed four categories of methods depending on whether sag extensibility and bending stiffness are taken into account: (i) methods using classic taut string theory that neglects both effects, (ii) approaches based on modern cable theory that account for sag-extensibility without bending stiffness, (iii) techniques that consider bending stiffness but neglects sag-extensibility, and (iv) approaches that take into account both effects. The approaches in the last two categories which involve bending stiffness have attracted attention in recent years due to their correspondence to many practical applications.

To help differentiate between the approaches in the four above-mentioned categories, a non-dimensional bending stiffness parameter was introduced to evaluate the effect of bending stiffness on free vibration of beam-like members. A simple relationship was proposed in MEHRABI and TABATABAI (1998) between the natural frequencies, axial force and the bending stiffness parameter of a fixed-fixed cable. Based on the bending stiffness parameter, certain methods, which can be applied to identify high tension forces in cables, are not accurate on short thick cables, tie-bars or members of trusses and space frame structures.

Regarding the axial force determination for axially loaded single beams such as tie-rods supporting arched and vaulted constructions, proposed methods [LUONG (2012)] include (i) static methods making use of static displacement and/or strain; (ii) mixed techniques combining static and dynamic identification; and (iii) purely dynamic methods.

BATI and TONIETTI (2001) described a single static test to identify the force in tie-bars, which requires the measurement of three vertical displacements under a concentrated static load, as well as the strains variations at three sections of the bar. TULLINI (2013) proposed static method to determine the axial force in slender beams by measuring the flexural displacements or curvatures at five cross-sections of the beam subjected to an additional concentrated lateral load. Nevertheless, the measures of displacement and/or strain are relatively sensitive to experimental errors, and impractical for structures that are positioned at considerable heights. Moreover, the procedure by TULLINI (2013) assumes infinite translational stiffness at the beam ends. This restrictive assumption unfortunately cannot be ascertained in practice.

Concerning dynamic approaches, LAGOMARSINO and CALDERINI (2005) developed an algorithm to identify the axial tensile force in tie-bars by using the first three natural frequencies of a Euler-Bernoulli beam model. The *Line Search* method, a gradient-based searching algorithm, was adopted. AMABILI et al. (2010) proposed a technique to identify the tensile force in tie-bars using the first four to six natural frequencies of tie-bars based on Timoshenko beam theory. The unknowns of the tensile force, the stiffness of the foundation and in some cases, the length of the bar inside the wall, were identified by minimizing a weighted difference between the calculated and identified natural

frequencies using a *Nelder–Mead* minimization procedure, also known as downhill search method. GENTILINI et al. (2013) studied the identification of the axial force in tie-bars based on dynamic testing, added masses and genetic algorithms. The discrepancy between the experimentally determined and numerically computed frequencies of a modified tie-bar system with a concentrated mass was minimized to determine the axial force and two different joint stiffnesses of the end constraints. All the above dynamic-based methods, however, make use of only the information of the natural frequencies, while the useful information obtained for the mode shapes is discarded. Moreover, the methods only investigated single structural members.

Concerning axially loaded members as part of a structure, GREENING and LIEVEN (2003) studied the axial load identification of a single redundant frame using a sensitivity-based finite element model updating approach, i.e. the *Newton* method. The loads in all members were updated based on the experimentally identified natural frequencies. Similarly, BAHRA and GREENING (2011) examined the axial force identification for space frames using the *Newton* method. They showed an improvement to the approach by GREENING and LIEVEN (2003) such that the number of updating parameters was reduced by updating a scalar factor on each axial load pattern. The factors on the axial load patterns were updated based on the state of equilibrium of all member axial forces. Nevertheless, difficulties in modelling joints were found. In addition, as sensitivity-based approaches were used, their success depends strongly on the initial assumptions of the design parameters. A challenge was noted to find a start point leading to convergence. The loads in the examined frameworks were identified to an encouraging degree of accuracy, but correct solutions have been obscure and considerably demanding to be found.

Based on the theoretical formulation for beams with unknown boundary conditions, analytical-based algorithms were proposed for the inverse estimation of the axial force in single beams or beams as part of a structure [LI et al. (2012), REBECCHI et al. (2013), MAES et al. (2013)]. However, the methods for single beams do not apply straightforwardly to truss structures.

Even with the cumulative efforts by many researchers, the existing methods continue to exhibit shortcomings with respect to the axial force identification of multi-member truss structures. Besides, investigations considering the joint flexibility estimation in combination with the axial force determination has not been well investigated.

2.1.4 Analytical-based Algorithms for Axial Force Identification

The analytical-based methods by LI et al. (2012), REBECCHI et al. (2013) and MAES et al. (2013) offers convenience in the testing and analysis procedure for a member as part of a structure. Because the analytical-based method by MAES et al. (2013) is used in the present work, the theoretical formulation of the analytical-based algorithms is described.

2.1.4.1 LI et al. (2012)

The method by LI et al. (2012) examined structural elements including tie-bars, diagonal braces and short thick cables. Using Euler–Bernoulli beam theory, considering the bending stiffness, by separating of variables for displacement of free-vibration motion of specific shape $\phi(x)$ and having time-dependent amplitude $Y(t)$, from Eq. (2.7) one has

$$v(x,t) = \phi(x) Y(t) \quad (2.18)$$

$$\frac{\phi^{iv}}{\phi(x)} + \frac{N \phi''(x)}{EI \phi(x)} = -\frac{\rho A \ddot{Y}(t)}{EI Y(t)} = \alpha^4 \quad (2.19)$$

where the single constant α^4 is designated for mathematical convenience. Eq. (2.19) yields two ordinary differential equations

$$\ddot{Y}(t) + \omega^2 Y(t) = 0 \quad (2.20)$$

$$\phi^{iv}(x) + \frac{N}{EI} \phi''(x) - \alpha^4 \phi(x) = 0 \quad (2.21)$$

Setting a complex number g^2 to be associated with N , i.e. g^2 is purely imaginary when $N < 0$ and purely real when $N \geq 0$, and expressing α^4 in terms of the natural frequency, the following expressions are obtained

$$g^2 \equiv \frac{N}{EI}, \quad \alpha^4 \equiv \frac{\rho A \omega^2}{EI} \quad (2.22a,b)$$

From Eq. (2.22a,b), the parameters q_1 and q_2 can be defined in Eq. (2.23a,b) as

$$q_1 = \sqrt{\left(\alpha^4 + \frac{g^4}{4}\right)^{1/2} + \frac{g^2}{2}}, \quad q_2 = \sqrt{\left(\alpha^4 + \frac{g^4}{4}\right)^{1/2} - \frac{g^2}{2}} \quad (2.23a,b)$$

Based on the relationship of g^2 , α^4 and q_1 and q_2 , the solution of the axial force can be obtained by solving the determinant of the characteristic matrix $[S]_{4 \times 4}$, whose components in measurement of acceleration, velocity or displacement are

$$S = \begin{bmatrix} \cos q_1 x_1 - \lambda_{15} \cos q_1 x_5 & \sin q_1 x_1 - \lambda_{15} \sin q_1 x_5 & \cosh \frac{\alpha^2}{q_1} x_1 - \lambda_{15} \cosh \frac{\alpha^2}{q_1} x_5 & \sinh \frac{\alpha^2}{q_1} x_1 - \lambda_{15} \sinh \frac{\alpha^2}{q_1} x_5 \\ \cos q_1 x_2 - \lambda_{25} \cos q_1 x_5 & \sin q_1 x_2 - \lambda_{25} \sin q_1 x_5 & \cosh \frac{\alpha^2}{q_1} x_2 - \lambda_{25} \cosh \frac{\alpha^2}{q_1} x_5 & \sinh \frac{\alpha^2}{q_1} x_2 - \lambda_{25} \sinh \frac{\alpha^2}{q_1} x_5 \\ \cos q_1 x_3 - \lambda_{35} \cos q_1 x_5 & \sin q_1 x_3 - \lambda_{35} \sin q_1 x_5 & \cosh \frac{\alpha^2}{q_1} x_3 - \lambda_{35} \cosh \frac{\alpha^2}{q_1} x_5 & \sinh \frac{\alpha^2}{q_1} x_3 - \lambda_{35} \sinh \frac{\alpha^2}{q_1} x_5 \\ \cos q_1 x_4 - \lambda_{45} \cos q_1 x_5 & \sin q_1 x_4 - \lambda_{45} \sin q_1 x_5 & \cosh \frac{\alpha^2}{q_1} x_4 - \lambda_{45} \cosh \frac{\alpha^2}{q_1} x_5 & \sinh \frac{\alpha^2}{q_1} x_4 - \lambda_{45} \sinh \frac{\alpha^2}{q_1} x_5 \end{bmatrix} \quad (2.24)$$

where x_1 to x_5 are the positions of the sensors along the beam and assuming that x_5 is the location of the reference sensor, λ_{ij} is the ratio of the modal displacements $\phi(x)$ in any two points among the five measurement points corresponding to a certain order mode.

Solving the determinant of $[S]$ gives the values of q_1 and q_2 , and the axial force value can be calculated as

$$N = EI(q_1^2 - q_2^2) \quad (2.25)$$

The method was tested on a rectangular beam in laboratory, providing reasonably good results. For the method to work, it requires at least five sensors because of the five unknowns of axial force N and four springs at boundary conditions. Theoretically, the use of any single mode is sufficient; however spurious solutions may occur. Therefore, the results obtained for several modes should be compared to find the correct solution.

In the work of LI et al. (2012), the identification of boundary conditions were also investigated. The translational and rotational springs at the beam ends were identified. However, the sensors are required to be placed at the beam ends. In practice, measurements of the mode shape displacements at the ends of a beam or a structural member are sensitive to the experimental errors due to the generally small movements of the member ends.

2.1.4.2 REBECCHI et al. (2013)

Similar to the method of LI et al. (2012), REBECCHI et al. (2013) proposed an analytically-based algorithm for the axial load identification of slender prismatic beams using one vibration frequency and five amplitudes of the corresponding mode shapes, based on Euler–Bernoulli beam theory. The method can be also applied to a beam with uncertain vibration length making use of the total length distance between the five sensors.

Making use of the non-dimensional coordinate $z = x/L$ ($0 < z < 1$), Eq. (2.7) can be expressed as

$$v^{iv}(z) - \eta v''(z) - \mathcal{G}^4 v(z) = 0 \quad (2.26)$$

where the parameters η and \mathcal{G}^4 are defined as

$$\eta \equiv \frac{NL^2}{EI}, \quad \mathcal{G}^4 \equiv \frac{\rho AL^4 \omega^2}{EI} \quad (2.27a,b)$$

The solution of the axial force N can be obtained by solving the Eq. (2.28), provided that the control points are assumed at sections having non-dimensional coordinates $z_0 = 0$, $z_1 = 1/4$, $z_2 = 1/2$, $z_3 = 3/4$ and $z_4 = 1$.

$$\frac{v_1 + v_3}{v_2} = \frac{(v_0 + v_4) / (2v_2) + 1 + 2 \cos(p_1 / 4) \cosh(p_2 / 4)}{\cos(p_1 / 4) + \cosh(p_2 / 4)} \quad (2.28)$$

where v_0, v_1, v_2, v_3 and v_4 are the mode shape amplitudes at one frequency; p_1 and p_2 are

$$\begin{aligned} p_1^2 &= \frac{1}{2}(\sqrt{\eta^2 + 4\mathcal{G}^4} - \eta) \\ p_2^2 &= \frac{1}{2}(\sqrt{\eta^2 + 4\mathcal{G}^4} + \eta) \end{aligned} \quad (2.29a,b)$$

2.1.4.3 MAES et al. (2013)

Based on Timoshenko beam theory, MAES et al. (2013) developed an analytical method to estimate the axial force for a beam as a member of a truss structure by local measurements. Two different approaches were considered, i.e. the modal characteristics approach and the frequency domain approach. The identified force resulting from the two approaches depends on the selected mode or is a combination of many modes.

From the transversal force and moment equilibrium for a free beam section adopting the Timoshenko beam theory, by performing separation of variables and assuming the transverse displacement to be harmonic at frequency ω , one has

$$a_1 \frac{d^4 \hat{v}(x)}{dx^4} + a_2 \frac{d^2 \hat{v}(x)}{dx^2} + a_3 \hat{v}(x) = 0 \quad (2.30)$$

where the parameters a_1 , a_2 and a_3 are defined as

$$a_1 \equiv EI \left(1 + \frac{N}{k_y GA} \right) \quad (2.31)$$

$$a_2 \equiv -N + \frac{EI\rho\omega^2}{k_y G} + \rho I\omega^2 + \frac{N\rho I\omega^2}{k_y GA}; \quad a_3 \equiv -\rho A\omega^2 + \frac{\rho^2 I\omega^4}{k_y G} \quad (2.32a,b)$$

For a fixed value of N , Eq. (2.30) has the solution

$$\hat{v}(x) = \sum_{k=1}^4 C_k \exp(\beta_k x) \quad (2.33)$$

where C_k are real constants depending on the boundary conditions, i.e. the connections of the bar to the rest of the structure, which are assumed as unknown because no assumptions are made with respect to these connections; the total unknowns therefore equal five including the axial force and the four unknown boundary conditions (two translational and two rotational springs); β_1 to β_4 are defined as

$$\begin{aligned} \beta_1 &= \sqrt{\frac{-a_2 + \sqrt{a_2^2 - 4a_1 a_3}}{2a_1}}, & \beta_2 &= -\sqrt{\frac{-a_2 + \sqrt{a_2^2 - 4a_1 a_3}}{2a_1}} \\ \beta_3 &= \sqrt{\frac{-a_2 - \sqrt{a_2^2 - 4a_1 a_3}}{2a_1}}, & \beta_4 &= -\sqrt{\frac{-a_2 - \sqrt{a_2^2 - 4a_1 a_3}}{2a_1}} \end{aligned} \quad (2.34a,b,c,d)$$

The value of the axial force can be achieved by minimizing the function Δ_n

$$\Delta_n = \frac{\| [B] \{C\} - \{m\} \|_2}{\sqrt{\| [B] \{C\} \|_2 \|\{m\}\|_2}} \quad (2.35)$$

where $\{m\}$ contains the value of the modal displacement at each of the sensor positions at a value of a frequency, and $\|\cdot\|_2$ denotes the Euclidean vector norm. The matrix $[B]$ and vector $\{C\}$ are as follows

$$[B] = \begin{bmatrix} \exp(\beta_1 x_1) & \exp(\beta_2 x_1) & \exp(\beta_3 x_1) & \exp(\beta_4 x_1) \\ \exp(\beta_1 x_2) & \exp(\beta_2 x_2) & \exp(\beta_3 x_2) & \exp(\beta_4 x_2) \\ \vdots & \vdots & \vdots & \vdots \\ \exp(\beta_1 x_n) & \exp(\beta_2 x_n) & \exp(\beta_3 x_n) & \exp(\beta_4 x_n) \end{bmatrix} \quad (2.36)$$

$$\{C\} = [B]^\dagger \{m\} \quad (2.37)$$

where $[B]^\dagger$ is the pseudo matrix of the coefficient matrix B .

Numerical simulations were used first to illustrate the method. The influence of both modeling errors and measurement errors was investigated, which concludes that the characteristics of the bar must be accurately known. After that, laboratory experiments were performed. A bar with rectangular cross section was first tested as a single beam. Next, the bar was mounted in a laboratory space truss. The modal characteristics approach and frequency domain approach both yield close results for the single beam, but varying results for the bar as part of a space truss. In the present work, only the modal characteristics approach is applied, because the frequency domain approach requires assumption of a frequency range for averaging the axial force values, which is subjected to individual judgment.

2.1.4.4 Axial Force Identification by Analytical-based Algorithms

To evaluate the similarities of the analytical-based methods, due to the differences in the laboratory setups and specimens of the individual work, the three methods are compared using a common set of data, which is the data set of natural frequencies and mode shapes from the laboratory experiments given in LI et al. (2012). The reference forces are the experimentally measured forces by LI et al. (2012). The characteristics of the rectangular beam in laboratory tests of LI et al. (2012) can be seen in Figure 2.1.

Furthermore, numerical simulation of the rectangular beam with the same characteristics is performed with ANSYS®. The purpose is to investigate the accuracy of the methods by numerical inputs, which are exempted from experimental errors. Experimental errors can result, for example, from inappropriate experimental setup, incorrect experimental performance or inaccurate identification of the experimental parameters. Without the influence of the experimental errors, it was examined if the

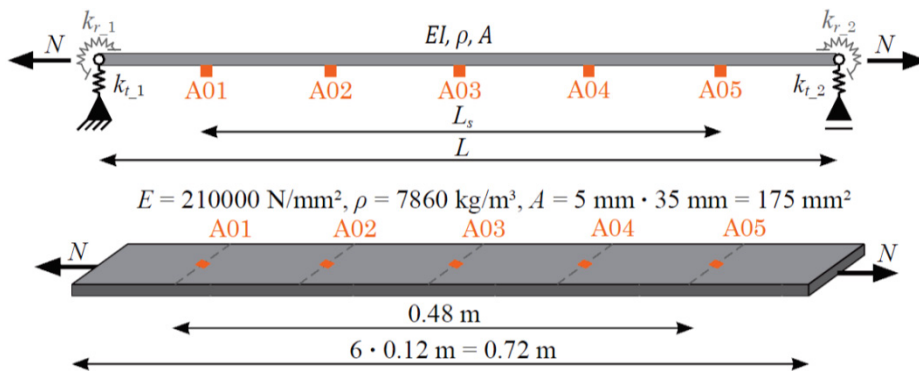


Figure 2.1 – Rectangular beam in the laboratory tests by LI et al. (2012).

analytical-based methods give precise results according to the theory for the beam with the characteristics as described in LI et al. (2012).

In Table 2.1, the results of the identified forces by the three analytical-based methods are compared, using two data sets of the frequencies and mode shapes, i.e. from experiments of LI et al. (2012) and numerical calculations. Note that only the frequencies and mode shapes at the positions of the five sensors of the first mode of a single beam were used. The results are also plotted in Figure 2.2.

For the experimental data set, the method of MAES et al. (2013) gives better results than that of the other two methods. When using the data set from numerical calculations, improvement of the identified forces by all three methods can be seen, implying that experimental errors affect the accuracy of the results. If the errors induced from experiments can be minimized, all three analytical-based methods give accurate results according to the theoretical formulation.

Only in the work of MAES et al. (2013), laboratory tests were also carried out for bars as part of a structure, i.e. as member of a space frame. The results of the identified forces in tabular form in the work of MAES et al. (2013) are represented in graphical form in Figure 2.3. For a single beam, the results of the identified forces based on the second to third modes match reasonably well to the experimental measured forces. The results based on the first mode were likely affected by the mass of the sensors, which become significant when the mass of the sensors is relatively high. When the beam is installed as a member of a space truss, however, the results of different modes vary significantly. The identified forces from the first six modes, except for the fourth and fifth modes, deviate from the experimentally measured forces with an averaged difference of approximately 5 kN to the true applied force that is increased from 0.14 to 14.13 kN.

Some remarks about the analytical-based algorithms are summarized as follows. The methods of LI et al. (2012) and REBECCHI et al. (2013) use Euler-Bernoulli beam theory, while the method of MAES et al. (2013) uses Timoshenko beam theory. All the methods require the instalment of at least five sensors on a bar. If translational or rotational degrees of freedom of the boundary conditions are known, the number of required sensors can be less than five. More than five sensors will provide additional data and may improve the results. The sensors must be equally installed [REBECCHI et al. (2013)] or can be randomly distributed [LI et al. (2012), MAES et al. (2013)]. Equal distances between sensors were usually implemented. In the work of REBECCHI et al. (2013), the influence of the location of the instrumented sections was examined. It was found that the results of the identified forces depend on the location of the installed sensors. Based on the laboratory setup in REBECCHI et al. (2013), better results were obtained when the greatest possible distance between the measurement points of a beam was adopted. For all methods, the knowledge of the length of the beam is not mandatory, but only the length between the outmost installed sensors on the member and the distances between the sensors are required.

All three methods provide more than one results of the identified force of a member for each of the mode considered. The result of a set of the identified forces based on different modes is used as a quality check, such that the result of the true force should appear most frequently and with small fluctuations between different values. In the method of MAES et al. (2013), two approaches were used, modal characteristics and frequency domain approach. In the second approach, the result of the identified force was averaged from a certain range of identified forces, although the selection of this range is not

Table 2.1 – Comparison of identified forces between different analytical-based methods using data sets from laboratory tests of LI et al. (2012) and numerical calculations.

LI et al. (2012)	Experimental f_n and ϕ_n [LI et al. (2012)]						Numerical f_n and ϕ_n (FEM)			
	LI		REBECCHI		MAES		LI & REBECCHI		MAES	
	N^a [kN]	Δ [kN]	N^a [kN]	Δ [kN]	N^a [kN]	Δ [kN]	N^a [kN]	Δ [kN]	N^a [kN]	Δ [kN]
0.00	2.78	–	2.79	–	1.40	–	0.00	–	0.01	–
5.00	7.25	2.25	7.25	2.25	6.17	1.17	4.95	–0.05	5.00	0.00
10.00	11.23	1.23	11.23	1.23	10.73	0.73	10.01	0.01	9.99	–0.01
15.00	15.82	0.82	15.82	0.82	15.45	0.45	14.92	–0.08	15.00	0.00
20.00	20.56	0.56	20.56	0.56	20.39	0.39	20.06	0.06	20.00	0.00
25.00	25.45	0.45	25.45	0.45	25.37	0.37	25.05	0.05	25.00	0.00
30.00	30.32	0.32	30.32	0.32	30.14	0.14	29.94	–0.06	30.00	0.00

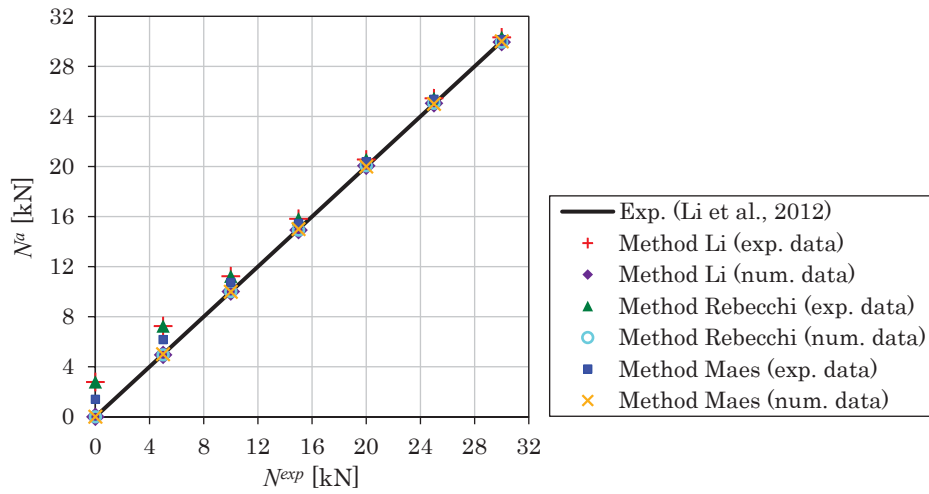


Figure 2.2 – Identified forces by different analytical-based methods using data sets from laboratory tests of LI et al. (2012) and numerical calculations.

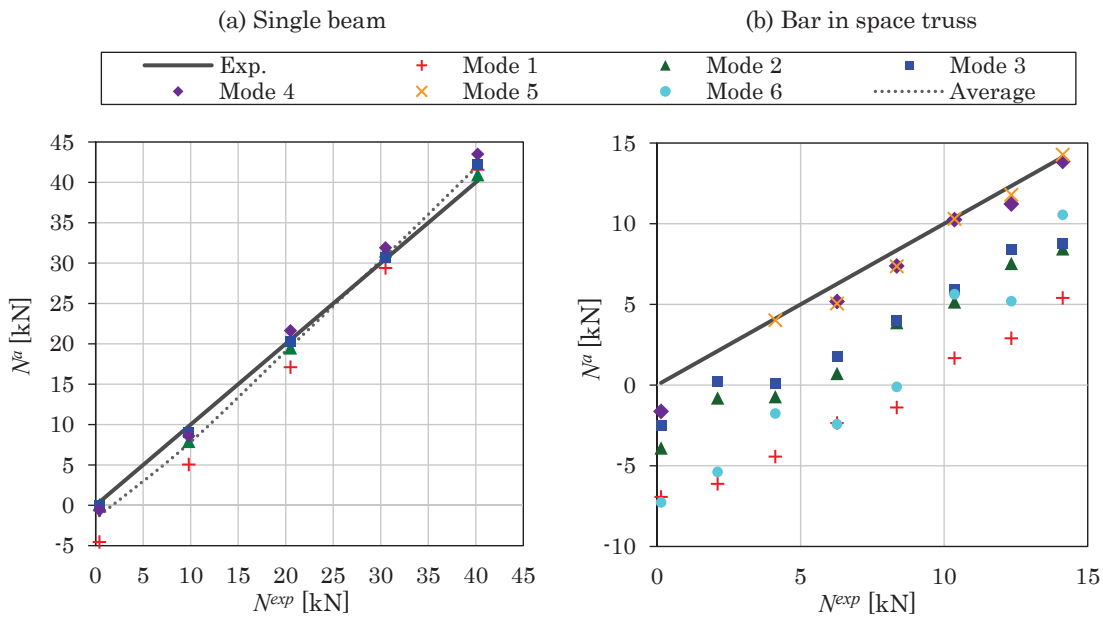


Figure 2.3 – Graphical representation of the results of the identified and measured forces from the laboratory tests given in the work of MAES et al. (2013).

generalized and depends on a problem as well as individual judgment. Some recommendations were given in the work of REBECCHI et al. (2013) about the selection of a proper flexural mode shape to increase the accuracy of the identified force. Flexural mode shapes to be selected should have maximum amplitudes in the frequency response functions (FRF) of control points in the proximity of midspan of the member. Furthermore, the amplitudes of the five mode shapes at five instrumented sensor locations should have the same sign. Mode shapes with small amplitudes that are close to a straight line should be systematically eliminated in the identification process, because the quality of the acquisition and identification of these mode shapes may be not high. It was also stated that the problem of selecting a proper mode shape may be more challenging for a beam as member of a structure, because global modes may interfere with local modes.

In the work of LI et al. (2012), laboratory tests were carried out for a single rectangular beam. In REBECCHI et al. (2013)'s work, laboratory tests were conducted for a three-span-continuous beam; the corresponding reference model to be used in the identification process was a single beam with unknown boundary conditions. In the most recent work of MAES et al. (2013), two types of laboratory experiments were performed, i.e. (i) for a single axially loaded rectangular steel bar; after that (ii), the same rectangular bar was mounted in a laboratory-scaled space truss. Therefore, only in MAES et al. (2013)'s work, the analytical-based method was examined by laboratory tests for a member belonging to a built-up structure.

Besides, the laboratory tests and identification process were only performed for tension members. Theoretically, the analytical-based methods can be applied to identify the compressive forces. However, the feasibility and accuracy of the methods for compression members, as well as for members of asymmetric profiles, require investigation.

The advantages of the analytical-based methods are the simplicity or practicability of the application and analysis procedure for a single beam, such as tie-rods in historic arches and vaults, or for a specific member in a truss structure, whose axial force is of interest. Several limitations are (i) the results of the identified force are influenced by the location of the instrumented sections; (ii) a possible range of the identified force is acquired because of possibly diverse results from different modes; and (iii) only the axial force on specific members of a structure is to be identified, i.e. members where measurement sensors are installed. The forces on other members without measurements are not known. The issue regarding the further analysis to obtain the forces in all members of a structure is not yet covered. For a complex structure, such analysis may not be straightforward. In other words, a global model of a structure is not available to predict the structural responses under alternative loading arrangements. Moreover, a practical investigation of the methods for bars as part of a structure is still limited.

2.2 Modelling and Analysis of Semi-Rigid Connections

For truss structures composed of axially loaded members connecting at joints, the common assumption of all pinned joints allows the individual members to act as bars supporting primarily an axial force. This simplifies greatly hand calculations to analyse the forces in the structure and contributed significantly to the popular use of trusses. However, joints in practice do not really permit free rotation. The analysis of a pinned-jointed truss is thus an approximation.

Beside assumption of pinned joints, rigid or semi-rigid joints are also used for layout of the structural members in the form of a truss structure, e.g. truss girders, offshore structures or space trusses. For rigid joints, bending effects are introduced in the structural members. Nevertheless, the bending effects are in many cases neglected in the analysis of trusses.

Considering the historical development from pin-jointed trussed framework to rigid-jointed frame, early in 1851 Karl Culmann (1821–1881) introduced the term *trussed framework*¹⁸ and developed a trussed framework theory, implicitly assuming frictionless pins at the joints [CULMANN (1851)]. In the same year, Johann Wilhelm Schwedler (1823–1894) described the pinned-jointed trussed framework model that, whereas the frames are thought of as rigid construction, the small resistances caused by the small elastic bending at joints are negligible when compared with the resistance of the strut, or the individual framework components can be assumed to be capable of rotation at joints [SCHWEDLER (1851)].

During the last decades of the 19th century, the contradiction of the pin-jointed trussed framework model to the as-built reality of the iron trussed framework with riveted joints led to the development of the theory of secondary stresses in truss structures [KURRER (2008)]. The truss members converging at the riveted joints are not only subjected to axial tension or compression forces, but to bending moments, too; the latter generate bending stresses. Friedrich Engesser (1848–1931) and Emil Winkler (1835–1888) grouped bending stresses together under the term *secondary stresses* [KURRER (2008)]. The quantification of secondary stresses requires rather cumbersome calculations compared to the pin-jointed trussed framework model because the structural system of the trussed framework with rigid joints is highly statically indeterminate.

In 1878, Heinrich Manderla (1853–1889) submitted a complete solution to enable the calculation of the secondary stresses in simple trussed frameworks with rigid joints on the basis of second-order theory, which appeared in the journal *Allgemeine Bauzeitung* in Vienna in 1880 [MANDERLA (1880)]. Manderla also introduced unknown displacement parameters into the mathematical elastic theory for the calculation of truss systems. In 1879, Friedrich Engesser (1848–1931) published an approximation method for determining the secondary stresses [ENGESSER (1879)], which neglected the bending stiffness of the web members and analysed the top and bottom chords as continuous beams with imaginary supports at the joints.

Winkler made his name through comprehensive contributions to the theory of secondary stresses. He introduced the difference between end tangents and member chord angles of rotation at the joint, and also considered eccentric truss joints [WINKLER (1881)]. As reported in one of the trussed frameworks analysed by Winkler, the increase in stresses compared with those calculated from the pin-jointed trussed framework model is, on average, 14 % for concentric joints and 20 % for eccentric joints (eccentricity of 50 mm).

Furthermore, Otto Mohr (1835–1918) contributed to the theory of secondary stresses by clear differentiation between the joint angles of rotation and the member angles of rotation for the ambiguous determination of the deformed state of a trussed framework with rigid joints [MOHR (1892/93)]. In 1910, Willy Gehler (1876–1953) summarized the

¹⁸ Trussed frameworks in the 1840s and early 1850s were still dominated by composite systems made of timber, cast iron and wrought iron [KURRER (2008)].

development of the theory of secondary stresses in iron truss bridges and practical calculation procedure after Mohr [GEHLER (1910)]. Based on comprehensive measurements carried out on the railway bridge across the River Elster on the Dresden–Elsterwerda line, Gehler concluded that Mohr’s procedure for determining the secondary stresses provided results that are in good compliance with the values observed in reality.

In the analysis of a realistic structure, the accuracy of the analysis can be greatly improved if the effects of joint flexibility are considered [e.g. LUI and LOPES (1997), LUONG et al. (2016), LUONG et al. (2017)]. The dynamic behaviour of a flexibly connected frame differs significantly from a rigid or pinned-jointed frame [CHAN (1994)].

During the last decades, extensive research has been conducted on the analysis and design of steel frames with semi-rigid connections. To estimate the actual behaviour of joints, numerous studies were made on semi-rigid connections, for instance state of the art reports [e.g. ZOETEMEIJER (1983), JOHNES et al. (1983), ANDERSON et al. (1987), CHEN et al. (1995)], numerical studies [e.g. CHAN (1994), GALVÃO et al. (2010), RAMIRES et al. (2012), NGUYEN and KIM (2013)] and experiments [e.g. KAWASHIMA and FUJIMOTO (1984), NADER and ASTANEH (1991), LIEW et al. (1997), DA SILVA et al. (2008)].

Modern design codes recognize the concept that the actual joints exhibit an intermediate behavior between the two extreme cases of pinned and rigid. Provisions in several design codes of practice have also been made for the design of steel frames with semi-rigid joints [e.g. DIN EN 1993-1-8: EUROCODE 3 (2005)]. EUROCODE 3 (2005) includes procedures and formulations to define both the stiffness and resistance of the semi-rigid joints from their

Table 2.2 – Brief overview of the work relating to semi-rigid connections of steel frames.

Year	Author	Connection model	Analysis type	
			Static	Dynamic
1942	JOHNSTON and MOUNT	Linear	•	
1960	BAKER	Linear	•	
1963	MONFORTON and WU	Nonlinear	•	
1970	ROMSTAD and SUBRAMANIAN	Bilinear	•	
1981	MONCARZ and GERSTLE	Nonlinear	•	
1982	STUTZKI	Linear	•	
1984	KAWASHIMA and FUJIMOTO	Linear		•
1988	SIVAKUMARAN	Bilinear	•	•
1991	NADER and ASTANEH	Linear and nonlinear	•	
1992	FARIS and KITIPORNCHAI	Nonlinear	•	
1994	CHAN	Linear	•	•
1995	BHATTI and HINGTGEN	Nonlinear	•	
1995	ZHU et al.	Nonlinear	•	•
1995	WONG et al.	Linear	•	•
1997	LUI and LOPES	Bilinear		•
1997	LIEW ET AL.	Linear and nonlinear	•	
2001	SEKULOVIC and SALATIC	Nonlinear	•	
2002	SEKULOVIC et al.	Nonlinear		•
2003	HADIANFARD and RAZANI	Linear	•	
2008	DA SILVA et al.	Nonlinear	•	
2009	TÜRKER et al.	Linear		•
2010	GALVÃO et al.	Nonlinear	•	•
2012	RAMIRES et al.	Bilinear	•	
2013	NGUYEN and KIM	Linear and nonlinear		•
2014	ATTARNEJAD and PIRMOZ	Nonlinear		•
2014	RAZAVI and ABOLMAALI	Nonlinear	•	•

geometrical and mechanical properties. An analytical procedure, called Component Method (CM), allows one to evaluate the stiffness and resistance characteristics of the joint by assembling those of all the constitutive components.

In the analysis of the semi-rigid frame structures, the connections are assumed to be able to transfer the vertical shear and have the capacity to transfer some moment. When a moment is applied to a connection, the connected members rotate relative to each other. The rotational behavior of the joint can be described by means of the moment-rotation curve. The curve defines three main properties as rotational stiffness, moment resistance and rotation capacity. Many studies are aimed at obtaining these moment-rotation curves or the associated properties to incorporate them in the frame analysis.

Considering the mathematic models for semi-rigid connections to represent moment-rotation relationship curves, the models can be grouped into two categories, i.e. linear and nonlinear semi-rigid connection models (see Table 2.2). Linear models are convenient in formulation and implementation assuming that the stiffness of connections is constant. In the nonlinear semi-rigid connection models, the stiffness of connections is varied corresponding to different loading magnitudes [GALVÃO et al. (2010)].

According to NGUYEN and KIM (2013), numerical results show that the use of different semi-rigid connection models does not substantially affect the behaviour of frames that are subjected to small connection moments and small deflection range. SEKULOVIC et al. (2002) discussed that the linear model has been widely used for its simplicity and is good in cases when the connection moment is small. In addition, a nonlinear model is necessary only when the connection rigidity may rapidly decrease compared with its initial value. ZHU et al. (1995) stated that the effect of the nonlinear behaviour of structural joints on the structural response is more apparent under cyclic and dynamic loading conditions. In the selection of a connection model, the accuracy as well as simplicity and versatility of the chosen model are among guiding parameters.

To incorporate the flexibility of the nodal connections in the analysis of the structures, the stiffness of rotational springs may be indicated by using modulus of elasticity, moment of inertia and length of a related bar. A stiffness matrix in local coordinates of a bar having semi-rigid end constraints is given in TÜRKER et al. (2009). For practical purposes, constraint parameters in the form of stiffness indexes or percentages of semi-rigid connection have been introduced to assess the degree of joint flexibility [e.g. KAWASHIMA and FUJIMOTO (1984), YU and SHANMUGAM (1986), SEKULOVIC and SALATIC (2001), TÜRKER et al. (2009)]. The stiffness index s_{kri} and fixity factor γ_{kri} representing the semi-rigid connection are expressed as

$$s_{kri} = \frac{k_{ri}L}{EI} \quad (2.38)$$

$$\gamma_{kri} = \frac{k_{ri}L}{3EI + k_{ri}L} \quad (2.39)$$

where k_{ri} is the rotational spring stiffness at i end of a member, EI is the flexural stiffness and L is the length of the member. The stiffness index takes the value of zero for pinned condition and tends to infinity for rigid connection, while the fixity factor takes values from zero to one corresponding to pinned to rigid condition.

2.3 Finite Element Model Updating for Civil Engineering Structures

Finite element model updating is proved to be a powerful tool to assist engineers in the structural assessment process. It helps to refine selected uncertain input parameters and validate the assumptions of the numerical model of various types of structures. Since the 1990s, finite element model updating emerged as important in the fields of mechanical and civil engineering. Contrast to the use of model updating for system identification in control engineering, model updating in civil engineering is performed *off-line* with the aim to generate improved numerical models to predict the responses under alternative loading arrangements or modified structural configurations. Therefore, as a demand upon model updating in civil engineering, the updated model must not simply reproduce the test results but also be physically meaningful.

In structural dynamics, model updating methodologies can be categorized basically into the direct methods and the iterative approaches [BAKIR et al. (2008)]. The direct methods update directly the elements of the stiffness and mass matrices of the finite element model in a one-step procedure without regard to changes in physical parameters. The updated system matrices represent the measured parameters, but unfortunately have little physical meaning and cannot be related to physical changes of the original finite element model. Some direct methods can be found for instance in FRISWELL and MOTTERSHEAD (1995). Wavelet-based direct algorithms were proposed by ZABEL (2003).

The iterative methods, on the other hand, update physical parameters of the finite element model until a sufficient degree of accuracy with respect to the measured data is achieved. Parametric changes are made to the model and the updated mass and stiffness matrices have physical meaning. In iterative methods, typically an objective function is improved by a step-by-step approach. A set of parameters are updated to minimize the objective function that quantifies the difference between measured and theoretical data. The experimentally derived and numerically calculated features in vibration-based model updating are typically natural frequencies and mode shapes. The uncertain parameters that need to be updated are such as material or geometrical properties, loading, boundary conditions, etc.

There are different approaches that have been proposed in the literature for iterative model updating. The approaches can be distinguished between local and global optimization methods. While local methods converge to the minimum that is closest to the initial parameter set, global methods try to find the global minimum.

Generally, three groups of standard optimization methods are (i) gradient-based methods, e.g. quasi-Newton, augmented Lagrangian, sequential quadratic programming, etc. [TEUGHELS (2003), CHEW et al. (2016)]; (ii) response surface methods [BATILL et al. (1999), GANGULI (2002), REN and CHEN (2010)]; and (iii) nature-inspired algorithms, e.g., genetic algorithms, evolutionary strategies, particle swarm optimization [GOLDBERG (1989), ZABEL and BREHM (2009), YU and GEN (2010), MARWALA (2010), YANG (2014)].

Conventional gradient-based methods have a satisfactory convergence rate, but they may get stuck into local minimum depending on the starting point. BAHRA and GREENING (2006) discussed the sensitivity-based updating of loading in frameworks using the Newton method. This method makes use of the local curvature of the original function, based on which an approximate quadratic model function is calculated in each point of the iterative process and minimized to obtain the consecutive point. The iterative process

ends when the minimum is reached. LINK and WEILAND (2009) stated that sensitivity-based approaches are widely used techniques for parameter estimation. BROWNJOHN et al. (2001) described the sensitivity-based finite element model updating method for structural assessment of bridges. The shortcoming of the sensitivity-based approaches is that its success strictly depends on the assumptions of the starting values of the target parameters to be close to the optimum; that unfortunately cannot be ensured in real-life applications.

The global search methods, such as genetic algorithms and particle swarm optimization, are used in model updating with highly flexible applicability [ZABEL and BREHM (2009)]. Examples of applications are model updating of railway bridges [CANTIENI et al. (2008), ZABEL and BREHM (2008), ZABEL and BREHM (2009), RIBEIRO et al. (2012)], or inverse identification of axial force in tie-rods [GENTILINI et al. (2013)]. The advantages of the global search methods are that they are in general robust, the choice of the starting position has little influence on the final results, as well as they present a better global behaviour. The general drawback of the global search methods is high computational costs since they are based on probabilistic searching without the use of gradient information. For a respective problem, it is essential to choose an appropriate objective function and optimization algorithm.

2.3.1 Background of Selected Optimization Techniques

According to NOCEDAL and WRIGHT (1999), a good algorithm should possess the following properties: (i) robustness – a good performance on a wide variety of problems in their class; (ii) efficiency – requirement of not too much computational costs or storage; and (iii) accuracy – ability to identify a solution with precision, without being overly sensitive to errors in the data or arithmetic rounding errors of computer systems. These goals may often conflict. In numerical optimization, tradeoffs between different objectives are considered central issues, for instance between convergence rate and storage requirements, or between robustness and speed, and so on.

2.3.1.1 Gradient-based Methods

The gradient-based optimization algorithms were introduced by SCHITTKOWSKI (1985). They mainly use quasi-Newton methods, such as nonlinear programming using a quadratic or linear least-square algorithm, e.g. Nonlinear Programming by Quadratic Lagrangian (NLPQL). Starting from a predefined initial parameter set, the gradient-based methods employ the local derivatives of the objective function to find next local optimum. A stepwise convergence to an optimum is performed by line search algorithms using gradients. Gradient-based optimization is known for fast convergence, but has the problem of getting stuck in local optima. Therefore, gradient-based methods are recommended to solve smooth nonlinear optimization problems with preferably small number of the design variables.

2.3.1.2 Response Surface Methods

Also known for low computational costs, the response surface methods replace the model responses by mathematical surrogate functions or approximation model instead of time consuming solver calls. The analyses are performed in two steps. First, a response surface is generated on a suitable set of discrete support points using appropriate

approximate functions. Then the optimization itself is carried out on the response surface, for which gradient-based and/or evolutionary algorithms are applied. To approximate the response surface, different methods can be used, such as least square or moving least square approximations. The accuracy of the methods depends on whether the resulting response surface is well qualified to represent global trends of the optimization problem. Adaptive response surface methods contain an improvement with regard to the certainty that the trends are sufficiently well represented, thus they are used to enhance approximation quality around the optimum. Although the response surface methods can offer extreme fast convergence, they have limitations to reasonable smooth problems, i.e. low dimensional single-objective optimization problems, and the continuous variables should not exceed ten variables [ZABEL and BREHM (2009)].

2.3.1.3 Nature-inspired Algorithms

Nature-inspired algorithms are modern-type methods, also referred to as artificial or computational intelligence techniques. They have good universality and are less dependence on structural shape. Nature-inspired algorithms initiate natural processes like biological evolution, such as adaption, selection and variation, i.e. evolutionary algorithms, or swarm intelligence, i.e. particle swarm optimization. They are area of research that are of increasing interest and have multi-disciplinary applications.

Genetic algorithms belong to evolutionary algorithms, a class of stochastic search methods. Based on Darwin's principle *survival of the fittest*, a population of artificial individuals searches design space of possible solutions for better approximation. Evolutionary algorithms are population-based¹⁹, fitness-oriented²⁰, and variation-driven²¹ [YU and GEN (2010)]. Classical evolutionary algorithms include evolution strategies [RECHENBERG (1973)], evolutionary programming [FOGEL et al. (1966)] and genetic algorithms [HOLLAND (1975)]. Several recognized advantages of evolutionary algorithms are the capacity to handle large number of parameters and find near global minimum. In addition, they can be suitable for optimization problems with a high number of variables and/or constraints.

Particle swarm optimization imitates social behavior of a swarm, moving into directions of previous optimal positions [KENNEDY and EBERHART (1995)]. Swarm intelligence influences by personal and global behavior. Three important parameters influence speed and spread of the swarm, i.e. separation, alignment, and cohesion²². In predefined global search strategy, swarm movement is intensive at beginning and damped throughout the optimization process. The method is less efficient if discrete design variables and many constraint conditions exist. With continuous variables, the particle swarm optimization converges generally close to global optimum. The efficiency of algorithm is improved by qualified start population.

¹⁹ Evolutionary algorithms process a whole group of candidate solutions, called a *population*, simultaneously.

²⁰ Every solution in a population is called an *individual*, which has its *code* – gene representation, and its *fitness value* – performance evaluation. Fitter individuals are preferred by evolutionary algorithms.

²¹ Individuals undergo a number of variation operations to mimic genetic gene changes. Evolutionary algorithms use recombination to mix information of more candidate solutions into a new one.

²² *Separation* refers the behaviour of avoiding the crowded local flockmates; *alignment* is the behaviour of moving towards the average direction of local flockmates; *cohesion* is the behaviour of moving towards the average position of local flockmates.

A review by CHAUHAN and SAINI (2014) concluded that artificial intelligence techniques are promising techniques. FADAEE and RADZI (2012) reviewed six different optimization techniques and identified genetic algorithms and particle swarm optimization as most useful and promising multi-objective optimization methods. Genetic algorithms excel in solving global, centrally managed optimization tasks. Swarm intelligence, on the other hand, is designed to solve problems in a decentralized, distributed way.

Recent research also gives attentions to hybrid optimization methods, in which individual nature-inspired approaches are used as parts of hybrid intelligent systems to overcome the limitations of a single algorithm. Examples are combination of particle swarm optimization with simulated annealing [WANG et al. (2007)], or use of domain-specific operators in genetic algorithms [GIL and HAN (2011)], and so on.

2.3.1.4 Remarks about Selected Optimization Techniques

Considering the application of the optimization techniques in the present work, the advantages and disadvantages of the aforementioned optimization algorithms are summarized as follows.

Gradient-based optimization methods offer low computational costs. However, for target functions with multiple local minima, it is difficult to find the global optimum. The number of the design variables is preferably small. Besides, the success of the gradient-based optimization is decisively influenced by the choice of the starting point.

The response surface methods can also offer fast convergence. In addition, they have the capability of finding global optimum. However, with a large parameter number, for instance of approximately more than twenty, problems arise in the formation of the approximation function. With a higher number of parameters, the response surface methods work inefficiently.

Genetic algorithms and particle swarm optimization are both capable of handling large numbers of parameters and find near global optimum. Furthermore, the success of these techniques does not depend on the initial starting point. The drawback is high computational costs.

2.3.2 Background of Experimental Modal Identification

Since the rapid development of digital computers in the 1960s, experimental modal analysis has become an extremely active research topic [MAIA and SILVA (1997), EWINS (2000)]. Historically, the four main groups of communities have been using vibration testing and analysis are mechanical engineering, oil industry, aerospace engineering and civil engineering. The different disciplines have benefited from each other from their individual progress.

2.3.2.1 Historical Development of Vibration Analysis

According to BRAUN et al. (2002), early studies related to vibrations already dated back to ancient times. Progress was made by Galileo in 1581, who observed the period of a simple pendulum to be nearly independent of the amplitude of vibration. A century later, Newton has put a firm basis for the basic principles of dynamics. Further development of the science of mechanics was accounted by Euler (1707–1783). By the

year 1788, Lagrange has developed most of the analytical tools used in vibration studies. Rayleigh has written a first book that is devoted entirely to the theory of vibration *Theory of Sound* (1887), which together with textbooks of Timoshenko (1928) and Den Hartog (1934) formulated the important principles of the classical vibration theory.

Since the beginning of the industrial revolution, vibration problems have faced engineers to constant challenges, for instance interaction of steam-driven trains with relatively flexible metal bridges caused vibration problem and fatigue. At the beginning of the 20th century, vibration problem was found for example from rotor dynamics of turbine generator sets, when central electric power stations were installed for cities. Moreover, development of airplanes and helicopters has set new vibrational challenges. In 1940, the collapse of the Tacoma Narrows suspension bridge has intrigued engineers, physicists and mathematicians in the past decades to find the explanation for the vibration-related failure.

In the latter half of the 20th century, technology advancement regarding improved sensors and actuators as well as development of digital computer has facilitated engineering applications and solution for large vibration problems. In 1965, the proposal of the Fast Fourier Transform (FFT) by COOLEY and TUCKEY (1965) led to a rapid advance of commercialized electronic hardware analyzers for more precise measurements. Together with powerful computer software to perform finite element analysis, it enabled dynamic analysis of complicated real-scale structures. Nowadays, the field related to vibration is incredibly broad with multi-disciplinary applications.

2.3.2.2 Overview of Modal Identification Methods

The available experimental modal analysis techniques can be classified according to the function of the excitation source as (i) *input-output* or *experimental modal analysis* (EMA); (ii) *output-only* or *operational modal analysis* (OMA); and (iii) *combined experimental-operational modal analysis*. An overview of the most techniques can be found for instance in CUNHA et al. (2006), and more recently in REYNDERS (2012).

EMA are based on the estimation of a set of FRF relating to an applied force. In EMA, the structure can be excited by one or several dynamic forces. The excited dynamic forces as well as the response of the structure to those forces are recorded. The modal parameters are extracted in the frequency range of interest. EMA has been well established and has vast applications, especially in mechanical engineering. For civil engineering (CE), however, EMA techniques are not suitable for large structures, such as bridges, towers, etc., where applied excitation forces might not have enough impact so that the contribution of the measured excitation is insignificant to the total structural response. In addition, the condition of the in-situ test for large structures is rather operational than laboratory testing, in which the effect of ambient excitation or operational loading, such as wind or traffic, in many cases might not be neglected.

OMA are developed to overcome the limitation of EMA, based on the premise that wind, traffic or human activities can adequately excite the structures. In OMA, modal parameters are extracted from the dynamic response to (partly) unmeasured operational forces. Nevertheless, OMA is also subjected to some shortcomings. The first shortcoming concerns an incomplete modal model from output-only measurement, because the mode shapes cannot be scaled in an absolute sense, e.g., to unit modal mass. A possible solution is to add or remove a significant amount of mass to or from the structure and perform

a second measurement; however, this is not always practical. Secondly, considering ambient excitation, the result may be confined to a narrow frequency band and thus the quality of the extracted modes might be limited to only a certain number of modes. Furthermore, most experimental and operational modal analysis algorithms only yield point estimates for the modal parameters, meaning the information on their uncertainty is not known when estimation is made from a single test.

During the last years, there has been increasing interest to combine modal testing techniques, also called hybrid vibration testing or Operational Modal Analysis with eXogenous inputs (OMAX), where artificial force is used, and operational forces are included not as noise but as useful excitation in the identified system model. The amplitude of the artificial forces can be equal to, or lower than that of the operational forces. For modal testing of large structures, this aspect is crucial that allows the use of small and practical actuators which is easier to transport. More details are given in REYNDERS (2012).

The mathematical methods for processing the modal analysis data can be classified according to the domain in which they are performed, i.e. the frequency or the time domain. Depending on the simplicity and the feasibility of the application in the field, the methods can be used in separate phases of the data processing. The pre-processing phase concerns the verification of the acquired data by means of checking the frequency content. For this stage, the most used method in civil engineering is the Peak Picking method.

The post-process phase is frequently carried out when more reliable results are required and more time can be devoted to the task. The most used methods in civil engineering are the Frequency Domain Decomposition, the Enhanced Frequency Domain Decomposition and the Stochastic Subspace Identification. Next, a brief description of several common techniques is given.

2.3.2.3 Peak Picking

The Peak Picking (PP) method, a frequency domain technique, is the simpler and more practical method for modal identification. In spite of some drawbacks, the PP method provides fast results and is useful as a pre-process tool when dynamic monitoring is performed. Systematized by FEBER (1993), this method determines the natural frequencies of the structures as the peaks of the Average Normalized Power Spectral Densities (ANPSD). The damping factors are determined using the Half Power Bandwidth Method (HPBM), and the components of the mode shapes are determined by the values of the transfer functions at the natural frequencies, see for example PEETERS and DE ROECK (1999). The main limitations of the PP method are that picking the peaks is often a subjective task as well as identifying close frequencies is difficult. In addition, operational deflection shapes are obtained instead of mode shapes and the damping estimates are unreliable.

2.3.2.4 Frequency Domain Decomposition

The Frequency Domain Decomposition (FDD), a frequency domain technique, performs an approximate decomposition of the system response into a set of independent single degree of freedom (SDOF) systems, one for each mode. Each of the estimated spectral density matrices is decomposed using the Singular Value Decomposition (SVD)

algorithm, in which the singular values are the estimates of the auto spectral density of the SDOF systems, and the singular vectors are the estimates of the mode shapes [BRINCKER et al. (2000)]. The technique is non-parametric and the estimated modes are purely the result of signal processing. BRINCKER et al. (2000) improved the FDD method by presenting the Enhanced Frequency Domain Decomposition method (EFDD). It is closely related with the FDD method but include additional procedures to evaluate the damping and to get enhanced estimates of the frequencies and mode shapes of a system.

2.3.2.5 Stochastic Subspace Identification

The Stochastic Subspace Identification (SSI), a time domain technique, has been proved to be powerful, robust and one of the most accurate techniques. It fits a parametric model directly to the raw-times series data from the sensors. The SSI method was originally proposed by VAN OVERSCHEE and DE MOOR (1991) and modified by PEETERS and DE ROECK (1999). Generally, it is investigated for a set of parameters to minimize the deviation between the system's measured and predicted responses. For the parametric model estimation, a reasonable number of parameters should be chosen. The modal identification is performed by constructing stabilization diagrams and selecting the stable poles in a certain system order.

The novel approach of the reference-based stochastic subspace identification (SSI/ref) introduced by PEETERS and DE ROECK (1999) reformulated the classical algorithm using the covariances between the outputs and only a limited set of reference outputs instead of the covariances between all outputs. Since the dimension of the problem is reduced, it has beneficial effects on the computational costs. The implementations of the SSI/ref as SSI-cov/ref, i.e. covariance-driven, and SSI-data/ref, i.e. data-driven, give similar and reliable accuracy. The SSI-data/ref presents some advantages over the SSI-cov/ref, but it is considered to be slower [PEETERS (2000)] and its application is more demanding than the SSI-cov/ref.

2.3.3 Model Updating Framework

A framework for model updating, as explained by BREHM (2011), consists of the following distinct but interconnected tasks: sensitivity analysis, pre-test analysis, execution of experiments, feature extraction, and model updating. In each step, there always exist several sources of uncertainties or errors. ZABEL and BREHM (2009) classified three distinguished groups of errors that affect the quality of the model updating process. They are errors associated with the numerical model, errors associated with the measured data, and errors associated with the applied model updating method.

Considering the numerical model of a structure, it is often described by finite element methods, in which the chosen discretisation may be inadequate or often the regions of joint connections and boundary conditions may be poorly presented. Regarding the measured data, random and systematic errors may occur. Insufficient mounting of the sensors to the structure can also lead to unwanted effects. In this case, incomplete description of the system behaviour by the measured data may occur due to the difference between the limited number of measurement points and the usually larger number of degrees of freedom of the model. More details can be found in MOTTERSHEAD and FRISWELL (1993), FRISWELL and MOTTERSHEAD (1995), and NATKE (1998).

With respect to the model updating method, ZABEL and BREHM (2009) discussed that the performance and results of model updating depend on the chosen objective function, the choice of parameters to be modified, as well as the optimization technique and respective parameters controlling the optimization algorithm.

To select the parameters to be updated, parameters that are uncertain should be updated. Moreover, the updating parameters should influence the output data or the objective function considerably. Updating parameters which have similar effect on the model output may make the parameter estimation problem ill-conditioned. Example is updating the two unknown boundary conditions of a single beam that are represented by rotational spring stiffness. Because the identification problem is symmetric, the output of the numerical frequencies of the beam are identical by exchanging the boundary conditions. In this case, different values of the design parameters can lead to the same output value.

The issue of unique estimation of parameters was discussed in FRISWELL and MOTTERSHEAD (1995). This situation arises because the measured data in general is not sufficient in quantity to enable unique parameters to be estimated. Mode shape data should be used, although this data is generally less accurate than the natural frequencies. As an alternative way to increase the amount of data available, one can test the structure in slightly different configurations or with mass or springs added to the structure [NALITOLELA et al. (1990), NALITOLELA et al. (1992)]. This technique is sometimes called *perturbed boundary condition testing* [LAMMENS et al. (1993)]. The structure and the theoretical model are perturbed; the measured eigenvalues before and after each mass or stiffness addition are used to update the parameters. The method requires that the structural perturbation is modelled accurately.

Using added mass, GENTILINI et al. (2013) has studied the vibration of a modified tie-rod for the inverse identification of the axial force and the rotational spring stiffnesses of both end constraints. The use of additional masses has been also successfully adopted to identify structural parameters of beams such as mass density and flexural rigidity [SKRINAR (2002), TURKER (2008)].

2.4 Proposed Methodology

The proposed methodology aims to identify the axial forces and corresponding stresses of truss structures, as well as provide information about the joint flexibility of semi-rigid joints. The method should have practical testing procedure on in-situ trusses and be not particularly sensitive to assumptions about the initial values of the design parameters.

The proposed approach combines the finite element model updating and analytical-based methods. In addition, the global analysis of a truss structure is combined with the local analysis of its members. The vibration-based finite element model updating using global search optimization techniques is adopted. As reviewed, global optimization-based approaches do not rely significantly on the initial parameter set and have been employed for solving complex optimization problems [MUSILEK et al. (2015)].

Particularly, the following optimization algorithms are examined in the present work: (i) an adaptive response surface method (ARSM), (ii) a genetic algorithm (GA) and (iii) a particle swarm optimization (PSO). The feasibility and suitability of the methods with respect to the inverse identification of the axial forces and estimation of joint stiffness of truss structures are investigated.

Beside the choice of an optimization algorithm, to ensure a successful and physically meaning updated model, focus was placed on the aspects of selecting the updating parameters as well as developing a meaningful objective function. This is assisted by the performance of a sensitivity analysis prior to an optimization process.

Regarding a modelling strategy to properly represent the semi-rigid joints, the following assumptions are considered: (i) the material is assumed to remain elastic throughout the analysis; (ii) small strains, displacements and rotations are considered, as the connection moments of truss structures are normally small; (iii) slip and friction effects are not included. A finite element model is developed using linear elastic rotational spring elements at the end constraints and joints. The numerical model considers the dynamical response of semi-rigid connections and also includes the geometrical nonlinearity due to stress stiffening effects.

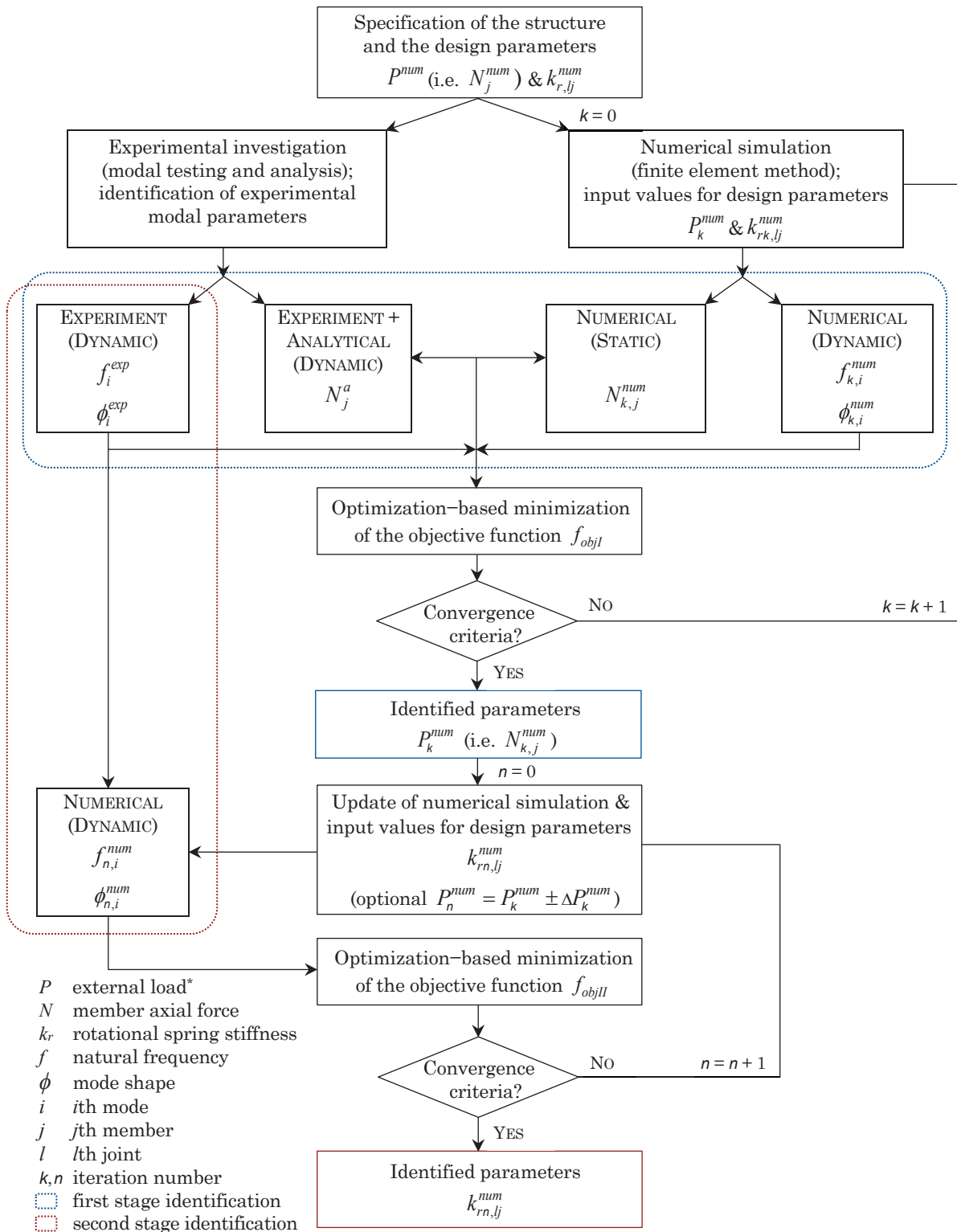
2.4.1 Sensitivity Analysis

Using an initial model, a sensitivity analysis is performed to examine the influence of changes in preselected uncertain model input parameters on changes in the selected assortment of possible features. The selection of uncertain model input parameters is greatly important, as only sensitive model input parameters can be identified with sufficient accuracy. A global sensitivity analysis can be carried out, which is a correlation analysis using the Pearson correlation coefficient or Spearman correlation coefficient. In the present work, a global sensitivity analysis, based on a stochastic sampling strategy and Spearman correlation coefficient, is performed prior to the optimization process to investigate the effects of the input parameters and identify the important uncertain parameters, i.e. design parameters, that most influence the objective function to be used in the model updating process.

2.4.2 Proposed Two-Stage Model Updating Procedure

Based on the results of the sensitivity analysis, a two-stage optimization procedure is proposed to determine the axial forces and estimate the joint stiffness of truss structures. In the first stage of the optimization process, the axial forces are to be identified. The calibration of the finite element model of the truss with the unknowns of the load and the rotational stiffness of the joints, whose initial values can be chosen randomly based on engineering-judgement, is carried out based on experimentally identified global natural frequencies and mode shapes. Furthermore, the axial forces in selected individual members of the truss are used as additional information. The analytical-based algorithm developed by MAES et al. (2013) is applied, in which the axial forces in selected members are estimated from the natural frequencies and five amplitudes of the corresponding mode shapes of a local member.

From the identified forces in the first stage, the joint stiffnesses are estimated to a higher degree of accuracy in the second stage of optimization procedure. The validation criterion is the modal parameters of the global natural frequencies and mode shapes. The updating parameters are the joint stiffnesses and optionally the forces, but the variation of the forces should be kept small so that the axial force effects do not get dominant over the influences of the joint flexibility. The results of the second stage optimization are the rotational spring stiffnesses of joints indicating the level of semi-rigid connections. A schematic representation of the proposed methodology is shown in Figure 2.4.



*The load P is referred to the unknown external load(s) and used as the updating parameter in the proposed methodology. The member axial force N is calculated by static analysis and static equilibrium of the numerical model of the truss with the applied load P .

Figure 2.4 – Schematic diagram of the proposed methodology to identify the axial forces and estimate the joint stiffnesses of truss structures.

2.4.3 Definition of Objective Functions

For the first stage of the optimization, an objective function which includes terms related to the residuals of the frequencies and mode shapes as well as additional information of the member axial forces in selected members is minimized. Thus, the objective function f_{objI} in the first stage to identify the axial forces is defined as

$$f_{objI} = a \sum_{i=1}^{nmodesf} \frac{|f_i^{num} - f_i^{exp}|}{f_i^{exp}} + b \sum_{i=1}^{nmodes\phi} |\text{MAC}(\phi_i^{exp}, \phi_i^{num}) - 1| + c \sum_{j=1}^{nbars} \frac{|N_j^{num} - N_j^a|}{N_j^{ref}} \quad (2.40)$$

where a , b and c are weighting factors for the terms of the objective function, assuming in general cases to be equal to one; f_i^{exp} , f_i^{num} , ϕ_i^{exp} and ϕ_i^{num} are the experimentally identified and numerically calculated natural frequencies and mode shapes of mode i ; $nmodesf$ and $nmodes\phi$ are the total number of modes and $nbars$ is the total number of selected members. N_j^{num} is the numerically calculated axial force by static load equilibrium in selected member j ; N_j^a is the analytically-based identified axial force based on MAES et al. (2013); N_j^{ref} is the axial force equal to $A_j \sigma_j^{ref}$, where A_j is the cross-sectional area and σ_j^{ref} is the reference stress in the individual member j , assuming at an intermediate level of 50 N/mm² to avoid a too low or too high value. N_j^{ref} is used as the divisor instead of N_j^a , because N_j^a may be less accurate for low values of axial stresses, as well as it may differ itself significantly between a low and high value of the force.

In the second stage of optimization, the objective function f_{objII} to identify the joint stiffnesses is defined as

$$f_{objII} = a \sum_{i=1}^{nmodesf} \frac{|f_i^{num} - f_i^{exp}|}{f_i^{exp}} + b \sum_{i=1}^{nmodes\phi} |\text{MAC}(\phi_i^{exp}, \phi_i^{num}) - 1| \quad (2.41)$$

which contains the residuals of the natural frequencies and modal assurance criterion (MAC) indices or mode shapes.

2.4.4 Mode Pairing Criteria

The mode pairing technique establishes the correspondence between the most likely numerical modes with the experimentally identified modes. To assure a correct sensitivity analysis and a well-shaped objective function in the optimization process, correct assignment of the modes plays a vital role.

Based on the results of the numerical study, truss structures can possess closely-spaced modes as well as similar modes of vibration. Therefore, the energy-based modal assurance criterion (EMAC) proposed by BREHM et al. (2010) is applied for the mode pairing criteria, in addition to the traditional MAC. The EMAC allows classification of the mode shapes taking into account the relative Modal Strain Energy (MSE) of a defined cluster of degrees of freedom. Therefore, information extracted from the measurements related to specific modes can be utilized in a more beneficial way. The modal assurance criteria (MAC) is given by

$$\text{MAC}_{ij} = \frac{(\{\hat{\Phi}\}_i^T \{\hat{\Phi}\}_j)^2}{(\{\hat{\Phi}\}_i^T \{\hat{\Phi}\}_i)(\{\hat{\Phi}\}_j^T \{\hat{\Phi}\}_j)} \quad (2.42)$$

where $\hat{\Phi}_j$ is the numerically derived vector containing the coordinates from numerical mode j th corresponding to the experimental degrees of freedom and $\hat{\Phi}_i$ is the experimentally obtained vector containing the experimental information of mode i th.

The MSE, the relative MSE for selected clusters of degrees of freedom and the EMAC [BREHM et al. (2010)] are calculated as

$$\text{MSE}_j = \frac{1}{2} \sum_{k=1}^n \sum_{l=1}^n \{\hat{\Phi}\}_{jk}^T [K]_{kl} \{\hat{\Phi}\}_{jl} = \frac{1}{2} \{\hat{\Phi}\}_j^T [K] \{\hat{\Phi}\}_j = \frac{1}{2} \omega_j^2 \quad (2.43)$$

$$\Pi_{jk} = \frac{\text{MSE}_{jk}}{\text{MSE}_j} = \frac{\sum_{l=1}^n \{\hat{\Phi}\}_{jk}^T [K]_{kl} \{\hat{\Phi}\}_{jl}}{\{\hat{\Phi}\}_j^T [K] \{\hat{\Phi}\}_j} \quad (2.44)$$

$$\text{EMAC}_{ijk} = \Pi_{jk} \text{MAC}_{ij} \quad (2.45)$$

where MSE_j is the total MSE for mode j , Π is the relative MSE for mode j with respect to cluster k . Concerning the information to be extracted from the finite element model, they are the stiffness matrix of the whole structure and/or the stiffness matrix of selected degrees of freedom that belong to a defined cluster. A defined cluster should reflect the information extracted from the distribution of measurement points as well as their measurement directions related to a specific mode, for instance a cluster can be defined to include only the degrees of freedom of in-plane vibration, if the measurements only allow the in-plane degrees of freedom to be extracted. Moreover, the information of the numerically computed modal parameters of the structure, i.e. natural frequencies and mode shape coordinates, is required, which can be extracted from the finite element programme after the modal analysis of the numerical model is performed.

The relative MSE is in the range between zero and one. The relative MSE is connected to the MAC by multiplication. Therefore, the range of the EMAC is bounded between zero and one. The value of zero represents no consistent correspondence, whereas a value of one indicates a highly consistent correspondence. The assignment of modes is given similarly to the MAC, where the numerical mode with the largest value is assigned to the respective experimental mode.

2.4.5 Optimization Process

A flow chart of the optimization process is shown in Figure 2.5. A numerical model based on the finite element method is developed. Static analysis is performed to obtain the stress distribution in the truss members. Dynamic analysis is performed for the structure in its prestress state, and numerical natural frequencies and mode shapes are calculated for each loading condition. The results of the modal parameters are extracted. In addition, the stiffness matrix of the truss structure is exported to calculate the relative MSE.

Based on the experimental modal information, the mode pairing is carried out with the calculation of the MAC and EMAC matrices. The objective function, as defined in Eq. (2.40) or Eq. (2.41) depending on whether the optimization is in the first or second stage, is calculated. Finally, the application of an optimization technique is performed. The estimation of a new set of the parameters is made, which are bounded between the lower and upper limits, for the minimization of the objective function residuals. The implementation and execution of the proposed methodology is carried out using three software packages, e.g. ANSYS® for the finite element method, Matlab® regarding the computation process and OptiSLang® concerning the iteration process using the optimization techniques. The iterative process is continued until the convergence criterion is satisfied or when the generations reach the maximum value.

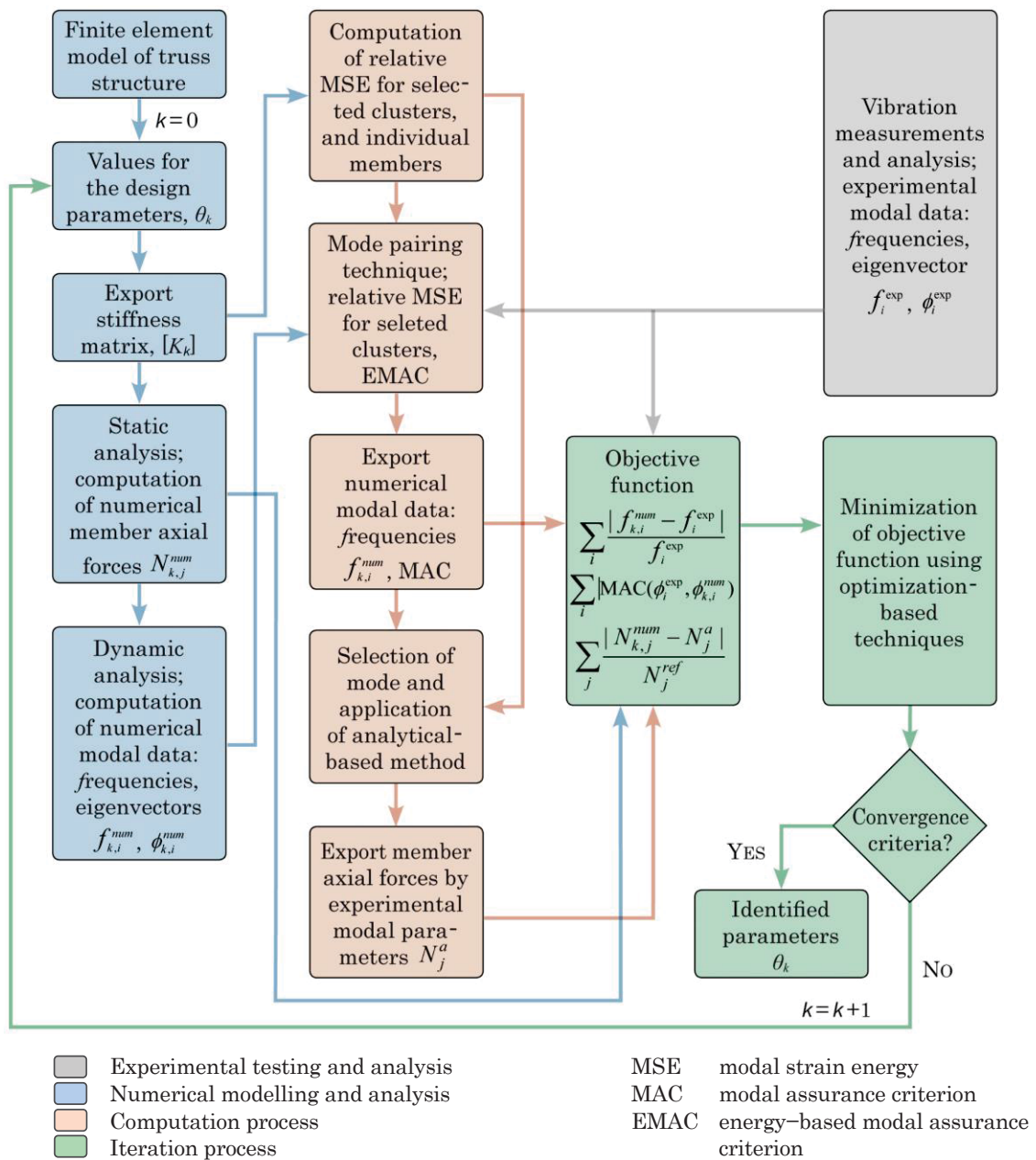


Figure 2.5 – Flowchart of the optimization process of the proposed methodology.

2.5 Discussions

In the literature, although many methods have been presented for the axial force identification based on vibration measurements, most of the methods considered only single structural members. Moreover, few of them concern the estimation of the rigidity of the structural joints and end constraints.

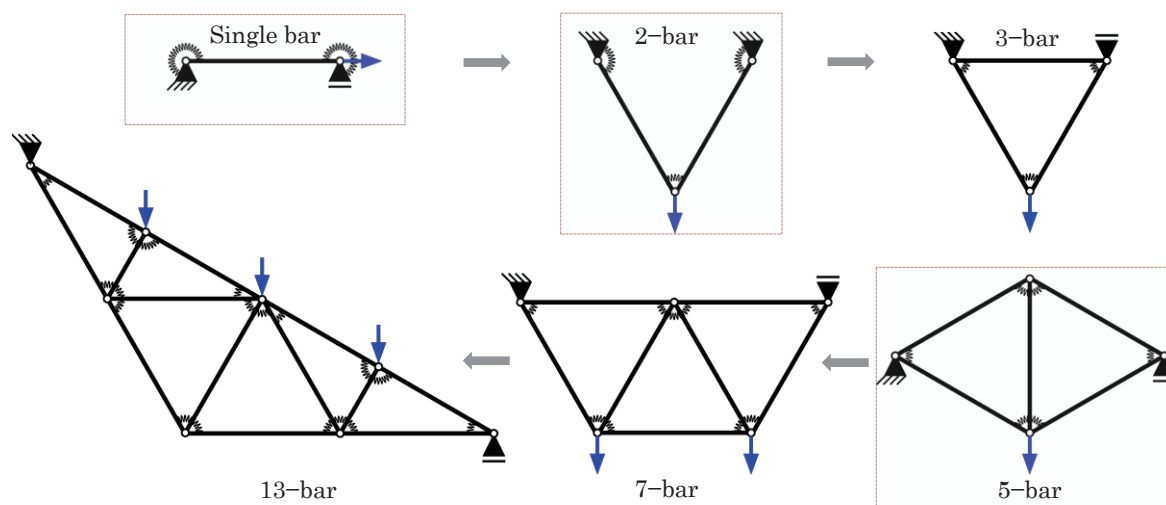
The use of a dynamic-based approach is attractive for existing truss-type structures to determine their state of stress and assess the safety condition, due to the nature of minimum intervention of dynamic-based approaches and based on the sensitivity of the modal parameters to the effects of stress stiffening and joint rigidity of truss-type constructions.

As reviewed, finite element model updating methods are proven to be powerful techniques. With the use of global search optimization strategies, they allow more flexibility in the applications. Nevertheless, engineering judgements and reasonable selection of the updating parameters are essential to avoid unrealistic solutions.

To achieve the success of a vibration-based model updating approach, the key aspects include accurate identification of the experimental parameters, construction of an appropriate numerical model, definition of a meaningful objective function, as well as selection of an effective optimization algorithm.

3

VERIFICATION OF METHODOLOGY BY NUMERICAL STUDY



Numerical simulation allows subsequent experiments to be carried out effectively. This chapter focuses on the construction of finite element models for three types of systems from simple to more complex structures. Numerical sensitivity studies are presented to understand the influences of selected parameters on the static as well as dynamic responses of the systems. The feasibility and robustness of the proposed methodology to identify the axial forces and estimate the joint flexibility are discussed.

3.1 Overview of Investigated Systems

Three types of systems were chosen to be examined closely: (i) single bars, (ii) a two-bar truss-like system, and (iii) a five-bar truss. They were developed step by step from a simple single bar to a more complicated truss structure. The simple systems, whose structural properties with physical meaning and high reliability, were studied first to provide foundation to understand more complex systems. The investigated systems were designed to be lightweight truss-type structures and characterized mainly by axial forces. They were also constructively relevant for subsequent laboratory experiments.

3.2 Single-Bar Systems

The single bar was modelled by the finite element method based on Timoshenko beam theory. Semi-rigid connections were considered by introducing rotational springs to the two ends of the bar, as shown in Figure 3.1.

First, to understand the fundamental influences of structural input parameters on the dynamic responses of the single-bar system, a preliminary parametric study was conducted, which is provided in Appendix B. The independent effect of several selected input parameter on the natural frequency of the first mode of the single-bar system was examined. The input parameters are tensile stress, rotational spring stiffness of constraints, cross-sectional area, length of the member, modulus of elasticity, and mass density. A single variation was investigated for each parameter.

The tensile stress, rotational spring stiffness, cross-sectional area and modulus of elasticity have positive effects on the frequency values; whereas the length and mass density have negative effects. The positive effect means the frequency values increase when the input parameter increases. Vice versa, if the frequency values decrease when the input parameter increases, the input parameter has a negative effect. The degree of nonlinear effect varies for the parameters. For the case studies of the preliminary parametric study, the parameters tensile stress and rotational spring stiffness have the most significant effects on the first frequencies, followed by the geometrical properties of the single bar.

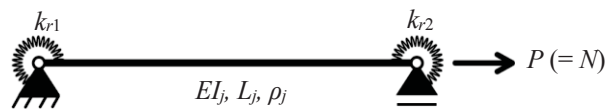


Figure 3.1 – Single bar model.

Table 3.1 – Geometrical and material properties of single bars in the numerical study.

Bar	L [mm]	\emptyset [mm]	A [mm ²]	I [mm ⁴]	E [N/mm ²]	ρ [kg/m ³]	λ_s [-]
B1	2700	20	314.16	7853.98	205 000	7850	540
B2	1500	20	314.16	7853.98	205 000	7850	300
B3	1000	20	314.16	7853.98	195 000	7850	200
B4	1510	9.5	70.88	399.82	205 000	7850	636

L – length; \emptyset – diameter (of solid circular cross-section); A – cross-sectional area; I – moment of inertia; E – modulus of elasticity; ρ – mass density; λ_s – slenderness ($\lambda_s = L\sqrt{A/I}$).

For the numerical study to implement and verify the proposed methodology, single bars of different geometrical and mechanical characteristics were chosen (see Table 3.1). Subsequently in the laboratory experiments, these bars were tested either as single bars or bars as part of a structure. For the numerical model, the programme ANSYS® was used. The bar was modelled with BEAM188 elements, which is based on Timoshenko beam theory including shear-deformation effects; one bar is divided into 40 elements.

The different cases of the axial load were selected. They are given in Table 3.2. The non-dimensional parameter ζ is to evaluate the effect of the bending stiffness on free vibration of a bar-like member. When ζ is larger than 50, an accurate relationship was proposed between the natural frequencies, axial force and the bending stiffness parameter of a fixed-fixed cable [MEHRABI and TABATABAI (1998)]. Although this range covers wide applications for cables in cable-stayed bridges, other significant applications such as diagonal braces, tie-bars and short thick cables are not considered. It is noteworthy to mention that the present work aims to assess a range of ζ less than 50 for beams and beam-like structural members.

Regarding the connection rigidity, the different case studies are provided in Table 3.3. To assess the degree of joint flexibility, constraint parameters in the form of stiffness indexes or percentages of semi-rigid connection have been introduced for practical purposes [e.g. KAWASHIMA and FUJIMOTO (1984), TÜRKER et al. (2009)]. In the present work, the fixity factor was used to represent the degree of joint flexibility from zero (pinned condition) to one (rigid condition).

As previously discussed, linear elastic rotational springs are used to account for the uncertain rotational joint stiffness, assuming the cases of small moments and deflections of truss connections, as well as slip and friction are not included. Concerning the numerical modelling of the rotational springs in ANSYS®, the connection elements were modelled with torsional spring-damper rotational elements (COMBIN14). They are created by the superposition of two or more nodes at the ends of connected members at joints. The elements were linked by coupling the coincident nodes.

Table 3.2 – Load cases of single-bar systems in the numerical study.

Load case	σ [N/mm ²]	B1		B2		B3		B4	
		N	ζ	N	ζ	N	ζ	N	ζ
		[kN]	[-]	[kN]	[-]	[kN]	[-]	[kN]	[-]
S1	25	7.85	5.96	7.85	3.31	7.85	2.26	1.77	7.02
S2	100	31.42	11.93	31.42	6.63	31.42	4.53	7.09	14.04
S3	175	54.98	15.78	54.98	8.77	54.98	5.99	12.40	18.58

ζ – bending stiffness parameter ($\zeta = L\sqrt{N/EI}$).

Table 3.3 – Case studies of connection rigidity of single-bar systems in the numerical study.

Connection stiffness	k_r [Nm/rad]				s_{kr} [-]	γ_{kr} [-]
	B1	B2	B3	B4		
CS1 (Pinned)	0.00	0.00	0.00	0.00	0.00	0.00
CS2	0.60	1.07	1.53	0.05	1.00	0.25
CS3	1.79	3.22	4.60	0.16	3.00	0.50
CS4	5.37	9.66	13.78	0.49	9.00	0.75
CS5	33.99	61.18	87.30	3.04	95.00	0.95
Almost Rigid	177.11	318.79	454.86	16.12	297.00	0.99

k_r – rotational spring stiffness; s_{kr} – stiffness index ($s_{kr} = k_r L / EI$); γ_{kr} – fixity factor ($\gamma_{kr} = k_r L / (3EI + k_r L)$).

Table 3.4 – Parameters of target systems for the numerical study of the single bars.

Target system	Designation	Bar type	λ_s [-]	EI [Nm ²]	$P^{true} = N^{true}$ [kN]	σ^{true} [N/mm ²]	$k_{r1}^{true} = k_{r2}^{true}$ [kNm/rad]	γ_{kr}^{true} [-]
1	B1_S1_CS1	B1	540	1610.07	7.85	25	0.00	0.00
2	B1_S1_CS3				7.85	25	1.79	0.50
3	B1_S2_CS2				31.42	100	0.60	0.25
4	B1_S2_CS4				31.42	100	5.37	0.75
5	B1_S3_CS3				54.98	175	1.79	0.50
6	B1_S3_CS5				54.98	175	33.99	0.95
7	B2_S1_CS2	B2	300	1610.07	7.85	25	1.07	0.25
8	B2_S2_CS3				31.42	100	3.22	0.50
9	B2_S3_CS4				54.98	175	9.66	0.75
10	B3_S2_CS2	B3	200	1531.53	31.42	100	1.53	0.25
11	B3_S3_CS5				54.98	175	87.30	0.95
12	B4_S1_CS3	B4	635.8	81.96	1.77	25	0.16	0.50

P – axial load; N – member axial force; σ – member axial stress; *true* – values of parameters of target systems.

Because experimental data are not yet available in the numerical study, *target systems* were used, based on which the simulated experimental data were calculated. Table 3.4 presents the twelve target systems in the numerical study. The target systems were generated by different combinations of four bars (B1 → B4), three levels of axial stress (S1 → S3), and five sets of the connection stiffnesses (CS1 → CS5). Each target system is characterized by a specific value of free slenderness λ_s , flexural rigidity EI , axial stress σ , and fixity factor γ_{kr} .

3.2.1 Effects of Stress Stiffening and Joint Flexibility

To illustrate the effects of stress stiffening and joint flexibility on the static and dynamic responses, four single bars type B4 were considered, i.e. pinned vs. rigid and zero- vs. high-load systems. For the pinned system, the rotational spring stiffness were assumed to be infinitesimal; whereas for the rigid system, they tend to infinity. The spring stiffnesses at the two end constraints are assumed identical. The applied axial load takes

Table 3.5 – Numerical natural frequencies of the first six modes of the single bar B4 without and with stress stiffening based on different static analyses for the stress stiffening.

Mode	f_n [Hz]								
	Pinned system ($k_r \rightarrow 0$)				Rigid system ($k_r \rightarrow \infty$)				
	$N = 0$ kN		$N = 17.14$ kN ($\sigma \approx 242$ N/mm ²)		$N = 0$ kN		$N = 17.14$ kN ($\sigma \approx 242$ N/mm ²)		
	without stress stiffening		stress stiffening		without stress stiffening		stress stiffening		
Ana.	Num.	linear	nonlinear	Ana.	Num.	linear	nonlinear		
1	8.36	8.36	58.71	58.73	58.69	18.81	18.93	64.63	64.58
2	33.45	33.42	120.95	120.96	120.88	52.26	52.18	133.10	132.99
3	75.62	75.17	189.89	189.88	189.74	102.43	102.25	208.79	208.60
4	134.15	133.59	268.21	268.12	267.89	169.32	168.95	294.34	294.05
5	209.40	208.64	357.95	357.71	357.36	252.93	252.25	391.67	391.24
6	301.37	300.28	460.64	460.12	459.62	353.26	352.09	502.12	501.54

Ana. – Analytical formulae based on Euler–Bernoulli beam theory, i.e. Eq (2.4) and Eq. (2.8);

Num. – Numerical finite element method based on Timoshenko beam theory;

stress stiffening linear – static linear analysis prior to dynamic analysis;

stress stiffening nonlinear – static geometric nonlinear analysis prior to dynamic analysis.

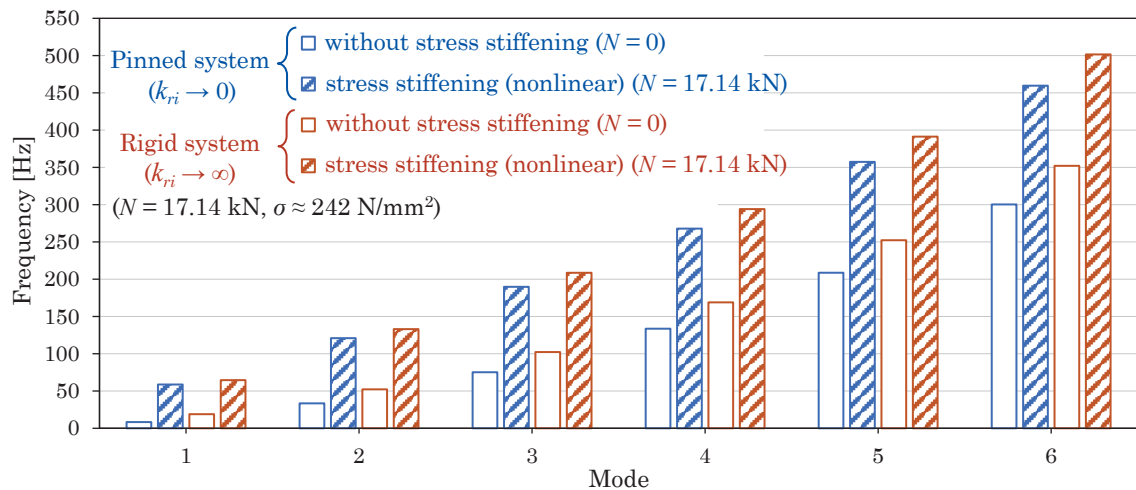


Figure 3.2 – Numerical natural frequencies of the first six modes of the pinned vs. rigid single bar system B4 without and with the effects of stress stiffening in the numerical study.

two values of zero and 17.14 kN. The load of 17.14 kN for the high-load system is equivalent to a normal stress of about 242 N/mm² in the bar. To take into account stress stiffening, static analysis of the numerical model was performed prior to the dynamic analysis to obtain the stress distribution in the member. The effect of the stress was accounted for in the subsequent dynamic analysis.

Concerning the types of the static analysis, as the inclusion of stress stiffening or geometric stiffness is often linked with nonlinear geometrical analysis, two types of static analysis were performed. They are linear static analysis, i.e. stress stiffening only, and geometric nonlinear static analysis, i.e. stress stiffening and large deformations.

In addition, as previously reviewed, closed-form solutions only exist in the cases of a rigid-rigid beam excluding axial force effects (i.e. Eq. (2.4)), and a pinned-pinned beam including stress stiffening (i.e. Eq. (2.8)). Thus, numerical finite element method was employed for other cases of boundary conditions of a single bar and for complex structures. To compare the results of the modal parameters by the closed-form solutions and the finite element method, Table 3.5 provides the analytically and numerically calculated natural frequencies of the first six modes of the bar B4 comparing the effects of stress stiffening based on the different static analyses.

Table 3.6 – Numerical natural frequencies of the first six modes of the six target systems compared to the pinned system at zero-load of the single bar B1 in the numerical study.

Mode	Pinned, zero- load	Target system											
		1		2		3		4		5		6	
		f_n [Hz]	Δ [%]	f_n [Hz]	Δ [%]	f_n [Hz]	Δ [%]	f_n [Hz]	Δ [%]	f_n [Hz]	Δ [%]	f_n [Hz]	Δ [%]
1	5.5	11.8	114.7	13.0	136.4	21.9	297.7	23.2	322.1	28.8	422.6	31.3	468.1
2	22.0	30.3	37.9	32.3	46.9	47.7	116.9	50.3	128.8	60.6	175.4	65.8	198.9
3	49.5	58.6	18.4	61.0	23.3	80.5	62.7	84.2	70.2	98.1	98.2	106.1	114.4
4	87.9	97.4	10.7	100.0	13.8	122.1	38.8	126.7	44.1	143.1	62.7	154.0	75.2
5	137.3	146.9	7.0	149.7	9.0	173.3	26.2	178.6	30.1	196.8	43.3	210.6	53.4
6	197.6	207.3	4.9	210.2	6.4	234.8	18.8	240.6	21.8	260.1	31.6	276.5	40.0

The results using the finite element model agree with that from the analytical formulae. Some differences of the frequencies of higher modes are found due to the assumptions of the Euler–Bernoulli or Timoshenko beam theories.

In the cases of minor bending or deformations, the linear static analysis provides similar results to the geometric nonlinear static analysis. Nevertheless, the types of the static analysis prior to the dynamic analysis can affect the results of the modal parameters, such as in the case of a framework that experiences out-of-plane bending while subjected to stress stiffening [GREENING and LIEVEN (2003)]. Therefore, the geometric nonlinear static analysis was adopted for all subsequent analyses. It is assumed that more accurate results can be achieved by the static geometric nonlinear analysis than the linear static analysis in general cases.

In Figure 3.2, the effect of stress stiffening on the frequencies of the bar B4 is significant due to a wide variation of the stress. Nevertheless, the effect of the joint flexibility cannot be neglected. From the static analysis, the assumption of pinned or rigid joints has only small effects on the stresses of the members, as the bending stress due to own weight of the considered member as well as the rotational stiffness of the joints is insignificant compared to the normal stress. However, assumptions of pinned or rigid joints affect the structural dynamic behaviour. Thus, the numerical model of a bar should consider the unknown joint flexibility to approximate accurately the dynamic responses.

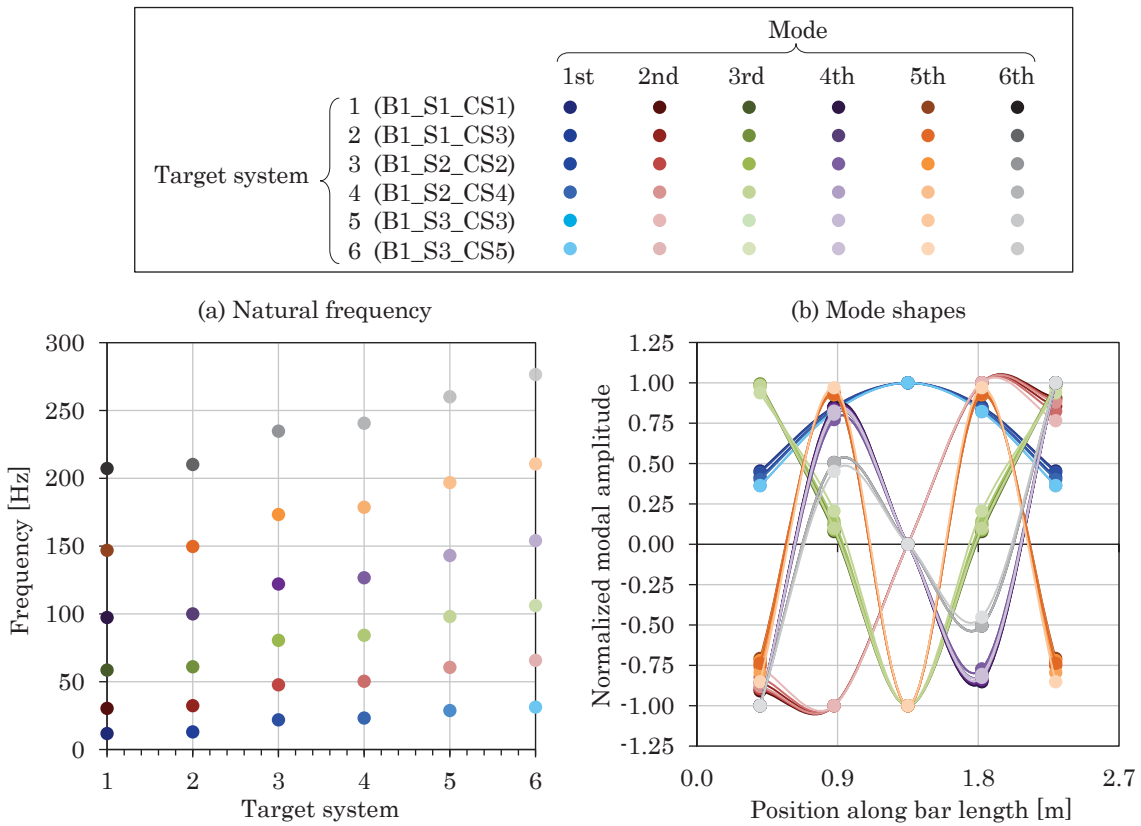


Figure 3.3 – Numerical modal parameters of the first six modes of six target systems of single bar B1 in the numerical study.

Another investigation was conducted considering the bar type B1. For this bar, six target systems were formed by combinations of the input parameters of the axial force and boundary conditions. The numerically calculated natural frequencies of the six target systems of the bar B1 are given in Table 3.6, in comparison to that of the pinned–pinned bar at zero–applied load. The differences in the natural frequencies of the systems can be recognised clearly.

Figure 3.3 presents the numerical frequencies and mode shapes of the first six modes of the target systems of bar B1. The mode shapes are normalized to maximum modal displacements that are equal to one. They are drawn representatively at five points, assuming five sensors are used in the experiments. The five points are equally distributed along the bar length. The distance between the assumed installed sensors is 472.5 mm, while the total length of the five points is 1890 m.

Some changes in the mode shapes can be seen. Nevertheless, unlike natural frequencies, the magnitudes of the changes in the mode shapes usually cannot be measured accurately in the experiments. FRISWELL and MOTTERSHEAD (1995) have discussed that natural frequencies can be identified from experimental measurements in general to a much greater accuracy than mode shapes.

To evaluate the mutual effects of stress stiffening and the joint rigidity on the natural frequencies, the frequencies of the first mode of the single beam B4 is plotted versus the rotational spring stiffness and axial force in Figure 3.4. The rotational spring stiffness at both end constraints are assumed identical; they are varied from pinned to nearly rigid. The tensile stress is varied from zero to approximately 250 N/mm².

The effect of the axial tensile stress is significant. The frequency–load relationship is parabolic for pinned–pinned beam and near–parabolic for other support conditions.

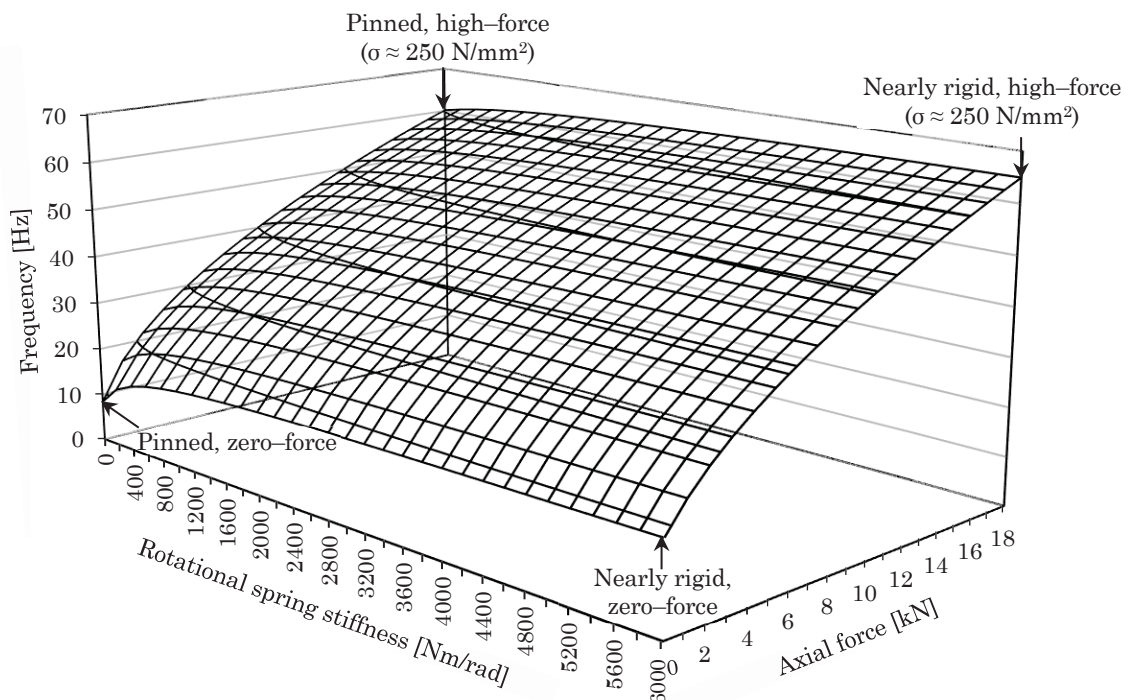


Figure 3.4 – The numerical natural frequencies of the first mode of single bar B4 at varying constraint conditions and stress stiffening.

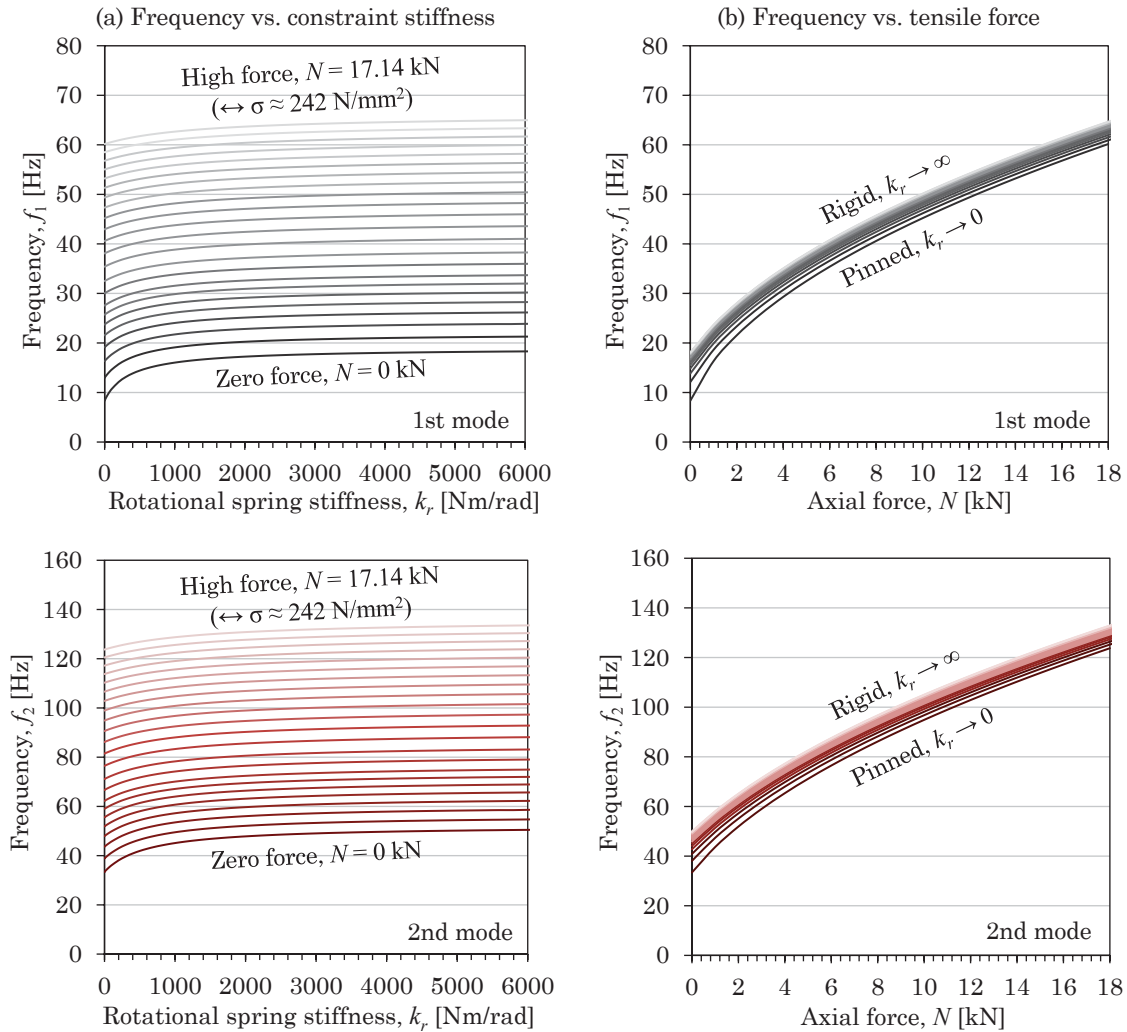


Figure 3.5 – Numerical natural frequencies of the first two modes of single bar B4 at varying stress stiffening and constraint conditions.

If the effect of slenderness of a bar is also considered together with the effects of stress stiffening and constraint flexibility, the stiffness of a structural member depends on three components: (i) mechanical stiffness i.e. elastic stiffness component; (ii) tensional stiffness i.e. geometric stiffness component; and (iii) constraint stiffness, e.g. rotational stiffness component. LAGOMARSINO and CALDERINI (2005) discussed that when each of these factors changes, the total stiffness matrix of the member will be affected. When increasing the tensile force, the tensional stiffness contribution tends to dominate over other mechanical and constraint contributions. Similarly, for increasing rotational stiffness, the system becomes less sensitive to the effect of tensile force. For increasing slenderness, the contribution provided by constraint stiffness becomes less significant compared to other contributions (see Appendix B).

Considering different modes of vibration, Figure 3.5 presents the frequencies of the first two modes of the single bar B4 at various axial forces and constraint flexibility. Upon axial loading of the member, the natural frequencies of all modes experience a modification to their magnitudes. In terms of percentage, the relative changes of the natural frequencies of the first mode are larger than that of the second mode, although the changes in absolute values of the second mode are higher than that of the first mode.

3.2.2 Selection of Modes to use Analytical-based Algorithm

As the analytical-based algorithm proposed by MAES et al. (2013) is used as part of the proposed methodology, a case study is carried out to examine the effects of the locations of the instrumented sensors on the identified axial force. Moreover, discussion about the selection of a mode for the use of the analytical-based algorithm is made.

Numerically calculated mode shapes were extracted at five assumed sensor locations for the finite element model of the single bar B1. Two arrangements of the sensors on the single bar were assumed, as given in Figure 3.6. The first setup assumes that the sensors are equally distributed over the length of the bar B1; whereas the second setup considers an unequal distribution of the sensors. For comparison, the axial forces were calculated for the two setups using all three analytical-based methods of LI et al. (2012), REBECCHI et al. (2013) and MAES et al. (2013). The results are presented in Figure 3.7.

As discussed, the analytical-based approaches from the literature is affected by the locations of the sensors. By the methods of LI et al. (2012) and MAES et al. (2013), the sensors can be distributed randomly. By the method of REBECCHI et al. (2013), the five sensors must be equally distributed to achieve reasonable estimation of the axial force.

For all methods, spurious solutions of the identified forces can occur for the modes where the sensor locates at a modal node. At this location, the modal displacement is very close or equal to zero. For instance, for the second, fourth and sixth mode, the sensor S3 is located at a modal node, giving rise to large errors on the identified axial forces by all methods. The true axial force value can be one of the possible solutions, but additional spurious values occur. The spurious zeros can be positive and negative identified forces.

By using the first mode of vibration, the results of the forces by the methods of LI et al. (2012) and MAES et al. (2013) give correct values for both arrangements of sensors in all case studies of target systems. A relevant remark is that using the first mode that is in the form of the first vibration mode of a single beam reduces the possibility of spurious solutions. This agrees with the discussions given in the work of REBECCHI et al. (2013).

3.2.3 Sensitivity Analysis

The sensitivity analysis was performed to determine the parameters that have significant influences on the static and dynamic responses to be included into the optimization process. The characteristics of the parameters in the sensitivity analysis

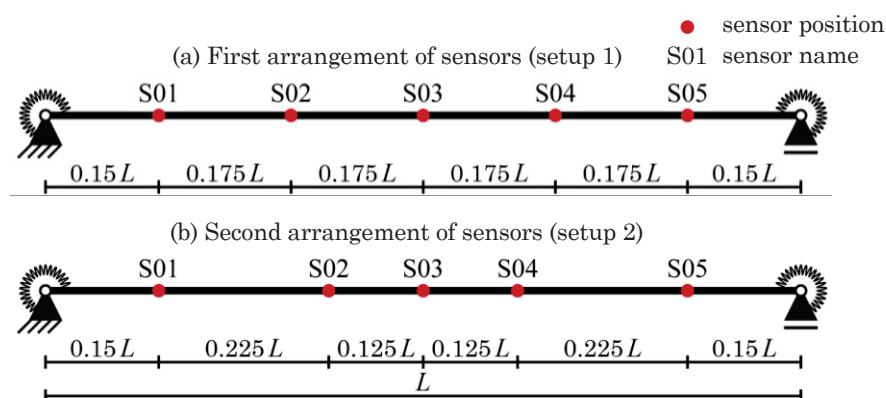


Figure 3.6 – Different arrangements of sensors on single bar system B1 in the numerical study.

are defined in Table 3.7. The parameters of the load and rotational spring stiffness of the supports were assumed as the main unknowns. The rotational spring stiffness at the two end supports of the symmetric single-bar systems were assumed identical. The variations of the other parameters were chosen in limited ranges. The measurements of the geometry and sensor positions can be made using callipers with a reasonable level of accuracy. As for the mechanical properties of steel, they are normally reliable. In the case of historic iron, broader variation ranges for the material properties may need to be considered.

Several sensitivity analyses were carried out to evaluate different choices of the updating parameters. The analyses include:

- updating the spring parameter only, which involves 1 design input parameter (i.e. the rotational spring stiffness), and 9 output responses including 8 modal responses (4 natural frequencies and 4 MAC values) and 1 static force response;
- updating load and spring parameters, which involves 2 design parameters and 9 output responses;
- updating all parameters including the load, rotational spring stiffness as well as the parameters related to the mechanical and geometrical properties of the system, which involves 11 design parameters and 9 output responses.

The analysis in which only the spring parameter of the joints or end constraints is updated assumes that the load is known exactly. This is not the case in practice, but the analysis aims to investigate numerically the influence of solely the constraint stiffness

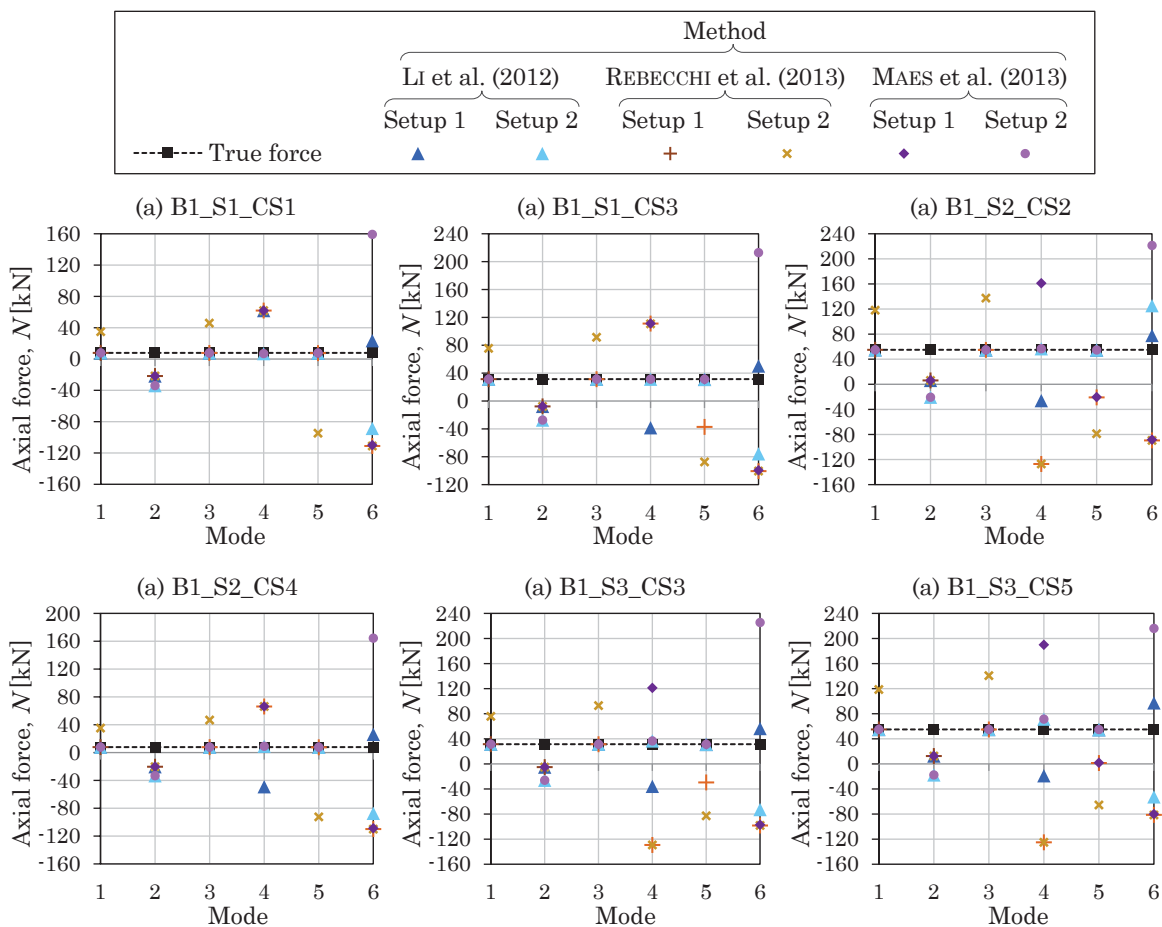


Figure 3.7 – Identified axial forces using analytical-based methods in the numerical study of bar B1.

on the output responses and the accuracy of the optimization to estimate the end stiffness without the uncertainty regarding the load.

In contrast to sensitivity analyses that considers a single variation of each parameter at one time, all input parameters were varied simultaneously. The advantage is to obtain global sensitivities for all pairs of parameters with a single sample set. The multivariate samples were generated by using the Latin Hypercube method, which is a stochastic sampling strategy.

Figure 3.8 shows the results of a global sensitivity analysis through Spearman linear correlation matrix for a target system of the bar B1, i.e. the system B1_S1_CS1. The sensitivity analysis was based on 200 Latin hypercube samples, with the parameter intervals presented in Table 3.7. The colours indicate the different direction of association between the input parameters and the output responses.

The correlation matrix shows that the flexibility of the end constraints has a considerable influence on the frequencies and MAC values; while the tensile force or tensile stress has a significant influence on the modal parameters as well as the numerically computed static force. The effects of other parameters are insignificant compared to the axial load and constraint flexibility effects, but it is worth noting the limited variation ranges of the other parameters.

To compare the target systems and examine the effects of stress stiffening and constraint flexibility as well as slenderness, the sensitivity analyses were carried out for other single bars. The results for the target system B1_S3_CS5 (single bar B1) (see Figure 3.9) and target system B3_S2_CS2 (single bar B3) are discussed next.

Concerning the target systems B1_S1_CS1 and B1_S3_CS5, the bar has the same geometrical and mechanical characteristics (type B1). Because the tensile stress is higher for the system B1_S3_CS5 than the system B1_S1_CS1, when updating both the load and the rotational spring stiffness, the effect of the constraint stiffness is reduced.

To evaluate the effect of slenderness, as the bar B3 is not as slender as the bar B1, the sensitivity analysis of the target system B3_S2_CS2 reveals that the effect of the

Table 3.7 – Characterization of the parameters of the numerical models for the sensitivity analysis.

Parameter	Designation	Value	Variation	Unit
P	Applied load	*	before buckling load to high tensile load (tensile stress approx. 200 N/mm ²)**	kN
γ_{kr}	Fixity factor	*	pinned to almost rigid***	–
E	Modulus of elasticity	205 000 (B1, B2, B4) 195 000 (B3)	+/- 1 %	N/mm ²
ρ	Mass density	7850	+/- 0.2 %	kg/m ³
A	Cross-sectional area	314.16 (B1, B2, B3) 70.88 (B4)	+/- 1 % +/- 2 %	mm ²
m_s	Mass per sensor	10	+/- 5 %	g
x_{s1}	Position sensor 1****	0.150L	+/- 1 mm	mm
x_{s2}	Position sensor 2	0.375L	+/- 1 mm	mm
x_{s3}	Position sensor 3	0.500L	+/- 1 mm	mm
x_{s4}	Position sensor 4	0.625L	+/- 1 mm	mm
x_{s5}	Position sensor 5	0.850L	+/- 1 mm	mm

*Different values for target systems (see Table 3.4).

**–1.50 / 60.00 (B1); –5.00 / 60.00 (B2); –10.00 / 60.00 (B3); –1.50 / 15.00 (B4);

***0.00 / 0.99;

****Position of sensor to one end support (see Figure 3.6(b)); L – member length.

constraint flexibility is more significant. The results of the sensitivity analyses agree with the previous discussion about the stiffness components of a structural member.

Overall, for slender truss structures, the axial force or stress stiffening has significant effect on the output parameters from the static as well as dynamic analyses of the numerical model. The constraint stiffness has influence on the dynamic response of the modal parameters. In general cases, the effect of the constraint stiffness becomes less significant in the presence of the effect of stress stiffening.

Based on the results of the sensitivity analyses, two stages of the optimization process were suggested to identify the design parameters with better accuracy. First, the load and the resulted axial forces can be identified accurately such that the objective function comprises the output parameters of both the static and dynamic responses of the numerical model. After the load is identified, the constraint stiffness can be estimated more accurately if the objective function takes into account the modal parameters and the updating parameter is primarily the constraint stiffness.

3.2.4 Identification of Axial Forces and Joint Stiffness

The optimization phase allows the identification of the assumed unknown parameters of the axial forces and rotational spring stiffness. For clarity, the parameters of the target systems that are used to calculate the simulated experimental data in the numerical

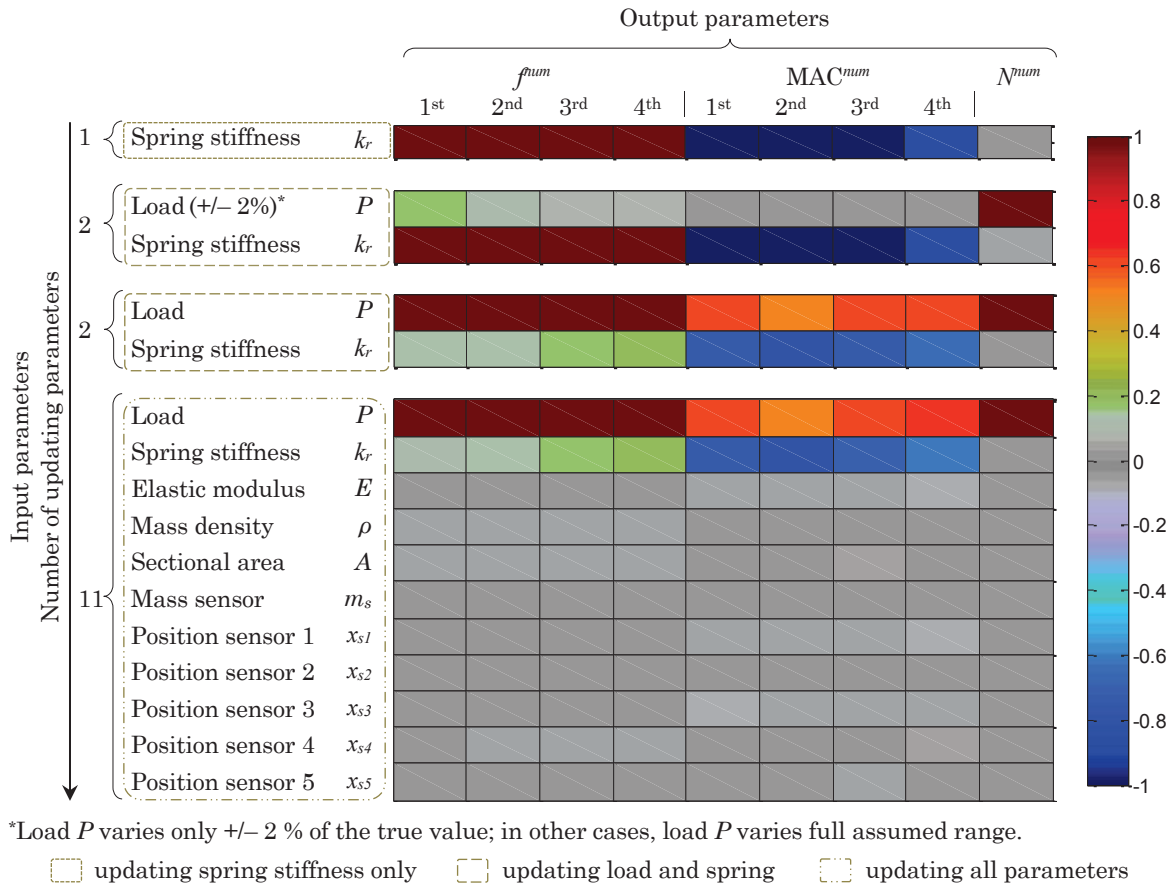


Figure 3.8 – Spearman correlation matrix between the parameters and responses of the numerical model of the single bar target system B1_S1_CS1.

study are denoted as *true*, whereas the parameters identified from the proposed methodology are denoted as *id*.

The first four simulated experimental modes of the target systems were used in the identification process. The axial load was varied simultaneously with the rotational spring stiffness. As the identification problem is symmetric, the rotational spring stiffnesses at the two end constraints were assumed to be identical. The optimization of the single-bar model involved 2 design parameters (P , k_r (or γ_{kr})), 8 modal responses (4 natural frequencies and 4 MAC values) and 1 static force. The variations of the design parameters are as indicated in Table 3.7. In the second optimization stage of the proposed methodology, the identified load or axial force from the first stage was assumed to be within a 2 % variation to account for possible errors on the axial force identification, while the main purpose is to determine the joint rigidity parameter. Latin hypercube method was used to generate randomly the initial population. Four independent optimization runs with random initial populations were performed and the mean values were adopted.

As mentioned, different optimization techniques were applied, which belong to the response surface methods and population-based or nature-inspired methods. The implementation of the optimization techniques was made using the programme OptiSLang[®] [Dynardo GmbH]. The ARSM was based on linear order of approximation with a start range of 0.5, minimum iterations of 5, maximum iterations of 20 and minimum range of 10^{-6} . The GA and PSO were based on an initial population consisting of 15 individuals and 50 generations, for a total of 750 individuals. The crossing rate was

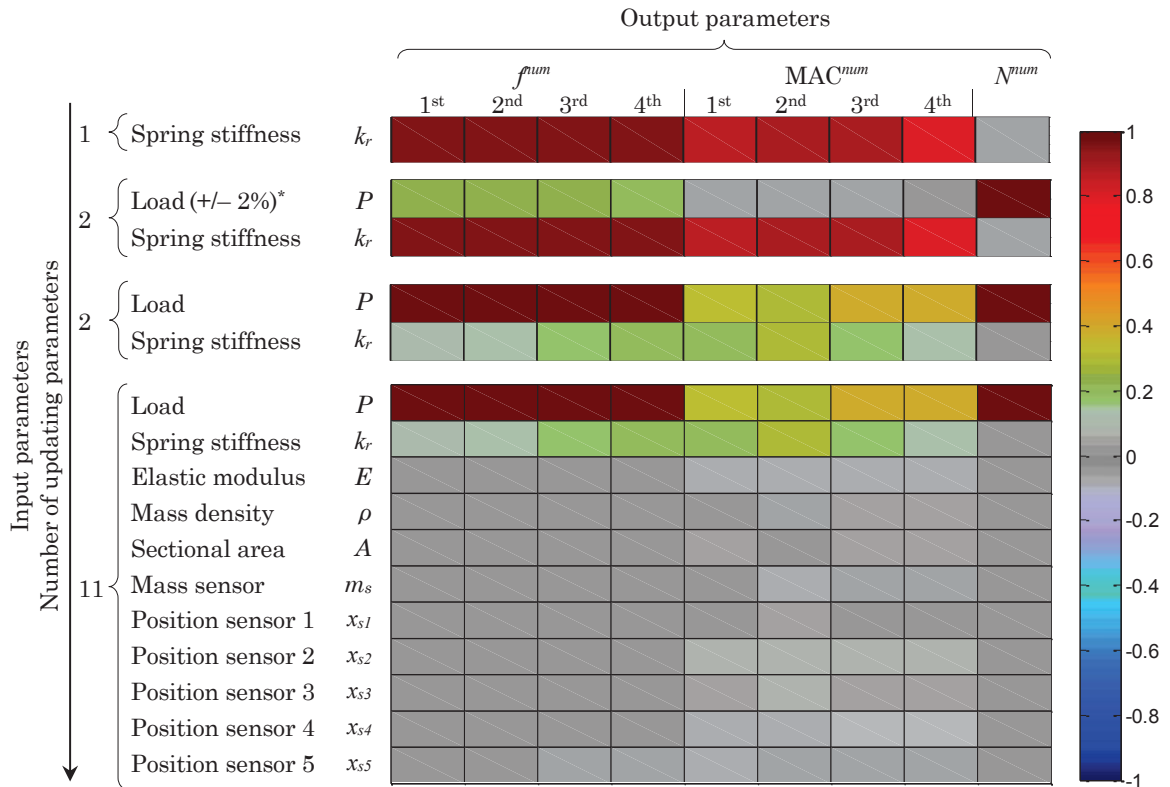


Figure 3.9 – Spearman correlation matrix between the parameters and responses of the numerical model of the single bar target system B1_S3_CS5.

set equal to 50 % and the mutation rate was equal to 15% with a standard deviation along the optimization between 0.10 and 0.01.

The results of the axial force and joint stiffness identification using the proposed methodology for the single-bar systems are given in Table 3.8. The identified axial forces match well to the true ones. The different optimization techniques provide in general similar results. The ARSM gives the largest difference of the identified force to the true one of -0.63 kN for a case of the first target system at the stress of 25 N/mm². The largest difference by the GA is -0.36 kN and by the PSO is 0.32 kN. In most cases, the differences between the identified and true forces in absolute values are smaller than 0.10 kN.

Table 3.8 – Results of the identified axial forces and corresponding stresses, as well as the identified rotational spring stiffness and fixity factors, in the numerical study of single-bar systems.

Target system	Designation	Technique	*SPR	Proposed methodology					
			$\frac{\gamma_{kr}^{id,SPR}}{\gamma_{kr}^{true}}$	N^{id}	σ^{id}	Δ	k_r^{id}	γ_{kr}^{id}	$\frac{\gamma_{kr}^{id}}{\gamma_{kr}^{true}}$
			[-]	[kN]	[N/mm ²]	[kN]	[kNm/rad]	[-]	[-]
1	B1_S1_CS1	ARSM	–	7.22	23.00	–0.63	0.39	0.18	–
		GA	–	7.60	24.20	–0.25	0.22	0.11	–
		PSO	–	7.73	24.62	–0.12	0.11	0.06	–
2	B1_S1_CS3	ARSM	1.00	7.79	24.78	–0.06	1.73	0.49	0.98
		GA	1.00	7.69	24.47	–0.16	1.96	0.52	1.04
		PSO	1.00	7.76	24.71	–0.09	1.86	0.51	1.02
3	B1_S2_CS2	ARSM	1.00	31.37	99.87	–0.05	0.46	0.20	0.80
		GA	0.96	31.34	99.76	–0.08	0.64	0.26	1.04
		PSO	1.00	31.44	100.09	0.02	0.50	0.22	0.88
4	B1_S2_CS4	ARSM	1.00	31.39	99.91	–0.03	5.01	0.74	0.99
		GA	1.01	31.06	98.86	–0.36	5.77	0.76	1.01
		PSO	1.00	31.41	99.98	–0.01	5.35	0.75	1.00
5	B1_S3_CS3	ARSM	1.00	54.96	174.95	–0.02	1.34	0.43	0.86
		GA	1.00	55.00	175.07	0.02	1.65	0.47	0.94
		PSO	1.00	54.95	174.91	–0.03	1.71	0.49	0.98
6	B1_S3_CS5	ARSM	1.00	54.96	174.95	–0.02	31.25	0.95	1.00
		GA	1.00	55.00	175.06	0.02	30.24	0.94	0.99
		PSO	1.00	54.97	174.96	–0.01	34.12	0.95	1.00
7	B2_S1_CS2	ARSM	1.00	7.82	24.88	–0.03	1.08	0.24	0.96
		GA	0.97	7.76	24.71	–0.09	1.13	0.24	0.96
		PSO	1.00	7.65	24.34	–0.20	1.05	0.26	1.04
8	B2_S2_CS3	ARSM	1.00	31.40	99.96	–0.02	3.08	0.49	0.98
		GA	1.00	31.39	99.90	–0.03	3.28	0.50	1.00
		PSO	1.00	31.38	99.88	–0.04	3.20	0.50	1.00
9	B2_S3_CS4	ARSM	1.00	54.93	174.83	–0.05	9.65	0.74	0.99
		GA	1.00	54.92	174.81	–0.06	9.68	0.75	1.00
		PSO	0.99	55.30	176.03	0.32	9.68	0.75	1.00
10	B3_S2_CS2	ARSM	1.00	31.35	99.77	–0.07	1.49	0.24	0.96
		GA	1.00	31.44	100.08	0.02	1.63	0.26	1.04
		PSO	1.00	31.42	100.01	0.00	1.57	0.25	1.00
11	B3_S3_CS5	ARSM	1.00	54.93	174.83	–0.05	85.62	0.95	1.00
		GA	1.00	54.85	174.58	–0.13	86.87	0.95	1.00
		PSO	1.00	54.80	174.45	–0.18	88.48	0.95	1.00
12	B4_S1_CS3	ARSM	1.00	1.78	25.12	0.01	0.13	0.43	0.86
		GA	1.00	1.74	24.61	–0.03	0.17	0.50	1.00
		PSO	1.00	1.78	25.10	0.01	0.14	0.46	0.92

Assumption: $k_r^{id} = k_{r1}^{id} = k_{r2}^{id}$;

*SPR – updating the parameter(s) of the rotational spring stiffness only, assuming the force is known exactly.

The identified fixity factors by the proposed methodology indicate correctly joint rigidity with respect to a hinged or rigid condition in all cases. However, exact values of the fixity factors like the true ones were usually not achieved, especially for small values of the rotational spring stiffness or low values of the fixity factors.

The ratios of the identified to the true fixity factors were calculated, while a ratio of 1.00 indicates an excellent agreement of the identified results. The ARSM gives the ratios of the identified to the true fixity factors in the range from 0.80 to 1.00. The GA and PSO provide better results of the fixity factors or constraint stiffness than the ARSM. The GA gives the ratios from 0.94 to 1.04. The range of the ratios obtained by the PSO is from 0.88 to 1.02.

As mentioned, to investigate the accuracy of the optimization in estimating the joint stiffness if the load is known exactly, optimization runs were performed assuming the scenario that the rotational spring stiffness or the rigidity factor was the only unknown, which was included as the only updating parameter. The objective function contains the modal parameters of the natural frequencies and MAC indices.

The results of the ratios of the identified rigidity factors ($\gamma_{kr}^{id,SPR}$) to the true ones (γ_{kr}^{true}) are also provided in Table 3.8, which range from 0.96 to 1.00. The identified rigidity factors by the optimization with only the updating parameter of the spring stiffness are highly accurate. This proves the considerable influence of the joint stiffness on the dynamic responses.

Table 3.9 – Assumptions of different initial starting values of the design parameters of the axial force and rigidity factor in numerical study of single-bar systems.

Optimization	Assumed initial start values of design parameters
A	Initial starting values 50 % smaller than true values
B	Initial starting values 20 % smaller than true values
C	Initial starting values 100 % higher than true values
D	Initial starting values 200 % higher than true values

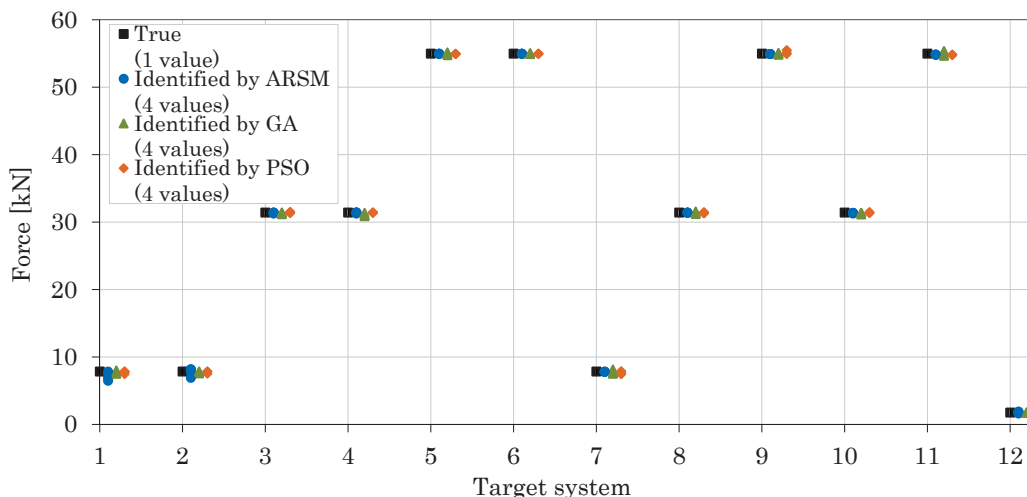


Figure 3.10 – Results of all identified axial forces of four optimization runs with different initial parameter sets using three different optimization techniques in the numerical study of the single-bar systems.

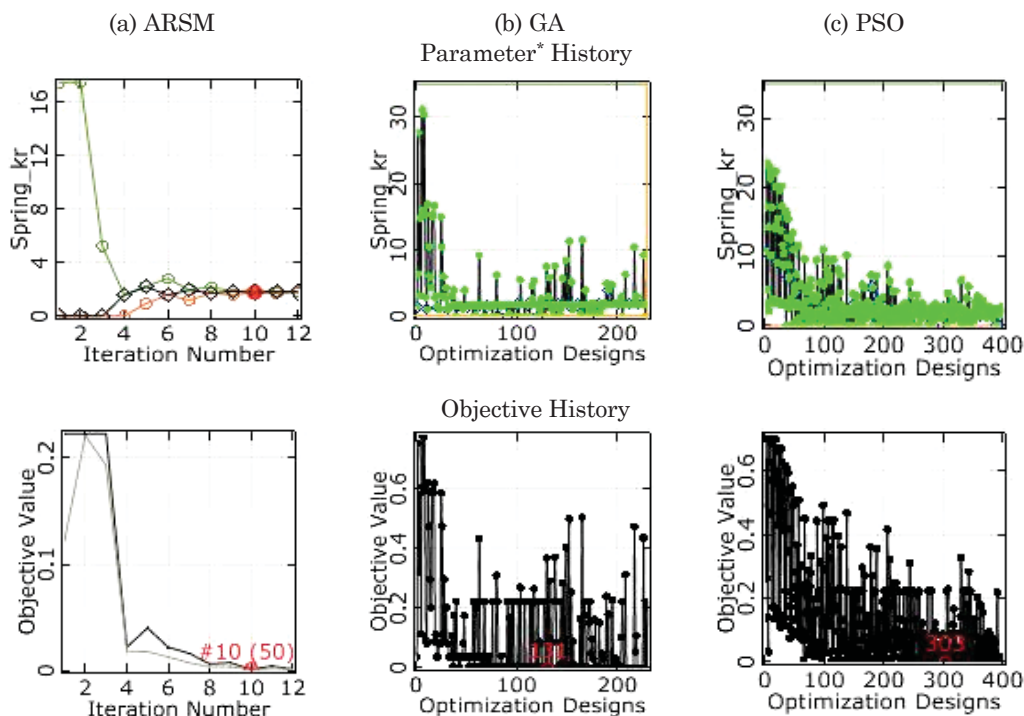
Regarding the different optimization stages of the proposed methodology, the identified axial forces from the first stage are sufficiently accurate. The identified forces in the second stage optimization show that they are not necessarily improved compared to that from the first stage. For the joint flexibility, the results of the joint rigidity factors were improved in the second stage optimization compared to that in the first stage.

3.2.5 Computational Efficiency of Optimization Techniques

To examine the dependency of the optimization techniques on the assumptions of the initial starting point, optimization runs based on different initial populations were carried out. Table 3.9 shows the initial starting values of the design parameters that were assumed to be 50 % smaller, 20 % smaller, 100 % higher and 200 % higher than the true values for four optimization runs A to D. For the single-bar systems, the design parameters are the axial force and rigidity factor of the end constraints.

The results of the identified axial forces of all four optimization runs are presented in Figure 3.10. The identified forces are highly consistent in all runs. Moreover, the optimization runs led to very similar values of the frequencies and MAC indices, which demonstrates the robustness of the optimization-based techniques. The PSO shows the most consistent results, followed by the GA and lastly, the ARSM.

Concerning the computationally efficiency, Figure 3.11 shows an example of convergence diagrams of the ARSM, GA and PSO for an optimization of the target system B1_S1_CS3. Because the GA and PSO are stochastic methods, the scatters of the objective values are larger compared to the ARSM. The ARSM is more computationally



* Updating parameter is only the rotational spring stiffness assumed identical at the two supports; the objective function contains the modal parameters of the natural frequencies and MAC indices.

Figure 3.11 – Convergence of optimization by different optimization techniques in the numerical study of the target system B1_S1_CS3.

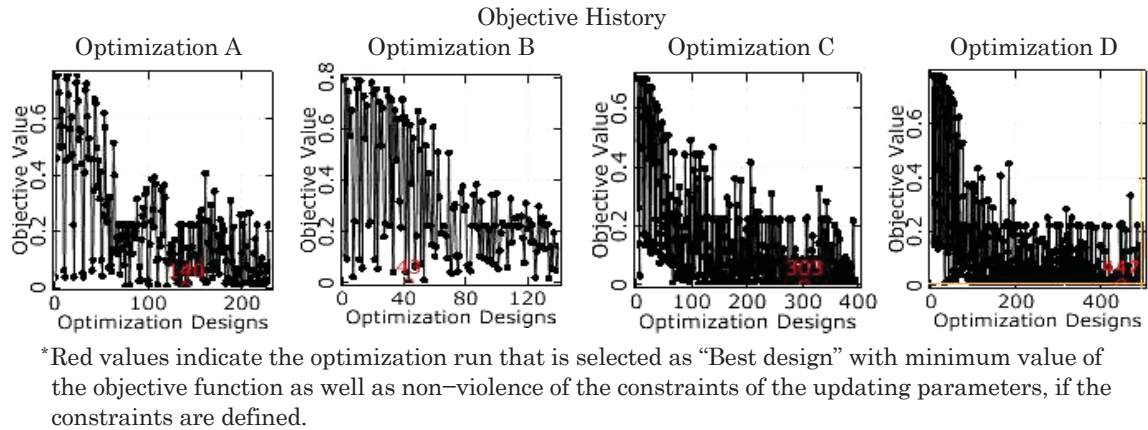


Figure 3.12 – Convergence of optimization with different initial parameter sets by the PSO in the numerical study of the target system B1_S1_CS3.

efficient than the other two techniques, whereas the PSO requires in general the most computational efforts.

The non-dependence of the initial starting point of the optimization-based methods has been illustrated in Figure 3.10. Although the starting values of the design parameters do not need to be close to the optimum, Figure 3.12 illustrates that the efficiency of the optimization can be increased when the initial populations are close to the optimum. The optimization B with the initial starting values closer to the true values than the optimizations A, C, D and thus, requires the least computational cost; whereas the optimization D with the initial population am furthest to the true values requires the most computational cost.

3.2.6 Error Analysis

In practice, it is expected that there are deviations due to uncertainties in measurement data and structural properties. Numerical errors are present because the model gives an imperfect representation of the true structure. Measurement errors are inherently present during the experiments due to measurement noise.

PARK et al. (2006) considered two model uncertainty types for a single-bar model, i.e. uncertainty associated with the identified natural frequencies and uncertainty in the structural parameters of the bar. The first type of uncertainty may arise when a true natural frequency locates between two frequency responses; while the second type can include errors in the stiffness parameters, the mass parameters and the damping parameters. In the numerical error study by PARK et al. (2006), the first uncertainty was assumed by considering the frequency resolution to be the same frequency resolution in the experimental study, i.e. $\Delta f = 0.25$ Hz. The frequencies were approximated to nearest

Table 3.10 – Numerical error analysis of the single-bar systems.

Error case	Error associated with	Designation	True value	Variation	Unit
ER1	material and geometrical properties	Modulus of elasticity	E^{true}	+/- 1 %	N/mm ²
		Mass density	ρ^{true}	+/- 0.2 %	kg/m ³
		Bar diameter	d_{bar}^{true}	+/- 1 mm	mm
ER2	sensor properties and locations	Mass per sensor	m_s^{true}	+/- 5 %	g
		Sensor location	x_s^{true}	+/- 1 mm	mm

frequency response values, which were multiples of Δf in the first case study, then in the second case study the frequencies of the first case study were further added by $+\Delta f$. For the uncertainty in the structural parameters, PARK et al. (2006) investigated only the deviation in the stiffness parameter, i.e. the elastic modulus was increased by 1 % and 10 %. It was discussed that the mass of the bar can be evaluated with much less uncertainty; the effect of the mass change to the vibration characteristics can be inferred from the effect of the stiffness change; as well as the effect of the damping change to the resonant frequencies is in general negligibly small. The additional mass and stiffness of the instrumented sensors were not examined. The results show that the maximum errors of the identified tensile force and spring constant of the bar are 0.8 % and 7.8 %, as a result of a variation in the natural frequencies or the elastic modulus in the case studies. The uncertainty in structural parameters has much smaller impact on the accuracy of the parameter identification than the uncertainty in the natural frequencies.

MAES et al. (2013) performed an error analysis for a seven-member truss girder considering the parameters of the geometrical properties, material properties as well as sensor properties. It was assumed that the bar section A and the moment of inertia I are characterized by an error of 0.1 %; the Young's modulus E and the material density ρ are also characterized by a small error of 0.1 %; the mass of each sensor m_s and its mass moment of inertia are subjected to an error of 1 %. In addition, a maximum error in the

Table 3.11 – Results of the identified axial forces and stresses as well as the identified fixity factors in the numerical error analysis of the single-bar systems.

Target system	Designation	Technique	ER1+ER2					
			N^{id}	σ^{id}	Δ	Δ	γ_{kr}^{id}	$\frac{\gamma_{kr}^{id}}{\gamma_{kr}^{true}}$
			[kN]	[N/mm ²]	[kN]	[%]	[-]	[-]
1	B1_S1_CS1	ARSM	7.16	22.79	-0.69	-9.64	0.38	-
		GA	7.63	24.29	-0.22	-2.88	0.06	-
		PSO	8.08	25.72	0.23	2.85	0.01	-
2	B1_S1_CS3	ARSM	7.74	24.64	-0.11	-1.42	0.51	0.98
		GA	8.02	25.53	0.17	2.12	0.49	1.02
		PSO	7.99	25.43	0.14	1.75	0.46	1.09
3	B1_S2_CS2	ARSM	31.57	100.49	0.15	0.48	0.29	0.86
		GA	31.62	100.65	0.20	0.63	0.22	1.14
		PSO	31.44	100.08	0.02	0.06	0.26	0.96
4	B1_S2_CS4	ARSM	31.29	99.60	-0.13	-0.42	0.77	0.97
		GA	31.52	100.33	0.10	0.32	0.75	1.00
		PSO	31.32	99.69	-0.10	-0.32	0.74	1.01
5	B1_S3_CS3	ARSM	54.82	174.48	-0.16	-0.29	0.45	1.11
		GA	54.82	174.50	-0.16	-0.29	0.49	1.02
		PSO	54.85	174.59	-0.13	-0.24	0.50	1.00
6	B1_S3_CS5	ARSM	54.79	174.40	-0.19	-0.35	0.94	1.01
		GA	54.80	174.43	-0.18	-0.33	0.95	1.00
		PSO	55.00	175.07	0.02	0.04	0.95	1.00
7	B2_S1_CS2	ARSM	7.83	24.92	-0.02	-0.26	0.25	1.00
		GA	7.26	23.10	-0.60	-8.26	0.26	0.95
		PSO	8.00	25.46	0.15	1.88	0.24	1.05
8	B2_S2_CS3	ARSM	30.44	96.89	-0.98	-3.22	0.51	0.99
		GA	31.43	100.03	0.01	0.03	0.49	1.02
		PSO	31.22	99.39	-0.19	-0.61	0.51	0.98
9	B2_S3_CS4	ARSM	54.43	173.26	-0.55	-1.01	0.75	1.01
		GA	55.30	176.02	0.32	0.58	0.76	0.99
		PSO	55.08	175.34	0.11	0.20	0.76	0.99

Assumption: $\gamma_{kr}^{id} = \gamma_{kr1}^{id} = \gamma_{kr2}^{id}$.

sensor position was assumed as 0.5 mm. Sensor noise, assuming to be zero mean and white, was added in the time domain for each of the calculated response signals with a standard deviation of the assumed measurement noise of 10^{-5} ms^{-2} . The sensitivity of the sensors²³ has a maximum error in absolute value of 0.04 %. In the numerical study, MAES et al. (2013) assumed a single variation of each uncertain parameter, but chose the sign of the parameter variations such that a worst case scenario was obtained. The results show that the identified axial force was affected by small errors in the input parameters. Besides, the error sensitivity was dependent on the mode considered. The error of the axial force when considering the first mode of vibration is 5.32 %; for all other modes of the six modes considered, higher errors were obtained.

In the present work, an error analysis study was carried out to examine the influence of the measurement and modelling errors on the axial force identification and joint flexibility estimation. The selected uncertainty types are shown in Table 3.10. They are uncertainties related to the structural parameters, including errors in the stiffness and mass parameters. The errors in the damping parameters for truss-type structures are excluded, as discussed by PARK et al. (2006) that the effect of the damping change to the resonant frequencies is negligibly small.

In Table 3.11, the results of the error analyses for the single-bar systems are provided. The optimization by the proposed methodology involves 11 updating parameters of the axial force and joint rigidity factor as well as the uncertain parameters in the error cases ER1 and ER2, in which the parameters concerning the sensor location correspond to five sensor locations. The updating parameters were varied simultaneously. The unknown axial force and rigidity factor were varied in the ranges as indicated in Table 3.7, while the other uncertain parameters were varied in the assumed ranges as defined in Table 3.10. For the sake of simplicity, only nine target systems were included.

The axial forces can still be identified reasonably accurately under the impact of the uncertainties in the structural parameters. The rigidity factor of the end constraints can be also identified fairly well due to the impact of the uncertainty in the structural parameters. Regarding the absolute deviations, the largest deviation to the true force is -0.98 kN by the ARSM, corresponding to a relative error of -3.22% to the true force.

3.2.7 Estimation of Joint Stiffness at Symmetric Locations of Structures

As mentioned, the identification problem of the end constraint stiffnesses of a single bar is symmetric. It means the updating algorithm fails in assigning the rotational stiffness to the proper bar end, as a change of the boundary condition at one end would yield identical output response of the modal parameters to the same change of the boundary

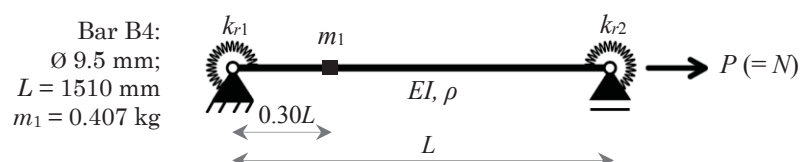


Figure 3.13 – Single bar model with an added mass.

²³ A sensor characteristic used for the conversion of a sampled voltage signal to an acceleration signal [MAES et al. (2013)]. In practice, the sensitivity of a sensor is often determined for a single, fixed calibration frequency.

Table 3.12 – Parameters of target systems for the numerical study of the bar B4 with added mass.

Target system	Designation	N^{true} [kN]	σ^{true} [N/mm ²]	k_{r1}^{true} [kNm/rad]	γ_{kr1}^{true} [-]	k_{r2}^{true} [kNm/rad]	γ_{kr2}^{true} [-]
1	B4m_S1_CS1_CS4	1.72	25	0.00	0.00	0.49	0.75
2	B4m_S2_CS4_CS2	7.09	100	0.49	0.75	0.05	0.25
3	B4m_S3_CS3_CS5	12.40	175	0.16	0.50	3.09	0.95

Assumption: k_{r1} and k_{r2} – two different rotational spring stiffness at bar ends.

condition at the other end. So far, the stiffnesses of the two end constraints of the single-bar systems were assumed identical.

FRISWELL and MOTTERSHEAD (1995) has discussed a technique called perturbed boundary condition testing. Using this technique, the structure can be tested in slightly different configurations or with added mass or springs to increase the amount of data available. GENTILINI et al. (2013) studied the vibration of modified beam system and made use of added mass for the structural parameter identification of tie-bars.

The identification of the different boundary conditions of a bar is examined next, assuming the rotational spring stiffnesses of the two end constraints are not identical. The technique using an added mass is applied, in which a mass is added near one end of a bar to make the system unsymmetrical. The position and size of the added mass should be selected to influence considerably the dynamic behaviour of the system. Some discussions about the position and size of an added mass are given in the work of GENTILINI et al. (2013).

In the case of the bar B4, an added mass of 0.407 kg is located at approximately 453 mm to one bar end (see Figure 3.13). The bar is 1510 mm long. In the numerical model, the mass was included using a point mass element.

Three case studies of target systems of the single bar B4 with added mass were carried out. The characteristics of the case studies are provided in Table 3.12. The axial loads were chosen that allow low to relatively high states of stress, i.e. 25 N/mm² to 175 N/mm². The rotational spring stiffnesses of the two end constraints were chosen to represent random non-identical constraint flexibility.

The results of the identified tensile forces are given in Table 3.13, while the results of the identified fixity factors are provided in Table 3.14. The axial forces were identified very well. The different rotational spring stiffnesses at the two ends were also identified correctly. For the second target system, the ratios of the identified to the true rigidity

Table 3.13 – Results of the identified axial forces and corresponding stresses in the numerical study of the single bar B4 with added mass.

Target system	Designation	Technique	N^{id} [kN]	σ^{id} [N/mm ²]	Δ [kN]
1	B4m_S1_CS1_CS4	ARSM	1.69	23.87	-0.03
		GA	1.76	24.77	0.04
		PSO	1.72	24.31	0.00
2	B4m_S2_CS4_CS2	ARSM	7.01	98.87	-0.08
		GA	7.06	99.56	-0.03
		PSO	7.02	99.08	-0.07
3	B4m_S3_CS3_CS5	ARSM	12.31	173.64	-0.09
		GA	12.28	173.26	-0.12
		PSO	12.43	175.32	0.03

Table 3.14 – Results of the rotational spring stiffness and fixity factors in the numerical study of single bar B4 with added mass.

Target system	Designation	Technique	k_{r1}^{id}	γ_{kr1}^{id}	$\frac{\gamma_{kr1}^{id}}{\gamma_{kr1}^{true}}$	k_{r2}^{id}	γ_{kr2}^{id}	$\frac{\gamma_{kr2}^{id}}{\gamma_{kr2}^{true}}$
			[kNm/rad]	[-]	[-]	[kNm/rad]	[-]	[-]
1	B4m_S1_CS1_CS4	ARSM	0.03	0.17	–	0.56	0.78	1.04
		GA	0.01	0.04	–	0.50	0.76	1.01
		PSO	0.02	0.11	–	0.54	0.77	1.03
2	B4m_S2_CS4_CS2	ARSM	0.52	0.76	1.01	0.07	0.30	1.20
		GA	0.53	0.76	1.01	0.06	0.26	1.04
		PSO	0.51	0.76	1.01	0.07	0.29	1.16
3	B4m_S3_CS3_CS5	ARSM	0.19	0.54	1.08	3.77	0.96	1.01
		GA	0.19	0.53	1.06	4.22	0.95	1.01
		PSO	0.16	0.49	0.98	2.94	0.95	1.00

factors of the second boundary condition by the ARSM and PSO are not as close to 1.00 as the other cases due to the small value of the end rotational spring stiffness. For other cases, the ratios of the identified rigidity factors to the true ones indicate a good agreement.

The numerical case studies of the single bars reveal that the proposed methodology with the use of the added mass in a non-symmetric position allows to identify different values of the rotational stiffness of the bar ends.

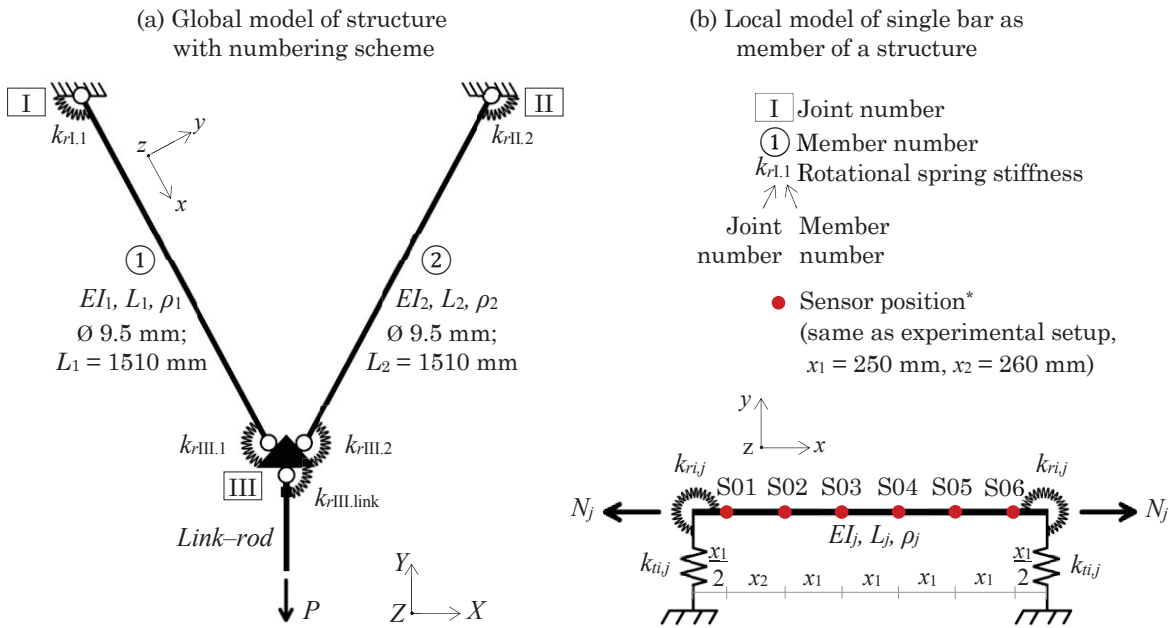
3.3 Two-Bar System

Numerical study has been carried out for the fundamental single-bar systems, whose vibration modes are identical in-plane and out-of-plane. The issue related to closely-spaced in-plane and out-of-plane modes of structural systems as well as similar modes of vibration due to coupled vibration of connected truss members is not addressed yet.

Considering an example of a two-member structure as shown in Figure 3.14(a). The structure has non-identical modes of vibration in the three-dimensional space. At joints, rotational springs are introduced to account for the unknown joint stiffness of the connections. As previously mentioned, the connection elements were modelled with torsional spring-damper elements (COMBIN14) in ANSYS®. The torsional spring-damper is purely rotational element with no mass and has three degrees of freedom at each node, i.e. rotations about the nodal x , y , and z axes. A spring constant was defined for each spring considered. When a single member of the structure is analysed, a beam model is assumed with translational and rotational springs (see Figure 3.14 (b)).

To evaluate the effects of joint flexibility and stress stiffening effects of the two-bar structure, four case studies were considered, i.e. pinned vs. rigid systems and zero- vs. high-load systems. Similar to the case studies of single bars, the rotational spring stiffness of all connections were assumed to be infinitesimal for the pinned system and tend to infinity for the rigid system. Two values of the applied load were assumed to be zero and 30 kN. The load of 30 kN for the high-load system results in an axial force and normal stress of approximately 17.14 kN and 242 N/mm² in each of the two members.

The results of the static analysis show that the assumption of pinned or rigid joints have insignificant effects on the stresses of the members. Compared to the normal stress, the



*In-plane degrees of freedom assumed to be from experiments are at six locations of instrumented sensors (S01 to S06) on a member, in the longitudinal and vertical directions of the member in its local coordinate system, i.e. x - and y -directions. For the analytical-based algorithm, S02 to S06 are used.

Figure 3.14 – Symmetric two-bar system for global and local analyses.

bending stress due to own weight of the considered member as well as the rotational stiffness of the joints is nearly negligible (see Appendix C).

Considering the dynamic analysis, the first sixteen modes of the pinned system are presented in Figure 3.15. As expected, the global modes of a structure are governed by the modal configurations of its members. Moreover, the constituted truss members vibrate interactively with each other in a coupling manner. As a result, similar vibration modes and closely-spaced in-plane and out-of-plane modes are found, for example the seventh mode to the tenth mode or the eleventh mode to the fourteenth mode.

Table 3.15 – Numerical natural frequencies of the first twelve modes the pinned and rigid symmetric two-bar structure without and with stress stiffening.

Mode	Pinned system ($k_r \rightarrow 0$)			Rigid system ($k_r \rightarrow \infty$)			
	$P = 0$ kN	$P = 30$ kN		$P = 0$ kN		$P = 30$ kN	
		f_n [Hz]	f_n [Hz]	Δ^* [%]	f_n [Hz]	Δ [%]	f_n [Hz]
1	7.14	36.52	411.66	10.61	48.60	42.17	490.80
2	7.40	42.43	473.50	16.65	125.08	51.70	598.87
3	8.80	58.70	566.86	19.58	122.46	65.09	639.55
4	9.71	59.42	511.93	19.71	102.95	64.98	569.24
5	10.18	64.35	532.25	34.38	237.82	78.10	667.33
6	13.71	61.21	346.50	25.92	89.04	71.23	419.56
7	33.79	120.99	258.02	53.60	58.59	134.18	297.05
8	34.11	120.25	252.58	56.93	66.91	134.69	294.92
9	34.19	120.65	252.93	48.94	43.15	140.98	312.40
10	34.26	122.82	258.55	59.46	73.57	137.50	301.40
11	75.41	189.75	151.64	104.49	38.57	210.18	178.73
12	75.85	191.40	152.35	107.64	41.92	215.13	183.64

*Difference to the natural frequency of the pinned zero-load system.

It is noted that for the investigated two-member system, the different geometrical characteristics of the connection plate in the three-dimensional space result in changed stiffness of the connection elements in-plane and out-of-plane. In addition, the vibration of the structure is associated with the coupled vibration of all the structural components of the system. Therefore, the modal parameters of some in-plane and out-of-plane vibration modes of the two-member system are highly similar but not identical.

In Table 3.15, the frequency values of the pinned and rigid two-bar systems considering stress stiffening are given. Due to the effects of the joint rigidity as well as stress stiffening, several modes of the rigid system and high-load system are interchanged with those of the pinned zero-load system, for instance the fifth and sixth modes. The order

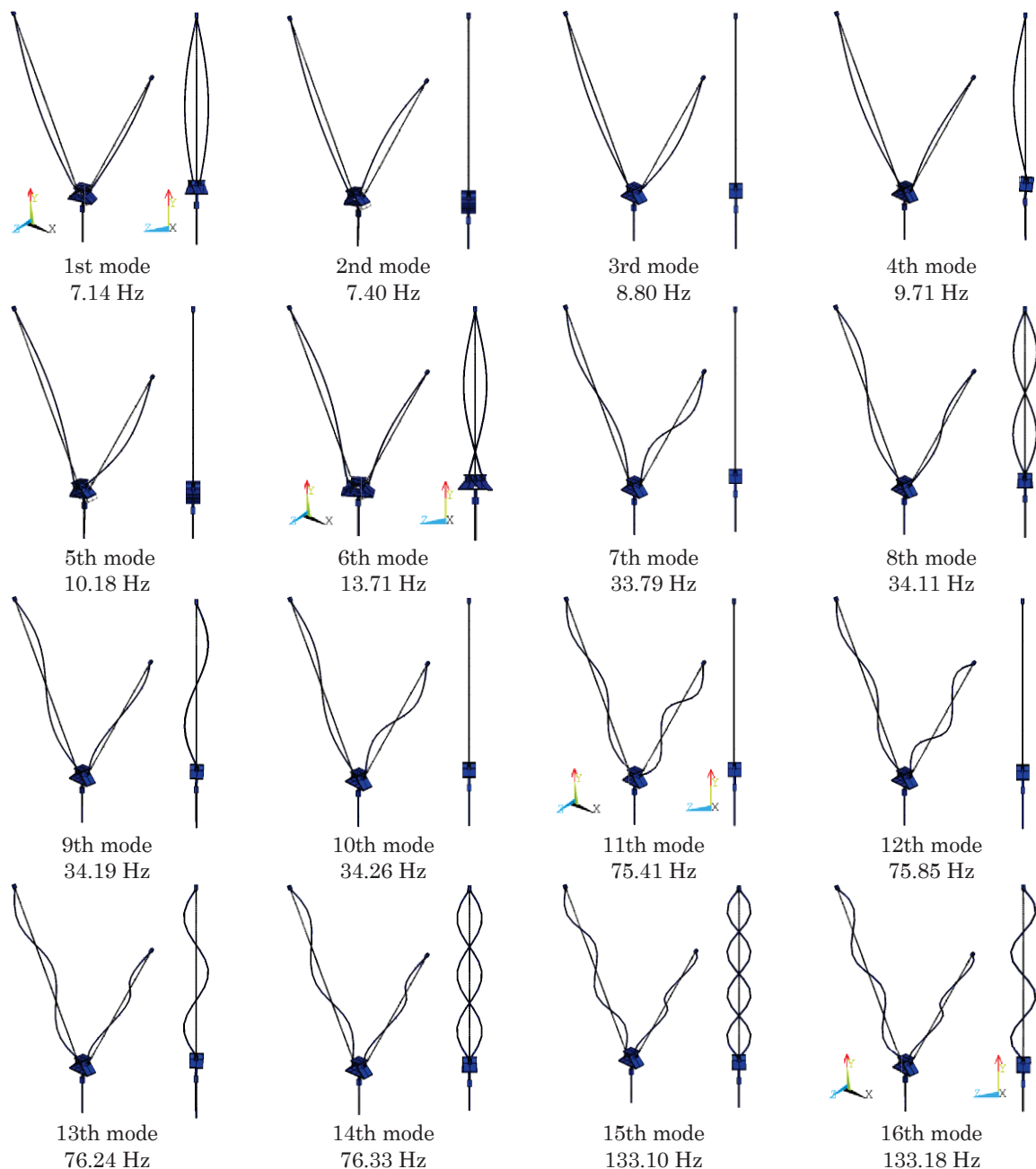


Figure 3.15 – Numerical natural frequencies and mode shapes of first sixteen modes of pinned system at zero-applied load in the numerical study of symmetric two-bar structure.

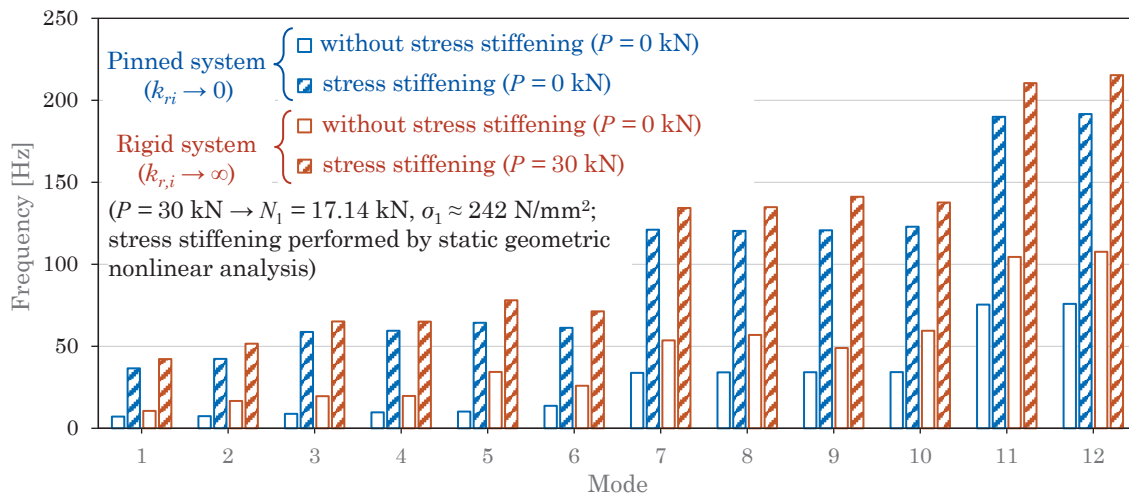


Figure 3.16 – Numerical natural frequencies of the first twelve modes of pinned vs. rigid system with and without stress stiffening in the numerical study of symmetric two–bar structure.

of the modes in Table 3.15 are sorted according to the modes of the pinned zero–load symmetric two–bar system.

In Figure 3.16, the natural frequencies of the pinned and rigid systems of the two–bar structure without and with the stress stiffening are presented. The effect of the stress stiffening is significant, as a wide variation of the stress was considered. The effect of the joint flexibility can be also seen on the natural frequencies of the systems. Similar conclusion for the two–bar structure to the single bar is that the numerical model should consider the unknown joint stiffness to correctly approximate the structural dynamics.

3.3.1 Global and Local Analyses of Truss Structures

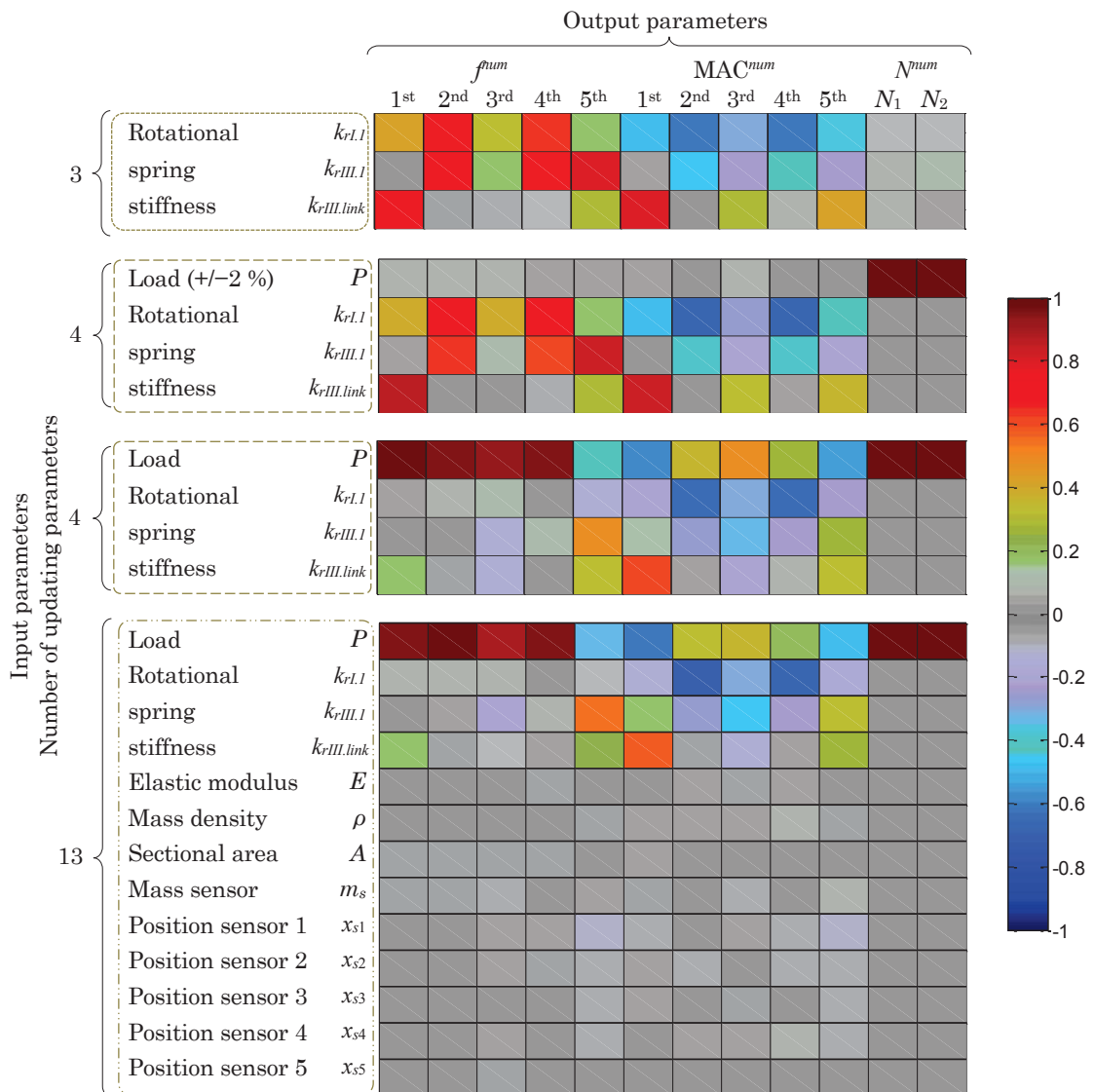
Considering the different approaches in the literature and for clarity, global analysis is referred in this work as analysis of the whole structure, while local analysis is associated with analysis of single truss members. The aspects relating the global and local modal configurations as well as coupled vibration of truss members are discussed.

For truss structures, the constituent truss members form a global coupled system. The coupled vibration of the member depends on the member connectivity at the joints, as well as the level of loading. In addition, when comparing the natural frequencies of a single member (i.e. Table 3.5) with that of the two–bar structure (i.e. Table 3.15), the slenderness of the truss members governs the magnitudes of the truss frequencies. For example, the first mode of vibration of the pinned zero–load single bar B4 at 8.36 Hz can be correlated to the third mode of the pinned zero–load two–bar structure at 8.80 Hz, where the vibration mode of the individual member of the two–bar structure is in the same form with that of the first mode of the single bar. The single bar type B4 has the same characteristics as the member of the two–bar structure. The difference in the values of the frequency is due to the modelling of the end portions of the members of the two–bar structure to the connections. Moreover, the second and third modes of the pinned zero–load single bar B4 at 33.42 Hz and 75.17 Hz can be correlated to the seventh and eleventh modes of the pinned zero–load two–bar structure at 33.79 Hz and 75.41 Hz. When the stress stiffening is considered, for instance the first three modes of the rigid high–load single bar B4 can be correlated to the third, seventh and eleventh modes of the rigid high–load two–bar structure, respectively.

3.3.2 Sensitivity Analysis

For the application and verification of the proposed methodology, three target systems were considered for the two-bar structure to simulate the experimental data. The unknowns are the applied axial load P at the end of the link-rod and the stiffness of all the rotational springs (see Table 3.16).

Three values of the axial stress were chosen as 25, 100 and 175 N/mm² representing low, intermediate and high tensile stress in the two members. The values of the rotational springs were chosen randomly to represent different constraint flexibility. The rotational springs at the symmetric locations of the two-bar structure were assumed to have identical stiffness, resulting in three unknowns of the stiffness of the rotational springs.



*Load P varies only +/- 2 % of the true value; in other cases, load P varies full assumed range.

□ updating springs only □ updating load and springs □ updating all parameters

Figure 3.17 – Spearman correlation matrix between the parameters and responses of the numerical model of the first target system in the numerical study of symmetric two-bar structure.

Table 3.16 – Parameters of the target systems in the numerical study of symmetric two–bar structure.

Target system	p^{true} [kN]	N^{true} [kN]	σ^{true} [N/mm ²]	$k_{rI.1}^{true}$ [kNm/rad]	$\gamma_{krI.1}^{true}$ [-]	$k_{rIII.1}^{true}$ [kNm/rad]	$\gamma_{krIII.1}^{true}$ [-]	$k_{rIII.link}^{true}$ [kNm/rad]	$\gamma_{krIII.link}^{true}$ -
1	3.04	1.77	25.00	0.00	0.00	0.05	0.25	0.49	0.75
2	12.37	7.09	100.00	0.49	0.75	0.16	0.50	3.09	0.95
3	21.70	12.40	175.00	0.05	0.25	3.09	0.95	0.16	0.50

Assumptions: $k_{rI.1}^{true} = k_{rII.2}^{true}$; $k_{rIII.1}^{true} = k_{rIII.2}^{true}$.

As previously discussed, a sensitivity analysis is performed prior to the optimization process to examine the input parameters with significant influences on the structural output responses. The characteristics of the parameters in the sensitivity analysis can be referred to Table 3.7, except that the variation of the load is from zero to 30 kN.

The results of a global sensitivity analysis through Spearman correlation coefficient for the first target system of the two–bar structure are presented in Figure 3.17, which are based on 200 Latin hypercube samples. Similar to the result of the sensitivity analysis for the single bar, the member axial stresses have significant effect on the output parameters from the static as well as dynamic analyses of the numerical model. The joint flexibility affects considerably the modal parameters of the natural frequencies and mode shapes. Taking into account that the truss–like structure is modelled as symmetric, the geometrical characteristics of the connection plate are different in the three–dimensional space, which result in changed stiffness of the connection elements in–plane and out–of–plane. As a result, the influence of $k_{rIII.link}$ is most significant when the mode of vibration involves out–of–plane rotation of the connection plate. The influence of the joint flexibility is reduced when the effect of the load or stress stiffening is present.

3.3.3 Identification of Axial Force and Joint Stiffness

The proposed methodology was implemented using the first five simulated experimental modes to identify the load and the rotational spring stiffness of joints. The simulated experimental modes were assumed to be in–plane modes of vibration. The load was varied simultaneously with the spring stiffness or the fixity factors in the range from zero to 30 kN. The fixity factors were varied from 0 (pinned) to 0.99 (almost rigid). The values of the initial populations were assumed random with no pre–knowledge of the design parameters.

Table 3.17 – Results of the identified axial forces and stresses in the numerical study of symmetric two–bar structure.

Target system	Technique	P^{id} [kN]	Δ [kN]	N_1^{id} [kN]	σ_1^{id} [N/mm ²]	Δ [kN]	N_2^{id} [kN]	σ_2^{id} [N/mm ²]	Δ [kN]
1	ARSM	3.05	0.01	1.78	25.08	0.01	1.78	25.08	0.01
	GA	3.03	-0.01	1.77	24.91	-0.01	1.77	24.91	-0.01
	PSO	2.99	-0.04	1.75	24.65	-0.02	1.75	24.65	-0.02
2	ARSM	12.39	0.02	7.10	100.17	0.01	7.10	100.17	0.01
	GA	12.42	0.05	7.12	100.43	0.03	7.12	100.43	0.03
	PSO	12.41	0.04	7.11	100.32	0.02	7.11	100.32	0.02
3	ARSM	21.70	0.01	12.41	175.06	0.00	12.41	175.06	0.00
	GA	21.66	-0.04	12.38	174.71	-0.02	12.38	174.71	-0.02
	PSO	21.70	0.00	12.41	175.02	0.00	12.41	175.02	0.00

Table 3.18 – Results of the identified rotational spring stiffness and fixity factors in the numerical study of the symmetric two-bar structure.

Target system	Technique	$k_{r1.1}^{id}$	$\gamma_{kr1.1}^{id}$	$\frac{\gamma_{kr1.1}^{id}}{\gamma_{kr1.1}^{true}}$	$k_{rIII.1}^{id}$	$\gamma_{krIII.1}^{id}$	$\frac{\gamma_{krIII.1}^{id}}{\gamma_{krIII.1}^{true}}$	$k_{rIII.link}^{id}$	$\gamma_{krIII.link}^{id}$	$\frac{\gamma_{krIII.link}^{id}}{\gamma_{krIII.link}^{true}}$
		[kNm/rad]	[-]	[-]	[kNm/rad]	[-]	[-]	[kNm/rad]	[-]	[-]
1	ARSM	0.01	0.06	–	0.06	0.27	1.10	6.57	0.75	1.00
	GA	0.02	0.12	–	0.04	0.21	0.85	7.51	0.77	1.03
	PSO	0.03	0.13	–	0.06	0.25	1.01	6.99	0.76	1.01
2	ARSM	0.43	0.80	1.06	0.21	0.50	1.00	34.24	0.96	1.01
	GA	0.35	0.68	0.91	0.45	0.45	0.90	30.67	0.92	0.96
	PSO	0.39	0.71	0.95	0.16	0.50	1.00	38.01	0.94	0.99
3	ARSM	0.04	0.18	0.72	3.64	0.96	1.01	2.54	0.53	1.06
	GA	0.07	0.24	0.97	2.68	0.94	0.99	2.22	0.50	1.00
	PSO	0.07	0.27	1.10	2.90	0.95	1.00	2.19	0.50	0.99

Similar to the study of the single bar, the identified load from the first stage of optimization was applied in the second stage of optimization with an assumed variation of $\pm 2\%$ to account for possible error in the identification of the load. The narrow variation of the load was chosen in the second stage of optimization to allow dominant influences of the joint flexibility on the output parameters of the modal parameters.

The optimization of the two-bar model involved 4 design parameters (the load and 3 joint rigidity factors), 10 modal responses (5 natural frequencies and 5 MAC values) and 2 static forces in the two members. The results of the identified load and axial forces in the members of the symmetric two-bar structure are given in Table 3.17. An excellent agreement between the identified and true forces was obtained. The different optimization techniques provide similar results. The maximum difference between the identified forces and the true forces is 0.05 kN.

Table 3.18 gives the results of the identified rotational spring stiffness and fixity factors of the symmetric two-bar structure. A good agreement between the identified and the true fixity factors was acquired. For most of the cases, the ratios between the identified and the true fixity factors are close to one. The PSO provides slightly better results. The GA also provides satisfactory results. The ARSM gives for a case of the third target system a relatively low ratio of 0.72. However, it is worth mentioning that for this case, the value of the rotational spring stiffness is small. Thus, a small change in the value of the rotational spring stiffness can result in a considerable change in the value of the fixity factor. In other words, it is more difficult to identify accurately the rotational spring stiffness or the fixity factor for the cases of small values of the rotational spring stiffness.

The numerical results of the symmetric two-bar structure indicate that the proposed methodology is able to identify the axial forces as well as the joint stiffnesses of the two-bar truss-like structure. The assumption is identical joint stiffnesses at symmetric locations of the structure due to symmetric identification problem.

3.3.4 Error Analysis

As previously discussed, some deviations would be expected due to uncertainties in measurement data and structural properties. The impact of the uncertainties to the structural parameter identification of the two-bar structure is assessed by assuming variations of structural parameters as defined in Table 3.10, in addition to the variations of the axial forces and joint rigidity factors.

Table 3.19 – Results of the identified axial forces and stresses in the numerical error analysis of the symmetric two-bar structure.

Target system	Technique	P^{id}	Δ	N_1^{id}	σ_1^{id}	Δ	N_1^{id}	σ_2^{id}	Δ
		[kN]	[kN]	[kN]	[N/mm ²]	[kN]	[kN]	[N/mm ²]	[kN]
1	ARSM	2.87	-0.16	1.68	23.67	-0.09	1.68	23.67	-0.09
	GA	2.90	-0.14	1.69	23.88	-0.08	1.693	23.88	-0.08
	PSO	3.05	0.01	1.78	25.04	0.01	1.78	25.04	0.01
2	ARSM	12.38	0.01	7.09	100.08	0.01	7.09	100.08	0.01
	GA	12.38	0.01	7.10	100.11	0.01	7.096	100.11	0.01
	PSO	12.47	0.10	7.15	100.80	0.06	7.145	100.80	0.06
3	ARSM	21.55	-0.15	12.32	173.84	-0.08	12.32	173.82	-0.08
	GA	21.38	-0.31	12.23	172.48	-0.18	12.23	172.48	-0.18
	PSO	21.75	0.06	12.44	175.47	0.03	12.44	175.47	0.03

An optimization was carried out, in which all uncertain parameters were included into the optimization process. For simplicity, the focus of the error analysis was the identification of the load and the axial forces or corresponding stresses of the two-bar structure. The results of the identified forces and stresses are provided in Table 3.19. The forces can still be determined with a high level of accuracy. The largest absolute deviation of the identified load to the true one is -0.31 kN and to the true member force is -0.18 kN by the GA, corresponding to a relative error of -1.45 % to the true load.

3.3.5 Estimation of Joint Stiffness at Symmetric Locations of Structures

As examined for a single bar, the identification of different joint stiffnesses of symmetric locations is feasible with added mass. To investigate the possibility to estimate different joint stiffnesses at symmetric locations of the two-bar structure, several modifications were considered on the two-bar system to make the system unsymmetrical.

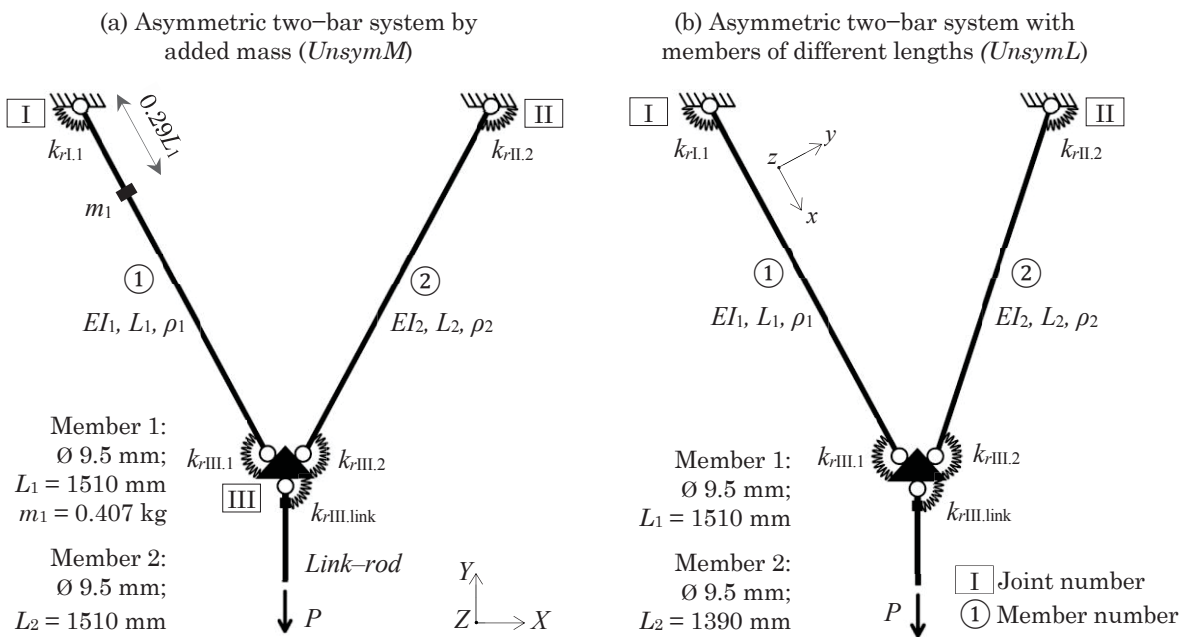


Figure 3.18 – Two types of asymmetric two-bar systems to examine the estimation of different joint stiffnesses at symmetric locations of the structure.

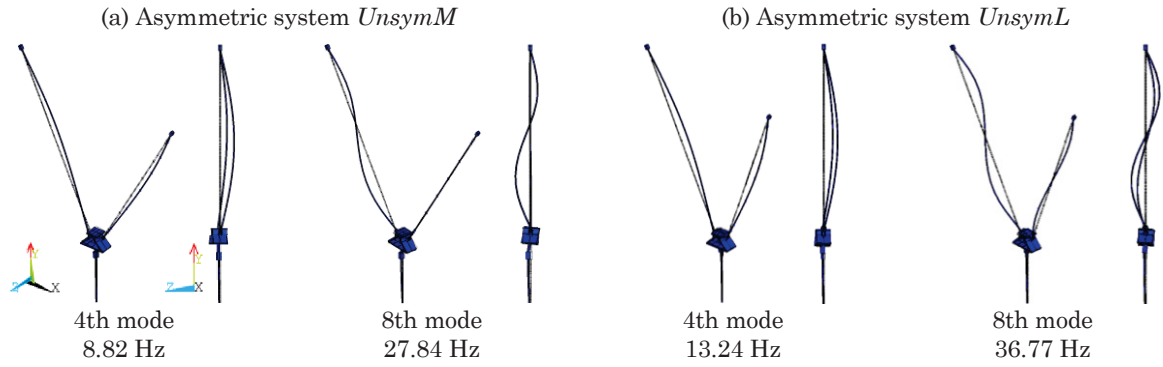


Figure 3.19 – Examples of numerical natural frequencies and mode shapes of the asymmetric two-bar systems assuming pinned connections at zero-applied load showing different vibration behaviour of the two members.

Two types of an asymmetric two-bar structure were investigated. The first asymmetric two-bar system is named *UnsymM*. For this system, a mass of 0.407 kg is added to one of the two members, i.e. the first member, at a distance of 440 mm to the higher end of the member (see Figure 3.18(a)). The position of the added mass was chosen based on the dynamic analyses examining different locations of the mass. At the selected location, the effect of the mass is sufficiently significant on the vibration behaviour of the structure compared to the system without mass.

The second asymmetric two-bar system is referred to as *UnsymL*, which is formed by concerning different lengths of the two members (see Figure 3.18(b)). This system has one member of about 1510 mm long and the other member is approximately 1390 mm long. The system *UnsymL* was examined as it is interesting to investigate the identification of the joint stiffnesses that is not bounded by a symmetric identification problem. For existing structures in practice, the technique of added mass can be applied, but the modification of the member lengths is not applicable to existing structures.

The vibration characteristics of the asymmetric two-bar systems are compared with that of the symmetric system. Figure 3.19 demonstrates two examples of the vibration modes of the systems *UnsymM* and *UnsymL*. Unlike the symmetric two-bar structure, the two

Table 3.20 – Parameters of the axial forces and corresponding stresses of the target systems in the numerical study of the asymmetric two-bar structures.

Target system	Asymmetric system	P_1^{true} [kN]	N_1^{true} [kN]	σ_1^{true} [N/mm ²]	N_2^{true} [kN]	σ_2^{true} [N/mm ²]
1	<i>UnsymM</i>	3.04	1.77	25.01	1.77	25.00
2	<i>UnsymM</i>	21.70	12.40	175.00	12.41	175.00
3	<i>UnsymL</i>	12.37	5.38	75.84	7.95	112.12

Table 3.21 – Parameters of the rotational spring stiffness and fixity factors of the target systems in the numerical study of the asymmetric two-bar structures.

Target system	Asymmetric system	$k_{rI.1}^{true}$ [kNm/rad]	$\gamma_{krI.1}$ [-]	$k_{rIII.1}^{true}$ [kNm/rad]	$\gamma_{krIII.1}$ [-]	$k_{rIII.link}^{true}$ [kNm/rad]	$\gamma_{krIII.link}^{true}$ [-]	$k_{rII.2}^{true}$ [kNm/rad]	$\gamma_{rII.2}^{true}$ [-]
1	<i>UnsymM</i>	0.49	0.75	0.00	0.00	0.74	0.25	0.16	0.50
2	<i>UnsymM</i>	0.05	0.25	3.09	0.95	2.23	0.50	0.49	0.75
3	<i>UnsymL</i>	0.16	0.50	0.05	0.25	6.68	0.75	3.09	0.95

Assumptions: $k_{rIII.2}^{true} = k_{rII.2}^{true}$ (for *UnsymM*); $k_{rIII.2}^{true} = k_{rIII.1}^{true}$ (for *UnsymL*).

members of the asymmetric systems vibrate more distinctly. When both members vibrate, the modified member with the added mass of the *UnsymM* and the shorter member of the *UnsymL* vibrate not as strongly as the other member.

The parameters of the target systems for the asymmetric two–bar structures are given in Table 3.20 for the load, axial forces and corresponding stresses, as well as in Table 3.21 for the rotational spring stiffness and fixity factors. The three target systems have different states of stress from low, intermediate to relatively high, i.e. 25 N/mm² to 175 N/mm². It is noted that for the system *UnsymM*, the added mass has small effect on the stresses of the members. As a result, the two members have nearly identical stresses. However, for the system *UnsymL*, reasonably, the two members experience highly different stresses. The applied load of about 12 kN results in an axial force of approximately 5.4 kN in the first member and nearly 8.0 kN in the second shorter member, as well as an equivalent normal stress of about 76 N/mm² in the first member and 112 N/mm² in the second member.

For the implementation of the proposed methodology, the unknowns were assumed to be the load applied at the end of the link–rod and the rotational spring stiffness of four among the five joints. To focus on the identification of the rotational spring stiffness at the higher end of the second member, which was assumed to be identical to that of the first member for the symmetric two–bar structure, and to simplify the identification problem, four among the five unknowns of the rotational spring stiffness were considered, in comparison to three in the case of the symmetric system.

Table 3.22 – Results of the identified axial forces and stresses in the numerical study of the asymmetric two–bar structures *UnsymM* and *UnsymL*.

Target system	Technique	P^{id}	Δ	N_1^{id}	σ_1^{id}	Δ	N_2^{id}	σ_2^{id}	Δ
		[kN]	[kN]	[kN]	[N/mm ²]	[kN]	[kN]	[N/mm ²]	[kN]
1	ARSM	3.05	0.01	1.78	25.14	0.01	1.78	25.14	0.01
	GA	2.96	-0.08	1.73	24.36	-0.05	1.73	24.35	-0.05
	PSO	3.12	0.09	1.82	25.69	0.05	1.82	25.69	0.05
2	ARSM	21.71	0.01	12.41	175.02	0.01	12.41	175.05	0.01
	GA	21.72	0.02	12.42	175.07	0.02	12.42	175.09	0.02
	PSO	21.76	0.06	12.44	175.49	0.04	12.44	175.50	0.04
3	ARSM	11.67	-0.70	5.07	71.53	-0.31	7.50	105.84	-0.45
	GA	11.70	-0.66	5.09	71.75	-0.29	7.52	106.15	-0.42
	PSO	11.76	-0.61	5.11	72.15	-0.26	7.56	106.64	-0.39

Table 3.23 – Results of the identified rotational spring stiffness and fixity factors in the numerical study of the asymmetric two–bar structures *UnsymM* and *UnsymL*.

Target system	Technique	$k_{rI.1}^{id}$	$\gamma_{krI.1}^{id}$	$\frac{\gamma_{krI.1}^{id}}{\gamma_{krI.1}^{true}}$	$k_{rIII.1}^{id}$	$\gamma_{krIII.1}^{id}$	$\frac{\gamma_{krIII.1}^{id}}{\gamma_{krIII.1}^{true}}$	$k_{rIII.link}^{id}$	$\gamma_{krIII.link}^{id}$	$\frac{\gamma_{krIII.link}^{id}}{\gamma_{krIII.link}^{true}}$	$k_{rII.2}^{true}$	$\gamma_{krII.2}^{true}$	$\frac{\gamma_{krII.2}^{id}}{\gamma_{krII.2}^{true}}$
		[kNm/rad]	[-]	[-]	[kNm/rad]	[-]	[-]	[kNm/rad]	[-]	[-]	[kNm/rad]	[-]	[-]
1	ARSM	0.45	0.73	0.98	0.00	0.00	-	0.71	0.24	0.97	0.15	0.48	0.95
	GA	0.47	0.74	0.99	0.00	0.02	-	0.72	0.24	0.98	0.17	0.50	1.01
	PSO	0.50	0.75	1.01	0.00	0.00	-	0.74	0.25	1.00	0.17	0.51	1.01
2	ARSM	0.04	0.20	0.79	3.07	0.95	1.00	2.25	0.50	1.01	0.48	0.75	0.99
	GA	0.07	0.31	1.25	4.29	0.96	1.01	2.96	0.57	1.14	0.63	0.80	1.06
	PSO	0.14	0.35	1.39	0.49	0.75	0.79	2.57	0.54	1.07	1.32	0.89	1.19
3	ARSM	0.36	0.69	1.38	0.09	0.35	1.39	7.86	0.78	1.04	8.01	0.98	1.03
	GA	0.30	0.65	1.30	0.08	0.33	1.31	7.10	0.76	1.01	7.54	0.98	1.03
	PSO	0.24	0.60	1.20	0.08	0.33	1.32	5.65	0.72	0.96	6.13	0.97	1.03

For the system *UnsymM*, the rotational spring stiffnesses of the two ends of the second members were assumed identical. For the system for the system *UnsymL*, the rotational spring stiffnesses at the lower ends of the first and second members were assumed identical. Five simulated experimental in-plane modes were used.

The results of the identified forces are provided in Table 3.22. Very good results were obtained for the system *UnsymM* with a maximum difference of the identified to the true forces of 0.09 kN. Reasonable results were achieved for the system *UnsymL*, in which a maximum difference of the forces of -0.70 kN was obtained. The different optimization techniques give similar results.

In Table 3.23, the results of the identified rotational spring stiffness and fixity factors are shown. It was noted that small values of the rotational spring stiffness were more difficult to be estimated accurately, for example the rotational spring stiffness of the first member of the second and third target systems. However, a correct relation to a pinned and rigid condition of the different joint stiffnesses could be identified in general.

The numerical case studies of the asymmetric two-bar structures by added mass or modification of the length of the symmetric system reveal that the proposed methodology is able to provide reasonable estimation of different values of the rotational stiffnesses in a non-symmetric identification problem.

3.4 Five-Bar Truss System

Following the numerical study of the two-bar structure, a five-bar truss was developed and studied. The three-dimensional finite element model of the five-bar truss is presented in Figure 3.20. The programme ANSYS® was used. Two-node beam elements were used based on Timoshenko beam theory. The model for the five-bar truss has 225 nodes and 302 beam elements. For modeling the connections, rotational springs with varying stiffness are introduced to ten connection points at the beginning and end of the members and at the joint to the link-rod. The mechanical properties for the system were assumed as the mass density of 7850 kg/m^3 , the modulus of elasticity of $205\,000 \text{ N/mm}^2$ and the Poisson's ratio of 0.30. The geometrical and mechanical characteristics of the members of the five-bar truss is given in Table 3.24.

To illustrate the complication in the dynamic behaviour of a multiple-member truss-type structure when the number of members is increased, Figure 3.21 presents the natural frequency values of the modes up to 120 Hz of the five-bar truss in comparison to the two-bar system. The structures were assumed to be nearly rigid. As a multiple-member system gets more complex, the number of modes increases substantially. Besides, the five-bar truss consists of both tensile and compressive members. The frequency values of the compression members are reduced at higher applied forces,

Table 3.24 – Geometrical and mechanical properties of the five-bar truss in the numerical study.

Member	L [mm]	Cross-section [mm]	A [mm ²]	I [mm ⁴]	E [N/mm ²]	ρ [kg/m ³]	λ_s [–]
1	1493	Ø 9.5	70.9	399.8	205 000	7850	628.6
2	1484	Ø 9.5	70.9	399.8	205 000	7850	624.8
3	1917	Ø 9.5	70.9	399.8	205 000	7850	807.2
4	1066	L40x40x4	304.0	46081.0	205 000	7850	86.7
5	1060	L40x40x4	304.0	46081.0	205 000	7850	86.1
Link-rod	396	Ø 12	113.1	1017.9	205 000	7850	132

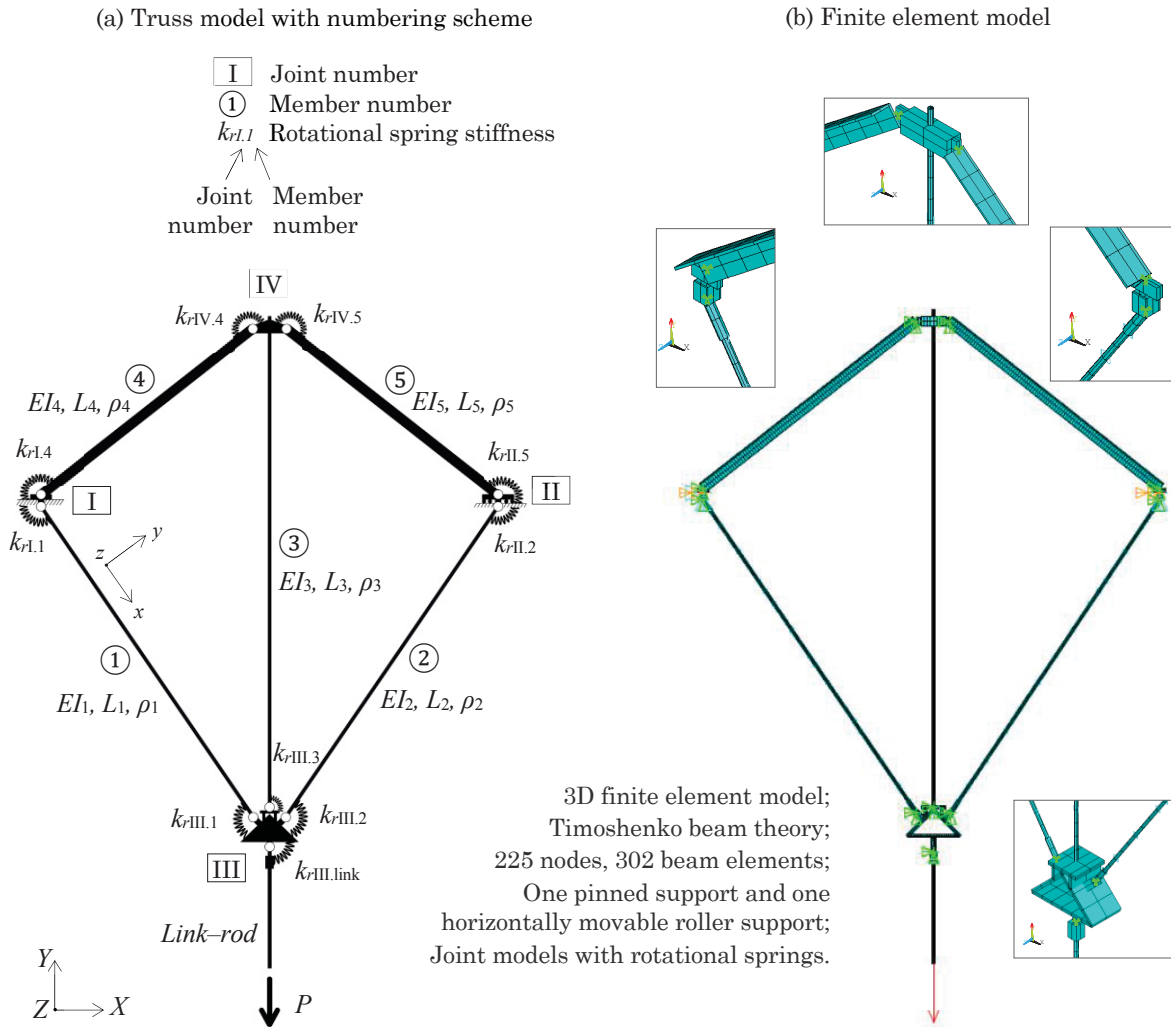


Figure 3.20 – Numerical global model of the five-bar truss system.

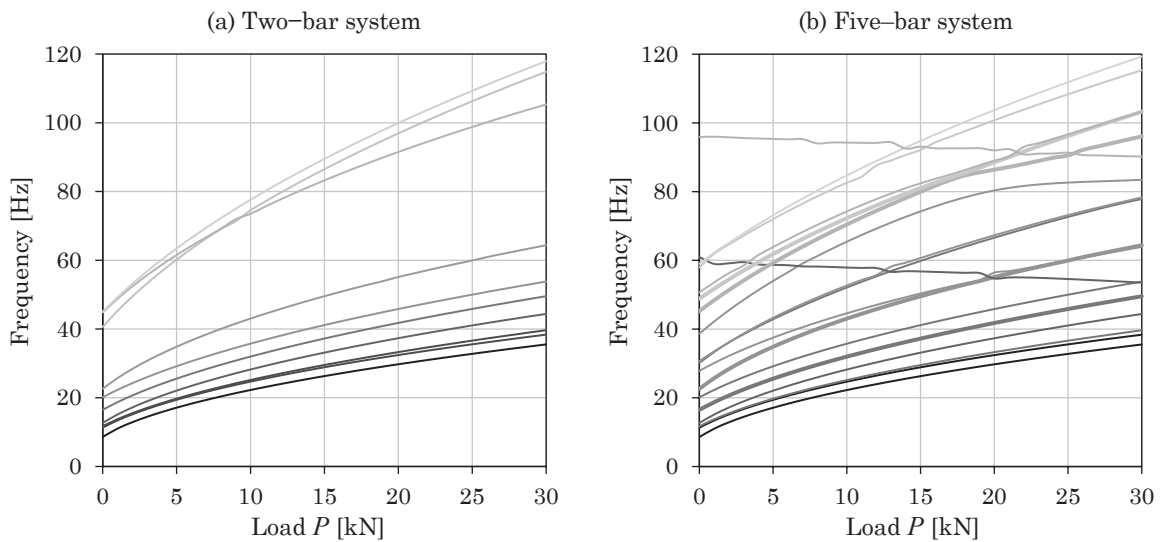


Figure 3.21 – Numerical natural frequencies of the modes in the frequency range up to 120 Hz of the two-bar and five-bar systems assuming nearly rigid joints.

Table 3.25 – Numerically calculated axial forces and normal stresses of the five-bar truss at different applied loads.

P [kN]	N [kN]					σ [N/mm ²]							
						Link							Link
	Bar 1	Bar 2	Bar 3	Bar 4	Bar 5	–rod	Bar 1	Bar 2	Bar 3	Bar 4	Bar 5	–rod	
5.0	2.00	2.03	1.73	-1.43	-1.44	5.0	28.29	28.68	24.46	-4.71	-4.75	44.26	
15.0	5.92	6.00	5.20	-4.22	-4.26	15.0	83.57	84.65	73.41	-13.89	-14.01	132.75	
25.0	9.83	9.96	8.68	-7.01	-7.07	25.0	138.75	140.52	122.50	-23.06	-23.26	221.24	
35.0	13.74	13.92	12.14	-9.81	-9.88	35.0	194.04	196.52	171.43	-32.27	-32.51	309.73	

whereas the frequency values of the tension members are increased. These counteracting effects by the coexistence of compressive and tensile forces in a truss cause intricate variation of frequencies as well as interchange of modes. Thus, attention must be paid in sorting a correct order of the modes when the load of the system is varied.

Numerical analyses were performed to understand the static and dynamic behaviour of the five-bar truss system. The static calculations of the axial forces and normal stresses of the five-bar truss due to different loads are provided in Table 3.25. A load from 5 kN to 35 kN results in a low to relatively high states of normal stress in the tension members, e.g. about 28 N/mm² to 194 N/mm² in the first member. Note that the five-bar truss is not absolutely symmetric. The axial forces and stresses in the first and second members are similar but not the same.

Regarding the dynamic analysis, the numerical model allows all the modes to be estimated. The modal natural frequencies and the modes of vibration are determined via free vibration. Figure 3.22 shows the first sixteen modes of a semi-rigid five-bar truss at zero-applied load. For this example, the assumed values of all fixity factors are not pinned but semi-rigid of 0.75 because it is interesting to observe the modes of vibration of the compression top chords, which occur at lower modes of the semi-rigid system than the pinned system. The natural frequencies of the five-bar truss are associated with different types of modes of vibration. A relevant classification for each mode is according to the in-plane and out-of-plane characteristics. The out-of-plane modes include the modal vibrations in translational direction of a three-dimensional space. Some in-plane

Table 3.26 – Parameters of the axial forces and stresses of the target systems in the numerical study of the five-bar structure.

Target system	P^{true} [kN]	N_1^{true} [kN]	σ_1^{true} [N/mm ²]	N_2^{true} [kN]	σ_2^{true} [N/mm ²]	N_3^{true} [kN]	σ_3^{true} [N/mm ²]
1	4.41	1.77	25.00	1.80	25.36	1.53	21.53
2	18.00	7.09	100.01	7.18	101.34	6.24	88.01
3	31.59	12.40	174.97	12.57	177.34	10.95	154.48

Table 3.27 – Parameters of the rotational spring stiffness and fixity factors of the target systems in the numerical study of the five-bar structure.

Target system	$k_{rI,1}^{true}$ [kNm/rad]	$\gamma_{krI,1}^{true}$ [-]	$k_{rIII,1}^{true}$ [kNm/rad]	$\gamma_{krIII,1}^{true}$ [-]	$k_{rIV,3}^{true}$ [kNm/rad]	$\gamma_{krIV,3}^{true}$ [-]	$k_{rIII,link}^{true}$ [kNm/rad]	$\gamma_{krIII,link}^{true}$ [-]	$k_{rIV,4}^{true}$ [kNm/rad]	$\gamma_{krIV,4}^{true}$ [-]
1	0.49	0.75	3.13	0.95	0.00	0.00	0.05	0.25	26.57	0.50
2	3.13	0.95	0.05	0.25	0.13	0.50	0.16	0.50	79.72	0.75
3	0.05	0.25	0.16	0.50	0.38	0.75	0.00	0.00	504.86	0.95

Assumptions: $k_{rI,1}^{true} = k_{rIII,1}^{true}$; $k_{rIII,1}^{true} = k_{rIII,2}^{true}$; $k_{rI,4}^{true} = k_{rIII,5}^{true} = k_{rIV,4}^{true} = k_{rIV,5}^{true}$.

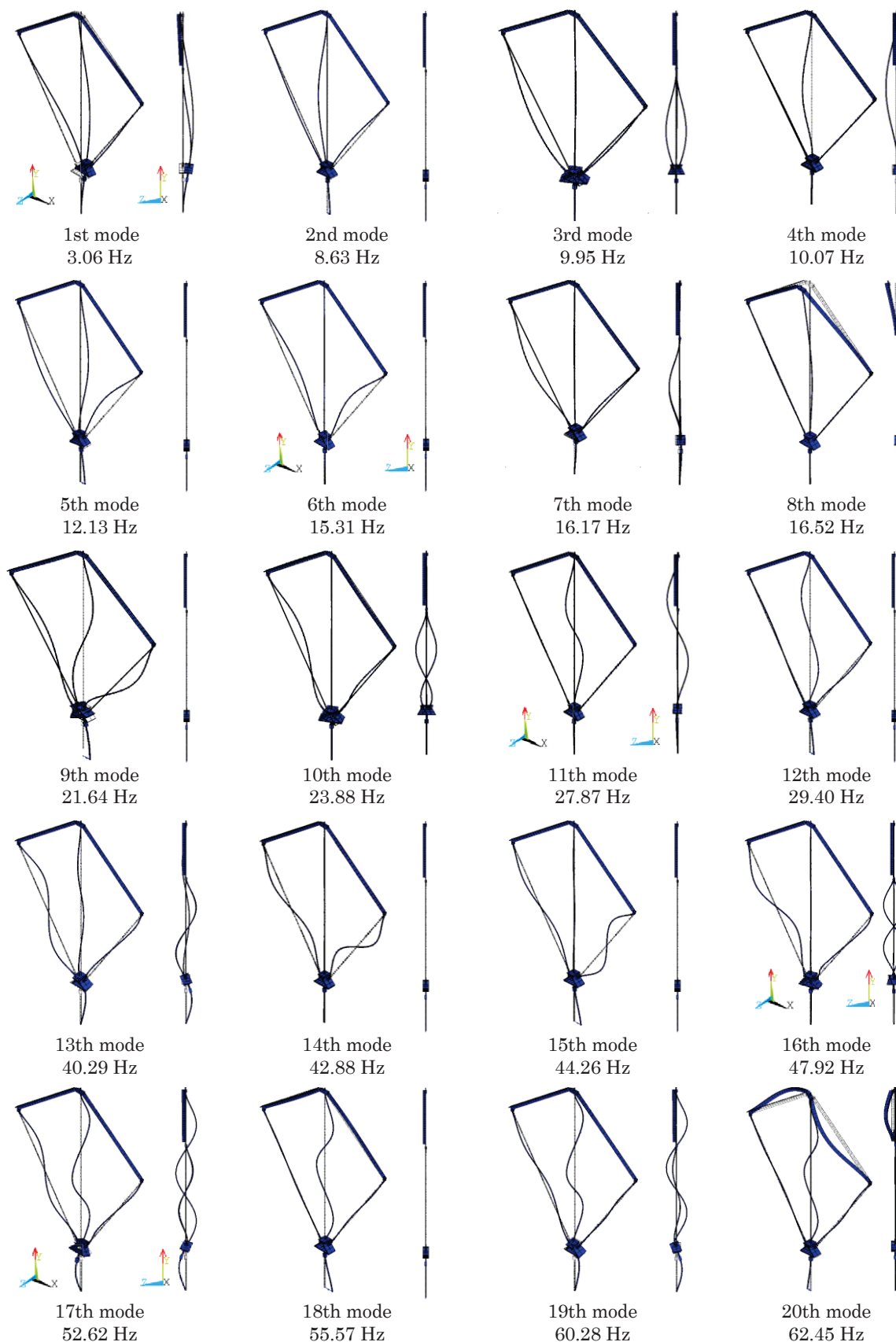


Figure 3.22 – Numerical natural frequencies and mode shapes of first sixteen modes of a semi-rigid five-bar truss ($\gamma_{kr} = 0.75$) at zero-applied force.

modes are coupled with out-of-plane modes. These particular modes are characterized by two sets of movements, in-plane and out-of-plane vibrations simultaneously or followed by one another (see mode 20th in Figure 3.22 for example).

Three target systems were considered for the implementation of the proposed methodology. The characteristics of the target systems are presented in Table 3.26 and Table 3.27. The unknowns are the applied load P at the end of the link-rod and the stiffness of the rotational springs. The rotational spring stiffness at symmetric location of the truss were assumed to have identical stiffness. The load P were chosen to result in three states of axial stresses of approximately 25, 100, and 175 N/mm² in the first member. The rotational spring stiffness were randomly chosen to represent different constraint flexibility, keeping into consideration the diversity of the case studies.

3.4.1 Mode Pairing Criteria

For the mode pairing, the technique making use of the modal strain energy (MSE) is discussed. GREENING and LIEVEN (2003) and BREHM et al. (2010) stated that the mode pairing task is complex because the order of the numerical modes change as a result of variations on the numerical parameters to be updated during the optimization process. In addition, the available numbers of degrees of freedom of experimental modes are often limited.

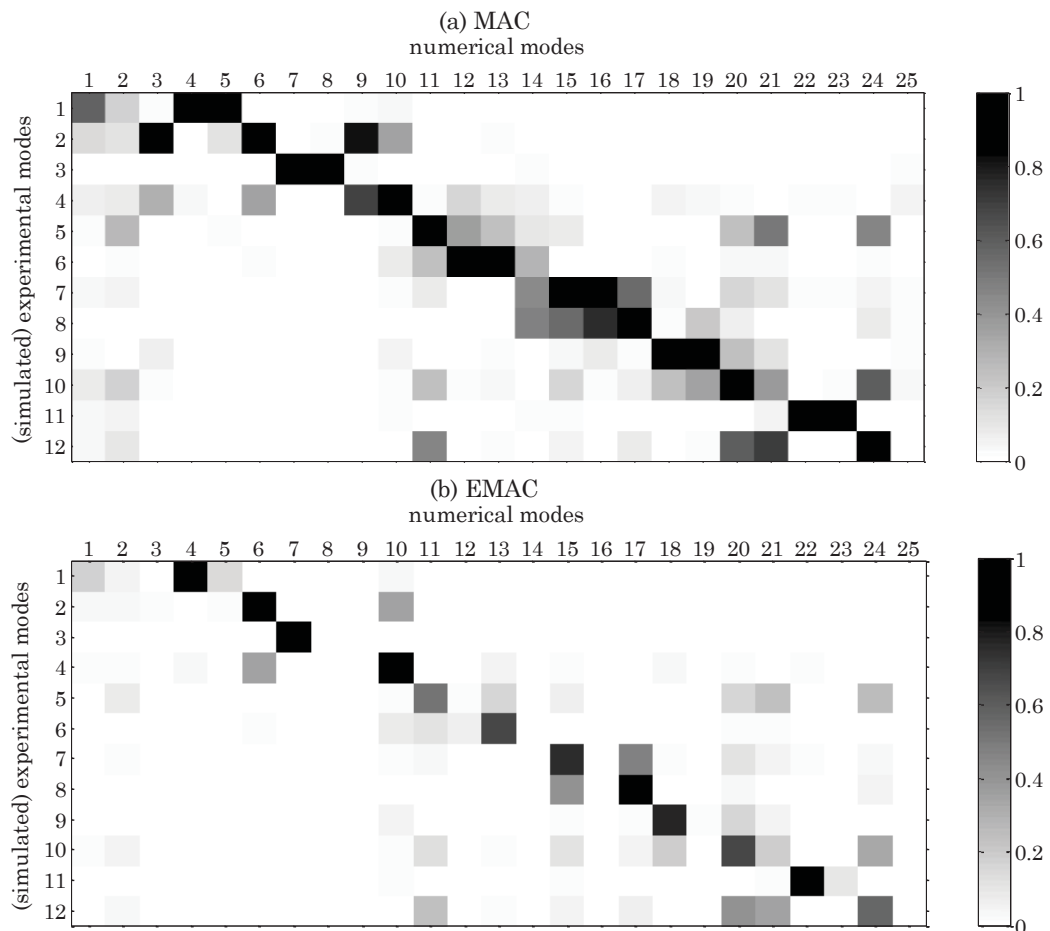


Figure 3.23 – Pairing of the simulated experimental and numerical frequencies by the MAC and EMAC in the numerical study for the second target system of the five-bar truss.

Based on the results of the modal analysis of the numerical model, the in-plane and out-of-plane modes of the five-bar truss can be closely-spaced and have similar modes of vibration. It was assumed that only the in-plane degrees of freedom of the modes are acquired from the experiments. Based on this assumption, the EMAC was applied for the mode pairing in addition to the MAC. The clusters of in-plane and out-of-plane degrees of freedom of a mode were selected separately. The MSE and relative MSE are calculated for the in-plane degrees of freedom.

To give an example of the mode pairing using the EMAC, the second target system at an intermediate state of stress was used. Twelve modes were chosen as simulated experimental modes for the second target system among thirty numerically calculated modes based on the values of the relative MSE of the in-plane degrees of freedom of at least 0.50 to allow a sufficient level of the vibration in-plane.

The simulated experimental and numerical modal parameters were computed based on the characteristics of the stress state and joint flexibility of the second target system. When the experimental modal parameters are available, the numerical modal parameters are calculated based on a five-bar truss system, whose stress state and joint fixity factors are generated randomly during each run of the optimization process of the proposed methodology.

For each mode, the MAC, MSE, relative MSE for the clusters of in-plane degrees of freedom and the EMAC were calculated. Figure 3.23 shows the MAC and EMAC values for the twelve simulated experimental modes and thirty numerical modes of the second target system of the five-bar truss.

As similar modes of vibration appear, for instance the in-plane and out-of-plane numerical seventh and eighth modes or the twenty-second and twenty-third modes, the traditional MAC was unable to assign reliably the correct numerical modes to the simulated experimental modes. The EMAC allows the classification of the mode shapes taking into account the relative MSE of the in-plane degrees-of-freedom of the truss. The EMAC shows correct assignments of the modes, illustrating the beneficial use of the EMAC for the mode pairing for truss structural systems.

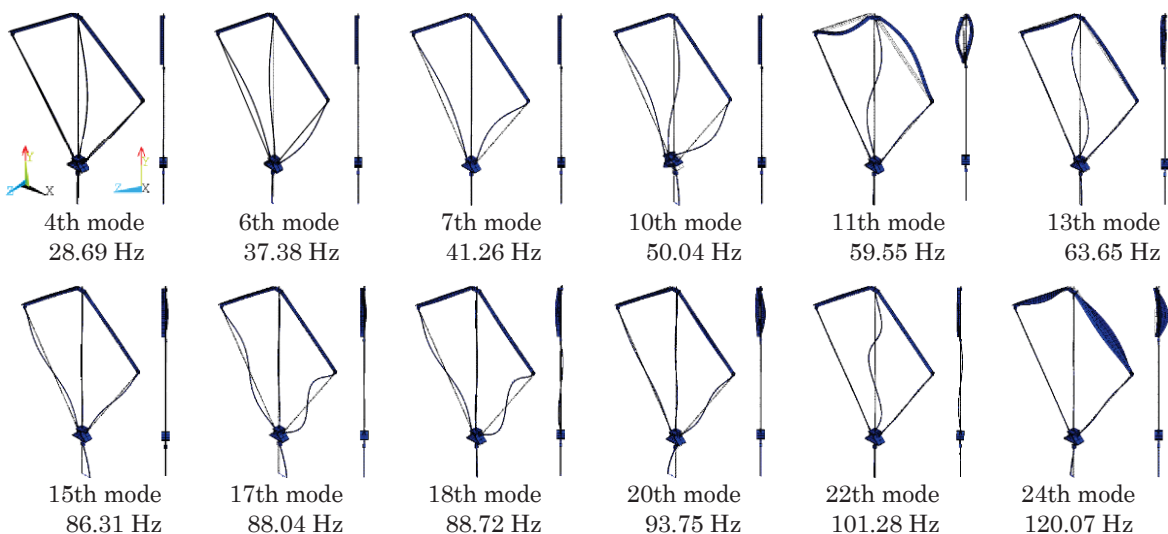


Figure 3.24 – Numerically calculated natural frequencies and mode shapes of twelve modes of the second target system as simulated experimental modes in the numerical study of the five-bar truss.

Table 3.28 – Relative modal strain energy (MSE) of members of the five-bar truss in the numerical study of the second target system.

Bar	Relative MSE											
	Simulated experimental mode											
	1	2	3	4	5	6	7	8	9	10	11	12
1	0.09	0.34	0.48	0.29	0.00	0.01	0.15	0.23	0.13	0.02	0.01	0.00
2	0.10	0.31	0.50	0.30	0.01	0.01	0.13	0.27	0.25	0.03	0.02	0.05
3	0.63	0.22	0.01	0.24	0.14	0.40	0.14	0.10	0.12	0.15	0.79	0.04
4	0.06	0.01	0.00	0.00	0.19	0.13	0.17	0.12	0.15	0.21	0.06	0.15
5	0.06	0.02	0.01	0.01	0.19	0.13	0.14	0.10	0.12	0.24	0.04	0.31
Link-rod	0.05	0.11	0.00	0.15	0.00	0.01	0.04	0.04	0.01	0.04	0.00	0.02
In-plane (total)	0.98	1.00	1.00	0.99	0.53	0.68	0.77	0.87	0.78	0.68	0.92	0.56
Out-of-plane (total)	0.02	0.00	0.00	0.01	0.47	0.32	0.23	0.13	0.22	0.32	0.08	0.44

3.4.2 Selection of Modes to use Analytical-based Algorithm

The proposed methodology uses information of the axial forces in selected individual members of the truss that are identified by the analytical-based algorithm by MAES et al. (2013). As previously explained, the analytical-based algorithm gives more than one solutions of the identified force for members of a truss structure, because each mode provides a solution of the identified force. The selection of the modes of individual bars for the use of the analytical-based methods is evaluated.

The relative MSE was calculated for individual members of a truss structure. The twelve simulated experimental modes of the second target system of the five-bar truss are presented in Figure 3.24. The results of the relative MSE of the twelve modes are shown in Table 3.28. For each mode, the vibration of each member in relation to other members and the dominant vibration of which members in certain modes can be recognized. For example, the third member, i.e. bar 3, the slenderest member of the five-bar truss structure, vibrates strongly in the first simulated experimental in-plane mode.

Table 3.29 – Selection of identified axial member forces based on analytical-based method using the relative MSE in the numerical study of the second target system of the five-bar truss.

Mode	Bar 1			Bar 2			Bar 3		
	$N_1^{true} = 7.09$ [kN]			$N_2^{true} = 7.18$ [kN]			$N_3^{true} = 6.24$ [kN]		
	N_1^{a*}	Δ	Π_1^{IP**}	N_2^a	Δ	Π_2^{IP}	N_3^a	Δ	Π_3^{IP}
	[kN]	[kN]	[-]	[kN]	[kN]	[-]	[kN]	[kN]	[-]
1	6.79	-0.30	0.09	6.91	-0.27	0.10	6.07	-0.17	0.63
2	6.82	-0.27	0.34	6.91	-0.28	0.31	6.06	-0.18	0.22
3	6.82	-0.27	0.48	6.91	-0.28	0.50	6.07	-0.17	0.01
4	6.82	-0.27	0.29	6.90	-0.28	0.30	6.04	-0.20	0.24
5	5.37	-1.72	0.00	7.50	0.32	0.01	6.05	-0.19	0.14
6	6.80	-0.29	0.01	6.88	-0.30	0.01	5.87	-0.37	0.40
7	6.69	-0.40	0.15	3.23	-3.95	0.13	5.87	-0.37	0.14
8	6.55	-0.54	0.23	6.74	-0.44	0.27	5.98	-0.26	0.10
9	6.57	-0.52	0.13	6.63	-0.56	0.25	6.04	-0.20	0.12
10	2.61	-4.48	0.02	5.97	-1.22	0.03	6.05	-0.19	0.15
11	7.12	0.03	0.01	6.94	-0.25	0.02	6.06	-0.18	0.79
12	9.91	2.82	0.00	8.44	1.26	0.05	5.21	-1.03	0.04

*Analytical-based method based on MAES et al. (2013);

**IP – in-plane;

■ Maximum value of relative MSE for modes in the form of the first vibration mode of a single bar.

To choose the modes for the use of the analytical-based method to be integrated into the proposed methodology, the mode with the highest relative MSE in the form of the first mode of a single beam was selected to avoid the issue regarding the zero-modal displacement at a node of a mode shape. The selection criterion agrees with the recommendations given by REBECCHI et al. (2013) about the selection of a proper flexural mode shape to increase the accuracy of the identified force.

Table 3.29 shows the identified axial forces of the first to third members based on the analytical-based method by MAES et al. (2013) for the twelve modes. Because the results for bar 4 and bar 5 for the L-profile members show however no satisfactory results, only the identified forces of the solid circular first to third members of the five-bar truss were used. Using the simulated experimental modal data, which are accurate

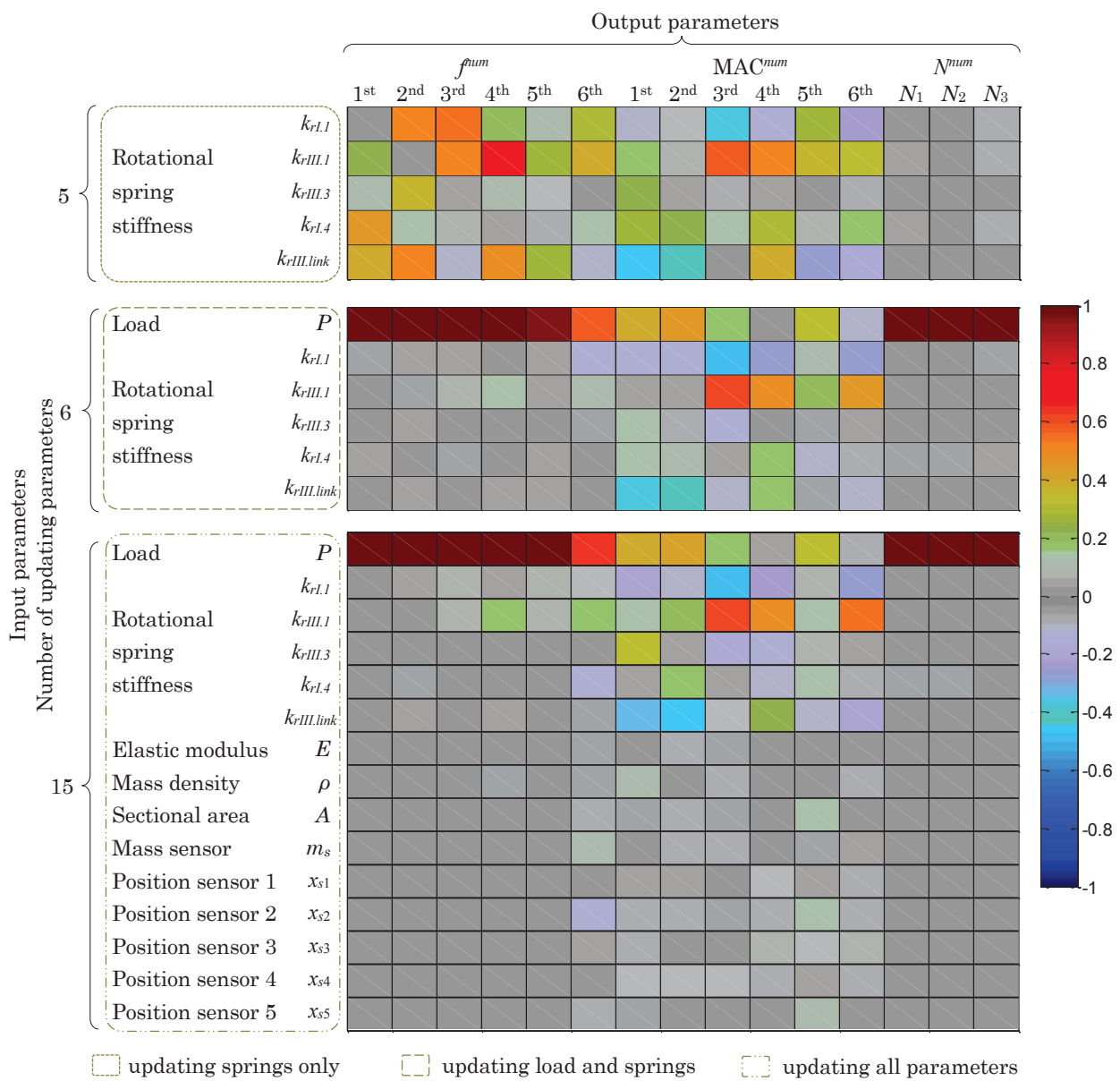


Figure 3.25 – Spearman correlation matrix between the parameters and responses using simulated experimental data of the third target system in the numerical study of the five-bar truss.

without the influence of experimental errors, the analytical-based method by MAES et al. (2013) provides in general a good match to the true axial forces. Variation of the identified forces occurs in some cases, due to mode shapes with small amplitudes that are in some cases close to a straight line or zero-modal displacement. Based on the maximum values of the indicator factor, the third mode was selected for the first and second bars, while the first mode was chosen for the third bar. The primary interest is the reliability of the selection of modes that can possibly give potentially correct results. The selected modes all give a highly reasonable estimation of the axial forces.

3.4.3 Sensitivity Analysis

The characteristics of the parameters of the numerical model, including their designation, the assumed lower and upper limits for the sensitivity analysis are based on Table 3.7, except that the variation of the load is from zero to 30 kN like for the two-bar system.

The results of the sensitivity analysis for the third target system of the five-bar truss are presented in Figure 3.25, which are based on 200 Latin hypercube samples. Similar to the sensitivity analyses of the single-bar and two-bar systems, the effects of the rotational springs are significant on the modal parameters, if the axial force effects are not dominant. The influences of the other parameters on the output responses are less significant compared to the load. The information obtained from the sensitivity analysis for the analysed numerical parameters is useful to apply the two-stage optimization process of the proposed methodology to identify the axial forces and joint flexibility of the five-bar truss.

3.4.4 Identification of Axial Forces and Joint Stiffness

It has been known from the sensitivity analysis that the load or the axial forces have significant influence on the static response as well as modal parameters. To implement the proposed methodology, the first six simulated experimental modes were used. The load was varied from zero to 30 kN, and the fixity factors were varied from 0 (pinned) to 0.99 (almost rigid). The initial values of the axial force and the rotational spring stiffness of the connections were assumed having no pre-knowledge of the true values, which are the values of the target systems.

Table 3.30 – Results of the identified axial forces and stresses in the numerical study of five-bar truss.

Target system	Technique	P^{id} [kN]	Δ [kN]	N_1^{id} [kN]	σ_1^{id} [N/mm ²]	Δ [kN]	N_2^{id} [kN]	σ_2^{id} [N/mm ²]	Δ [kN]	N_3^{id} [kN]	σ_3^{id} [N/mm ²]	Δ [kN]
1	ARSM	4.39	-0.02	1.77	24.90	-0.01	1.79	25.25	-0.01	1.52	21.44	-0.01
	GA	4.48	0.07	1.80	25.41	0.03	1.83	25.76	0.03	1.55	21.90	0.02
	PSO	4.42	0.01	1.78	25.01	0.01	1.81	25.37	0.01	1.54	21.54	0.01
2	ARSM	18.24	0.24	7.18	101.35	0.10	7.28	102.69	0.10	6.32	89.20	0.08
	GA	18.17	0.17	7.16	100.94	0.07	7.25	102.28	0.07	6.30	88.84	0.06
	PSO	18.29	0.29	7.20	101.59	0.11	7.30	102.95	0.11	6.34	89.43	0.10
3	ARSM	31.22	-0.37	12.25	172.78	-0.15	12.41	175.07	-0.16	10.84	152.96	-0.11
	GA	31.25	-0.34	12.26	172.92	-0.15	12.42	175.19	-0.15	10.85	153.09	-0.10
	PSO	31.36	-0.23	12.30	173.56	-0.10	12.46	175.84	-0.08	10.89	153.66	-0.06

Table 3.31 – Results of the identified rotational spring stiffness and fixity factors in the numerical study of the five–bar truss.

Target system	Technique	$k_{rI.1}^{id}$	$\gamma_{krI.1}^{id}$	$\frac{\gamma_{krI.1}^{id}}{\gamma_{krI.1}^{true}}$	$k_{rIII.1}^{id}$	$\gamma_{krIII.1}^{id}$	$\frac{\gamma_{krIII.1}^{id}}{\gamma_{krIII.1}^{true}}$	$k_{rIII.3}^{id}$	$\gamma_{krIII.3}^{id}$	$\frac{\gamma_{krIII.3}^{id}}{\gamma_{krIII.3}^{true}}$	$k_{rIII.link}^{id}$	$\gamma_{krIII.link}^{id}$	$\frac{\gamma_{krIII.link}^{id}}{\gamma_{krIII.link}^{true}}$	$k_{rIV.4}^{id}$	$\gamma_{krIV.4}^{id}$	$\frac{\gamma_{krIV.4}^{id}}{\gamma_{krIV.4}^{true}}$
		[kNm/rad]	[-]	[-]	[kNm/rad]	[-]	[-]	[kNm/rad]	[-]	[-]	[kNm/rad]	[-]	[-]	[kNm/rad]	[-]	[-]
1	ARSM	0.41	0.71	0.95	4.74	0.97	1.02	0.00	0.03	–	0.74	0.25	1.00	86.60	0.77	1.53
	GA	0.44	0.72	0.96	3.44	0.95	1.01	0.00	0.00	–	0.73	0.25	1.00	23.03	0.46	0.93
	PSO	0.49	0.75	0.99	3.51	0.95	1.01	0.01	0.06	–	0.75	0.25	1.01	27.79	0.50	1.00
2	ARSM	2.17	0.91	0.96	0.05	0.20	0.73	0.05	0.26	0.52	1.58	0.40	0.79	87.09	0.77	1.03
	GA	2.43	0.94	0.98	0.06	0.26	0.96	0.08	0.37	0.75	1.93	0.46	0.91	81.56	0.75	1.01
	PSO	2.81	0.94	0.99	0.05	0.24	0.89	0.14	0.50	1.00	2.11	0.49	0.95	80.08	0.75	1.01
3	ARSM	0.04	0.19	0.77	0.14	0.44	1.13	0.45	0.76	1.01	0.55	0.19	–	464.94	0.95	0.99
	GA	0.06	0.25	1.01	0.15	0.46	1.18	0.44	0.77	1.03	0.15	0.06	–	497.95	0.95	0.99
	PSO	0.06	0.26	1.04	0.13	0.44	1.11	0.36	0.74	0.98	0.21	0.08	–	511.12	0.95	1.00

Assumptions: $k_{rI.1}^{id} = k_{rII.1}^{id}$; $k_{rIII.1}^{id} = k_{rIII.2}^{id}$; $k_{rI.4}^{id} = k_{rII.5}^{id} = k_{rIV.4}^{id} = k_{rIV.5}^{id}$.

In the second stage of optimization, the identified load from the first optimization stage was also varied within $\pm 2\%$ to account for possible error in the identification of the load. The optimization of the five–bar model involved 6 design parameters (the load and 5 joint rigidity factors) and 12 modal responses (6 natural frequencies and 6 MAC values) and 3 static forces in the first to third tension members of circular solid cross–sections.

During the optimization, the modes with a MAC value equal or greater than 0.75 were to be selected. A minimum number of four paired modes was defined as a constraint, to aim for an optimized model with physical meaning.

In Table 3.30, the identified axial forces agree well to the true values of the target systems. The different optimization techniques provide similar results. The maximum difference between the identified and true load by the ARSM is -0.37 kN. The maximum difference between the identified and true member axial forces is -0.16 kN.

In Table 3.31, the identified fixity factors also represent in most cases correctly the degrees of joint stiffness of the five–bar truss with respect to a pinned or rigid condition. The PSO gives the most satisfactory results. The ratios between the identified and the true fixity factors are closer to one than the other two techniques. The ARSM provides the highest deviations of the results of the rigidity factors compared to the PSO and GA.

The numerical results of the five–bar truss structure reveal that the proposed methodology is able to identify reasonably the axial forces as well as the joint stiffnesses of the truss–type structure.

3.5 Discussions

From the numerical study of three partial systems of truss–type structures, i.e. single bars, a two–bar system and a five–bar truss, the following remarks are drawn.

- A truss structure subjected to an increasing axial force becomes less sensitive to the influence of the rotational stiffness of the end constraints and joint connections.
- A truss structure of higher slenderness also becomes less sensitive to the influence of the rotational stiffness of the end constraints and joint connections.
- Sensitivity analyses give useful information that can be extracted for subsequent optimization process.

-
- Sensitivity analyses reveal that the modal parameters are influenced by the axial forces or axial stresses as well as the joint flexibility.
 - Sensitivity analyses show that the numerical calculated static forces in the investigated truss-type structures is sensitive to the load but insensitive to the joint flexibility.
 - The numerical study of different systems reveals that the proposed methodology can identify tensile forces at various stress states with good accuracy. For all case studies, the identified axial forces match fairly well to that of the target systems.
 - The numerical simulation also reveals that the proposed methodology can estimate correctly the joint rigidity factors of truss-type systems in relation to the pinned or rigid conditions. For all case studies, reasonable estimation of the fixity factor in relation to a pinned to rigid condition was achieved. The rigidity factor provides useful assessment in terms of the percentage of rigidity of semi-rigid connections.
 - About the choice of the objective function, the objective function for the identification of the axial forces contains three terms; the first two terms are related to the natural frequencies and the MAC values, while the third term is associated with the axial forces of the individual truss members that are estimated by an analytical-based method. The objective function for the estimation of the rotational spring stiffness contains only the terms related to the modal parameters, i.e. natural frequencies and MAC values.
 - The numerical error analysis shows that the identified axial forces are not significantly vulnerable to the uncertainty associated with structural parameters.
 - The numerical error analysis reveals that the uncertainty in structural parameters of truss structures has less impact on the accuracy of the parameter identification than the uncertainty in natural frequencies.
 - The numerical study reveals that a modification of a symmetric truss-type structure such as by adding mass to the truss members can determine joint stiffness at symmetric locations of a structure.

4

VALIDATION OF METHODOLOGY BY LABORATORY EXPERIMENTS



The proposed methodology discussed in the previous chapter is readily applied to bench-scale systems in the laboratory. This chapter describes the laboratory tests for the single bars, two-bar system and five-bar truss. The results of the identification of the axial forces and corresponding stresses as well as the estimation of the joint stiffness by the proposed methodology are presented. The conclusions that emerged from the experiments are given.

4.1 Overview of Laboratory Experiments

The assemble of the partial systems of truss-type structures and the laboratory experiments were carried out at *Versuchstechnische Einrichtung* (VTE), Institute of Structural Engineering, Department of Civil Engineering at Bauhaus-Universität Weimar. The laboratory tests consisted of static measurements of the applied loads and the strains in selected members of the systems to verify the results of the identified axial forces. In addition, dynamic measurements were performed to identify the modal parameters of the systems. Based on the experimentally identified modal parameters, the proposed methodology was applied to determine the axial forces and joint stiffnesses of truss-type structures. Three types of systems were tested in the laboratory, from simple to more complex structures, i.e. single-bars, a two-bar system and a five-bar truss. The laboratory systems have similar geometrical and mechanical properties like those in the numerical study.

4.2 Single-Bar Systems

The setup of the experiments for the single bars were made using the available specimens and material at the laboratory facility. The single bars are steel circular solid bars type *DYWIDAG* with a core diameter of 20 mm. The mechanical properties of the bars were provided by the manufacturer as follows: the steel grade of S900/1100, mass density of 7850 kg/m³ and modulus of elasticity of 205 000 N/mm². Several tests were performed for bars of different slenderness by changing the length of the members (see Table 4.1). Note that the system B3 in the laboratory experiment is different from the system B3 in the numerical study in the value of the modulus of elasticity. The drawings of the performed tests are provided at the end of the Appendix.

As shown Figure 4.1, the tie-bar was inserted in a test frame (bar type B1). At one end of the entire bar of about 4000 mm long, a hydraulic actuator was used to apply the load. To create a prestress state and define the end constraint of the designed single bar, after an axial load was applied, one end of the single-bar system was tightened by a nut. After the nut was fixed, the hydraulic actuator was released. The prestress was controlled by a load cell with an accuracy of 2 mV/V, as well as measured by a strain gauge installed on the bar. As one end constraint of the bar could be moved, the length of the bar was adjusted to examine three single-bar systems of different slenderness. Table 4.2 gives the values of axial forces that are calculated from the measured strains for different tests of the single bars. The increments of the forces were to allow relatively low to intermediate states of stress, for instance approximately 35 N/mm² to around 154 N/mm² for the bar type B2 and similarly for other bar types.

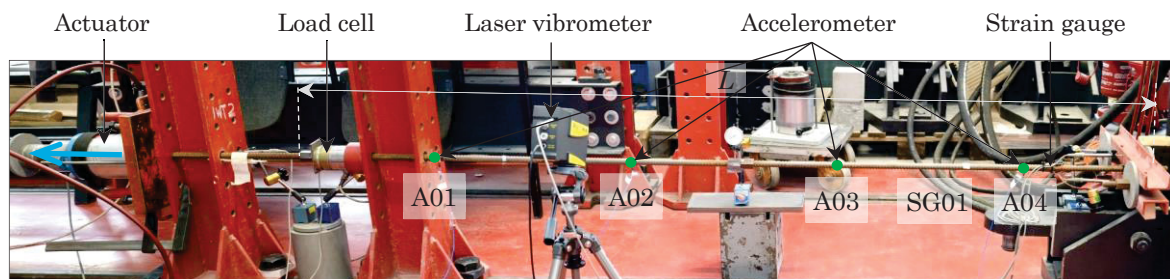


Figure 4.1 – Overview of the laboratory test for the bar B1.

Table 4.1 – Summary of single-bar systems in the performed laboratory tests.

Bar	L [mm]	\emptyset [mm]	A [mm ²]	I [mm ⁴]	E [N/mm ²]	ρ [kg/m ³]	λ_s [-]
B1	2700	20	314.16	7853.98	205 000	7850	540
B2	1500	20	314.16	7853.98	205 000	7850	300
B3	1000	20	314.16	7853.98	205 000	7850	200

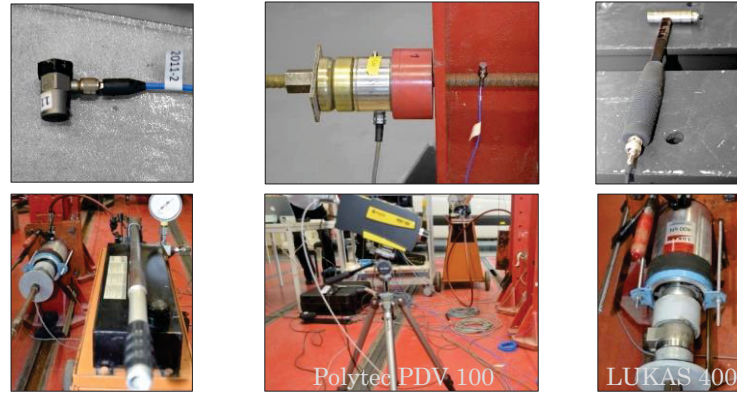


Figure 4.2 – Equipment in the laboratory tests of the single bars.

The equipment used in the laboratory tests for the single-bar systems are shown in Figure 4.2. For the dynamic tests, due to the limitation in the installed positions of the sensors on the bar, four instead of five piezoelectric accelerometers PCB/352C33, having sensitivity of 100 mV/g and weight of about 6 g, were mounted to a bar at an equal distance of $0.225L$ from each other, where the length L is indicated for different bars (see Figure 3.6(b)). The accelerometers were measuring in longitudinal direction along the length of the bars and vertical directions perpendicular to the cross-section of the bars. They are labelled A01 to A04. The outer accelerometers A01 and A04 were placed at a distance of $0.150L$ from the ends of the bar. In addition to the measurements by accelerometers, a laser vibrometer Polytec PDV 100 was used in some tests to compare the results with that of the accelerometers. The sensor light of the laser vibrometer was setup to coincide with the accelerometer A02 for comparison purpose.

The vibration measurements were conducted with hammer excitation using an impact hammer PCB/086C03 with soft tip, which is able to measure a pulse up to 2.2 kN with sensitivity of 2.25 mV/N and has a weight of about 0.16 kg. The instruments were connected to a signal conditioner and a data acquisition system of the National Instruments. The sampling rate was set as 2048 Hz.

Table 4.2 – Values of applied forces and corresponding stresses from the measured strains in the laboratory experiments of the single bars.

Load step	B1		B2		B3	
	P^{exp} [kN]	σ^{exp} [N/mm ²]	P^{exp} [kN]	σ^{exp} [N/mm ²]	P^{exp} [kN]	σ^{exp} [N/mm ²]
1	13.27	42.23	11.10	35.33	9.94	31.64
2	22.41	71.34	18.08	57.55	26.10	83.08
3	32.65	103.94	30.11	95.84	34.06	108.42
4	40.70	129.56	48.30	153.74	44.64	142.09
5	46.63	148.42	–	–	–	–

The procedure to carry out the tests was as follows. First, one end of the bar, where the load cell was installed, was tightened by a nut. Dynamic measurements were made at initial condition of zero–applied load. Hammer excitations were applied at two or three locations along the bar. After that, the nut at the left end of the bar was released. An axial force was applied to the bar by the hydraulic actuator. The left end of the bar was tightened again and a prestress condition was created in the bar. Two to three vibration measurements were performed with hammer excitations for each load step, with a duration of about sixty seconds on average for one measurement.

4.2.1 Modal Parameter Identification

The natural frequencies and amplitudes of the corresponding mode shapes of the single–bar systems were identified for each load step. The modal parameter estimation was carried out through the application of the stochastic subspace identification (SSI) method, i.e. the reference–based covariance–driven SSI–cov/ref, available in the MACEC software developed by the Structural Mechanics Division of the Civil Engineering Department of KU Leuven [PEETERS and DE ROECK (1999); REYNDERS and DE ROECK (2008); REYNDERS et al. (2011)]. An example of the stabilization diagram using the SSI at one load step for the single bar B1 is shown in Figure 4.3, which were estimated based on state models of order between 1 and 100.

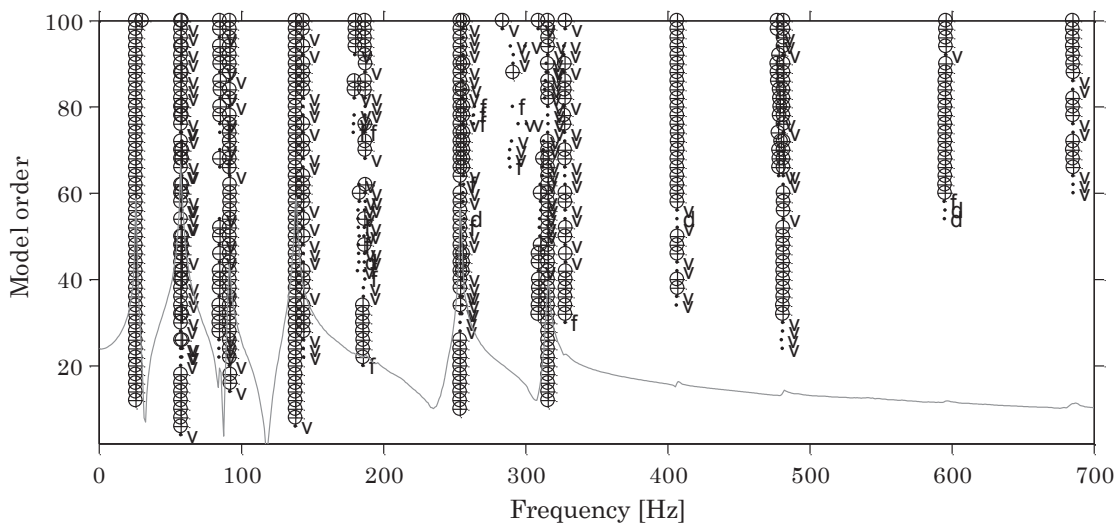


Figure 4.3 – Stabilization diagram in the laboratory experiment of the bar B1 at one load step.

Table 4.3 – Experimentally identified natural frequencies in the laboratory experiments of single bars B1, B2 and B3.

Load step	B1					B2				
	σ^{exp} [N/mm ²]	f_n^{exp} [Hz]				σ^{exp} [N/mm ²]	f_n^{exp} [Hz]			
		1st mode	2nd mode	3rd mode	4th mode		1st mode	2nd mode	3rd mode	4th mode
1	42.23	19.76	46.58	78.99	124.06	35.33	40.68	104.91	206.50	363.91
2	71.34	22.59	51.14	82.37	128.17	57.55	47.16	125.52	213.58	366.41
3	103.94	25.86	57.48	91.87	138.25	95.84	54.27	129.71	225.68	379.53
4	129.56	28.16	61.92	97.76	143.82	153.74	65.75	132.54	265.68	375.95
5	148.42	29.57	64.61	100.33	150.25	–	–	–	–	–

Regarding the measurements using the laser vibrometer in comparison to the traditional wired accelerometers, the laser vibrometer has the advantage that it does not add weight to the structure, due to the non-contact nature. The FRFs obtained from the laser vibrometer are highly comparable to that from the accelerometers. Nevertheless, higher frequency ranges than 200 Hz were not acquired as well by the laser vibrometer as by the accelerometers.

The identified natural frequencies for all load cases of the single bar B1 are compared with that of the bar B2 in Table 4.3. The effects of the tensile stress in increasing the values of the natural frequencies are clearly observed. Comparing between the bars of different slenderness, the identification of the natural frequencies and modal configurations could be obtained more consistently for bars with higher slenderness. In addition, more number of vibration modes were acquired for bars of higher slenderness.

The results of the experimentally identified natural frequencies using the SSI and numerically computed frequencies for the first six modes of the bar B1 are shown in Figure 4.4. The numerical pinned and nearly rigid models were used for the calculation of the numerical frequencies. In addition, the analytical formulae for certain cases of the boundary conditions and stress stiffening (i.e. Eq (2.4) and (Eq. (2.8)) were used to compare with the experimental and numerical results. The analytically and numerically calculated natural frequencies agree well. The experimentally identified frequencies are closer to the numerically computed natural frequencies of the assumed almost rigid bar system.

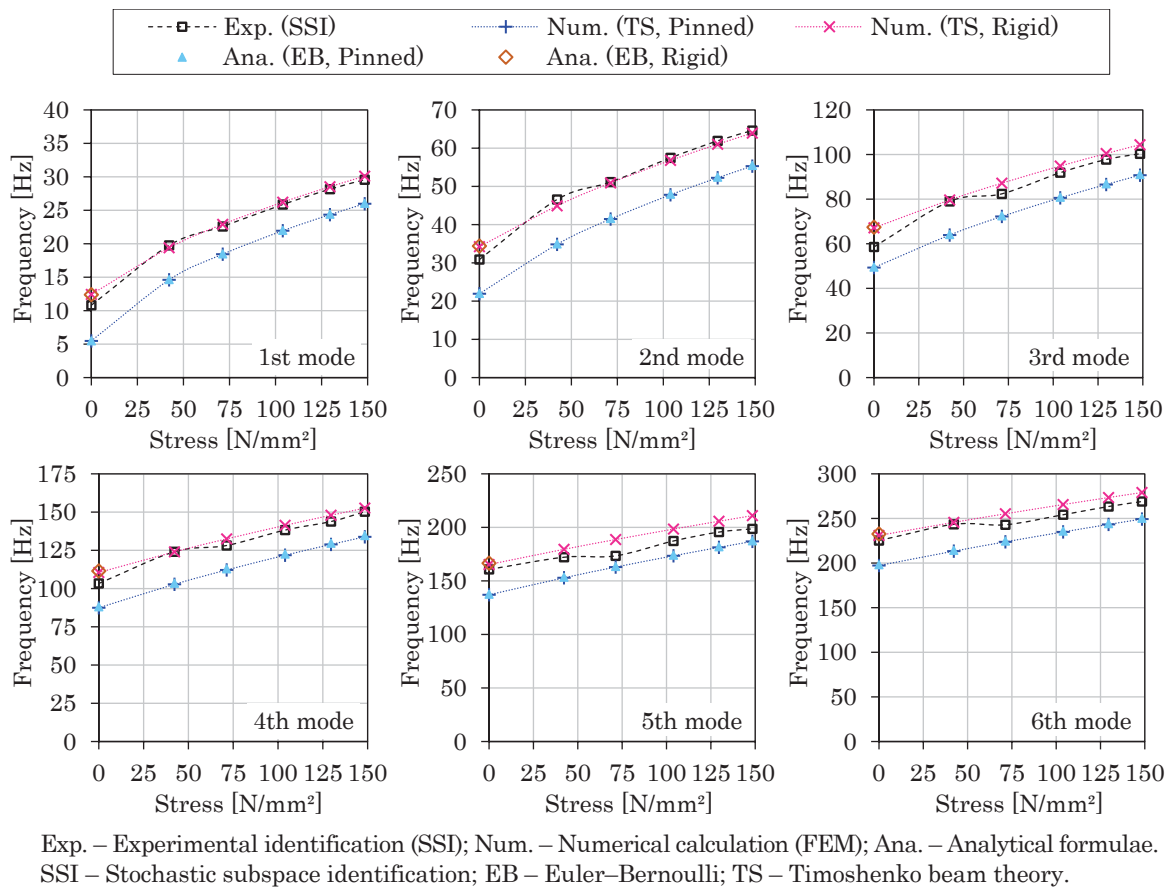


Figure 4.4 – Experimentally identified and analytically/numerically calculated natural frequencies at different stress states in the laboratory experiment of single bar B1.

Table 4.4 – Results of the identified axial forces and corresponding stresses as well as the rotational spring stiffness and fixity factors in the laboratory experiment of single bar B1.

Load step	Technique	N^{id}	σ^{id}	Δ	$k_{r1}^{id} = k_{r2}^{id}$	γ_{kr}^{id}
		[kN]	[N/mm ²]	[kN]	[kNm/rad]	[-]
1	ARSM	13.85	44.09	0.58	177.11	0.99
	GA	13.78	43.87	0.51	172.87	0.99
	PSO	13.82	44.00	0.55	177.11	0.99
2	ARSM	22.75	72.42	0.34	45.54	0.96
	GA	22.75	72.43	0.34	48.07	0.96
	PSO	22.76	72.45	0.35	48.85	0.96
3	ARSM	32.81	104.43	0.16	59.84	0.97
	GA	32.96	104.92	0.31	53.04	0.97
	PSO	32.83	104.49	0.18	78.79	0.98
4	ARSM	40.49	128.87	-0.21	51.82	0.97
	GA	40.72	129.61	0.02	57.41	0.97
	PSO	40.50	128.91	-0.20	56.54	0.97
5	ARSM	46.34	147.51	-0.29	96.78	0.98
	GA	46.38	147.62	-0.25	118.03	0.99
	PSO	46.28	147.33	-0.35	140.30	0.99

When referring to the previous Figure 3.5 together with the results of Figure 4.4, the effect of the axial tensile stress is significant considering different sing-bar systems. In addition, axial loading causes a modification to the magnitudes of the natural frequencies of all modes. The relative changes of the natural frequency values of the first mode in percentage are higher than that of higher modes, although the absolute changes of the natural frequencies of higher modes are more than that of the first mode.

4.2.2 Identification of Axial Force and Estimation of Joint Stiffness

The identification procedure using the proposed methodology as described in the numerical study was used to identify the unknown parameters of the axial force and rotational spring stiffness of the end constraints of the laboratory single-bar systems.

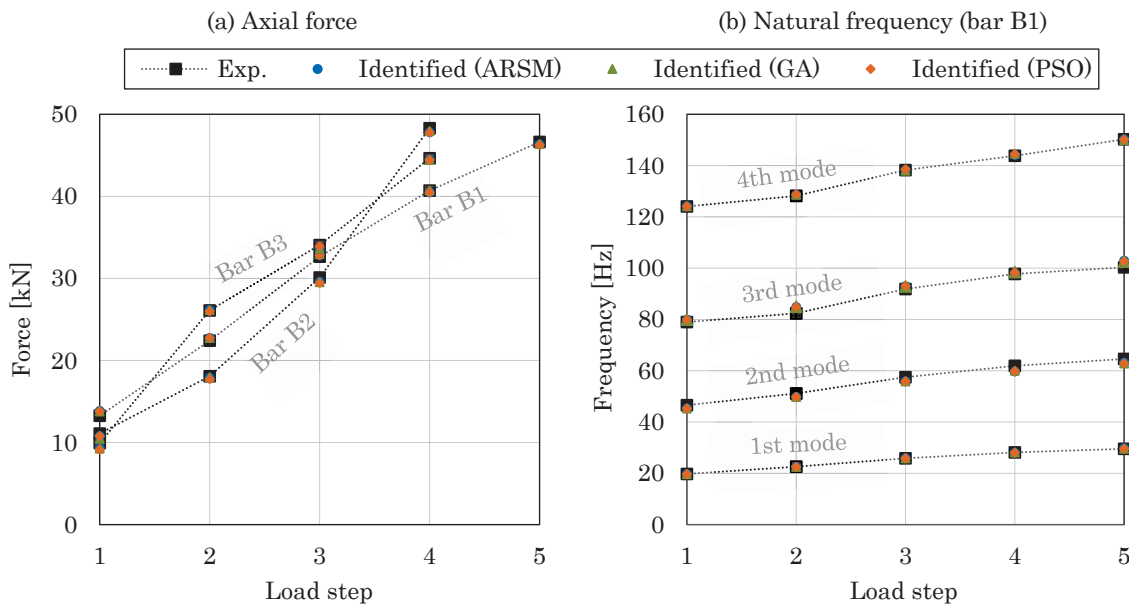


Figure 4.5 – Results of the identified axial forces and natural frequencies of the first four modes in the laboratory experiment of the single-bar systems.

The identification of the axial force for one single bar system was performed using the first four experimentally identified modes. Because one measurement point at midspan was not available, the five mode shape displacement points for the use of the analytical-based method were from four measurement points and one assumed point at midspan of the bar based on polynomial interpolation of the measurement data. The mode shapes were normalized to a maximum modal displacement that is equal to one. The initial values of the updating load were assumed as 10 kN, while the initial values for all fixity factors were 0.5.

Table 4.4 presents the results of the identified forces using the proposed methodology of single bar B1. The forces match reasonably well to the experimental values. Similarly, the results of the identified forces for the single bar systems B2 and B3 in Figure 4.5 show a good agreement to the experimentally measured forces. In addition, as seen in Figure 4.5, the identified natural frequencies agree with the experimentally identified ones. The MAC values are from 0.97 to 1.00.

4.3 Two-bar System

The laboratory experiments for three two-bar systems with the geometric and material characteristics like the systems in the numerical study were carried out. The first system is a symmetric system. The second and third systems are asymmetric structures. For clarity and similar to the numerical study, the asymmetric systems are referred to as *UnsymM* (system with added mass) and *UnsymL* (system whose members are of different lengths).

The symmetric two-bar system has each member of circular solid cross-section of 9.5 mm and a length of approximately 1510 mm (see Figure 4.6). The link-rod is considered as a connecting member to the hydraulic actuator for applying the load.

The asymmetric system *UnsymM* is based on the symmetric two-bar structure, but a mass of 0.407 kg is added to the first member at a distance of 440 mm to the higher end of the member. The added mass is shown in Figure 4.7.

The asymmetric system *UnsymL* has two members of different lengths, i.e. the first member is approximately 1510 mm long and the second member is about 1390 mm long (see Figure 4.8). The joint connections at the lower end of the first and second tension

Table 4.5 – Comparison of measured applied load of the hydraulic actuator by load cell and calculated member axial forces from the measured strains in the laboratory experiment of the symmetric two-bar system.

Load step	Measurements by strain gauges								Measurements by load cell
	local y				global Y				global Y
	σ_1^{exp}	σ_2^{exp}	N_1^{exp}	N_1^{exp}	N_1^{exp}	N_2^{exp}	N_{sum}^{exp}	Δ	P^{exp}
	[N/mm ²]	[N/mm ²]	[kN]	[kN]	[kN]	[kN]	[kN]	[kN]	[kN]
	Bar 1	Bar 2	Bar 1	Bar 2	Bar 1	Bar 2	Total	Total	
1	59.52	58.03	4.22	4.11	3.65	3.56	7.21	0.16	7.05
2	101.04	102.03	7.16	7.23	6.20	6.26	12.46	0.01	12.46
3	133.09	136.61	9.43	9.68	8.17	8.39	16.56	-0.18	16.74
4	172.04	177.76	12.19	12.60	10.58	10.92	21.50	-0.75	22.25
5	208.42	220.49	14.77	15.63	12.79	13.53	26.33	-0.12	26.45

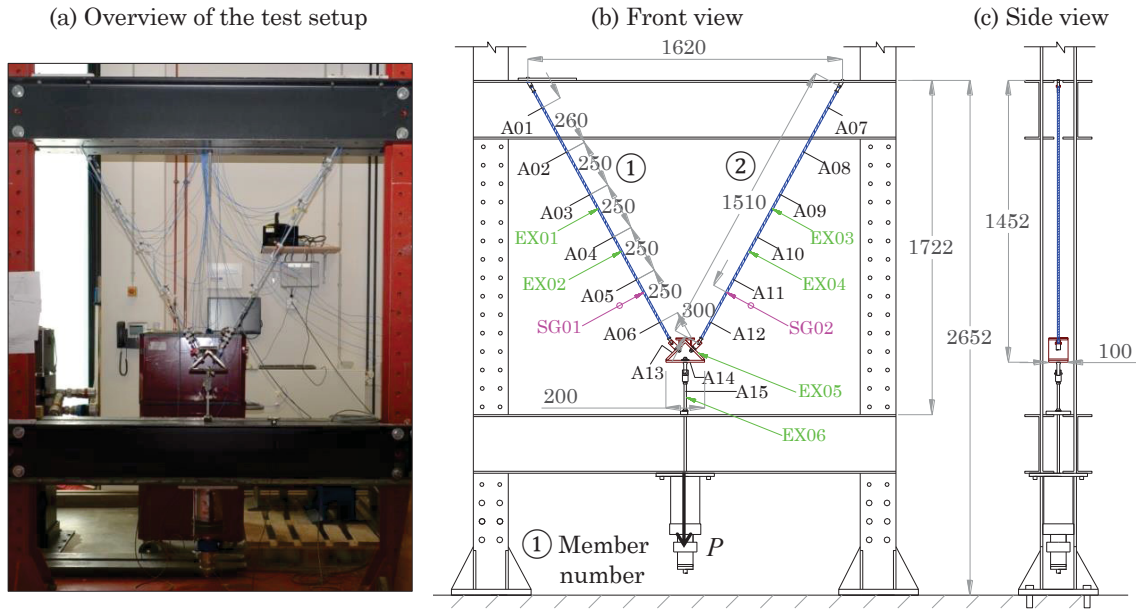


Figure 4.6 – Overview of the laboratory experiment of the symmetric two-bar system. A_i indicates accelerometers, SG_i strain gauge and EX_i indicates excitation points.

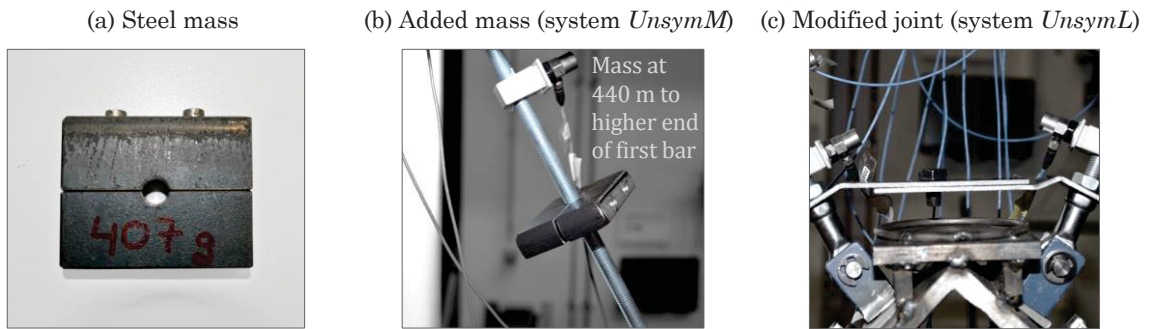


Figure 4.7 – Details of the laboratory test on the asymmetric systems *UnsymM* and *UnsymL*.

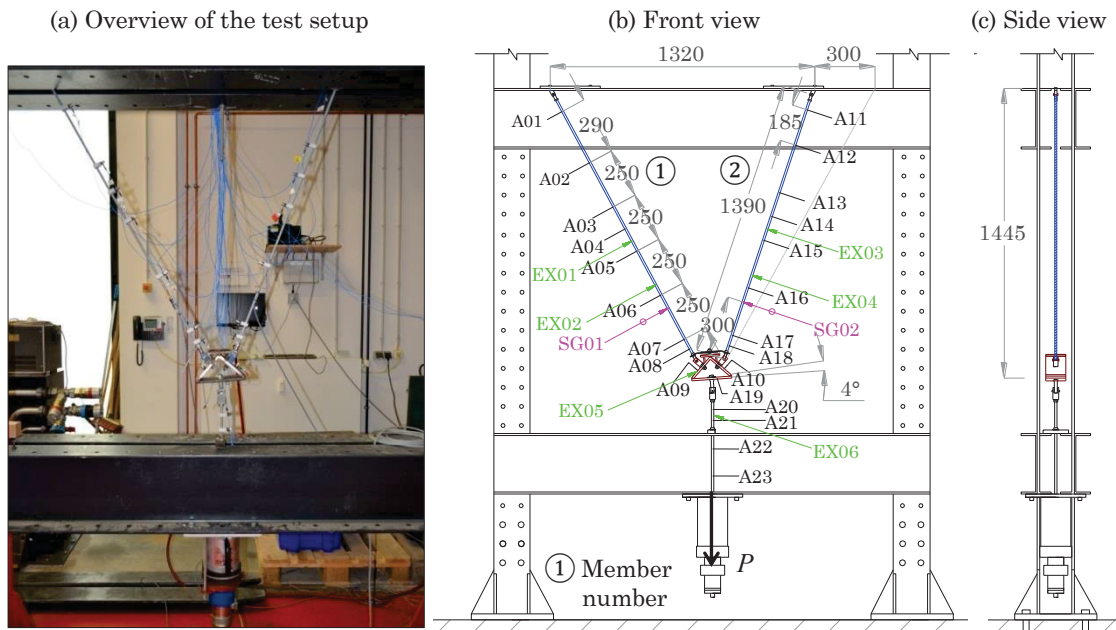


Figure 4.8 – Overview of the laboratory experiment of the asymmetric two-bar system *UnsymL*.

bars were set up to be linked together by a connecting plate (see Figure 4.7(c)). Thus, these joints are assumed to have the same rotational stiffness. The purpose was to examine a modification of the joint to evaluate the advantage of testing the structure in a slightly different configuration to reduce the number of unknown joint stiffnesses and facilitate the structural parameter estimation process using the proposed methodology.

Regarding the mechanical properties, the mass density of all two-bar systems is assumed as 7850 kg/m^3 . The modulus of elasticity of the steel members of the two-bar structures was determined by tensile tests performed at BAM as $205\,000 \text{ N/mm}^2$. The details of the tensile tests are described in the next section.

The overview of the test setups for the symmetric two-bar system and the asymmetric system *UnsymL* are presented in Figure 4.6 and Figure 4.8. For all three systems, tension loads were applied by the hydraulic actuator at the end of the link-rod in vertical pulling downward direction. The forces by the hydraulic actuator were measured by a load cell. In addition, two strain gauges were used to measure the strain in the members; one was used for each member. The strain values were recorded every 0.2 second.

Table 4.5 gives a comparison of the applied forces by the hydraulic actuator and the forces calculated from the measured strains in the two members for the symmetric system to double-check the accuracy of the measurements by static force equilibrium. Five load steps were performed in an increasing manner from approximately 7.1 kN to 26.5 kN. The applied loads result in an axial stress from about 59 N/mm^2 to 208 N/mm^2

Table 4.6 – Comparison of measured applied load of the hydraulic actuator by load cell and calculated member axial forces from the measured strains in the laboratory experiment of the asymmetric two-bar system *UnsymM*.

Load step	Measurements by strain gauges								Measurements by load cell
	local y				global Y				global Y
	σ_1^{exp}	σ_2^{exp}	N_1^{exp}	N_1^{exp}	N_1^{exp}	N_2^{exp}	N_{sum}^{exp}	Δ	P^{exp}
	[N/mm ²]	[N/mm ²]	[kN]	[kN]	[kN]	[kN]	[kN]	[kN]	[kN]
	Bar 1	Bar 2	Bar 1	Bar 2	Bar 1	Bar 2	Total	Total	
1	60.78	59.05	4.31	4.19	3.73	3.62	7.36	0.34	7.02
2	101.97	102.90	7.23	7.29	6.26	6.32	12.58	0.34	12.24
3	142.36	147.77	10.09	10.47	8.74	9.07	17.81	0.20	17.61
4	162.23	169.89	11.50	12.04	9.96	10.43	20.39	0.25	20.14
5	211.28	225.51	14.98	15.98	12.97	13.84	26.81	0.27	26.54

Table 4.7 – Comparison of measured applied load of the hydraulic actuator by load cell and calculated axial forces in the two members from the measured strains in the laboratory experiment for the asymmetric two-bar system *UnsymL*.

Load step	Measurements by strain gauges								Measurements by load cell
	local y				global Y				global Y
	σ_1^{exp}	σ_2^{exp}	N_1^{exp}	N_1^{exp}	N_1^{exp}	N_2^{exp}	N_{sum}^{exp}	Δ	P^{exp}
	[N/mm ²]	[N/mm ²]	[kN]	[kN]	[kN]	[kN]	[kN]	[kN]	[kN]
	Bar 1	Bar 2	Bar 1	Bar 2	Bar 1	Bar 2	Total	Total	
1	35.66	51.79	2.53	3.67	2.19	3.30	5.48	-0.09	5.57
2	50.41	71.32	3.57	5.06	3.09	4.60	7.69	0.03	7.66
3	73.54	104.03	5.21	7.37	4.52	6.78	11.30	0.26	11.04
4	95.43	134.16	6.76	9.51	5.86	8.79	14.65	0.44	14.21
5	117.95	167.27	8.36	11.86	7.24	10.99	18.23	0.54	17.69

in the first member, as well as an axial stress from about 58 N/mm² to 220 N/mm² in the second member measured by the strain gauges. As the assembled laboratory system is not absolutely symmetric, the axial forces and corresponding stresses in the two members are not absolutely the same. Moreover, with the application of increasing loads, the geometry and joint stiffness of the two members were changed differently, resulting in bigger differences between the member forces of the members at higher applied loads.

Similarly, for the systems *UnsymM* and *UnsymL*, the applied forces by the hydraulic actuator and the forces calculated from the measured strains in the two members are compared in Table 4.6 and Table 4.7. Five load steps were also performed for the system *UnsymM* from approximately 7.0 kN to 26.5 kN. The applied loads result in an axial stress from approximately 61 N/mm² to 211 N/mm² in the first member and 59 N/mm² to 226 N/mm² in the second member by strain gauge measurements on each member. The diagrams of the forces versus time during the experiment performance of the symmetric system and asymmetric *UnsymM* system are shown in Figure 4.9. The applied loads were maintained relatively constant for each dynamic measurement.

For the system *UnsymL*, the five load steps were increased from about 5.6 kN to 17.7 kN. The two members of the *UnsymM* have highly different stresses due to their different characteristics. The axial stress calculated from the measured strains in the first member was varied from 36 N/mm² to 118 N/mm², while the stress in the second member was varied from 52 N/mm² to 167 N/mm².

Concerning the dynamic tests, twelve accelerometers were installed for the symmetric and asymmetric *UnsymM* systems in total. Six piezoelectric accelerometers PCB/352C33 were attached on each member by glue. Regarding the system *UnsymL*, sixteen accelerometers were used; eight on each member. Measurements were carried out with hammer excitations at several positions on the two members of the system. The sampling frequency was set as 2048 Hz.

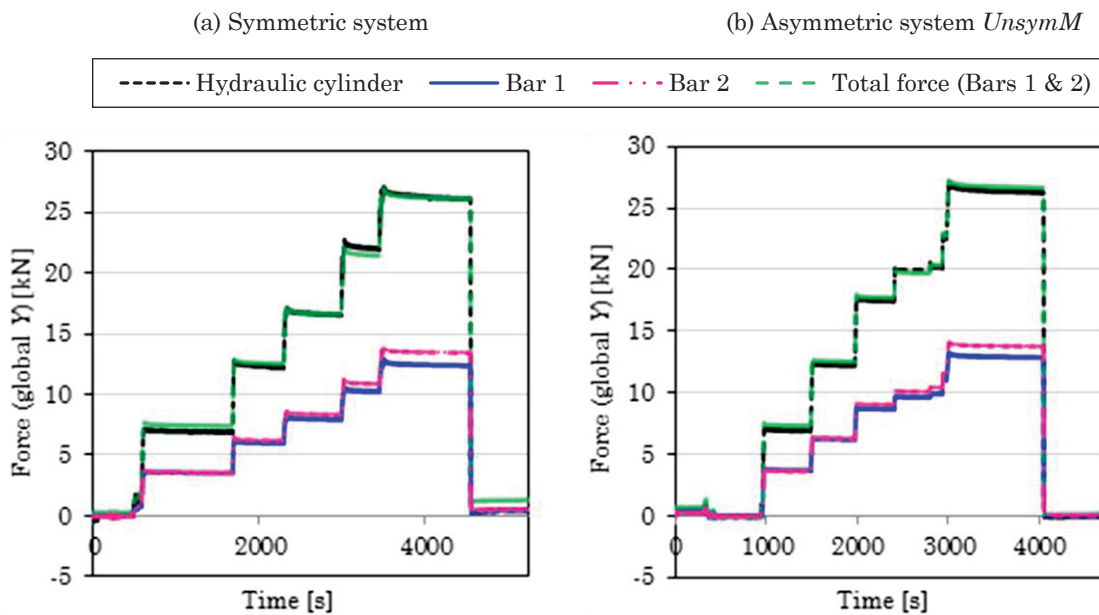


Figure 4.9 – Measured applied load of the hydraulic actuator by load cell and calculated axial forces in the two members from the measured strains during the measurements in the laboratory experiments of the two-bar systems.

4.3.1 Material Tests to Determine Stress–Strain Characteristics

Samples of the tension bars $\varnothing 9.5$ mm of the two-bar structure were available for the material tests to determine the stress–strain characteristics. The tests were performed at Bundesanstalt für Materialforschung und –prüfung (BAM). For the tensile tests, proportional bars with a diameter of 5 mm were manufactured in accordance with DIN EN 6892–1 (2009). The dimensions of the tensile specimens are given in Table 4.8.

The implementation of the small-scale tests was made at room temperature. The universal testing machine has a maximum tensile force of the hydraulic actuator of 100 kN. For the strain measurement, a strain gauge type HBM DD1 with a measuring length of 25 mm was used.

Table 4.8 – Characteristics of the tensile specimens of the two-bar structure for material tests [DIN EN 6892–1 (2009)].

d_0	L_0	d_1	r	h	L_c	L_t	Legend
5	25	M8	4	7	30	51	d_0 Initial diameter of the solid circular specimen in the test length L_0 Initial gauge length L_c Test length L_t Total length of the specimen

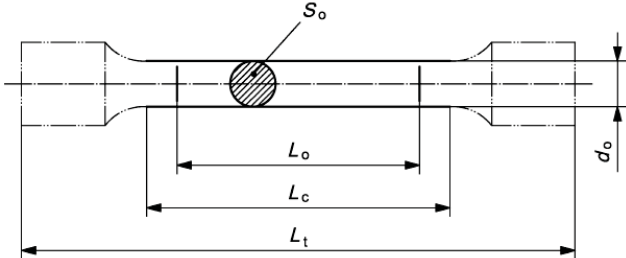


Table 4.9 – Results of the tensile tests for the specimens of the solid circular steel tension members of the two-bar system in the laboratory experiments.

		Stress, σ [N/mm ²]	Strain, ε [%]
Technical proportional limit	$f_{p0.01}$	400.7	0.206
0.2% strain limit	$f_{p0.2}$	498.6	0.443
Tensile strength	f_u	549.0	1.878

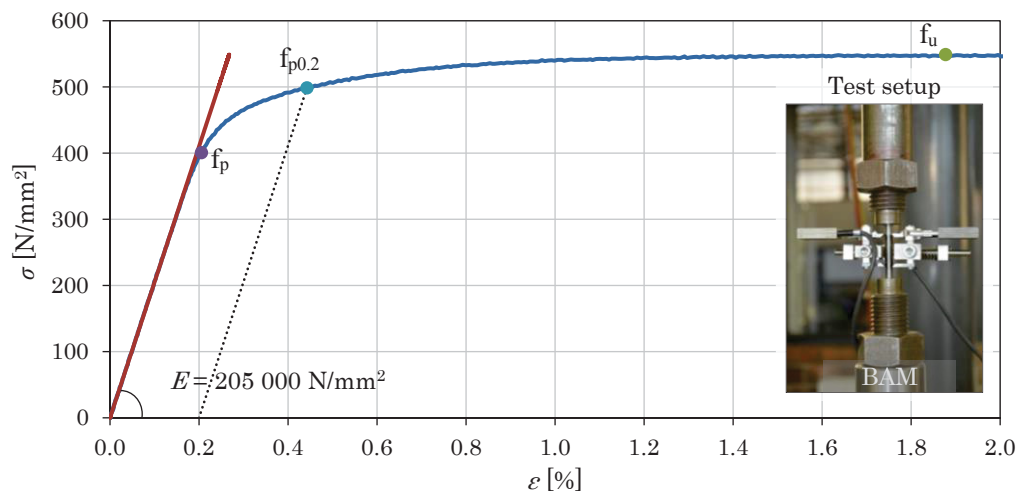


Figure 4.10 – Stress–strain curve from the tensile tests for the specimens of the solid circular steel tension members of the two-bar system in the laboratory experiments.

The tensile specimens were secured on the testing machine with a small locking force. The extensometer was attached to the sample. The tensile test was carried out under displacement control with a velocity of 0.02 mm/s until rupture of the specimen was reached. An assumption of a uniform elongation over the length of the specimen ($L_c = 30$ mm) gives a strain rate of 0.0007 s⁻¹, which corresponds to the requirements given in DIN EN 6892–1 (2009).

The measured stress–strain curve is shown in Figure 4.10. The investigated steel has no pronounced yield point. This results from the manufacturing of the cold forming process. The important characteristics of the investigated steel can be obtained from the measured stress–strain curve, as shown in Table 4.9. The modulus of elasticity was determined as $205\,000$ N/mm² by a linear interpolation of the stress–strain curve for the stress range from 100 to 250 N/mm².

4.3.2 Modal Parameter Identification

Similar to the single bars, the reference–based covariance–driven SSI was used to extract the modal parameters from the measured responses of the two–bar structures. Table 4.10 shows the experimentally identified frequencies of the first six modes of all three two–bar system at different states of stress in the laboratory experiments. The experimental modal parameters could be identified relatively well. The identified natural frequency values from the experiments of the two–bar structures are highly affected by the stress stiffening. Regarding the identified mode shapes, no significant differences between the various load states were found.

To demonstrate the effect of the added mass on the dynamic behaviour of the two–bar structure, the first six experimentally identified natural frequencies and mode shapes of the symmetric system and asymmetric system *UnsymM* at the first load step are presented in Figure 4.11. At the first load step, both systems have a similar stress state. The effect of the added mass on the natural frequencies of the asymmetric system *UnsymM*

Table 4.10 – Experimentally identified natural frequencies of the first six modes in the laboratory experiments of the symmetric and asymmetric two–bar structures.

Load step	System	σ_1^{exp} [N/mm ²]	σ_2^{exp} [N/mm ²]	f_n^{exp} [Hz]					
				1st mode	2nd mode	3rd mode	4th mode	5th mode	6th mode
1	<i>Symmetric</i>	59.52	58.03	26.40	33.28	42.28	70.86	74.38	114.57
2		101.04	102.03	34.51	42.38	54.06	87.94	91.72	141.72
3		133.09	136.61	38.77	48.43	60.67	99.23	102.68	154.87
4		172.04	177.76	43.31	54.83	67.55	111.65	114.75	172.52
5		208.42	220.49	47.52	59.92	73.28	121.12	124.26	186.05
1	<i>UnsymM</i>	60.78	59.05	23.22	29.88	39.90	58.47	72.25	110.72
2		101.97	102.90	29.56	37.99	51.22	73.72	88.79	130.53
3		142.36	147.77	34.26	43.63	57.23	84.54	102.21	134.05
4		162.23	169.89	36.33	46.47	61.00	88.55	106.86	111.88
5		211.28	225.51	41.68	53.07	68.53	101.52	121.57	150.41
1	<i>UnsymL</i>	35.66	51.79	21.37	30.43	38.56	61.84	76.14	101.23
2		50.41	71.32	25.15	34.47	43.30	68.62	85.38	110.82
3		73.54	104.03	29.08	40.00	50.31	79.41	98.88	125.07
4		95.43	134.16	31.64	44.32	55.54	88.09	109.56	130.23
5		117.95	167.27	34.59	48.81	61.16	96.45	119.64	147.86

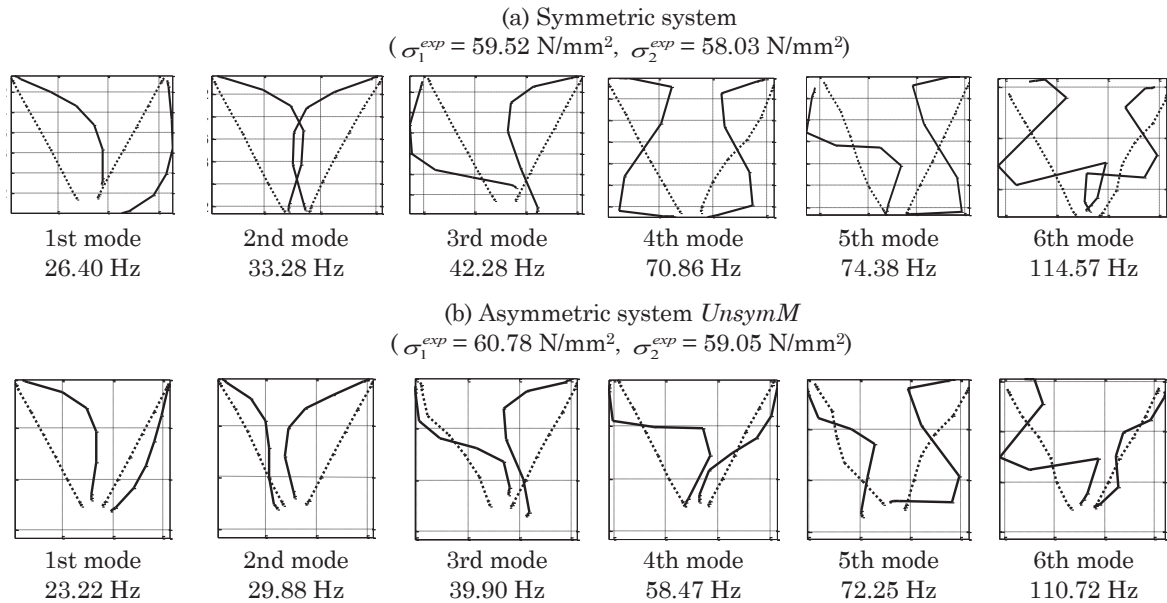


Figure 4.11 – Experimentally identified modal parameters of the first six modes at the first load step in laboratory experiments of the symmetric and asymmetric two-bar system *UnsymM*.

in comparison to the symmetric structure can be recognised clearly. In addition, the influence of the added mass can be also observed by investigating the shapes of the vibration modes. While the two members of the symmetric structure vibrates in similar forms, the members of the system *UnsymM* vibrates more distinctly from each other. Similar observations about more distinct vibrations of the members of the system *UnsymL* were also obtained.

4.3.3 Identification of Axial Force and Joint Stiffness

The identification procedure as described in the proposed methodology was implemented to identify the assumed unknowns of the axial forces and joint flexibility of the laboratory two-bar system. The first five to six experimentally identified modes were used in the

Table 4.11 – Results of the identified axial forces and stresses in the laboratory experiment of the symmetric two-bar system.

Load step	Technique	P^{id} [kN]	Δ [kN]	N_1^{id} [kN]	σ_1^{id} [N/mm ²]	Δ [kN]	N_2^{id} [kN]	σ_2^{id} [N/mm ²]	Δ [kN]
1	ARSM	6.52	-0.53	3.76	53.02	-0.46	3.76	53.02	-0.35
	GA	6.19	-0.86	3.57	50.32	-0.65	3.57	50.32	-0.55
	PSO	6.12	-0.93	3.53	49.79	-0.69	3.53	49.79	-0.58
2	ARSM	11.91	-0.56	6.83	96.33	-0.33	6.83	96.33	-0.40
	GA	11.84	-0.62	6.79	95.81	-0.37	6.79	95.79	-0.44
	PSO	11.94	-0.53	6.85	96.58	-0.32	6.85	96.58	-0.38
3	ARSM	16.30	-0.44	9.33	131.67	-0.10	9.33	131.67	-0.35
	GA	16.34	-0.40	9.35	131.97	-0.08	9.35	131.97	-0.33
	PSO	16.18	-0.57	9.25	130.55	-0.18	9.25	130.55	-0.43
4	ARSM	21.28	-0.97	12.17	171.65	-0.03	12.17	171.65	-0.43
	GA	21.53	-0.72	12.31	173.65	0.11	12.31	173.65	-0.29
	PSO	21.50	-0.75	12.29	173.43	0.10	12.29	173.41	-0.30
5	ARSM	26.34	-0.12	15.05	212.32	0.28	15.05	212.31	-0.59
	GA	26.26	-0.19	15.01	211.70	0.23	15.01	211.69	-0.63
	PSO	26.33	-0.13	15.05	212.25	0.27	15.04	212.24	-0.59

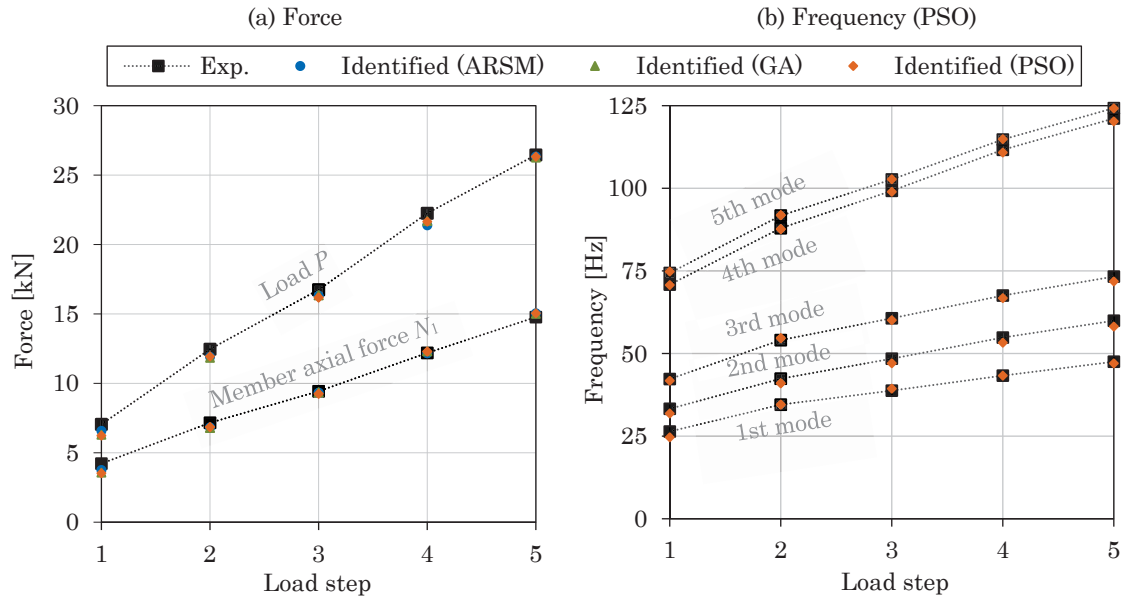


Figure 4.12 – Results of the identified axial forces and natural frequencies of the first five modes in the laboratory experiment of the symmetric two-bar structure.

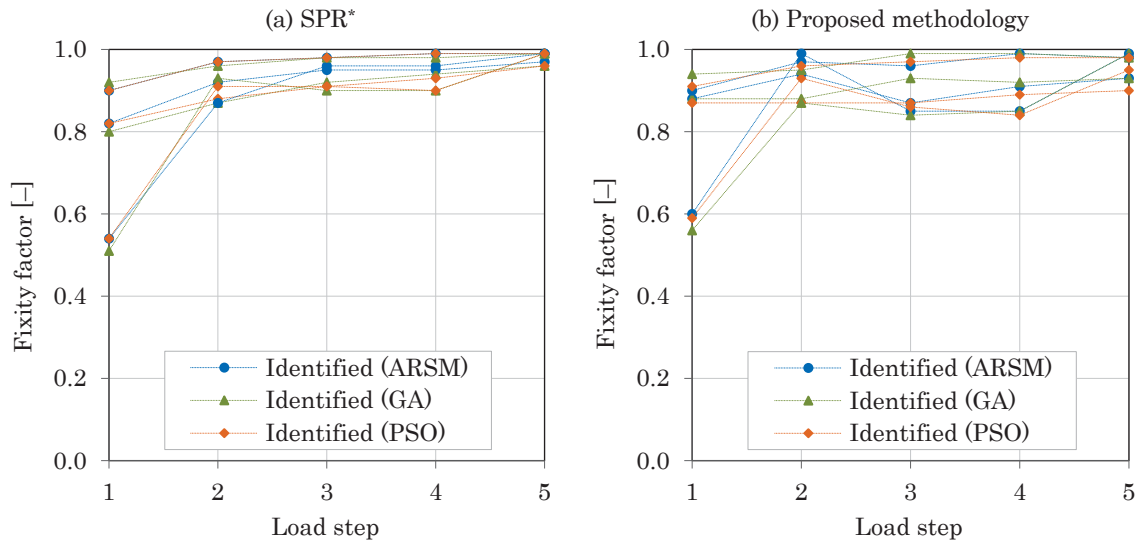
identification process. Like the numerical study, the updating parameters are the applied load to the system at the link-rod and the rotational spring stiffness of joints. For the symmetric system, it was assumed that the rotational spring stiffness at the symmetrical locations are identical. The load was varied from zero to 30 kN; the rigidity factors from zero to almost one. Similarly, the initial values of the updating load were assumed as 10 kN, while the initial values for all fixity factors were 0.5. The assumptions satisfy the condition that no prior-knowledge of the design parameters is necessary.

Regarding the selection of mode for the member force identification using the analytical-based algorithm by MAES et al. (2013), as previously discussed in Section 3.4.2, the criterion using the relative modal strain energy (MSE) was applied. For the two-bar systems, the experimentally identified second mode with the highest value of the relative

Table 4.12 – Results of the identified rotational spring stiffness and fixity factors in the laboratory experiment of the symmetric two-bar system.

Load step	Technique	$k_{rI.1}^{id}$	$\gamma_{krI.1}^{id}$	$k_{rIII.1}^{id}$	$\gamma_{krIII.1}^{id}$	$k_{rIII.link}^{id}$	$\gamma_{krIII.link}^{id}$
		[kNm/rad]	[-]	[kNm/rad]	[-]	[kNm/rad]	[-]
1	ARSM	1.25	0.88	1.55	0.90	3.30	0.60
	GA	1.15	0.88	2.59	0.94	2.86	0.56
	PSO	1.10	0.87	1.57	0.91	3.14	0.59
2	ARSM	2.36	0.94	5.70	0.97	38.86	0.95
	GA	1.17	0.88	3.40	0.95	15.14	0.87
	PSO	1.11	0.87	4.10	0.96	30.38	0.93
3	ARSM	1.10	0.87	4.19	0.96	12.86	0.85
	GA	2.11	0.93	11.69	0.99	11.77	0.84
	PSO	1.12	0.87	5.45	0.97	13.71	0.86
4	ARSM	1.71	0.91	11.26	0.99	12.53	0.85
	GA	1.99	0.92	16.12	0.99	12.55	0.85
	PSO	1.37	0.89	9.64	0.98	12.03	0.84
5	ARSM	2.23	0.93	8.85	0.98	220.45	0.99
	GA	2.21	0.93	9.19	0.98	220.45	0.99
	PSO	1.42	0.90	8.37	0.98	43.33	0.95

Assumptions: $k_{rI.1}^{id} = k_{rII.2}^{id}$; $k_{rIII.1}^{id} = k_{rIII.2}^{id}$.



*SPR – updating the parameter(s) of the rotational spring stiffness only, assuming the force is known.

Figure 4.13 – Results of the identified fixity factor $\gamma_{krIII,link}^{id}$ at different load steps in the laboratory experiment of the symmetric two-bar structure.

MSE was chosen for the respective component of the objective function considering the identified member force using the analytical-based algorithm.

Table 4.11 gives the identified applied loads as well as the member axial forces and corresponding stresses of the symmetric two-bar structure. The applied load and member axial force of the first member are plotted in Figure 4.12(a). A reasonable match between the experimentally measured and numerical identified forces was achieved for the different load states. The maximum deviation of the identified member forces for all cases is smaller than 0.70 kN. The performance of the three optimization techniques were comparable.

Regarding the identified modes, the identified natural frequencies of the first five modes at various load states are shown in Figure 4.12(b). The results of the PSO are presented,

Table 4.13 – Results of the identified axial forces and stresses in the laboratory experiment of the asymmetric two-bar system *UnsymM*.

Load step	Technique	P^{id}	Δ	N_1^{id}	σ_1^{id}	Δ	N_2^{id}	σ_2^{id}	Δ
		[kN]	[kN]	[kN]	[N/mm ²]	[kN]	[kN]	[N/mm ²]	[kN]
1	ARSM	6.80	-0.22	3.92	55.27	-0.39	3.92	55.26	-0.27
	GA	6.36	-0.66	3.67	51.75	-0.64	3.67	51.73	-0.52
	PSO	6.55	-0.47	3.78	53.26	-0.54	3.78	53.26	-0.42
2	ARSM	11.52	-0.72	6.61	93.21	-0.62	6.61	93.23	-0.68
	GA	11.39	-0.85	6.53	92.14	-0.70	6.53	92.14	-0.76
	PSO	11.49	-0.75	6.59	93.00	-0.64	6.59	93.00	-0.70
3	ARSM	17.20	0.59	9.84	138.82	-0.25	9.84	138.84	-0.63
	GA	17.22	0.61	9.86	139.03	-0.23	9.86	139.03	-0.62
	PSO	17.22	0.61	9.85	139.02	-0.24	9.85	139.02	-0.62
4	ARSM	19.57	-0.57	11.19	157.91	-0.31	11.19	157.91	-0.85
	GA	19.39	-0.75	11.09	156.46	-0.41	11.09	156.49	-0.95
	PSO	19.61	-0.53	11.22	158.29	-0.28	11.22	158.26	-0.82
5	ARSM	27.08	0.54	15.47	218.31	0.49	15.47	218.29	-0.51
	GA	27.02	0.48	15.44	217.81	0.46	15.44	217.84	-0.54
	PSO	27.09	0.55	15.48	218.42	0.50	15.48	218.35	-0.50

Table 4.14 – Results of the identified rotational spring stiffness and fixity factors in the laboratory experiment of the asymmetric two-bar system *UnsymM*.

Target system	Technique	$k_{rI,1}^{id}$ [kNm/ rad]	$\gamma_{krI,1}^{id}$ [-]	$k_{rIII,1}^{id}$ [kNm/ rad]	$\gamma_{krIII,1}^{id}$ [-]	$k_{rIII,link}^{id}$ [kNm/ rad]	$\gamma_{krIII,link}^{id}$ [-]	$k_{rII,2}^{true}$ [kNm/ rad]	$\gamma_{rII,2}^{true}$ [-]
1	ARSM	0.05	0.24	0.64	0.80	3.90	0.64	0.95	0.85
	GA	0.10	0.38	1.40	0.90	4.75	0.68	1.13	0.87
	PSO	0.07	0.30	1.06	0.87	5.85	0.72	0.84	0.84
2	ARSM	0.16	0.50	6.36	0.98	90.15	0.98	0.57	0.78
	GA	0.33	0.67	16.12	0.99	98.09	0.98	1.80	0.92
	PSO	0.30	0.65	9.23	0.98	71.63	0.97	1.74	0.91
3	ARSM	0.17	0.51	4.01	0.96	161.26	0.99	1.30	0.89
	GA	0.47	0.74	3.11	0.95	15.26	0.87	1.57	0.91
	PSO	0.42	0.72	7.75	0.98	10.61	0.83	0.41	0.72
4	ARSM	0.53	0.76	3.09	0.95	210.45	0.99	1.82	0.92
	GA	0.51	0.76	16.12	0.99	220.45	0.99	1.23	0.88
	PSO	0.46	0.74	0.52	0.76	220.45	0.99	2.20	0.93
5	ARSM	0.32	0.66	2.64	0.94	126.94	0.98	3.36	0.95
	GA	0.49	0.75	15.48	0.99	220.45	0.99	1.43	0.90
	PSO	0.52	0.76	1.70	0.91	173.66	0.99	1.56	0.91

Assumption: $k_{rII,2}^{true} = k_{rIII,2}^{true}$.

while the results of the ARSM and GA are similar. The identified frequencies by the proposed methodology agree well to the experimentally identified frequencies. Moreover, a high consistency of the paired mode shapes was achieved, with the obtained MAC values ranging from 0.93 to 0.99.

The identified rotational spring stiffnesses of the symmetric two-bar structure are provided in Table 4.12. A general trend was found that the joint rigidity was increased with increasing applied load. This is reasonable in practice as the joint flexibility depends on the relative stiffness of the member, which is related to the level of loading.

Furthermore, as discussed in the numerical study for the case studies of the single-bar systems, the optimization with only the updating parameters of the spring stiffness gives highly accurate results of the identified rigidity factors. This optimization assumes that

Table 4.15 – Results of the identified axial forces and stresses in the laboratory experiment of the asymmetric two-bar system *UnsymL*.

Load step	Technique	P_1^{id} [kN]	Δ [kN]	N_1^{id} [kN]	σ_1^{id} [N/mm ²]	Δ [kN]	N_2^{id} [kN]	σ_2^{id} [N/mm ²]	Δ [kN]
1	ARSM	5.40	-0.17	2.35	33.21	-0.18	3.48	49.10	-0.19
	GA	5.36	-0.21	2.34	33.00	-0.19	3.47	49.01	-0.20
	PSO	5.32	-0.25	2.32	32.76	-0.21	3.45	48.64	-0.22
2	ARSM	7.52	-0.14	3.27	46.10	-0.30	4.86	68.61	-0.20
	GA	7.41	-0.25	3.22	45.43	-0.35	4.79	67.56	-0.27
	PSO	7.38	-0.28	3.21	45.22	-0.37	4.77	67.31	-0.29
3	ARSM	11.10	0.06	4.82	68.03	-0.39	7.15	100.84	-0.22
	GA	11.05	0.01	4.81	67.82	-0.40	7.11	100.32	-0.26
	PSO	11.10	0.06	4.83	68.14	-0.38	7.14	100.66	-0.24
4	ARSM	14.85	0.64	6.45	91.05	-0.31	9.53	134.45	0.02
	GA	14.91	0.69	6.49	91.53	-0.27	9.56	134.84	0.05
	PSO	14.86	0.65	6.47	91.21	-0.30	9.53	134.46	0.02
5	ARSM	18.33	0.64	7.98	112.60	-0.38	11.73	165.51	-0.13
	GA	18.27	0.58	7.96	112.27	-0.40	11.69	164.96	-0.17
	PSO	18.33	0.64	7.98	112.51	-0.39	11.74	165.66	-0.12

Table 4.16 – Results of the identified rotational spring stiffness and fixity factors in the laboratory experiment of the asymmetric two-bar system *UnsymL*.

Target system	Technique	$k_{rI,1}^{id}$ [kNm/ rad]	$\gamma_{krI,1}^{id}$ [-]	$k_{rIII,1}^{id}$ [kNm/ rad]	$\gamma_{krIII,1}^{id}$ [-]	$k_{rIII,link}^{id}$ [kNm/ rad]	$\gamma_{krIII,link}^{id}$ [-]	$k_{rIII,2}^{true}$ [kNm/ rad]	$\gamma_{rIII,2}^{true}$ [-]
1	ARSM	0.11	0.40	0.70	0.81	8.97	0.80	0.58	0.78
	GA	0.06	0.27	1.48	0.90	5.24	0.70	0.35	0.68
	PSO	0.06	0.28	0.49	0.75	3.63	0.62	0.63	0.79
2	ARSM	0.08	0.32	1.09	0.87	33.75	0.94	0.18	0.52
	GA	0.23	0.58	2.03	0.93	39.71	0.95	0.28	0.63
	PSO	0.08	0.32	1.54	0.90	93.71	0.98	0.31	0.65
3	ARSM	0.32	0.66	3.50	0.96	93.55	0.98	0.29	0.64
	GA	0.78	0.83	3.11	0.95	13.15	0.86	0.41	0.72
	PSO	0.43	0.72	6.23	0.97	9.11	0.80	0.41	0.71
4	ARSM	0.18	0.52	0.73	0.82	12.63	0.85	1.01	0.86
	GA	3.00	0.95	1.09	0.87	6.56	0.75	0.44	0.73
	PSO	0.34	0.68	1.70	0.91	8.59	0.79	0.35	0.68
5	ARSM	7.59	0.98	3.12	0.95	7.84	0.78	0.56	0.78
	GA	3.06	0.95	16.12	0.99	7.49	0.77	0.30	0.65
	PSO	1.42	0.90	6.55	0.98	11.59	0.84	0.26	0.61

Assumption: $k_{rIII,1}^{true} = k_{rIII,2}^{true}$.

exact knowledge of the load is available; thus, the unknowns are only the joint stiffness or rigidity factors. As the values of the load were made available by load cell or strain gauges in the laboratory experiments for verification purpose, the optimization with only the joint rigidity factors as updating parameters were carried out. The results of the optimizations with only the spring stiffness were used to compare and evaluate the accuracy of the proposed methodology in identifying the joint rigidity of the laboratory two-bar structure.

Figure 4.13 presents the identified rigidity factors of the joint connection to the link-rod by the optimization with only the spring stiffness as well as by the proposed methodology. The results of the joint to the link-rod are presented because this joint shows more distinct rigidity levels at the different load steps compared to other joints. At the first load step of low applied force, the joint experienced a middle level of semi-rigidity; after that, the rigidity level was increased at higher applied forces. Compared with the optimization with only the spring stiffness, the proposed methodology identifies correctly the rigidity factor at the first load step. At higher loads, the proposed methodology also estimates reasonably the rigidity factors. It is noted that the identification of the joint stiffness for a system at higher stress states becomes less precise because the influence of the end constraints is reduced while the effect of the stress stiffening is increased. The three optimization techniques give comparable results.

The identified axial forces and axial stresses of the asymmetric systems *UnsymM* and *UnsymL* are provided in Table 4.13 and Table 4.15. The results show a satisfactory agreement between the experimentally measured and identified forces using the proposed methodology for both the asymmetric two-bar structures. The maximum deviation of the identified to the true forces for the system *UnsymM* is -0.95 kN. Better results of the identified forces were obtained for the system *UnsymL* with a maximum deviation to the true forces of 0.69 kN; smaller deviations were found in most cases.

The identified rotational spring stiffnesses and fixity factors of the asymmetric systems *UnsymM* and *UnsymL* are given in Table 4.14 and Table 4.16. For system *UnsymM*, the

joint rigidity level is also increased at higher applied loads. For system *UnsymL*, a less consistent trend was found in the cases of the joints at the connection to the link-rod and at higher end of the second member. Different joint stiffnesses could be identified.

The technique of added mass offers the advantage to estimate different joint stiffnesses that are normally cannot be included into the identification process due to the issue of symmetric identification problems. Besides, a slight modification of the structural configuration such as connecting the members at a joint can facilitate the identification process by reducing the number of the updating parameters of the joint flexibility.

4.4 Five-Bar Truss System

A five-bar truss structure with the same geometrical and mechanical properties as the five-bar truss in the numerical study was tested in the laboratory. The system was assembled based on the two-bar system from the previous laboratory test. One support was built to be not movable in longitudinal and vertical directions, while the other support was constructed as horizontally movable roller support. All connections were built to allow rotations of the connected members at joints.

The truss consists of three tension bars, two compression members and a link-rod that is connected to the hydraulic actuator to apply the load. The tension bars have solid circular cross-sections of \varnothing 9.5 mm. The two compression bars have L-profiles of 40x40x4.0 mm. The tension bar in the middle is approximately 1920 mm long, while the other two tension bars are about 1490 mm long. The compression top chords have a length of approximately 1060 mm. Due to the assembling of the structure, the truss is not absolutely symmetric. The exact geometrical characteristics of the system can be found in Table 3.24. Regarding the mechanical properties, all members are made of steel

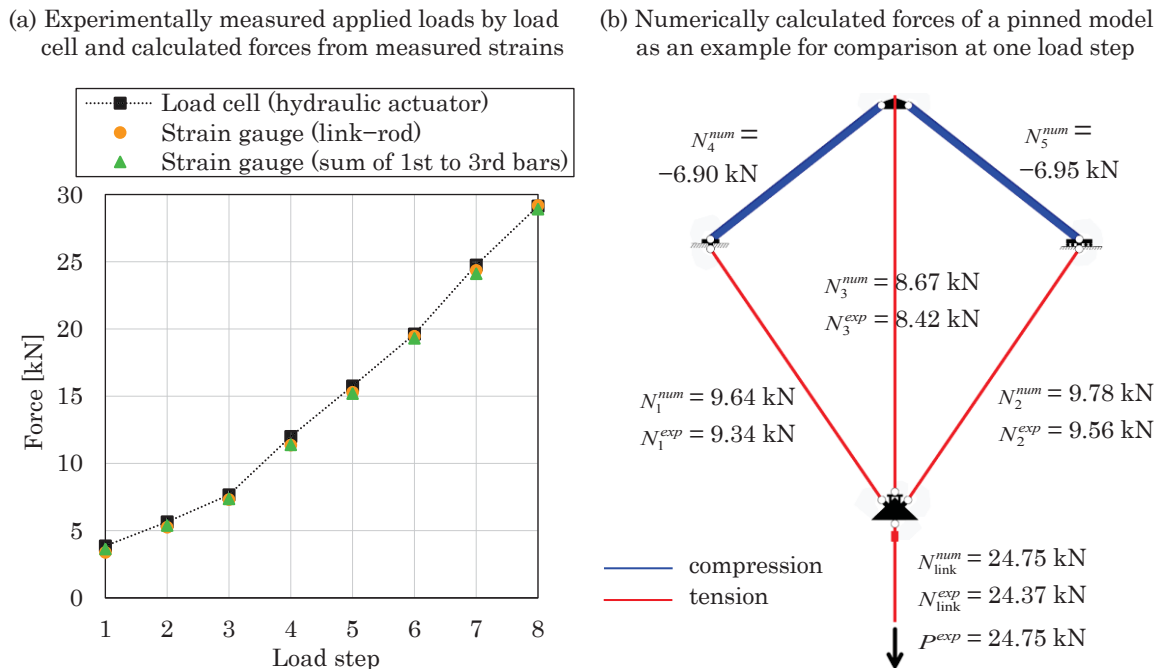


Figure 4.14 – Comparison of measured applied loads of the hydraulic actuator and calculated axial forces from the measured strains in the laboratory experiment of the five-bar truss.

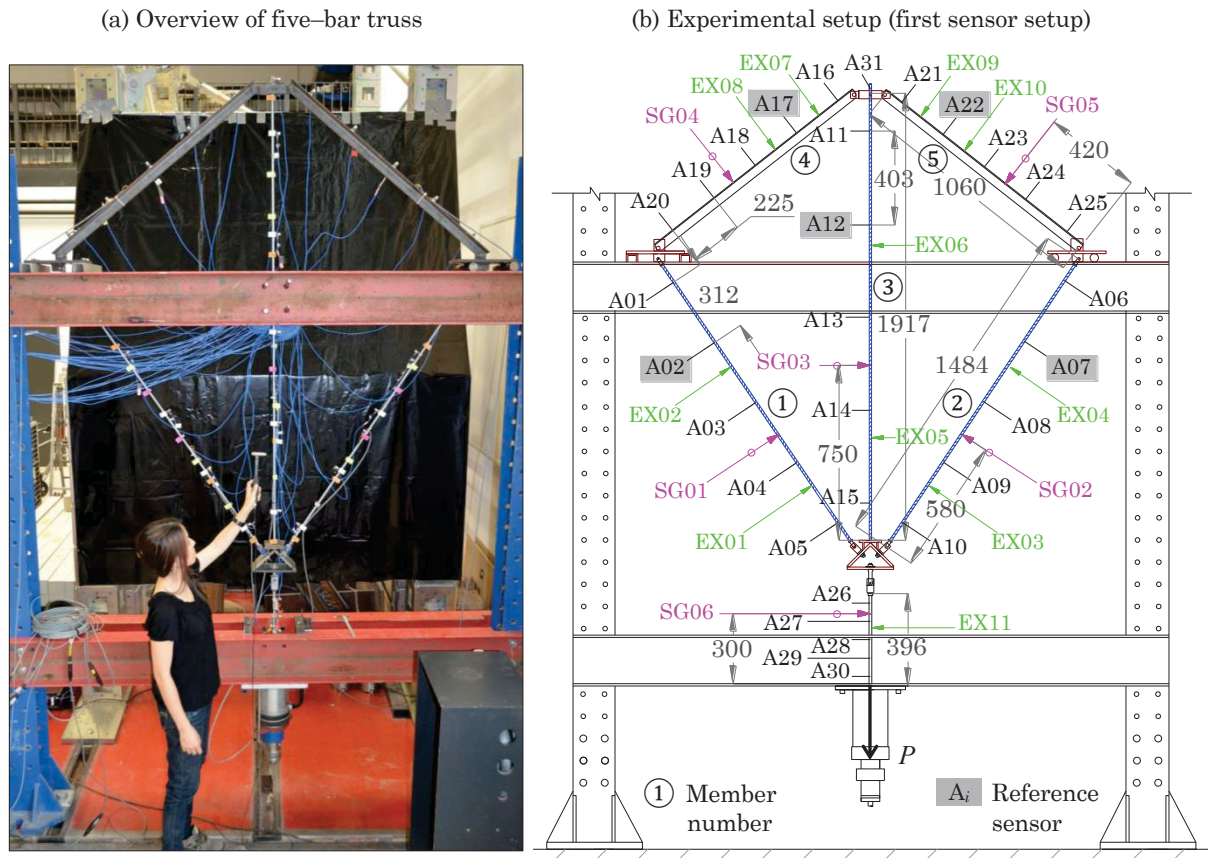


Figure 4.15 – Overview of the laboratory experiment of the five-bar truss structure.

A_i indicates accelerometers, SG_i indicates strain gauge and EX_i indicates excitation points.

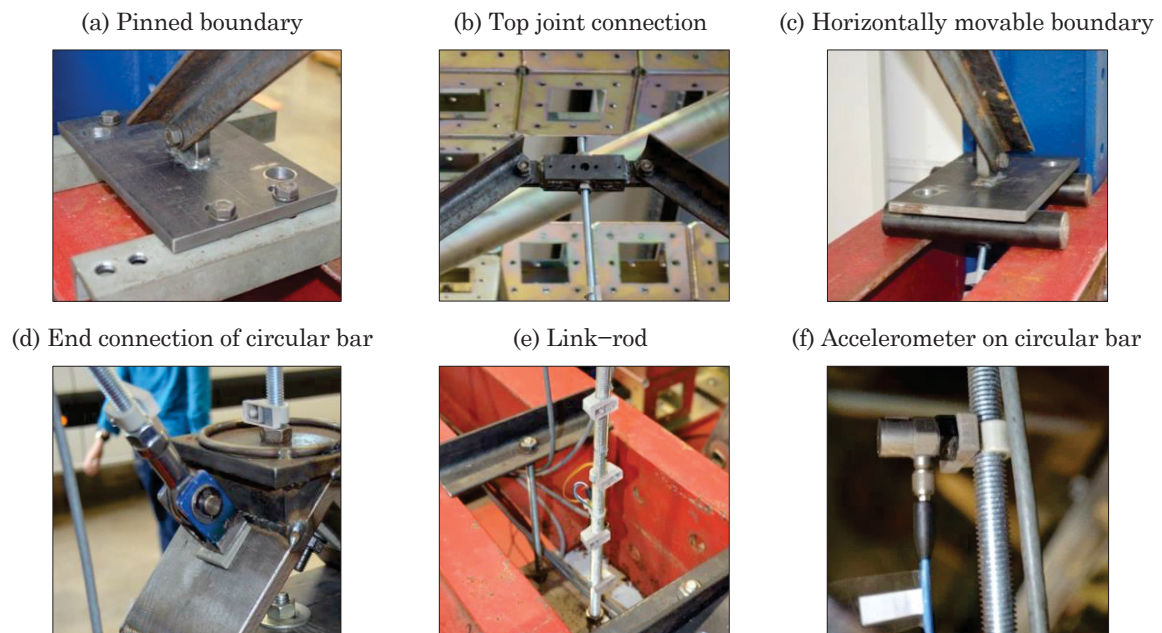


Figure 4.16 – Boundary conditions, joint connections and attached accelerometers on a tension truss member in the laboratory experiment of the five-bar system.

Table 4.17 – Measured applied forces of the hydraulic actuator and calculated member axial forces from the measured strains in the laboratory experiment of the five–bar truss.

Load step	Measurement of load cell	Measurement of strain gauges					
		Bar 1		Bar 2		Bar 3	
	P^{exp} [kN]	N_1^{exp} [kN]	σ_1^{exp} [N/mm ²]	N_2^{exp} [kN]	σ_2^{exp} [N/mm ²]	N_3^{exp} [kN]	σ_3^{exp} [N/mm ²]
1	3.86	1.70	23.93	2.02	28.44	0.56	7.84
2	5.65	2.38	33.63	2.69	37.90	1.18	16.61
3	7.66	3.15	44.47	3.42	48.31	1.91	26.88
4	12.00	4.65	65.56	4.91	69.29	3.46	48.79
5	15.76	6.06	85.42	6.30	88.90	4.95	69.84
6	19.62	7.58	106.87	7.82	110.28	6.54	92.27
7	24.75	9.34	131.83	9.58	135.08	8.42	118.84
8	29.14	11.09	156.42	11.32	159.75	10.33	145.67

with a mass density of 7850 kg/m³. The tension bars have the modulus of elasticity of 205 000 N/mm² according to the tensile tests performed at BAM. The modulus of elasticity of the compression top chords are also assumed to be 205 000 N/mm².

An overview of the five–bar truss laboratory system is shown in Figure 4.15(a). The load is applied to the system by hydraulic actuator at the end of the link–rod. The magnitude of the load is increased gradually, aiming to study the change in the modal parameters and the reliability of the proposed methodology according to different stress states.

To double–check the static equilibrium of the forces by different measurements, the applied forces of the hydraulic actuator measured by the load cell and the sum of the forces that are calculated from the measured strains in the members are compared in Figure 4.14. In addition, a static calculation of the numerical model at one load step, assuming pinned–jointed model, is shown to compare with the experimental measurements. A reasonable agreement of the forces by different measurements and between the experimentally measured and numerically computed forces is found.

Table 4.17 shows the values of the applied forces of the hydraulic actuator measured by the load cell as well as the resulted axial forces and corresponding stresses in the first to third tension bars that are calculated from the measured strains. The applied force was increased progressively from approximately 3.9 kN to 29 kN, corresponding to a low and intermediate stress of about 24 N/mm² and 156 N/mm² in the first tension member.

Table 4.18 – Experimentally identified natural frequencies of the first six modes in the laboratory experiment of the five–bar system.

Load step	f_n^{exp} (SSI) [Hz]					
	1st mode	2nd mode	3rd mode	4th mode	5th mode	6th mode*
1	15.56	19.04	23.94	33.27	42.42	–
2	17.92	24.58	27.24	37.54	45.58	57.09
3	20.42	27.39	30.47	41.62	49.95	56.97
4	24.67	32.20	35.91	48.60	58.00	56.06
5	27.70	36.04	40.31	53.73	63.37	55.92
6	30.59	39.80	44.55	57.62	69.70	55.56
7	33.62	43.76	48.95	63.71	75.13	55.25
8	36.53	47.44	53.30	69.61	80.00	54.52

*The order of the 1st to 6th mode is sorted according to the first load step; the 6th mode corresponds to the vibration mode of the compressive top chord, as a result, the frequencies are reduced at higher applied loads and cause interchange of modes at different load steps.

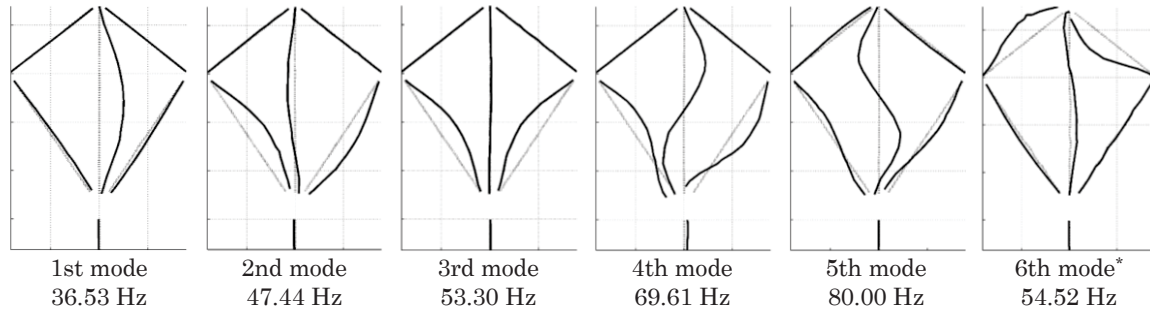


Figure 4.17 – Experimentally identified mode shapes of the first six modes at the eighth load step in the laboratory experiment of five-bar truss system.

The applied loads were limited taking into consideration the buckling loads of the compression top chords. It is noted that as the system is not absolutely symmetric, the forces are different for the first and second truss members of similar characteristics.

4.4.1 Modal Parameter Identification

The setups of the sensors are presented in Figure 4.15 and at the end of the Appendix. The experiments were performed in three setups to obtain sufficient resolutions of the mode shapes. The tests were implemented considering fixed reference points and roving measuring points. In total, 30 piezoelectric accelerometers PCB/352C33 were used in one setup. Excluding the link-rod, a total of 13 measurement points of each tension or compression member of the truss were obtained in three setups, resulting in a total of 65 measurement points for the five truss members in all three setups. The responses were evaluated in terms of accelerations in the vertical and longitudinal directions. Vibration measurements were carried out with hammer excitation on the members of the five-bar truss at a sampling frequency of 2048 Hz. The modal parameters were extracted from the measured responses using a reference-based covariance-driven SSI technique, similar to the single bars and two-bar structure.

The identified natural frequencies of the first six modes of the five-bar truss are provided in Table 4.18. The natural frequencies associated with the vibration modes of the tension members are increased with higher applied loads. However, the frequencies associated with the vibration modes of the compression top chords are decreased at the same time. The coexistence of both tensile and compressive forces causes interchange of modes. Thus, it is necessary to sort out the order of the mode carefully at different load steps.

Table 4.19 – Identified axial forces in the first tension member by applying the analytical-based algorithm for the first six modes in the laboratory experiment of the five-bar system.

Load step	N_1^a [kN]					
	1st mode	2nd mode	3rd mode	4th mode	5th mode	6th mode
1	1.53	1.83	1.36	0.98	0.72	-0.78
2	2.43	1.89	2.19	1.67	1.53	3.30
3	4.11	2.67	2.72	2.50	2.34	2.68
4	5.10	4.39	4.26	4.01	3.93	-
5	9.45	5.54	5.29	5.58	5.48	5.29
6	9.72	7.15	7.95	5.42	6.70	6.98
7	12.21	8.73	9.13	2.47	8.98	8.71
8	17.38	11.31	11.36	11.33	10.78	10.38

The configurations of the six experimentally identified modes of the five-bar structure are presented in Figure 4.17. Furthermore, to examine the selection of the modes to use the analytical-based algorithm, the analytical-based algorithm by MAES et al. (2013) was used to calculate the member forces based on the experimentally identified modes. The results of the estimated forces in the first tension member by the analytical-based method using the six experimental modes are provided in Table 4.19. The forces vary between the different modes. Theoretically, the forces can be determined accurately for different modes if the mode shape displacement does not coincide with a nodal point. However, the experimental data are subjected to measurement errors. Therefore, the measurements of the mode shape displacements can be sensitive to the experimental errors. In the case of the first member, the experimentally identified third mode with the highest value of the relative MSE was chosen. The choice of the mode in the form of the first vibration mode of a single beam gives a reasonable estimation of the forces.

4.4.2 Identification of Axial Force and Joint Stiffness

To implement the proposed methodology, the first four to six experimentally identified modes of the five-bar truss structure were used in the identification process. Similar to the numerical study, the updating parameters are the applied load and the rotational spring stiffness of the joints, assuming identical at symmetrical locations of the truss. Table 4.20 gives the results of the identified loads and member axial forces as well as corresponding stresses of the first two tension members of the five-bar structure. The forces in the other members including the compression members were also obtained by static force equilibrium but for simplicity, they are not presented.

Table 4.20 – Results of the identified loads, axial forces and axial stresses of the first to second tension members in the laboratory experiment of the five-bar truss.

Target system	Technique	P^{id} [kN]	Δ [kN]	Δ [%]	N_1^{id} [kN]	σ_1^{id} [N/mm ²]	Δ [kN]	Δ [%]	N_2^{id} [kN]	σ_2^{id} [N/mm ²]	Δ [kN]	Δ [%]
1	ARSM	3.78	-0.09	-2.07	1.53	21.53	-0.17	-10.00	1.55	21.84	-0.47	-23.27
	GA	3.58	-0.28	-7.25	1.45	20.44	-0.25	-14.71	1.47	20.74	-0.55	-27.23
	PSO	3.64	-0.23	-5.70	1.47	20.75	-0.23	-13.53	1.49	21.05	-0.52	-26.24
2	ARSM	5.47	-0.18	-3.19	2.19	30.88	-0.20	-7.98	2.22	31.32	-0.47	-17.47
	GA	5.50	-0.15	-2.65	2.20	31.04	-0.18	-7.56	2.23	31.47	-0.46	-17.10
	PSO	5.45	-0.20	-3.54	2.18	30.77	-0.20	-8.40	2.21	31.19	-0.48	-17.84
3	ARSM	8.01	0.35	4.57	3.18	44.91	0.03	0.95	3.23	45.51	-0.20	-5.56
	GA	7.32	-0.34	-4.44	2.91	41.11	-0.24	-7.62	2.95	41.67	-0.47	-13.74
	PSO	7.23	-0.44	-5.61	2.88	40.56	-0.28	-8.57	2.92	41.12	-0.51	-14.62
4	ARSM	12.19	0.19	1.58	4.82	67.96	0.17	3.66	4.88	68.87	-0.03	-0.61
	GA	11.28	-0.72	-6.00	4.46	62.92	-0.19	-4.09	4.52	63.77	-0.39	-7.94
	PSO	11.57	-0.43	-3.58	4.55	64.25	-0.09	-2.15	4.62	65.12	-0.30	-5.91
5	ARSM	15.59	-0.17	-1.08	6.15	86.74	0.09	1.49	6.23	87.89	-0.07	-1.11
	GA	15.27	-0.50	-3.11	6.02	84.94	-0.03	-0.66	6.10	86.07	-0.20	-3.17
	PSO	16.53	0.76	4.89	6.51	91.88	0.46	7.43	6.60	93.14	0.30	4.76
6	ARSM	18.75	-0.87	-4.43	7.38	104.16	-0.19	-2.64	7.48	105.57	-0.33	-4.35
	GA	20.21	0.60	3.01	7.96	112.24	0.38	5.01	8.06	113.74	0.24	3.07
	PSO	20.23	0.61	3.11	7.96	112.30	0.39	5.01	8.07	113.79	0.25	3.20
7	ARSM	24.12	-0.63	-2.55	9.48	133.79	0.14	1.50	9.61	135.55	0.03	0.31
	GA	24.17	-0.58	-2.34	9.50	134.07	0.16	1.71	9.63	135.86	0.06	0.52
	PSO	24.13	-0.63	-2.51	9.49	133.81	0.14	1.61	9.61	135.58	0.04	0.31
8	ARSM	29.75	0.61	2.09	11.68	164.77	0.59	5.32	11.83	166.92	0.51	4.51
	GA	29.68	0.54	1.85	11.65	164.40	0.57	5.05	11.81	166.57	0.48	4.33
	PSO	29.72	0.58	1.99	11.67	164.63	0.58	5.23	11.82	166.81	0.50	4.42

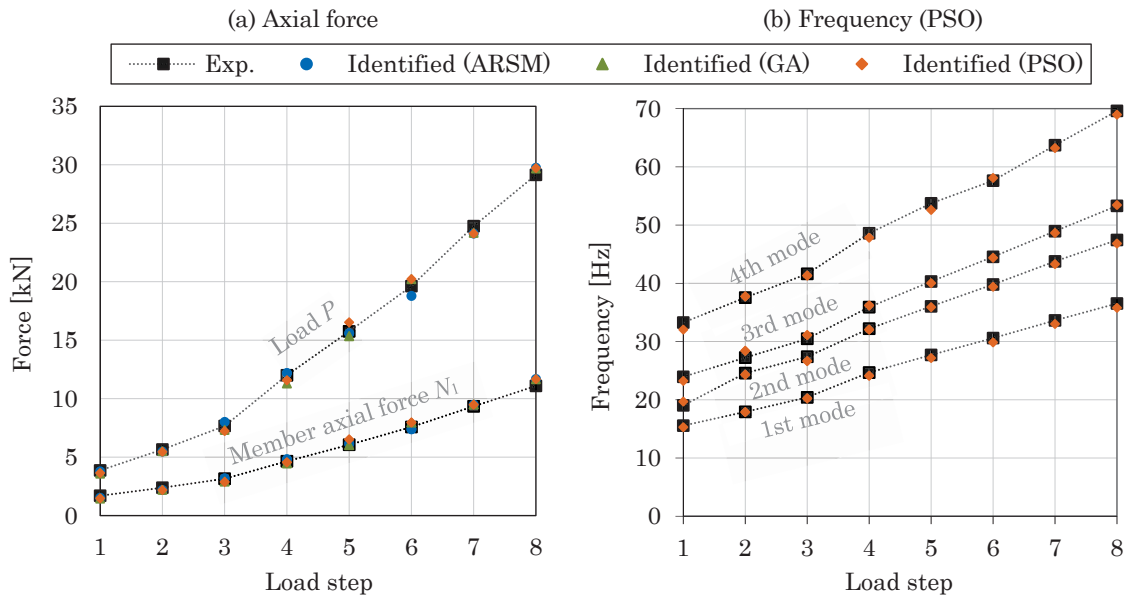


Figure 4.18 – Results of the identified axial forces and natural frequencies of the first four modes in the laboratory experiment of the five-bar truss.

The identified axial forces by the proposed methodology match reasonably well to the experimentally measured forces for all load states. Note that the experimental loads are those measured by a load cell at the hydraulic actuator, while the experimental member forces are the calculated forces from the measured strains for each of the truss member.

The differences between the identified forces and the experimentally measured ones fall below 0.9 kN in absolute value for all load steps and by all optimization techniques. The largest difference of the identified to the true force by the ARSM is -0.87 kN, which is equivalent to a relative difference of -4.43% . The GA and PSO perform generally more consistent than the ARSM, with a maximum deviation of -0.72 kN (-6.00%) and 0.76 kN (4.89%), respectively.

The identified forces by the proposed methodology are also plotted with the experimentally measured forces in Figure 4.18(a). Moreover, the numerically estimated and experimentally identified natural frequencies of the first four modes by the PSO are shown in Figure 4.18(b). Similar results of the estimated modal parameters were acquired by the ARSM and GA. The estimated and experimental obtained natural frequencies agree well. The MAC values range from 0.81 to 0.98, indicating a relatively good consistency of the estimated and experimentally identified mode shapes.

Table 4.21 provides the identified rotational spring stiffnesses and fixity factors. In general, the joints become more rigid at higher applied loads. For instance, the joint stiffness of the connection to the link-rod is close to a pinned connection at the lowest stage of the applied load but gets more rigid as the load is increased. It is again demonstrated that the assumption of pinned joints for the truss does not approximate accurately the dynamic responses of the structure's modal parameters. If considering the consistency of the increase in the level of the joint rigidity at higher applied loads, the GA provides in general the most consistent results. The ARSM shows in more cases a less consistent result compared to the other two techniques.

For the top chords that are less flexible members compared to the tension bars, the joint flexibility shows a reasonably consistent level of semi-rigidity. The changes in the joint

Table 4.21 – Results of the identified rotational spring stiffness and fixity factors in the laboratory experiments of five–bar system.

Load step	Technique	$k_{rI,1}^{id}$ [kNm/rad]	$\gamma_{krI,1}^{id}$ [-]	$k_{rIII,1}^{id}$ [kNm/rad]	$\gamma_{krIII,1}^{id}$ [-]	$k_{rIII,3}^{id}$ [kNm/rad]	$\gamma_{krIII,3}^{id}$ [-]	$k_{rIII,link}^{id}$ [kNm/rad]	$\gamma_{krIII,link}^{id}$ [-]	$k_{rIV,4}^{id}$ [kNm/rad]	$\gamma_{krIV,4}^{id}$ [-]
1	ARSM	0.51	0.75	1.50	0.90	0.48	0.79	0.10	0.04	76.24	0.68
	GA	0.61	0.79	1.96	0.92	6.59	0.89	0.16	0.07	62.22	0.52
	PSO	1.40	0.87	1.00	0.83	0.82	0.66	0.18	0.07	21.06	0.44
2	ARSM	1.53	0.90	2.80	0.94	2.55	0.95	5.90	0.72	18.86	0.41
	GA	0.92	0.83	3.69	0.95	2.22	0.95	132.75	0.97	22.20	0.46
	PSO	1.54	0.89	3.59	0.95	2.27	0.95	3.51	0.50	19.16	0.42
3	ARSM	0.82	0.71	9.09	0.95	1.95	0.94	7.60	0.74	21.78	0.45
	GA	1.99	0.92	3.40	0.95	4.94	0.97	211.35	0.99	21.49	0.45
	PSO	2.91	0.95	10.29	0.98	3.06	0.94	6.36	0.54	34.54	0.55
4	ARSM	0.90	0.69	5.59	0.96	2.27	0.95	113.37	0.86	24.33	0.48
	GA	2.14	0.93	4.63	0.96	8.26	0.99	110.22	0.99	28.94	0.52
	PSO	1.99	0.92	4.36	0.96	3.47	0.96	12.32	0.85	26.71	0.50
5	ARSM	0.99	0.55	7.74	0.97	3.22	0.59	3.42	0.53	17.95	0.40
	GA	4.21	0.96	2.72	0.94	8.22	0.98	133.33	0.97	22.04	0.45
	PSO	0.71	0.65	3.12	0.95	2.41	0.95	21.30	0.87	23.70	0.47
6	ARSM	12.12	0.98	4.45	0.95	12.44	0.99	13.07	0.80	25.01	0.48
	GA	3.41	0.95	1.38	0.89	7.18	0.98	220.45	0.99	25.42	0.49
	PSO	2.86	0.94	1.82	0.91	7.51	0.97	18.21	0.89	26.53	0.50
7	ARSM	2.14	0.66	1.21	0.88	6.52	0.86	4.21	0.65	27.29	0.51
	GA	11.42	0.98	3.28	0.95	9.84	0.99	110.22	0.99	28.09	0.51
	PSO	3.42	0.77	10.39	0.98	5.62	0.98	28.35	0.77	27.86	0.51
8	ARSM	8.17	0.56	16.41	0.99	2.06	0.93	12.14	0.79	31.36	0.54
	GA	16.31	0.99	12.49	0.99	1.51	0.92	151.82	0.98	33.47	0.56
	PSO	16.25	0.99	6.46	0.94	1.07	0.87	3.95	0.64	29.92	0.53

Assumptions: $k_{rI,1}^{id} = k_{rIII,1}^{id}$; $k_{rIII,1}^{id} = k_{rIII,2}^{id}$; $k_{rI,4}^{id} = k_{rIII,5}^{id} = k_{rIV,4}^{id} = k_{rIV,5}^{id}$.

rigidity of the compression top chords are reasonably small compared to the other joints. The level of the rigidity of the top chords depend on the structural characteristics of the members; thus, a high level of rigidity for the compression top chords was not reached.

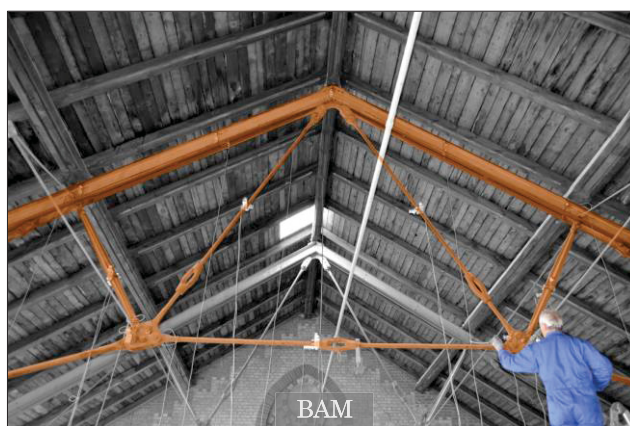
4.5 Discussions

The laboratory experiments of three types of systems that form part of a built–up truss structures were performed, i.e. single bars, two–bar systems and a five–bar truss. The following remarks are drawn.

- Truss structures can be considered easily excited structures; the modal parameters of truss structures could be identified relatively well.
- Better identification of the modal parameters was achieved for truss–type structures of higher slenderness and subjected to higher stress states.
- Five or more measuring points are recommended for truss members to estimate accurately the mode shapes and to apply the proposed methodology.
- The experimental study shows that the proposed methodology can identify the applied loads and the member axial forces with reasonably good accuracy.
- The joint rotational stiffness indicates in general an increasing trend in the rigidity level when the system is loaded and stresses.
- From the experimental studies, the proposed methodology is a feasible approach to identify the resulting tensile forces and the joint stiffnesses in axially loaded structural members as part of a truss–type structure.

5

RECOMMENDATIONS FOR IN-SITU EXPERIMENTS



An in-situ test on a historic Wiegmann–Polonceau roof truss in the city of Potsdam is described in this chapter. The feasibility of identifying the modal parameters of existing trusses is evaluated. Based on the experimental modal parameters, the possibility to estimate the axial forces by the proposed methodology in real-life applications is discussed. The findings provide foundation and recommendations for future in-situ tests on existing truss structures.

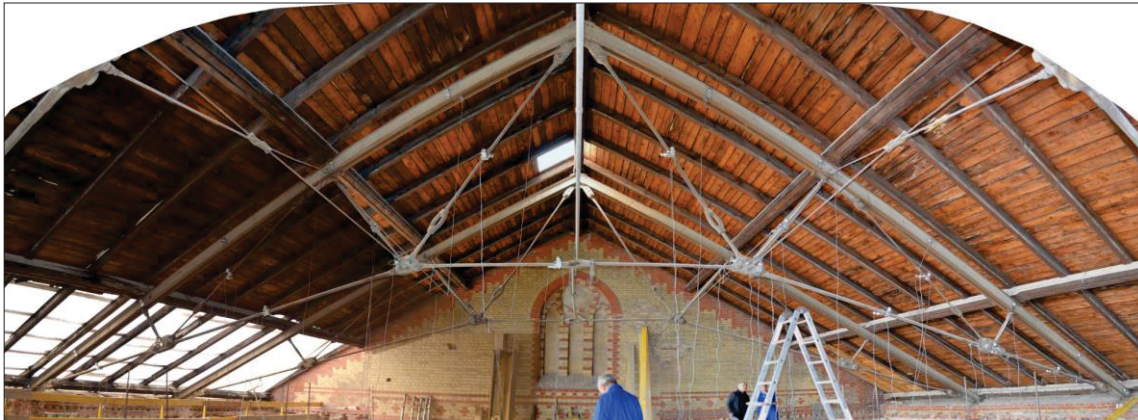
5.1 Purpose and Scope of In-situ Experiment

The in-situ experiment was performed to assess the possibility of identifying the modal parameters of an existing historic truss structure, based on the state of the work in 2012. The tests were carried out as a cooperation between Brandenburg University of Technology Cottbus-Senftenberg and Bundesanstalt für Materialforschung und -prüfung (BAM). The truss structure was chosen for the experiment as it sets a good example of an historic light-weight iron truss structure that is characterized primarily by axial forces. After the laboratory experiments were performed that allowed the development and validation of the proposed methodology, further analyses were made for the in-situ test to examine the axial force estimation of the existing truss.

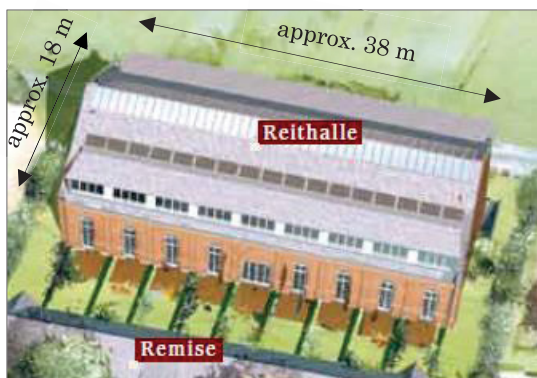
5.2 Description of Historic Truss Structure

The investigated historic Wiegman-Polonceau truss is located at a formerly horse riding building called *Reithalle*, which was constructed between 1885 and 1891 in the city of Potsdam, Germany [SIGEL et al. (2006)]. The building is approximately 18 m wide and 38 m long. The roof system consists of eight individual trusses at about 4.2 m from each other and connected with each other by horizontal tie bars. (see Figure 5.1).

(a) Overview of a single truss system



(b) Architectural illustration of the building in a renovated project for residential apartments.



(c) Overview of a series of truss systems

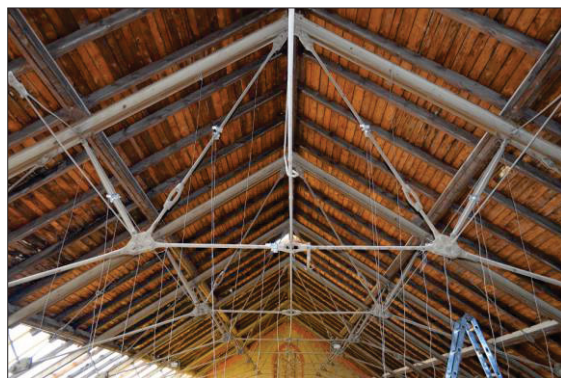


Figure 5.1 – In-situ experiments on a historic Wiegman-Polonceau truss.

From 2000 to 2013, renovation works were planned and carried out for the cultural heritage protected building within a residential apartment project, in which the building's exterior walls and the iron roof trusses were preserved.

Considering one single truss system, the truss is approximately 18 m wide and 6 m high and is positioned at about 5.8 m above the ground level. Several tension members of the

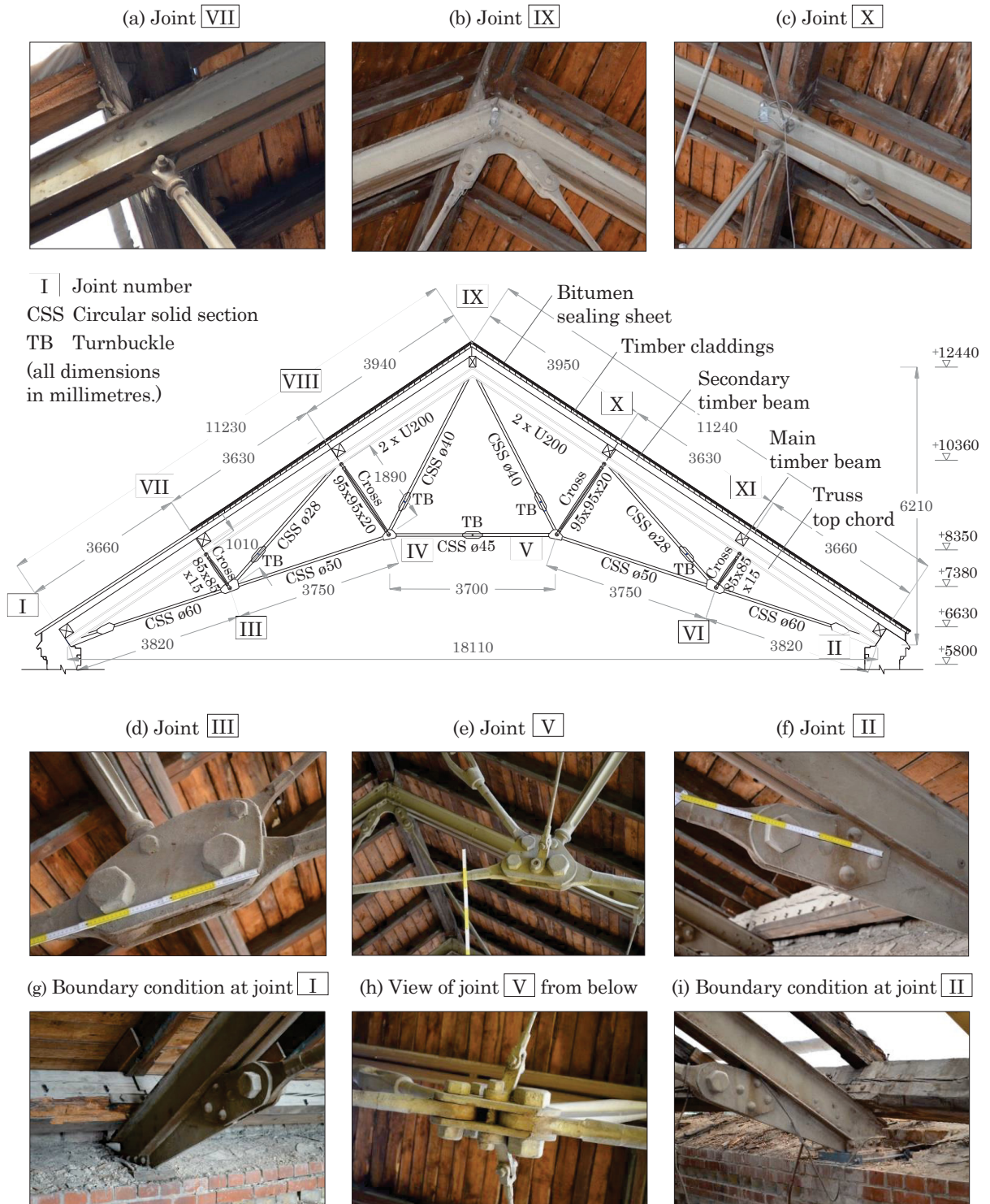


Figure 5.2 – Detailed view of one single truss system at *Reithalle* in Potsdam and selected joints.

truss have turnbuckles to allow compensation for differences in manufacture, i.e. the member dimensions could be adjusted during erection and preloading could be applied to achieve a desired deformation or prestress state of the truss. The shape of the strut members in compression is thickened in the middle to avoid buckling. This shape was assumed to be optimal and economical form for small cast iron compression members of the Wiegmann–Polonceau trusses. The view of one single truss system with numbering scheme and the details of several selected joints are given in Figure 5.2. The characteristics of several selected members are shown in Figure 5.3.

5.3 Finite Element Modelling

Before the in-situ experiment was carried out, a structural survey was conducted to measure the geometry of the structure and assess the loading components. After the structural survey, preliminary static and dynamic analyses were carried out using finite element models to examine the structural behaviour of the truss. The program ANSYS® was used. The mechanical properties of the truss are unknown. However, based on a literature research of the historical materials (see Table 1.1 in Chapter 1), the mechanical properties of the truss were assumed as the modulus of elasticity of the wrought iron of 195 000 N/mm² for all truss members, except the four compression struts.

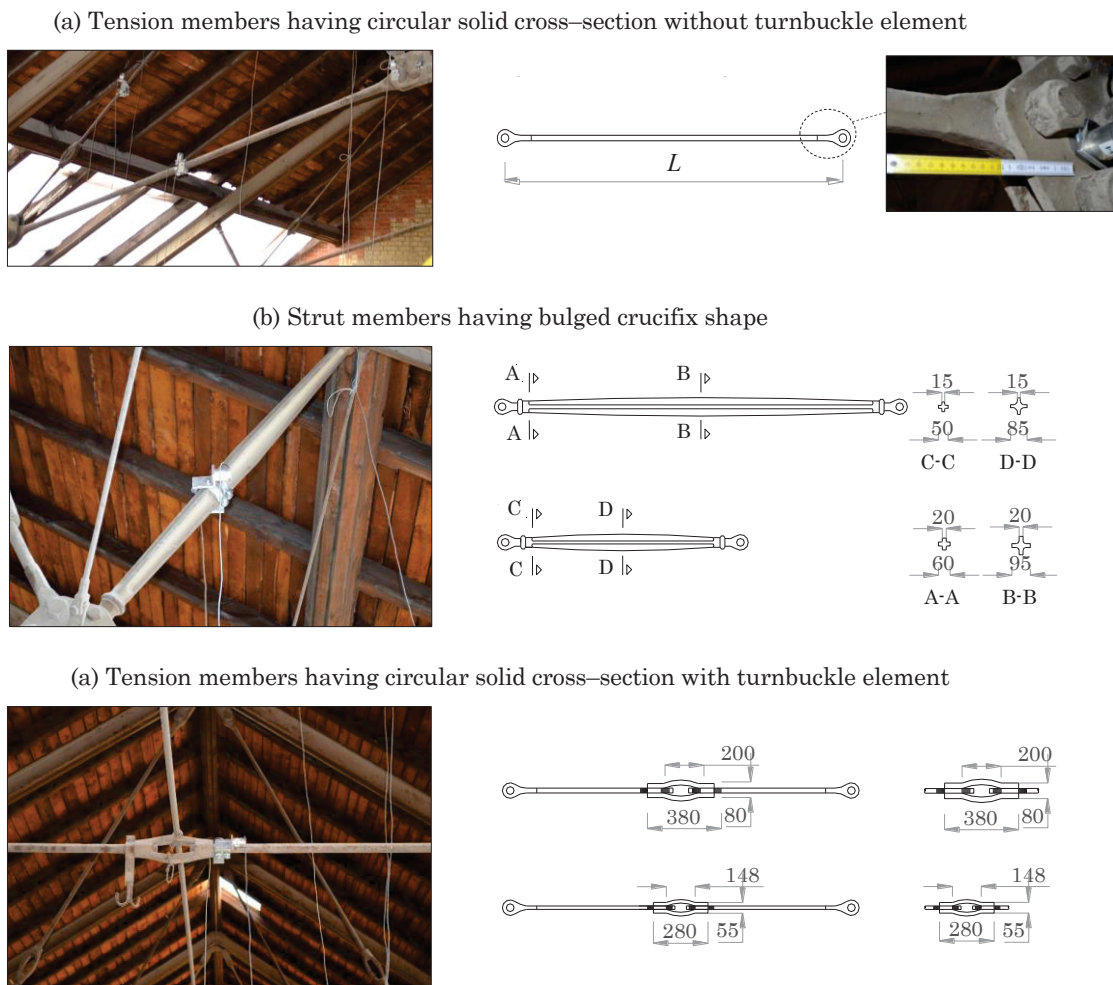


Figure 5.3 – Characteristics of selected members of the historic truss in the in-situ experiment.

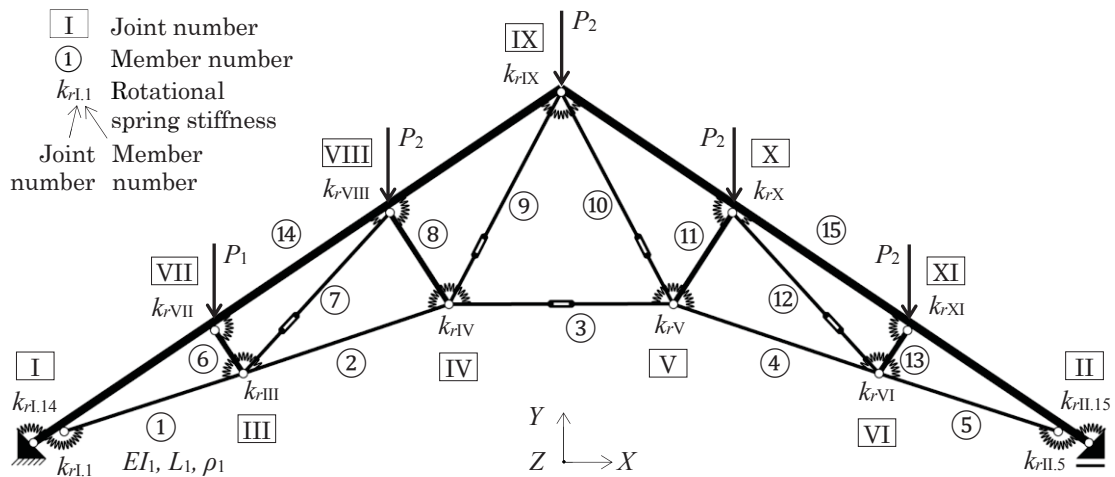


Figure 5.4 – Numerical model of the historic truss with numbering scheme.

These compression struts with the optimal shape were assumed to have the modulus of elasticity of the cast iron of $90\,000\text{ N/mm}^2$. The value of the mass density was chosen as 7850 kg/m^3 and the Poisson ratio of 0.3. The numerical model takes into account the shear deformation and rotational inertia based on Timoshenko beam theory.

The creation process of the finite element models shown in Figure 5.4 involved different assumptions and simplifications to evaluate appropriate assumptions as well as meaningful simplifications for the numerical models that can approximate the behaviour of the structure. In total, four finite element models were built, considering whether both the inertia and mass or only the mass of the gusset plates at the connections and the turnbuckles were included. In addition, different types of elements were examined.

The first model is referred to as a simplified finite element model that includes the mass of the gusset plates and turnbuckles, being modelled as point mass elements (see Figure 5.5a). The second model is also a simplified finite element model but more detailed than the first one, including the inertia and mass of the gusset plates as beam elements with

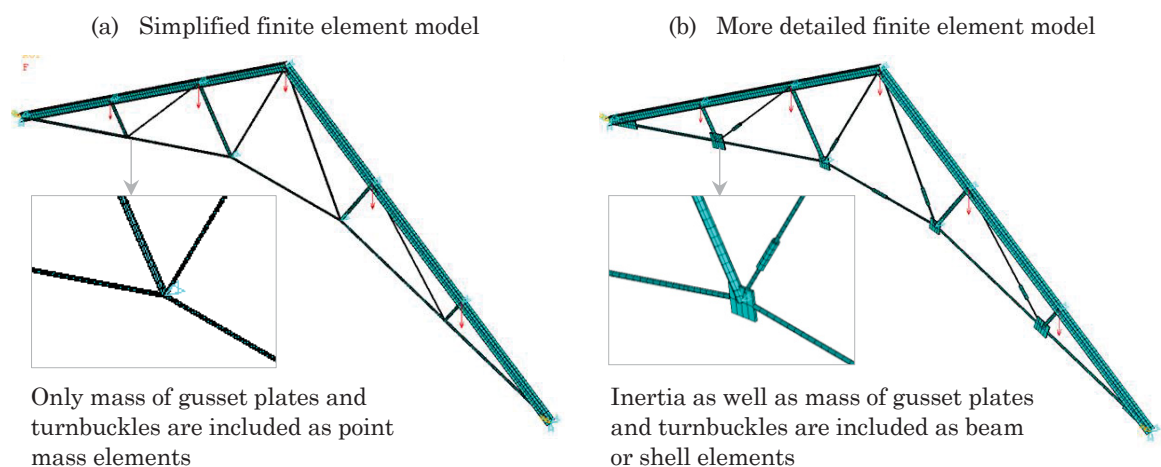


Figure 5.5 – Different finite element models of the truss to examine meaningful simplifications of the numerical models.

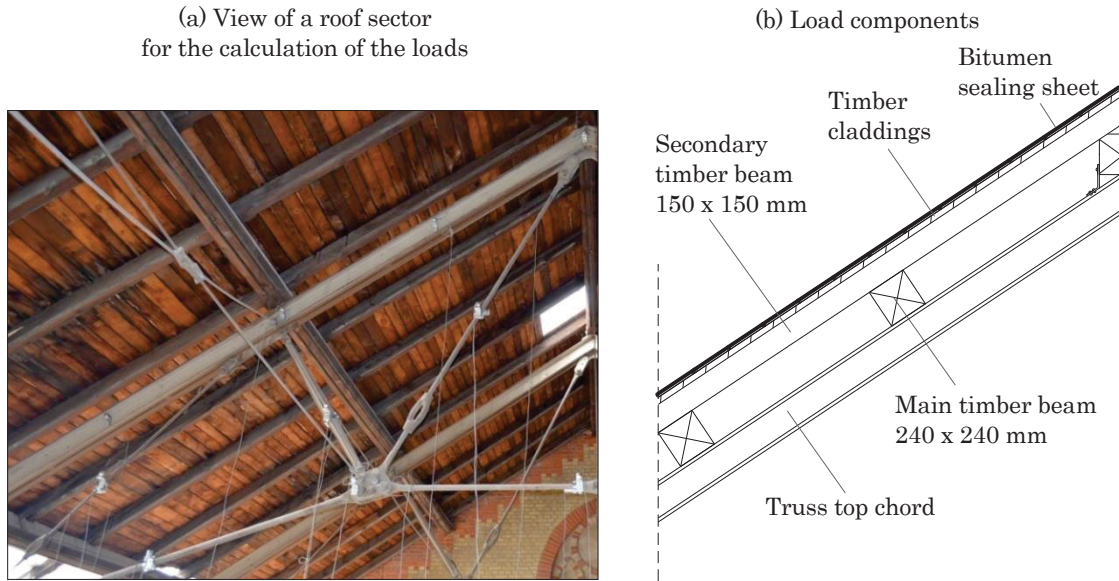


Figure 5.6 – The cross-section showing the components of the loads on the truss.

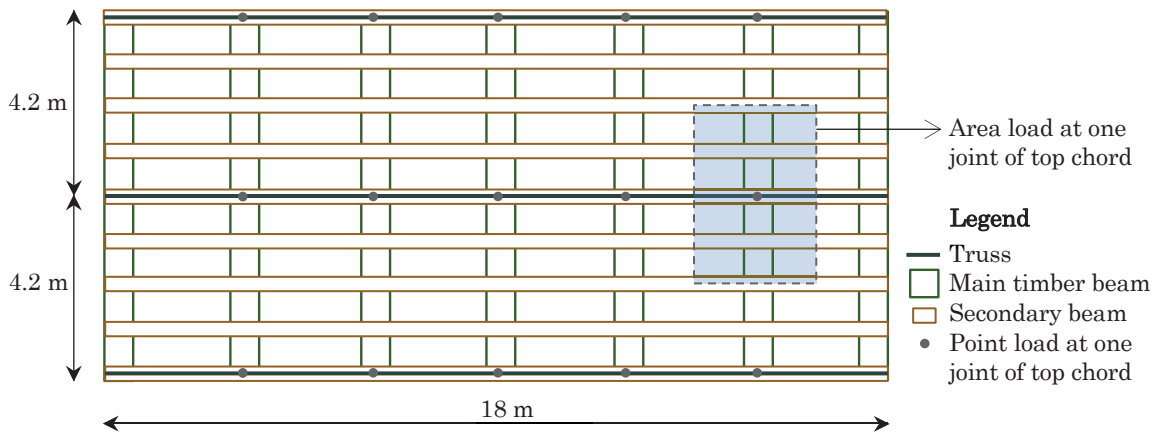


Figure 5.7 – Plan of a unit roof containing three trusses for the calculation of point loads of the roof.

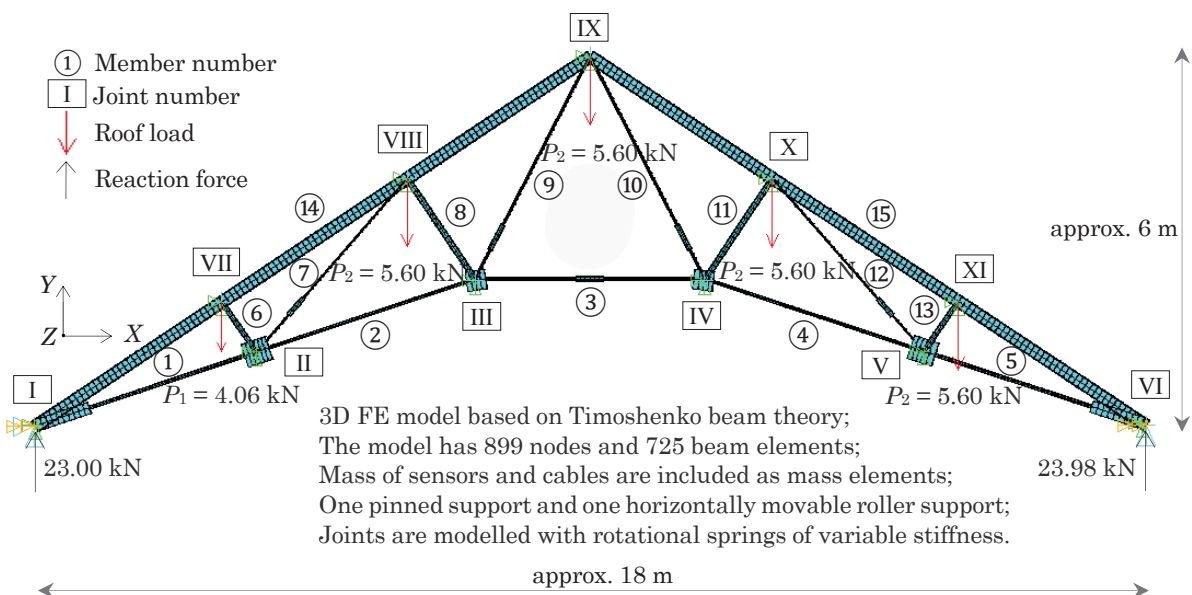


Figure 5.8 – Global finite element model of the truss with assumed applied roof loads.

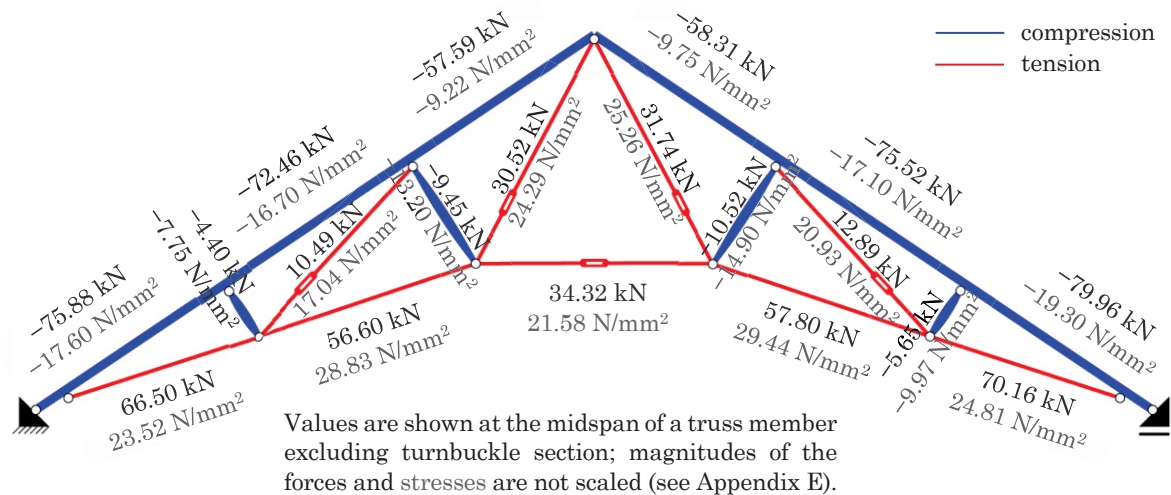


Figure 5.9 – Static axial force and axial stress distribution of global finite element model of the truss.

rectangular cross-sections, and the mass of the turnbuckles. The third model is a more detailed finite element model taking into account the inertia as well as mass of both the gusset plates and turnbuckles; the gusset plates were modelled as beam elements with rectangular cross-sections, while the turnbuckles as beam elements with circular hollow cross-sections (see Figure 5.5b). The fourth model is similar to the third one, except that shell elements were chosen for the gusset plates.

The truss model is restrained out-of-plane at nine points, i.e. two points at the boundary conditions, five points at all the joints of the top chord, as well as two points at the fourth, and fifth joints due to the tie-bars connecting the series of the truss systems in space.

For simplification, compression struts were assumed to be modelled as circular solid sections, and turnbuckles were modelled as circular hollow sections.

5.3.1 Static Analysis of Axial Force and Axial Stress Distribution

All models were subjected to the loads of the roof, applying as point loads at five joints on the top chords. The roof loads are resulted from the timber roof above the truss, including the main timber beams, secondary timber beams, timber claddings and bitumen sealing sheets. Figure 5.6 illustrates the load components acting directly on the top chord of the truss. A manual estimation of the roof loads was made. The total point load applied to each joint of the four joints on the top chords was calculated as 5.60 kN, whereas a point load on the remaining joint was estimated at a lower value of 4.06 kN due to the missing timber claddings and bitumen sealing sheets on one section of the roof.

At first, static analyses were performed for all models. An initial basic check of the generated models was done by checking the reaction forces, which are consistent for all models. The sum of the resistant forces applied at the supports was also checked to be equal the total applied dead and live loads. A further check of the model was done by analysing the vertical deflections. The maximum deflection of the truss was obtained similarly by all finite element models of approximately 8.9 mm. After that, dynamic analyses were conducted. The results of the natural frequencies and mode shapes show some differences between the models, demonstrating that modelling assumptions and simplifications affect the dynamic results of the truss. After the analysis process,

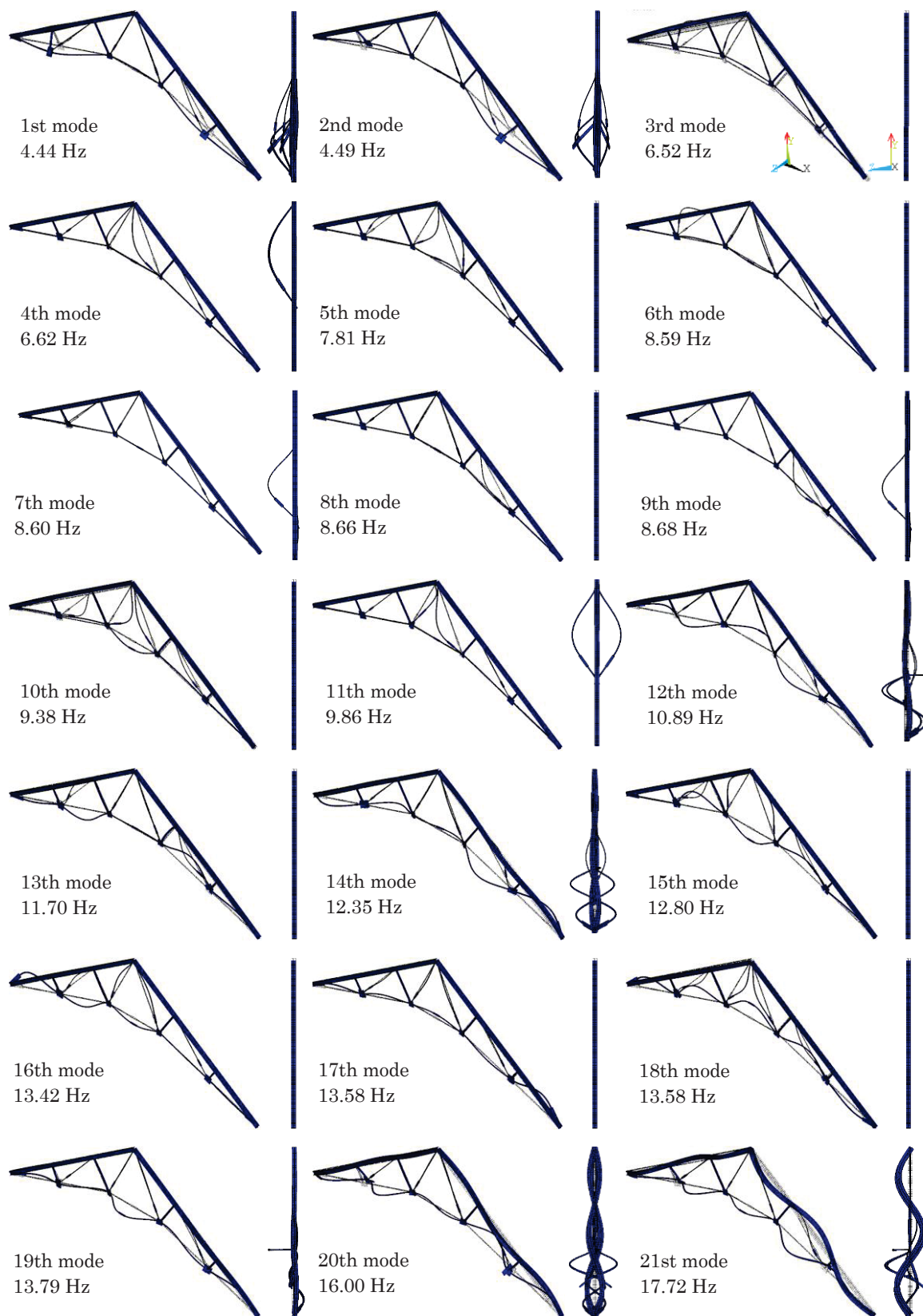


Figure 5.10 – Numerical natural frequencies and mode shapes of the first twenty-one modes of a semi-rigid system ($\gamma_{kr} = 0.15$) at zero-applied force in the in-situ experiment of the historic truss.

the more detailed models taking into account both the inertia and mass of the gusset plates and turnbuckles are recommended over the simplified models to increase the accuracy of the numerical analysis. The third numerical model will be presented in detail.

Figure 5.8 shows the third model together with the assumed roof loads. In total, the model was divided into 725 elements. The left support was modelled as pinned, whereas the right one was modelled as roller that is movable in horizontal direction. The mass of the measurement sensors are included in the truss model.

Figure 5.9 represents the static axial force and corresponding stress distribution of the finite element model. Because the truss geometry is not absolutely symmetric and due to the asymmetric applied roof loads, the resulted axial forces and stresses are not the same for the members of similar characteristics. The relatively low state of stress of the truss was because the building was under construction for the renovation project. Thus, some parts of the roof components were disassembled. In addition, at the time of the investigation of the truss, seasonal loads such as snow loads were not present.

5.3.2 Dynamic Analysis and Stress Stiffening

The first twenty-one modes of the historic truss assumed at zero-applied load are presented in Figure 5.10. A low value of the joint rigidity was chosen for all rotational springs to represent a semi-rigid system that is closer to a pinned truss. It is expected that the effects of stress stiffening will cause intricate variations of the frequencies as well as interchange of modes, since the structure exhibit closely-spaced modes and similar modes of vibration.

In the next part, the results of the in-situ dynamic measurement and analysis of single truss members will be presented. The numerical modelling and analysis strategy applied to individual members as part of a structure will be discussed. When analysing a single member of the truss, a finite element model based on Timoshenko beam theory was built as shown in Figure 5.11.

5.4 In-situ Experiment

The in-situ experiment was conducted considering two types of measurements using geophones and accelerometers. For the measurements using geophones, ambient vibration and hammer excitation measurements were carried out. The geophones were placed at selected connection nodes and middle of the truss members.

Regarding the local measurement, a single member of the truss was selected, which is the second member of the truss. This member offers several advantages for the numerical modelling, such as the geometrical property of the cross-sections can be

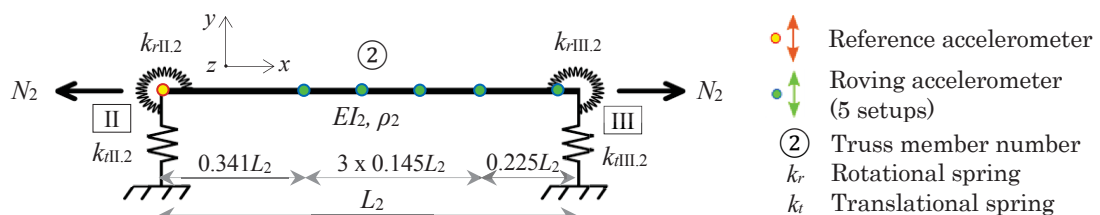


Figure 5.11 – Local measurement and analysis of a single bar as member of a global truss structure.



Figure 5.12 – Setting up of the equipment and performance of the in-situ experiment.

considered uniform symmetric with no presence of turnbuckle elements; therefore, a relative uniform axial stress distribution could be expected. In addition, the effect of the axial tensile force in the member can be studied without concerning the buckling behaviour. Two accelerometers were used, which measured in the transverse direction perpendicular to the local longitudinal direction of the member. One accelerometer was installed as reference, while the other one was moved along the member in five different setups (see Figure 5.11). Because of the on-going renovation work on-site at the time of testing, there were several restrictions as follows. The allowable time to setup and carry out the tests was strictly limited. Furthermore, there were limitations with respect to the number of accessible members for measurements, the number as well as the positions of the sensors to be installed on the truss member. The vibration measurements for the member were conducted with hammer excitation (see Figure 5.12).

5.4.1 Modal Parameter Identification

The experimental modal analysis for the truss member was performed adopting the reference-based covariance-driven SSI. Figure 5.13(a) shows the stabilization diagram of one test setup representing stable poles corresponding to natural frequencies.

In Figure 5.13(b), the identified frequencies and mode shapes of the first twelve modes of the second truss member can be seen, in which the mode shapes are normalized to a maximum modal displacement equal to one. It should be noted that the mode shapes plotted are based on not only the experimental measurements, but also an assumption of an additional location of mode shape displacements, whose values are assumed by polynomial interpolation of the measurement data or based on those from the fifth sensor in the experiment. The reason is the experimental data for this location was not available; while the additional location helps to create a better representation of the mode shapes. It can be noticed that the number of modes for a member of a truss system increases significantly compared to that of a single beam. Similar mode shapes occur at different frequencies, for example the mode of vibration in the form of the first mode shape of a single beam appears at 17.00 Hz as well as 20.19 Hz, which indicates a coupled vibration behaviour of the truss members.

The dynamic test of the global truss allowed the identification of natural frequencies and modal configurations of a large number of vibration modes. The global vibration of the truss is complicated such that closely-spaced and similar vibration modes occur. Due to a lack of measurement points, the identified mode shapes of the truss were not reflected accurately. When comparing with the mode shapes of the finite element model, clearer ideas can be obtained. The natural frequencies of the truss are composed of the frequencies of individual truss members coupled with the connected members.

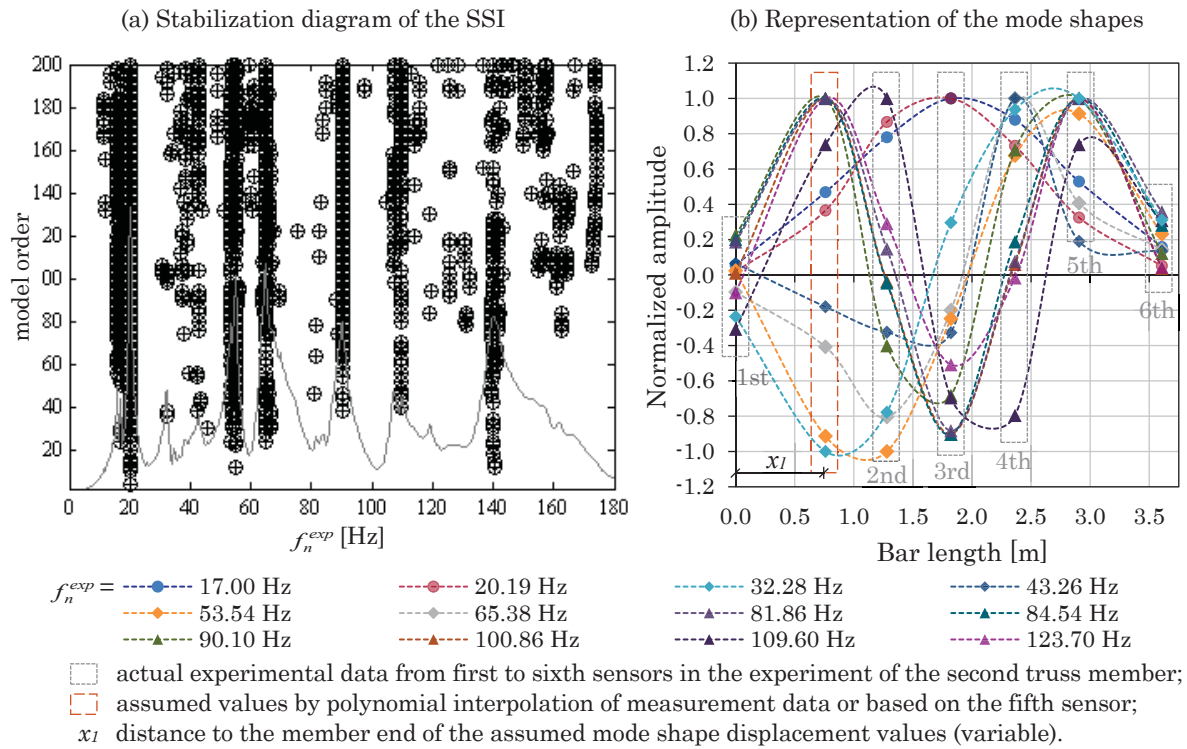


Figure 5.13 – Experimentally identified modal parameters from local measurement of the second truss member.

5.5 Analysis Strategies and Results

The local analysis of a single truss member, i.e. the second truss member, is described [LUONG et al. (2017)]. The finite element model as shown in Figure 5.11 was used; the model has uncertain parameters. A parametric study of uncertain parameters was carried out. The first uncertain parameter is the member axial force, considering that the loads of the roof were only estimated manually. The second uncertain parameter is the rotational spring stiffness of the joint connections. For simplification, the two constraint stiffnesses were assumed to have identical rotational spring stiffness. Beside the axial force and joint flexibility, other uncertain parameters include the modulus of elasticity of the wrought iron, the cross-sectional area and member length.

Table 5.1 – Assumed variations for the parameters of the finite element model of a truss member as single beam.

Parameter	Designation	Initial value	Variation	Limits (lower/upper)	Unit
N	Member axial force	56.60	+/- 17.9 %*	46.47 / 66.77	kN
σ	Member axial stress	28.83		23.67 / 34.01	N/mm ²
γ_j	Joint fixity factor	0.50	Pinned to rigid	0.00 / 1.00	–
E	Modulus of elasticity	195 000	+/- 5 %	185 000 / 205 000	N/mm ²
A	Cross-sectional area	1963.50	-11.64 % / +12.36 %	1734.94 / 2206.18	mm ²
L	Member length**	3500	+8.70 %	3500 / 3750***	mm

d – diameter of solid circular cross-sections; initial value of $d = 50$ mm, variations of d of +/- 3 mm;

*Variation is based on static analysis of the global truss model with +/-30% of the applied roof point loads.

**Variation depends on whether the portions of the member ends embedded in the joints are included or not, maximum distance is from bolt-to-bolt connections.

Table 5.1 provides an overview of the assumed variations of the parameters. The aim is to examine the effects of the parameters on the frequency values and find out appropriate assumptions of the parameters to give the results of the numerical frequencies that match to those identified from the experiments.

The results of the numerically calculated frequencies using the finite element model of the second truss member are shown in Table 5.2. For the case studies of the investigated single truss member, the parameters of the axial stress, the modulus of elasticity and cross-sectional area have less influences on the frequency values than the joint rigidity and member length, as the axial stress was assumed to be varied in a limited range. The joint rigidity has the most significant effect. A number of numerically calculated frequencies in the ranges that are most similar to the experimentally identified frequencies based on the mode of vibration that is in the form of the first mode of vibration of a single beam were identified. The possibility of the numerical frequencies that match to that from the experiment can be diverse, also when other combinations of the parameters are made.

From the preliminary parametric study, for the parameter of joint rigidity, the results of the frequencies show a consistent trend that the joint flexibility are closer to the rigid condition than the common assumption of hinged joints. This can be explained by the presence of friction and possible corrosion damages of historic truss structures.

5.5.1 Identification of Axial Force for Single Truss Member

The parametric study was useful to have a preliminary judgement about the parameters. However, a more exact identification of the parameters is required. The analytical-based algorithm by MAES et al. (2013) was used to estimate the axial force in a single member

Table 5.2 – Numerically calculated natural frequencies based on the finite element model of the second truss member.

σ	N	γ	E	A	L	f_1	Δ_1	f_2	Δ_2	f_3	Δ_3
[N/mm ²]	[kN]	[-]	[N/mm ²]	[mm ²]	[mm]	[Hz]	[%]	[Hz]	[%]	[Hz]	[%]
≈ 0.00	0.00*	0.00	185 000	1734.94	3750	6.70	–	26.79	–	60.22	–
23.67	46.47	0.00	195 000	1963.50	3750	10.10	50.75	31.41	17.25	66.20	9.93
					3500	11.19	67.01	35.55	32.70	75.44	25.27
		0.99	195 000	1963.50	3750	17.73	164.63	46.14	72.23	87.97	46.08
					3500	20.07	199.55	52.56	96.19	100.48	66.85
28.83	56.60	0.00	195 000	1734.94	3750	10.80	61.19	31.27	16.72	64.13	6.49
					3500	11.64	73.73	35.57	32.77	74.48	23.68
		0.00	195 000	2206.18	3500	11.76	75.52	37.55	40.16	79.81	32.53
						205 000	1963.50	11.91	77.76	37.00	38.11
		0.99	195 000	1963.50	3500	18.11	170.30	46.70	74.32	88.51	46.98
						185 000	1963.50	20.07	199.55	51.93	93.84
0.99	195 000	1963.50	3500	20.48	205.67	53.14	98.36	101.14	67.95		
				205 000	20.89	211.79	54.33	102.80	103.51	71.89	
34.01	66.77	0.000	195 000	1963.50	3750	11.20	67.16	32.87	22.70	67.77	12.54
					3500	12.33	84.03	37.03	38.22	77.02	27.90
		0.99	195 000	1963.50	3500	18.52	176.42	47.30	76.56	89.28	48.26
						205 000	2206.18	3500	21.98	228.06	57.35

*Zero-load model, i.e. self-weight only; calculated differences reference to frequencies of zero-load model;

■ Frequencies in most similar ranges with the experimentally identified frequencies based on the form of the mode shape similar to the first mode of vibration of a single beam.

of the truss, i.e. the second member. It requires the instalment of five or more sensors on a member. The identified axial force was obtained from each of the experimentally identified frequency and five amplitudes of the corresponding mode shapes of the member. In addition, the knowledge of the characteristics of the members, among which are the modulus of elasticity, bending stiffness and cross-sectional area, was required.

Using the twelve experimentally identified modal parameters of the single second truss member, the estimated axial forces of the member based on the analytical-based algorithm are, however, in most cases unreasonable due to possible inaccuracy in the measurement data of the mode shape displacements. Negative results of the forces were obtained for most cases. Examples of the identified axial force of the first two modes of the second truss member are provided in Table 5.3. Only for one case of the analyses of the twelve modes using different sets of mode shape displacements, a reasonable value of the axial force was achieved, i.e. 55.48 kN. For this case, the mode used in the analytical-based algorithm was the frequency of 20.19 Hz and the four amplitudes of the corresponding mode shapes displacements from the second to fifth accelerometers, as well as an assumed additional mode shape displacement based on polynomial interpolation of the measurement data.

From the preliminary analysis of the truss model and the parametric study, the initial values and variations of the parameters of the truss member were chosen (see Table 5.4). Because at least five sensors are required for the use of the analytical-based algorithm, whose positions should cover a sufficient length of the member and be not too near the end constraints, a first mode shape displacement was assumed at the position x_1 , whose value was based on polynomial interpolation of the measurement data or in some cases based on the data of the fifth sensor in the experiment.

As the knowledge of the member length is not necessary but only the distance of the sensors to an assumed end point of the member is required, the end point of the member can be random. It was assumed at the point at the bolt connection.

It can be noted that the mode shape displacements are sensitive to the measurement errors. If the values of the mode shape displacements are not accurately identified, it is challenging to identify correctly the axial forces based on the analytical-based algorithm to be used in the proposed methodology.

Table 5.3 – Identified member axial forces and stresses based on analytical-based algorithm using experimentally identified natural frequencies and different sets of mode shape displacements for the first two modes.

Mode	f_n^{exp} [Hz]	Five mode shape displacements by measurement data*		Four mode shape displacements by measurement data and an assumed point of mode shape displacement**	
		N^a [kN]	σ^a [N/mm ²]	N^a [kN]	σ^a [N/mm ²]
1	17.00	—***	—***	—***	—***
2	20.19	—***	—***	55.48	28.26

f_n^{exp} – Experimentally identified frequencies (SSI).

N^a – Member axial force; σ^a – Member axial stress (identified based on MAES et al. (2013)).

* Measurement data of six instrumented sensors along the member; five mode shape displacements were used excluding the first point at zero-length position.

** Measurement data of four instrumented sensors from second to fifth sensors; a point at the first location was added by polynomial interpolation of the measurement data or based on the fifth sensor.

*** Unreasonable values, i.e. negative and/or excessive values exceeding the maximum allowable stress.

Table 5.4 – Assumed values and variations of the parameters using an analytical-based algorithm.

Parameter	Designation	Assumed value	Variation	Range (lower / upper)	Unit
E	Modulus of elasticity	195 000	+/- 5 %	185 000 / 205 000	N/mm ²
A	Cross-sectional area	1963.50	-11.64 % / +12.36 %	1734.94 / 2206.18	mm ²
x_l	Distance to bolted joint*	760	-3.95 % / +2.63 %	730 / 780	mm

*of the assumed mode shape displacement; the other four distances, i.e. x_2 to x_5 , are from the second to fifth sensors in the experiment of the second truss member. At 738 m, the five locations on the mode shapes are equally distributed.

Table 5.5 – Identified member axial forces and stresses based on an analytical-based algorithm for the mode at 20.19 Hz using experimental mode shape displacements and an assumed additional mode shape displacement based on polynomial interpolation of the measurement data.

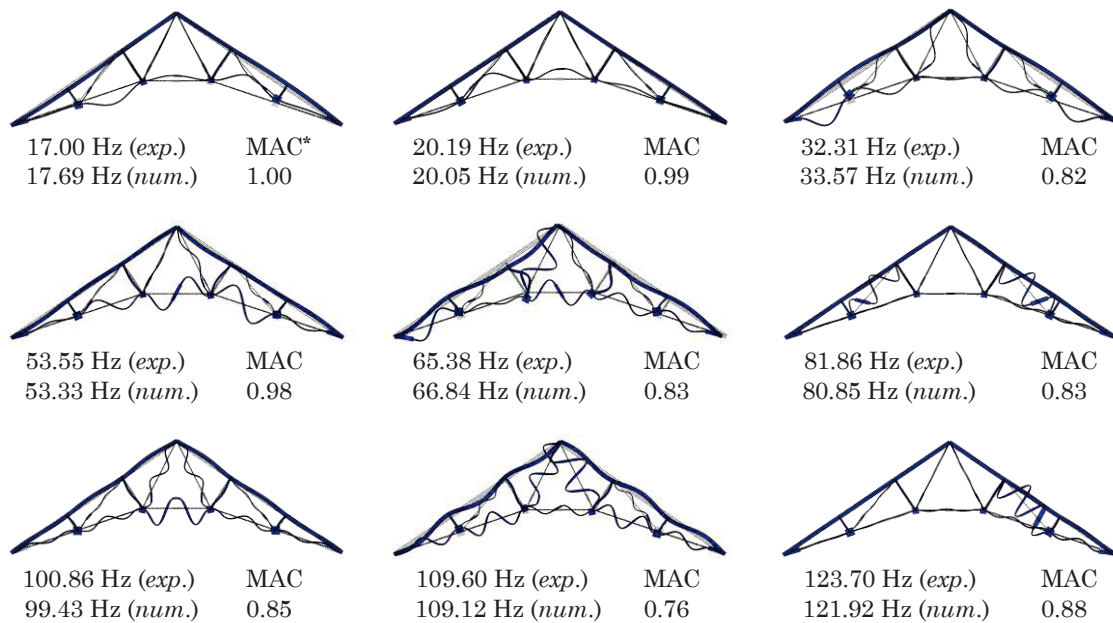
E [N/mm ²]	A [mm ²]	x_l [m]	N^a [kN]	σ^a [N/mm ²]
185 000	1963.50 ($d = 50$ mm)	760	61.75	31.45
195 000	1963.50 ($d = 50$ mm)	760	55.48	28.26
205 000	1963.50 ($d = 50$ mm)	760	49.22	25.07
195 000	1734.94 ($d = 47$ mm)	760	61.59	35.50
195 000	2206.18 ($d = 53$ mm)	760	45.37	20.57
195 000	1963.50 ($d = 50$ mm)	730	34.40	17.52
195 000	1963.50 ($d = 50$ mm)	780	72.15	36.75

The parameters in Table 5.4 were varied in the assumed ranges. The result of the identified axial forces based on the analytical-based algorithm using the mode at 20.19 Hz only are provided in Table 5.5. The identified force of 55.48 kN based on the corresponding input parameters are reasonable compared to the values in Table 5.2. Even though the variations of the input parameters cause varied identified forces, when considering the relevance of the input parameters and the corresponding axial forces compared to that in Table 5.2, the identified forces of 55.48 kN become most relevant.

5.5.2 Preliminary Calibration of the Numerical Model

Based on the analysis of the second member of the truss, a preliminary calibration of the parameters of the finite element model of the truss results in the following structural parameter characteristics: the loads P_1 of 4.04 kN, P_2 of 5.40 kN corresponding to a tensile force of about 55.52 kN and tensile stress of 28.28 N/mm² in the second truss member; the fixity factor of approximately 0.99 that is close to a rigid condition, the modulus of elasticity of 195 000 N/mm² and the cross-section of the second truss member of 1963.50 mm². For the investigated truss structure, the applied loads could be estimated reasonably, as the condition of the renovation progress on-site allowed a relatively clear view of the load components as well as accessibility to the structure. However, this is usually not the case for historic constructions.

The results of the local analysis were based on an assumption of an additional mode shape displacement due to the limitation of the positions of the instrumented sensors on the investigated truss member and insufficient measurement points. Thus, the results can vary depending on the assumptions of the location as well magnitude of the additional mode shape displacement. It is highly recommended for in-situ tests on existing truss structures to install at least five sensors on a member to cover a sufficient member length, when the testing condition allows such designs of experiments.



*MAC values using the experimental data of the second to sixth sensors of the second truss member.

Figure 5.14 – Numerical mode shapes of the truss model based on the pairing of the experimentally identified and numerically computed modes of the second truss member.

The natural frequencies and mode shapes of the nine in-plane modes of vibration of the finite element model of the truss in comparison with the experimentally identified modal parameters of the second truss member are shown in Figure 5.14. Only the results with a MAC value of at least 0.75 are presented. A reasonable degree of agreement between the experimentally identified and numerically calculated modal parameters was found.

5.6 Recommended Scheme for Future In-situ Experiments

A reliable application of the proposed methodology to identify the stress states and estimate the joint flexibility of truss structures require additional measurement data, considering the coupled vibration behaviour of multiple-member structures and the effects of the experimental uncertainties.

The findings from the in-situ test provide suggestions for future experiments on existing truss structures. A recommended scheme is given in Figure 5.15. The recommendations aim to give a stepwise procedure for the safety assessment of the stress state of existing real-scale truss-type structures.

The recommended scheme can be divided into five phases. The first and second phases concern the collection of all the possible data of the structure, including the historical information, geometrical survey, the mechanical materials characterization, a dynamic modal test and a numerical model analysis for static and dynamic calibration. The test planning can be designed at the end of the second phase. In the third phase, in-situ vibration measurements are performed. The modal parameter identification is conducted in the fourth phase. The proposed methodology is applied to determine the stress states and evaluate the joint flexibility of truss structures. In the last phase, conclusions are drawn to assess the safety of the truss structures. As with every engineering task, the decisive factor for the quality of the assessment solution is based on sound engineering-based judgements.

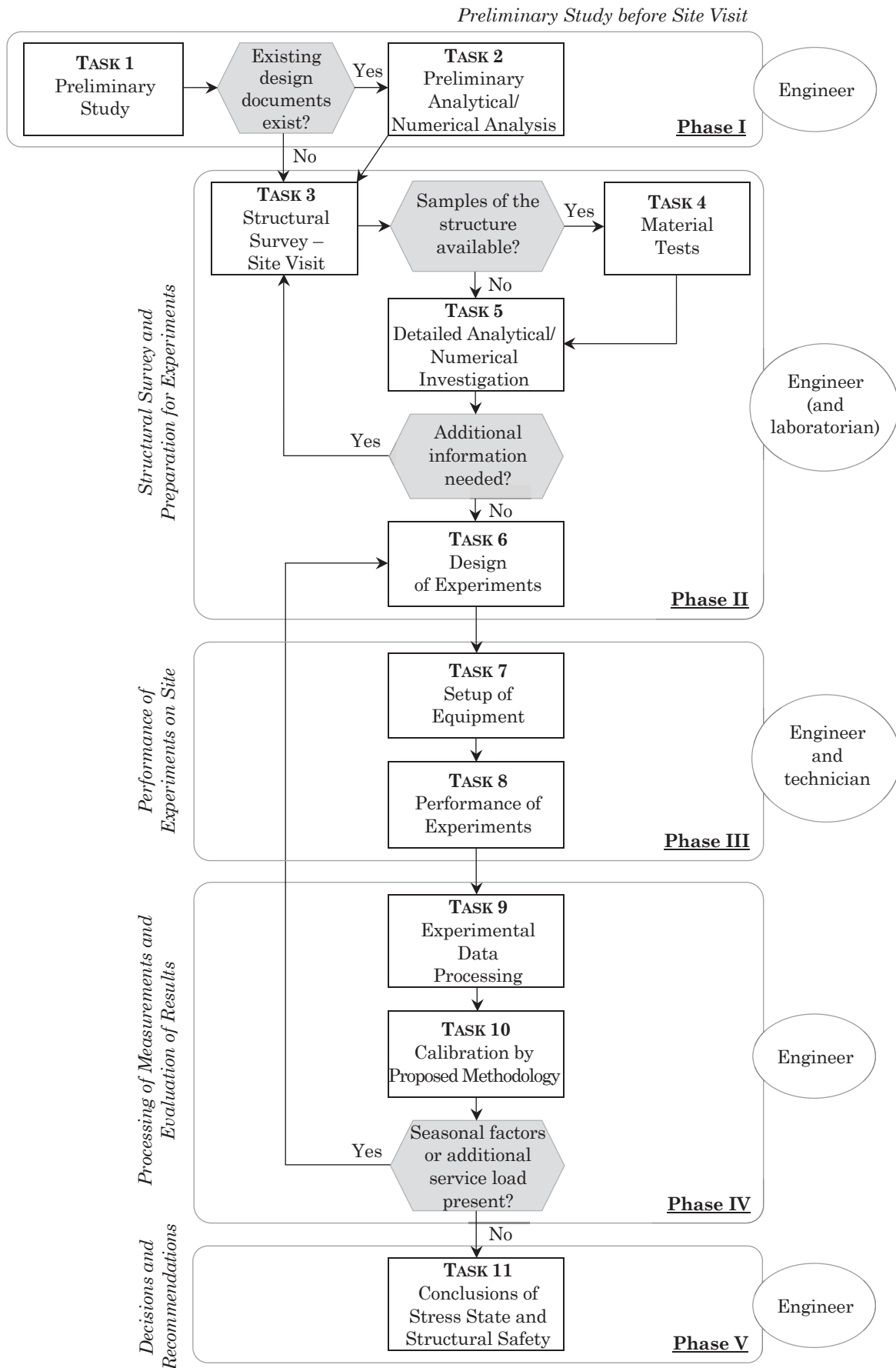


Figure 5.15 – Recommended scheme for in-situ testing on existing truss structures.

Phase I – Preliminary Study before Site Visit

TASK 1 – Preliminary Study

- (a) Study possible reasons to perform the structural assessment of the existing truss, e.g.
 - Change in conditions of use;
 - Designed service life reached;
 - Observation of deterioration;
 - Detection of damages, etc.
- (b) Study the construction history of the structure to have an idea about the possible material properties and structural characteristics.
- (c) Search and study existing structural documents, e.g. design notes, drawings, etc.

→ If existing design documents exist, proceed to Task 2; if not, proceed to Task 3.

TASK 2 – Preliminary Analytical / Numerical Analysis

- (a) Classify the types and sizes of members to take note of the member characteristics.
- (b) Assume the material properties based on the information in the existing documents or a research about the structure's construction history.
- (c) Calculate the loads, if information is available in existing design notes, or make assumptions of the loads.
- (d) Make simple calculations of the forces based on the structural self-weights and loads, or create a simple numerical model based on existing drawings, and perform the static analysis.
- (e) Understand the distribution of the static forces to identify the members in tension and compression, members with high stresses.
- (f) Perform the dynamic analysis to have ideas about the vibration behaviour of the structures and the range of the natural frequencies.
- (g) Calculate the member forces using the analytical-based algorithm [MAES et al. (2013)] based on the modal parameters.
- (h) Compare the results of the forces based on numerical static analyses and analytical-based solution to evaluate the assumptions of the member lengths, cross-sections, and material properties of individual members of the structure.

Phase II – Structural Survey and Preparation for Experiments

TASK 3 – Structural Survey – Site Visit

- (a) Measure the structural geometry, including
 - Dimensions of building; span and height of the truss structure, distance between trusses if there is more than one truss system;
 - Truss member lengths, cross-sections; gusset plates, connecting elements, etc.
- (b) Compare the measurements with existing drawings (if existing drawings are available), pay attention to assumed member lengths for preliminary calculations.
- (c) Take note of the member characteristics, if there is any additional mass, and/or turnbuckle elements.
- (d) Study the boundary conditions as well as connection joints and gusset plates.
- (e) Study the constraint conditions in-plane as well as out-of-plane.
- (f) Estimate the applied loads, take notes about the uncertainties and reasons that affect the load estimation.
- (g) Carry out visual and/or simple checks if any damage is present; take note of the locations, types and extent of damages.

- (h) Identify critical members including members with high stresses based on the preliminary calculations or numerical analysis and/or members being damaged.
- (i) Choose the most critical truss as the representative to be experimentally investigated if there is a series of trusses. The representative truss should characterize the common geometrical and connection characteristics of the truss series as well as is subjected to the highest or at least similar load level compared to other trusses.
- (j) Evaluate the interaction effects between the investigated truss and its neighbour trusses to better predict possible coupled vibration effects of the trusses in the three-dimensional space and the behaviour of the whole construction.
- (k) Consider the possibility of installing the testing equipment regarding the available conditions and accessibility.

→ If samples of the truss for the material tests can be taken, proceed to Task 4; if not, proceed to Task 5.

TASK 4 – Material Tests

- (a) Perform material tests to determine the mechanical properties of the structure, e.g. modulus of elasticity, etc. (refer for instance to DIN EN 6892–1 (2009) for types, requirements and instructions of the tests).
- (b) Compare and combine the results of the mechanical tests with the information of the construction history of the structure, to determine the assumptions for the material properties of the structure.

TASK 5 – Detailed Analytical / Numerical Investigation

- (a) Update the structural drawings based on the site measurements if necessary.
- (b) Create a detailed finite element model of the structure; make assumptions of the material properties based on the mechanical tests if they are available, and/or information in existing design documents, and/or research of the structure's construction history.
- (c) Pay attention to modelling assumptions of joints, i.e. joints are not assumed as pinned or rigid but can be modelled with rotational springs. For truss structures with small connection moments and without the effects of friction and slip, linear elastic spring models can be used. The assumptions of joints for slender trusses do not affect significantly the static analysis results of static forces, but affect the dynamic results.
- (d) Modell the structure considering the inertia as well as weight of gusset plates and turnbuckles if they are present, as well as other additional mass such as sensors, etc.
- (e) Modell a two- or three-dimensional structure depending on the constraint conditions and influences of elements in the three-dimensional space.
- (f) Perform the static analysis based on assumed loads to obtain the force distribution; the static geometric nonlinear analysis is recommended due to stress stiffening effects.
- (g) Perform the dynamic analysis to obtain the natural frequencies and mode shapes and analyse the modes of vibration, i.e. in-plane and out-of-plane, globally and locally.
- (h) Identify the members in tension and compression, members of slender cross-sections, members with uniform and symmetrical cross-sections, and those with no additional mass or turnbuckle elements, etc.
- (i) Calculate the forces using the analytical-based algorithm for selected members, preferably for slender tension members with uniform and symmetrical cross-sections. Natural frequencies and amplitudes of five mode shape displacements of one mode of the selected members are required. The five sensors should be equally distributed to facilitate the experimental setup. The use of modes in the form of the first vibration mode of a single beam is recommended as for other modes, spurious

solutions may occur due to points near a node of the structural mode shapes, i.e. points with zero modal displacement.

- (j) Compare the results of the forces based on the static analysis of the global numerical model and analytical-based solution of single members. If the results differ significantly, consider modifying the numerical model regarding the geometrical and/or mechanical properties as well as varying the locations of the five mode shape points. This also assists the design of the sensor location for the setup of experiments.

→ If additional information is needed, go back to Task 3; if not, proceed to Task 6.

TASK 6 – Design of Experiments

- (a) Define the number of measurement points according to the demand of the dynamic identification and based on the dynamic analysis of the numerical model.
- (b) Design the distribution of the sensors for the test setups depending on the analysed vibration behaviour of the structure; a recommendation is provided in Figure 5.16.
- (c) Design the number of test setups depending on the available number of sensors and available time for the tests; an example is shown in Figure 5.17.
- (d) Design the location of the reference sensors in case of several test setups, such that the reference points should not coincide with a node of the structural mode shapes.
- (e) Choose members for the use of the analytical-based algorithm to identify the forces in individual members. The measurement points for these members must be at least five points. General rules to select the members, as mentioned, are slender members in tension. It is also recommended to use members with uniform and symmetrical cross-sections. In addition, it is beneficial to choose a group of members connecting at a joint to check the joint static equilibrium, or more than two members to check the structural equilibrium of the global truss. A suggestion for a possible setup of sensors for the truss at *Reithalle* is shown in Figure 5.18. In case more sensors are available and/or more time can be given for the tests, other setups using more sensors will be more advantageous.
- (f) Consider the types of excitation; for lightweight truss structure, hammer excitation is recommended, whose execution is also practical.
- (g) Consider the types of sensors depending on the available equipment and accessibility to the structure. The types of sensors can be, for example, geophone, wired accelerometer, wireless accelerometer or laser vibrometer. For geophones and wired accelerometers, additional weights on the members should be included into the analysis of the numerical model, especially if many sensors are used on slender cross-sections. Sensors with light mass or non-contact sensors are advantageous.
- (h) Consider the application of additional mass on selected members, depending on the type of the structure and whether more precise identification of the joint stiffness is desired. This is because for a symmetrical truss, the identification problem for certain joint stiffness is symmetric. However, depending on the structural type and condition on-site, the application of additional mass may be impractical, as a significant mass may be required to create an effect on the dynamic response of the structure.
- (i) In cases where additional mass is to be applied for selected members, design the number and location of strain gauges for these members to check the change in the stress state before and after applying the mass, as a means of verification of the results. A general recommendation is that the strain gauges should be placed at the same vertical level of the centroid line of the member cross-section in its local direction. Depending on the sizes and types of cross-sections, strain gauges should be placed at both sides of the cross-sections. The location of the strain gauges can be designed based on the static analysis to avoid the positions of high bending stresses.

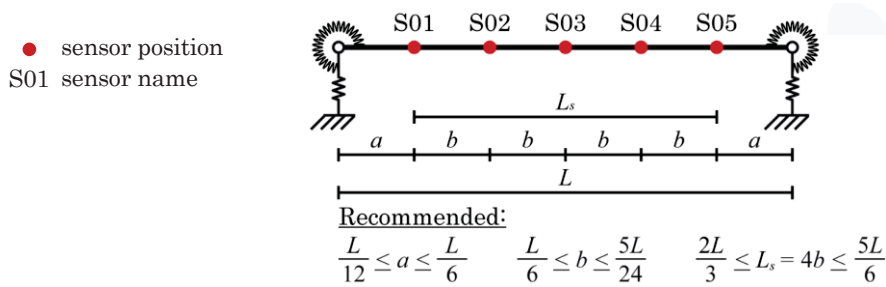


Figure 5.16 – Recommended positions of instrumented sensors on selected truss members.

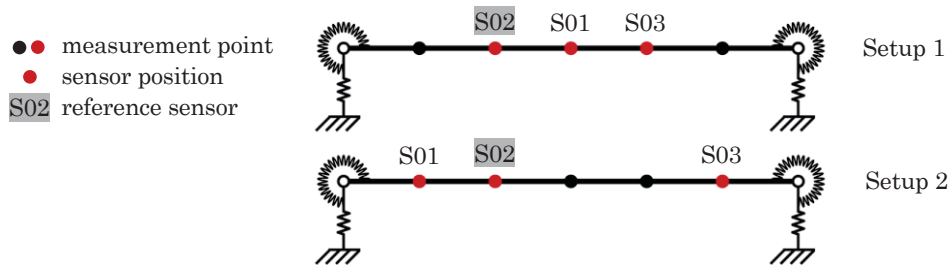


Figure 5.17 – Example of different setups in case of limited sensors on selected truss members.

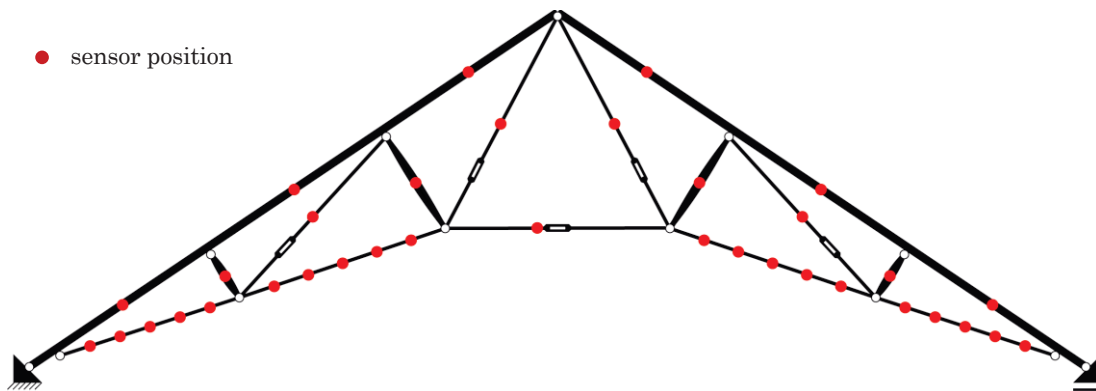


Figure 5.18 – Suggestion of a possible sensor setup for in-situ tests on a truss system.

Phase III – Performance of Experiments on Site

TASK 7 – Setup of Equipment

- As preparatory work, before installing the sensors, perform a light cleaning of the truss to remove dust. If paint coatings are applied to the members, a more thorough cleaning is recommended. Depending on the thickness of the paint coatings, thick coatings should be removed if possible to ensure intimate contact with the sensors.
- Proceed with some localized signal measurements before the overall measurements of each setup to monitor the level of the signals, characterize the signal-to-noise ratio and check the resonant frequencies involved. A simple FFT of the response measurements in a few key points, for example the reference points, can be made.
- Apply additional excitation to increase the signal-to-noise level or re-define the sampling frequency and the measurement duration to obtain more accurate results; change the types or positions of sensors if necessary.
- Make additional random excitation to avoid significant influences of noise on the results in case the signal-to-noise ratio is low.

TASK 8 – Performance of Experiments

- (a) Decide on the measuring duration to record a sufficiently large number of points to have resolution in frequency, considering the number of available sensors, the number of measurement points as well as the available time for the complete test.
- (b) Perform a preliminary check to quality of the data obtained; check the measured signals of every sensor in the setup recording phase and between each setup to avoid data losses or bad signal quality.
- (c) Carry out a preliminary modal analysis before finishing the tests, in order to be sure that the experimental results have sufficient quality for the success of the modal identification.

Phase IV – Processing of Measurements and Evaluation of Results**TASK 9 – Experimental Data Processing**

- (a) Combine different setups; study the dynamic behaviour using two or more identification methods to gain confidence in the results and possibility to proceed with more objective test procedures if necessary.
- (b) Choose a modal identification method or decide on different methods for comparison. Among the identification techniques, the SSI is considered as one of most accurate methods. Depending on the available software, the use of one method can be more computationally efficient over other ones.

TASK 10 – Calibration by Proposed Methodology

- (a) Build an initial numerical model that must be a relative representative of the actual physical structure, before performing the model updating and optimization process.
- (b) Use trial-and-error analysis to determine the initial assumptions for the unknowns, e.g. the loads and joint stiffnesses. To evaluate the assumptions for the joint stiffness, perform the analyses assuming first a pinned model, then a rigid model to check if the experimentally identified modal parameters are close or in between the results of those models. In addition, vary the other unknowns, in particular the loads, to evaluate reasonable assumptions.
- (c) Perform the static analysis to obtain the stress state, followed by the dynamic analysis to examine the calculated results in comparison with the identified results from the experiments.
- (d) Select the updating parameters, define the ranges of the updating parameters and perform the sensitivity analysis. Based on the results of the sensitivity analysis, reduce the number of updating parameters and decide the parameters that have significant influences on the objective function to be updated.
- (e) Perform the optimization process following the proposed methodology to identify the unknowns. The nature-inspired optimization techniques are recommended. Three or four optimization runs can be performed to check the consistency of the results. Depending on the identification problem and the sensitivity of certain parameters to certain output parameters, different objective functions should be used in different optimization stages.

→ If seasonal factors such as temperature and humidity or additional service loads play a role, consider performing the experiments in several campaigns → go back to Task 6; if not, proceed to Task 11.

Phase V – Decisions and Recommendations

TASK 11 – Conclusions of Stress State and Structural Safety

- (a) Conclude the loads and corresponding stress states of the truss structure based on the results of the numerical model calibration using the proposed methodology.
- (b) Identify critical members based on the stress states and/or local damages, if damages are present.
- (c) Evaluate the safety of the structure, for instance whether a substitution of critical members is necessary, reduction of loads is essential, and/or any repair or strengthening is required.
- (d) Decide on next future safety assessment checks.

5.7 Discussions

A representative in-situ dynamic test was performed on a historic truss in Potsdam to assess the identification of the modal parameters of existing multiple-member truss structures, based on the state of the research in 2012. The following remarks are drawn.

- The in-situ experiment shows that the natural frequencies of truss can be identified reasonably well. If sufficient sensors are used, the mode shapes can be also identified. The modal parameters of a truss indicate the characteristics of a coupled global system, in which the connected truss members vibrate interactively with each other.
- The numerical finite element models of different assumptions and simplifications recommend accurate modelling of the details of truss structures. The inertia as well as the mass of the gusset plates and turnbuckles should be considered to increase the accuracy of the numerical analyses.
- Local measurement and analysis strategy concerning individual members of a truss provides useful results to evaluate the behaviour of the truss.
- Uncertainties related to the geometrical characteristics of existing trusses as well as the experimental setup such as the positions of instrumented sensors influence the precision of the axial force identification.

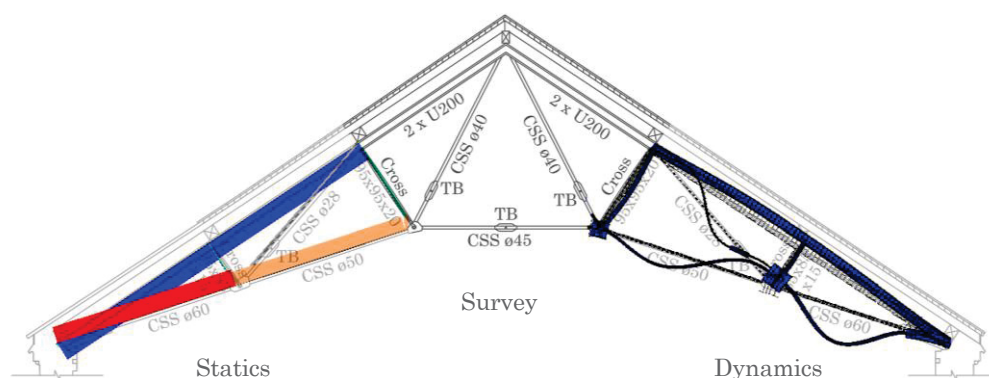
The topics to be further addressed by future investigation are as follows:

- Sufficient measurement data concerning at least five measurement points of selected truss members;
- Precise measurements of the structural geometry and dimensions of the experimental setup to reduce the errors on the estimated axial forces due to possible errors on the input variables;
- Accurate data acquisition and identification of the modal parameters from the measurements, in particular mode shape displacements;
- Selection of the joint rigidity parameters to be included as updating parameters in the optimization and assumptions of identical joint flexibility to reduce the updating parameters, as well as the identification of joint flexibility at symmetric locations of the truss by methods such as added mass.

Recommendations for a stepwise testing and analysis procedure were given, which are intended for future experimental-based investigations to assess the safety of existing truss structures.

6

CONCLUSIONS AND FUTURE RESEARCH



The results of the work are concluded, in which several main themes are discussed in details, i.e. dynamic behaviour of truss-like structures composed of axially loaded slender members; dynamic testing and identification of the modal parameters of truss-type structures; modelling of joints; finite element model updating strategies applied to truss structures; as well as different updating methods and nature-inspired optimization techniques. After that, the proposed methodology is summarized. Moreover, some thoughts about future work are given.

6.1 Conclusions

This thesis addresses the problem of the identification of multiple axial forces and corresponding stresses in axially loaded slender members of iron and steel truss structures by means of vibration measurements. The work was divided into four phases.

The first phase consists of a review of the state of the art methods for the axial force identification in axially loaded single structural members and members of truss-type systems. In addition, a review of the assessment of semi-rigid joints of truss and frame structures was included. Furthermore, main scientific developments in vibration-based finite element model updating and optimization strategies were reviewed.

The second phase focuses on the numerical study of selected systems from single bars to truss structures. Particularly, the second phase examines the influences of the model input parameters on the modal parameters. The numerical modelling and analysis of semi-rigid connections were also investigated. Moreover, the strategies for the model updating process were studied, which include mode pairing, development of an objective function, performance of sensitivity analyses, selection of updating parameters, and comparison of different optimization techniques. Based on the numerical simulation, a methodology was proposed to determine the multiple axial forces and estimate the joint rigidity of truss and truss-like structures.

The third phase concerns the laboratory experiments of three types of systems, i.e. single bars, a two-bar truss-like system and a five-bar truss. The experiments were carried out at different load steps to examine the dynamic responses of the systems at progressive states of stress. The application of the proposed methodology for the laboratory systems were investigated.

The fourth phase deals with the transfer of the methodology that was validated in the laboratory to real-life applications. Based on an in-situ experiment on a historic truss, the possible challenges when working with historic structures were addressed, as well as recommendations for future in-situ tests were drawn.

The conclusions from the work are presented next. For clarity, they are divided into several themes, in which the main observations are enumerated.

Dynamic behaviour of truss and truss-like structures composed of axially loaded slender members:

- For truss structures as a constitution of individual members connecting at joints, the constituent members form a global coupled system. The vibration behaviour of the structure is governed as a whole. The members vibrate interactively with each other in a manner that is indicated as coupling, the extent of which depends on the member connectivity at the joints and the relative stiffness of the members, including the loading level. Due to this coupling effect, similar modes of vibration of an individual member or a group of members occur. Thus, for a correct interpretation of the vibration behaviour of a member as part of a truss structure, the global behaviour of the system should be assessed.
- The magnitudes of the natural frequencies of a truss are governed by the slenderness of its members.

- Upon axial loading, all frequencies of truss members experience a modification to their magnitudes. The effect of the axial load on the natural frequencies can be clearly seen, whereas the stress stiffening effect on the mode shapes was not significantly found.
- As multiple load patterns can be existent for truss structures, the effect of structural loading on the dynamic performance of trusses gets more complicated for complex truss systems. Both compressive and tensile forces coexist with counteracting effects on the modal parameters. Tensile forces increase the natural frequencies of the tension members; whereas at the same time, compressive forces reduce the natural frequencies of the compression members. These counteracting effects in truss structures cause intricate variation of the frequencies and interchange of modes. As a consequence, when correlating the modes of a truss system at different stress states, attention must be paid in sorting the right order of the modes.
- Truss and truss-like systems are often nearly symmetric in geometry; thus, closely spaced modes are present due to truss members of similar characteristics.
- For truss structures unlike single bars, the vibration modes in-plane and out-of-plane are generally non-identical. However, they may be highly similar and closely spaced.

Numerical calculations show that the vibration modes of a truss system can be purely in-plane, purely out-of-plane or a combination of both. In reality however, a truss structure can often vibrate in a mixed manner in-plane as well as out-of-plane. To identify a vibration mode accurately, it is essential to analyse information of both natural frequencies and mode shapes.

Dynamic testing and identification of the modal parameters of truss-type structures:

- Modal analysis and testing is attractive for existing truss structures due to the advantages of non-destructiveness, practical testing procedure and reliable results. Besides, slender truss-type structures can be considered as easily excited structures; thus, the modal parameters should be identified without much difficulty.
- Studies carried out prior to testing, including detailed analyses of the numerical model, discussion of sensor types, sensor positions and different sensor setups, significantly contribute to the richness of the obtained measurement data and better understanding of the dynamic responses of the structures as well as better result interpretation.
- As it is important to estimate accurately the mode shapes, a sufficient number of measuring points is necessary for having enough resolution of the modes. For selected members of a truss, five or more measuring points are recommended.
- Natural frequencies can be measured to a greater accuracy than mode shapes in general. Based on the different laboratory experiments, the frequencies of slender truss-type structures at different stress states could be identified well. The mode shapes of the investigated systems could be also identified relatively well. Better identification of the modal parameters was obtained for truss systems whose members having higher slenderness and at higher stress states.

Modelling of joints:

- Joint rigidity affects the behavior of truss structures, in particular the dynamic behavior. Therefore, for the numerical modelling, joints should not be assumed as the extreme cases of pinned or rigid, but can be modelled with rotational springs to represent semi-rigid connections. Assuming the connection moments and deflections are small as well as the effects of friction and slip are not included, linear elastic spring elements can be applied to model the connections of truss-type structures.
- For practical estimation of the joint rigidity level, it is beneficial to introduce a stiffness parameter such as fixity factor. The fixity factor takes values from zero to one. Therefore, it is convenient for the understanding of different joint stiffnesses. Assuming a large value to represent a rigid condition for all springs is not recommended; whereas defining values corresponding to the rigidity condition for each spring, depending on the member's characteristic, is generally cumbersome.
- It was observed in the laboratory experiments that the rigidity of the joints tends to be increased at higher applied load, as the system is loaded and stressed.

Finite element model updating strategies applied to truss structures:

- Only well identified modes from the measurements are to be included into the model updating process.
- It is important to build an initial numerical model that must be of certain agreement to the investigated structure before an optimization process is carried out.
- In the process of building an initial numerical model, it is necessary to assume initial values for the unknowns. For this purpose, trial-and-error analysis should be carried out to bound the problem, based on the experimentally identified modal parameters. For example, regarding the unknown rotational spring stiffness, it is useful to analyse first the pinned and rigid models.
- Even though the starting values of the input parameters do not need to be close to the optimum, it is advantageous in increasing the efficiency of the optimization. In practice, a random value can be assumed as initial value for the updating parameter of the load, provided that the assumed value of the load allows reasonable ranges of the stresses of the structures, i.e. not exceeding the maximum allowable stress of the truss members.
- By means of the sensitivity analysis, the effects of the updating parameters on the output data can be understood. For slender truss structures, generally the axial force or corresponding axial stress have significant effect on the output parameters from the static as well as dynamic analyses of the numerical model. Therefore, when the force is included as an updating parameter, the effects of other parameters become less significant. Nevertheless, when considering the output parameters of only the modal parameters, the effects of the joint stiffness should not be neglected.
- For the updating process, the number of updating parameters should be limited; the parameters should be sensitive to the objective function.

- The choice of the objective function plays a crucial role. For instance, when the objective function comprises the output parameters calculated from both the static and dynamic analyses of the numerical model, the load and the resulted axial forces have a dominant effect on the objective function. But when the objective function takes into account only the modal parameters from the dynamic analysis, the joint stiffness can have pronounced effects on the objective function. Depending on the choice of the objective function, together with the choice of the updating parameters, the sensitivity of the updating parameters is varied.
- Several strategies were developed to increase the effectiveness of the optimization process and identify the design parameters accurately based on their sensitivity on the objective function. The strategies depend on the choices of
 - (i) which design parameters to be updated;
 - (ii) how many parameters to be updated; and
 - (iii) which output parameters to be included into the objective function.

To identify the load, the objective function should include the output parameters from both the static and dynamic analyses of the numerical model, i.e. member axial forces and modal parameters. The updating parameters can be the load and the rotational spring stiffness of the joints or only the load; in the latter case however, it is necessary to make assumptions for the joint stiffness. To identify the rotational joint stiffness, the objective function should include only the modal parameters, i.e. natural frequencies and mode shapes, as well as the updating parameter should be mainly the spring stiffness.

Therefore, a two-stage updating process can be carried out to identify first the load. After that, based on the result of the identified load, a second optimization procedure for the joint stiffness can be performed.

- From the numerical study, optimization with only the rotational springs as updating parameters have given results of the spring stiffness that match fairly well to the true spring stiffness, those were defined in the numerical study. To verify the identified spring stiffness in cases no experimental validation is available, the results obtained from the optimization with only the springs as updating parameters provide a means for comparison and check. This is only relevant to cases when the load is known, such as by measurements in laboratory experiments.
- An identification problem can be symmetric, such as the identification of the joint stiffness at symmetrical locations of a truss structure. In such cases, updating parameters of joint stiffnesses, those have similar effects on the model output, can hinder the success of the parameter estimation problem. Several suggestions to overcome this issue are to test the structure in slightly different configurations and/or add mass or springs to the structure, etc.

Different updating methods and nature-inspired optimization techniques:

- Compared to gradient- or sensitivity-based methods, global search optimization methods have the advantages of flexibility, independence of the initial parameter set and the capability to find global minimum; their disadvantage is associated mostly with high computational costs.
- Adaptive response surface method is more computationally efficient in comparison to nature-inspired optimization techniques. It can give relatively accurate results

especially in cases of smooth optimization problems and limited number of updating parameters. However, its performance appears less stable in case of more complex optimization problems and with a high number of updating parameters.

- Genetic algorithm, as a global optimizer based on evolutionary computing, allows and requires the use of information about the entire network or sequence being optimized. Therefore, it is endowed with the possibility to find (near) global optimum. For the application in the present work, genetic algorithm proves to be suitable. Possible limitation is its scalability due to the use of global information. In other words, genetic algorithm is suitable for global optimization, but may be less effective for local decisions.
- Particle swarm optimization, based on swarm intelligence, depends on the local information and interaction, which minimizes communication overhead associated with information across a network. As a result, its implementation is usually highly scalable, adaptable, and reasonably robust, which has been proved to be suitable in the present work. Nonetheless, depending on the problems, particle swarm optimization may get trapped in stagnation or premature convergence to a local optimum, and is not suitable for time-critical applications. Among the investigated optimization-based methods, particle swarm optimization requires in general the most computational costs.
- Based on the present study on truss structures, nature-inspired optimization techniques are identified to be promising, given that the updating problem is well-defined. As there is room for further exploration and improvements, it is expected that further advancement in many areas will likely benefit from novel, as-yet-unknown approaches, and from hybrid approaches combining multiple types of algorithms.

The proposed methodology is summarized as follows. The method is based on the finite element model updating using global search optimization techniques. The numerical model of truss structures is calibrated using experimental data of natural frequencies and mode shapes from vibration measurements. The results of the identification are the multiple axial forces or corresponding stresses in truss structures, as well as information about the joint rigidity in relation to pinned and rigid condition.

A two-stage model updating process is recommended. In the first stage, the primary aim is to determine the load and the resulted axial forces or stresses. Dynamic tests allow the identification of the natural frequencies and mode shapes, globally of the truss structure as well as locally of the individual bars. The validation criterion is based on the identified frequencies and global mode shapes of the truss. Moreover, additional information of the axial forces in selected individual bars of the truss is used, which is estimated from the natural frequencies and five amplitudes of the corresponding local mode shapes using an analytical-based algorithm. The tensile forces in selected tension members with uniform symmetrical cross-sections of the truss are identified. By static equilibrium of the global model, multiple axial forces in all truss members are obtained.

Based upon the results of the identified load, a second optimization procedure for the joint stiffness is subsequently performed. In this stage, only modal parameters of the global frequencies and mode shapes are used as validation criteria. The rotational spring stiffnesses of joints are identified as an indication of the level of semi-rigid connections.

Regarding the pairing of modes, an enhanced modal assurance criterion that allows the selection of desired clusters of degrees of freedom is adapted to use more beneficially the information extracted from the measurements relating to specific modes. Moreover, the modal strain energies are also used to select the relevant local mode shapes of selected individual bars of the truss.

The effectiveness of the methodology was verified by numerical study and validated by laboratory experiments. The results of the different experimental campaigns show that the identified axial forces match reasonably well with that from the experiments at different stress levels. Furthermore, the axial force identification is also reliable between different optimization runs.

For the joint stiffnesses, based on the numerical verification, the obtained results are also close to the true values. Nevertheless, unique results may not be achieved for optimization problems with a high number of updating joint stiffness parameters. With respect to the issue of symmetric identification of joint stiffness, the numerical study and laboratory experiments show that by modifying a symmetric truss-type structure such as by adding mass to the truss members, the identification problem becomes non-symmetric and the different rotational stiffnesses at symmetric locations of the structure can be estimated.

The advantages of the proposed methodology are that, by considering the global system, the method gives practically the results of the multiple axial forces and allows the global modelling of the structure, such as to predict the structural responses under alternative loading scenarios. Also, the methodology is relatively robust in the presence of uncertain parameters. The requirement of the proposed methodology is concerned with the reasonable accuracy of the initial numerical model.

About the vibration tests, a minimum number of five sensors per selected member are required. The outmost sensors should be installed to cover a sufficient length of the member and at certain distances to the end constraints. The present works suggests the total length of the outmost sensors to be between $2L/3$ and $5L/6$, and the distance of the sensor to the end constraint to be from $L/12$ to $L/6$ (see Figure 5.16).

Based on the investigated truss and truss-like systems, the application of the proposed methodology is for lightweight iron and steel truss structures composed of slender members that are primarily characterized by axial forces. Investigated member profiles of the laboratory systems were solid symmetrical profiles, e.g. solid circular cross-sections. Further investigation is recommended regarding the application of the methodology on in-situ (historic) trusses and under real-life conditions.

6.2 Future Research

For vibration-based structural parameter estimation of truss structures, finite element model updating using global search optimization strategies are attractive techniques, which involve multi-disciplinary and interactive development. To produce smooth applications in practice, several aspects can be considered for future research, as follows.

Further development for an in-situ examination methodology on real-life existing truss structures can be conducted. A guideline of measuring concepts and assessment strategies for practical application can be developed. One should take into account the

uncertainties related to the material and geometrical properties of historic structures, precision of the measurements and experimental setup as well as environmental factors, such as temperature, and so on.

In addition, an investigation of truss members of different types of profiles and different slenderness can be carried out, for example bulky asymmetrical profiles that are frequently used in truss bridges and truss frame structures. The identification of the axial forces in compression members of a truss can be also examined. In practice, certain compression members may have local damages such that redistribution of the axial forces in the truss occurs. Thus, analysis assuming the global truss model at a state of static equilibrium may be no longer valid. In such cases, a direct assessment of the forces in the compression members is required.

Besides, studies of space truss structures can be conducted. For space trusses, the effects of multiple load patterns are even more complicated. Moreover, there may be influences of structural elements in the third dimensional space. Another issue that can be also addressed is the effect of (excessive) static deflections on vibration.

Furthermore, the feasibility of the proposed methodology in cases of limited available information may be investigated, for instance when only certain members of a truss can be accessed for testing. Quantification of uncertainties in individual analysis process can be studied.

In the context of in-situ testing on real-life truss structures, an available integrated tool for direct on-site application shall certainly be interesting. It offers the advantage of cost-effective and fast quality checks in the construction phase, as well as safety checks and structural maintenance over the structure lifespan.

Another aspect that may be also studied further is the numerical modelling and experimental assessment of semi-rigid joints systematically to produce a catalogue of joint designs. In addition, the effects of friction and slip of joints may be considered. Over the past decades, a number of experimental programs involving the understanding of structural connections was performed, which encourages further development to the work related to semi-rigid connections.

Regarding model updating and selection of updating parameters, future research can look into the problem of parameterization of joints. Moreover, it is worth considering the aspects of attaching weights to the parameters. In addition, with respect to the issue of unique or symmetric identification problem for parameters such as joint stiffness, further investigation can be carried out to increase the amount of data available, for example to test the structure with added masses or in slightly different configurations.

With respect to the nature-inspired optimization methods, as typical for many modern approaches, their application evolves and unveils new research challenges. Several open issues include, for instance, concurrent handling of multiple constraints; investigation of parameter sensitivity, interactions, and tradeoffs; detailed evaluation of algorithm performance under real-world conditions, as well as from an application-centric perspective. For these purposes and considering the performance efficiency, further work can be concentrated on the reduction of the computational effort of the optimization-based methods.

REFERENCES

A

- ABRAMOVICH, H. and ELISHAKOFF, I. (1990), Influence of shear deformation and rotary inertia on vibration frequencies via Love's equations, *Journal of Sound and Vibration*, 137, pp. 516–522.
- ADDIS, B. (2006), The Crystal Palace and its Place in Structural History, *International Journal of Space Structures* 21 (1), pp. 3–19, DOI: 10.1260/026635106777641199.
- ADDIS, B. (2012), The Iron Revolution: How iron replaced traditional structural materials between 1770 and 1870. Before Steel: The introduction of structural irons and its consequences, M.a.S.J. Rinke (Ed.), Zurich: Niggli.
- AHN, KWON, KIM, H.K., and KIM, M.Y. (2003), Estimation of Stay Cable Tension by Error Correction Method, Proceedings of the fifth International Symposium on Cable Dynamics, Santa Margherita, Italy, September 2003.
- AMABILI, M., CARRA, S., COLLINI, L., GARZIERA, R., and PANNO, A. (2010), Estimation of tensile force in tie-rods using a frequency-based identification method, *Journal of Sound and Vibration*, 329 (11), pp. 2057–2067.
- ANDERSON, D., BIJLAARD, F., NETHERCOT, D.A., and ZANDONINI, R. (1987), Analysis and design of steel frames with semi-rigid connections, *IABSE Periodica / IABSE Survey S-39/87*, 4, pp. 61–78.
- ARCHIVE of CHAIR of CONSTRUCTION HISTORY and STRUCTURAL PRESERVATION (2002–2017), Brandenburgische Technische Universität (BTU) Cottbus–Senftenberg, In-situ surveys, documentation drawings, photo documentations, material testings.
- ATTARNEJAD, R. and PIRMOZ, A. (2014), Nonlinear analysis of damped semi-rigid frames considering moment–shear interaction of connections, *International Journal of Mechanical Sciences*, 81, pp. 165–173.

B

- BAHRA, A.S. and GREENING, P.D. (2006), Particularities of Newton's method in space frame force determination, utilising eigenpair functions, *Journal of Sound and Vibration*, 291 (1–2), pp. 462–490.
- BAHRA, A.S. and GREENING, P.D. (2009), Identifying axial load patterns using space frame FEMs and measured vibration data, *Mechanical Systems and Signal Processing*, 23 (4), pp. 1282–1297.
- BAHRA, A.S. and GREENING, P.D. (2011), Identifying multiple axial load patterns using measured vibration data, *Journal of Sound and Vibration*, 330 (15), pp. 3591–3605.
- BAKER, J.F. (1960), The steel skeleton, Volume one, Elastic behaviour and design, Cambridge University Press.
- BAKIR, P.G., REYNDERS, E., and DE ROECK, G. (2008), An improved finite element model updating method by the global optimization technique ‘Coupled Local Minimizers’, *Computers & Structures*, 86 (11–12), pp. 1339–1352.
- BARUCH, M. (1971), Determination of the stiffness of an elastic bar, *AIAA J.*, 9 (8), pp. 1637–1639.
- BATES, W. (1984), Historical Structural Steelwork Handbook. Properties of UK and European Cast Iron, Wrought Iron and Steel Sections including Designs, Load and Stress Data since the Mid 19th Century, The British Constructional Steelwork Association Ltd. London.
- BATI, B. and TONIETTI, S. (2001), Experimental methods for estimating in situ tensile force in tie-rods, Reston, VA, ETATS–UNIS, American Society of Civil Engineers.

- BATI, B.S., PUCETTI, P., and TONIETTI, S. (1992), Experimental methods for testing the pull tension of chains, Proceedings of the 13th World Conference on Non-Destructive Testing, Elsevier, Amsterdam.
- BATILL, S.M., STELMACK, M.A., and SELLAR, R.S. (1999), Framework for Multidisciplinary Design Based on Response-Surface Approximations, *Journal of Aircraft*, 36 (1), pp. 287–297.
- BAYCAN, C.M., UTKU, S., and WADA, B.K. (1991), Control of resonant frequencies in adaptive structures by prestressing, Second Japan/USA Joint Conference on Adaptive Structures, Nagoya, Japan, pp. 297–314.
- BERNER GROUP GmbH (2010), Exposé *Reithalle* Am Ruinenberg: Leben in der denkmalgeschützten *Reithalle* Potsdam, <https://www.yumpu.com/de/document/view/2329072/expose-reithallepotsdam-berner-group-berlin>.
- BHATTI, M.A. and HINGTGEN, J.D. (1995), Effects of connection stiffness and plasticity on the service load behavior of unbraced steel frames, *Eng J, AISC*, 32 (1), pp. 21–33.
- BLASI, C. and SORACE, S. (1994), Determining the axial force in metallic rods, *Structural Engineering International (IABSE)*, 4, pp. 241–246.
- BORGER, H. (1980), *Der Kölner Dom im Jahrhundert seiner Vollendung*, Bd. 2, Historische Museen der Stadt Köln.
- BRAUN, S., EWINS, D.J., and RAO, S.S. (2002), *Encyclopedia of Vibration*, 1st edition, Elsevier, Cornwall, UK.
- BREHM, M., ZABEL, V., and BUCHER, C. (2010), An automatic mode pairing strategy using an enhanced modal assurance criterion based on modal strain energies, *Journal of Sound and Vibration*, 329 (25), pp. 5375–5392.
- BREHM, M. (2011), *Vibration-based model updating: Reduction and quantification of uncertainties*, Ph.D. Thesis, Bauhaus-Universität Weimar.
- BRINCKER, R., ZHANG, L., and ANDERSEN, P. (2000), Output-only modal analysis by frequency domain decomposition, Proceedings of the ISMA25 Noise and Vibration Engineering, Leuven.
- BROWNJOHN, J.M.W., XIA, P.-Q., HAO, H., and XIA, Y. (2001), Civil structure condition assessment by FE model updating: methodology and case studies, *Finite Elements in Analysis and Design*, 37 (10), pp. 761–775.
- BUDELMANN, H., HOLST, A., and WICHMANN, H.-J. (2009), Magnetoelastische Spannkraftmessung in Bauwerken, *Beton- und Stahlbetonbau*, 104 (6), pp. 330–339.

C

- CANTIENI, R., BREHM, M., ZABEL, V., RAUERT, T., and HOFFMEISTER, B. (2008), Ambient testing and model updating of a filler beam bridge for high-speed trains, 7th European Conference on Structural Dynamics – EURODYN2008, Southampton, UK.
- CASAS, J.R. (1994), A combined method for measuring cable forces: the cable-stayed Alamillo Bridge, Spain, *Structural Engineering International*, 4 (4), pp. 235–240.
- CHAN, S.L. (1994), Vibration and modal analysis of steel frames with semi-rigid connections, *Engineering Structures*, 16 (1), pp. 25–31.
- CHAUHAN, A. and SAINI, R.P. (2014), A review on Integrated Renewable Energy System based power generation for stand-alone applications: Configurations, storage options, sizing methodologies and control, *Renewable and Sustainable Energy Reviews*, 38, pp. 99–120.
- CHEN, C.-C., WU, W.-H., LEU, M.-R., and LAI, G. (2016), Tension determination of stay cable or external tendon with complicated constraints using multiple vibration measurements, *Measurement*, 86, pp. 182–195.
- CHEN, W.F., GOTO, Y., and LIEW, J.Y.R. (1995), *Stability Design of Semi-Rigid Frames*, Wiley, New York, ISBN: 978-0-471-07670-4.
- CHEW, K.-H., TAI, K., NG, E.Y.K., and MUSKULUS, M. (2016), Analytical gradient-based optimization of offshore wind turbine substructures under fatigue and extreme loads, *Marine Structures*, 47, pp. 23–41.

- CLOUGH, R. W. and PENZIEN, J. (1995), *Dynamics of Structures*, Computers & Structures, Inc. University Ave., Berkeley, CA 94704, USA, 2nd edition, McGraw–Hill international Editions.
- COOLEY, J.W. and TUCKEY, J.W. (1965), An algorithm for the Machine Calculation of Complex Fourier Series, *Mathematics of Computation*, 19 (90), pp. 297–301.
- CROCI, G., BULIANI, G., ASCENSIG, G. (1988), Studies and experimentation on the Ludovisi Cloister in Rome, In: *Third Congress of the Italian Association for Restoration and Strengthening of Constructions*, Cataia, Italy, pp. 305–315.
- CULMANN, K. (1851), *Der Bau der hölzernen Brücken in den Vereinigten Staaten von Nordamerika*, *Allgemeine Bauzeitung* 16: 69 – 129.
- CUNHA, Á., E., C., MAGALHÃES, F., and MOUTINHO, C. (2006), *From Input–Output to Output–Only Modal Identification of Civil Engineering Structures*, Final Report F11, SAMCO Association, Europe.
- D**
- DA SILVA, J.G.S., DE LIMA, L.R.O., DA S. VELLASCO, P.C.G., DE ANDRADE, S.A.L., and DE CASTRO, R.A. (2008), Nonlinear dynamic analysis of steel portal frames with semi–rigid connections, *Engineering Structures*, 30 (9), pp. 2566–2579.
- DE BOUW, M. (2010), *Brussels Model Schools (1860–1920) – Structural Analysis of the Metal Roof Trusses*, Ph.D. Thesis, Vrije Universiteit Brussel Architectonische Ingenieurswetenschappen.
- DE BOUW, M. and WOUTERS, I. (2011), Polonceau versus Ardant: efficiency versus aesthetics?, *Structural Studies, Repairs and Maintenance of Heritage Architecture XII*, Editors C.A. Brebbia & L. Binda, WIT Press, ISSN 1743–3509, 118, pp. 319–331.
- E**
- ENGESSER, F. (1879), Über die Durchbiegung von Fachwerkträgern und die hierbei auftretenden zusätzlichen Spannungen, *Zeitschrift für Baukunde* 2: 590 – 602.
- ERLER, U. and SCHMIEDEL, H. (1988), *Brücken*, VEB Fachbuchverlag Leipzig, 1988, ISBN 3–343–00352–2.
- F**
- FADAEI, M. and RADZI, M.A.M. (2012), Multi–objective optimization of a stand–alone hybrid renewable energy system by using evolutionary algorithms: A review, *Renewable and Sustainable Energy Reviews*, 16 (5), pp. 3364–3369.
- FARIS, G.A. and KITIPORNCHAI, S. (1992), Elastoplastic nonlinear analysis of flexibly jointed space frames, *J Structural Eng*, 118 (1), pp. 108–27.
- FEBER, A. (1993), *Development of a Hybrid Bridge Evaluation System*, Ph.D. Thesis, University of British Columbia (UBC), Vancouver, Canada.
- FOGEL, L.J., OWENS, A.J., and WALSH, M.J. (1966), *Artificial intelligence through simulated evolution*, New York, John Wiley & Sons.
- FRISWELL, M.I. and MOTTERSHEAD, J.E. (1995), *Finite element model updating in structural dynamics*, Kluwer Academic Publishers, Dordrecht, Boston, London.
- G**
- GALVÃO, A.S., SILVA, A.R.D., SILVEIRA, R.A.M., and GONÇALVES, P.B. (2010), Nonlinear dynamic behavior and instability of slender frames with semi–rigid connections, *International Journal of Mechanical Sciences*, 52 (12), pp. 1547–1562.
- GANGULI, R. (2002), Optimum Design of a Helicopter Rotor for Low Vibration using Aeroelastic Analysis and Response Surface Methods, *Journal of Sound and Vibration*, 258 (2), pp. 327–344.
- GASPARINI, D.A. and PROVOST, C. (1989), Early Nineteenth Century Developments in Truss Design in Britain, France and the United States, *Construction History*, 5, pp. 21–33.
- GEHLER, W. (1910), *Die Entwicklung der Nebenspannungen eiserner Fachwerkbrücken und das praktische Rechnungsverfahren nach Mohr*, Berlin: Wilhelm Ernst & Sohn.

- GEIER, R., DE ROECK, G., and FLESCHE, R. (2006), Accurate cable force determination using ambient vibration measurements, *Structure and Infrastructure Engineering*, 2 (1), pp. 43–52.
- GENTILINI, C., MARZANI, A., and MAZZOTTI, M. (2013), Nondestructive characterization of tie-rods by means of dynamic testing, added masses and genetic algorithms, *Journal of Sound and Vibration*, 332 (1), pp. 76–101.
- GIL, J.-M. and HAN, Y.-H. (2011), A Target Coverage Scheduling Scheme Based on Genetic Algorithms in Directional Sensor Networks, *Sensors*, 11 (2), pp. 1888.
- GO, C.G. and LIOU, C.D. (2004), Load–response determination for imperfect column using vibratory data, *Journal of Sound and Vibration*, 269 (3–5), pp. 455–466.
- GOLDBERG, D.E. (1989), *Genetic Algorithms in Search, Optimization, and Machine Learning*, Addison–Wesley Professional.
- GOLDHAMMER, B.F. and JOHNSON, E.E. (1953), The determination of the critical Load of a column or stiffened panel in compression by the vibration method, *Proc. of SESA XI*
- GREENING, P.D. and LIEVEN, N.A.J. (2003), Identification and updating of loading in frameworks using dynamic measurements, *Journal of Sound and Vibration*, 260 (1), pp. 101–115.

H

- HADIANFARD, M.A. and RAZANI, R. (2003), Effects of semi–rigid behavior of connections in the reliability of steel frames, *Structural Safety*, 25 (2), pp. 123–138.
- HARTUNG, G. (1983), *Eisenkonstruktionen des 19. Jahrhunderts*, München: Schirmer–Mosel, ISBN 3–921375–70–3.
- HÄBLER, D. (2011), The “Elliptical Beams“ in the Winter Palace in Saint Petersburg – Survey, documentation and structural analysis, M.Sc. Thesis, BTU Cottbus.
- HELMERICH, R. (2005), *Alte Stähle und Stahlkonstruktionen: Materialuntersuchungen, Ermüdungsversuche an originalen Brückenträgern und Messungen von 1990 bis 2003*, Forschungsbericht 271, Bundesanstalt für Materialforschung und –prüfung (BAM), Wirtschaftsverlag NW, Verlag für neue Wissenschaft GmbH, Berlin, ISBN 3–86509–362–0.
- HERES, B. (2006), The Iron Roof Trusses of the New Hermitage in St. Petersburg – Structural Survey, Analysis and Assessment of a Masterpiece of Structural Steelwork from the 1840s, *Proceedings of the International Congress on Construction History*, Queens' College, Cambridge University March – April 2006, 2, pp. 1555 – 1568.
- HIGGINS, COX, and FRANK (2005), Acoustic Monitoring on the Fred Hartman Bridge: Understanding the Condition of Stay Cables, *Proceedings of the Sixth International Symposium on Cable Dynamics*, Charleston, SC (USA), September 2005.
- HIROSHI, Z., SHINKE, T., and NAMITA, Y. (1996), Practical formulas for estimation of cable tension by vibration methods, *Journal of Structural Engineering*, 122 (6), pp. 651–656.
- HOLLAND, J.H. (1975), *Adaptation in natural and artificial systems*, University of Michigan Press.
- HOLST, A., WICHMANN, H.-J., HARIRI, K., and BUDELMANN, H. (2006), Monitoring of Tension Members of Civil Structures – New Concepts and Testing, *Proc. of 3rd European Workshop on Structural Health Monitoring*. 5–7 July 2006, Granada, Spain.
- HOLZER, S.M. (2006), Vom Einfluß des Analysewerkzeugs auf die Modellbildung – Zur statischen Analyse des Wiegmann–Polonceau–Trägers in der 2. Hälfte des 19. Jahrhunderts, *Bautechnik*, 83 (6), pp. 428–434.
- HOLZER, S.M. (2012), Triumph of the computable. The development of structural systems in the 19th century, 2nd European Summer School on Construction History (CH.ESS), “The Birth of Modern Engineering – Iron, Steel and Reinforced Concrete”, Vrije Universiteit Brussels.
- HOLZER, S.M. (2012), Towards a history of *structural analysis* in the 19th century, 2nd European Summer School on Construction History (CH.ESS), “The Birth of Modern Engineering – Iron, Steel and Reinforced Concrete”, Vrije Universiteit Brussels.

HORTON, W.H., CUNDARI, F.L., and JOHNSON, R.W. (1967), The analysis of experimental data obtained from stability studies on elastic column and plate structures, *Israel J. of Tech.*, 5 (1–2), pp. 104–113.

HORTON, W.H. and STRUBLE, D.E. (1970), Non-destructive test techniques in the prediction of the buckling load of a column, 13th Annual Israel Conference on Aviation and Astronautics, Tel Aviv–Haifa.

J

JACOBSON, M.J. and WENNER, M.L. (1968), Predicting buckling loads from vibration data, *Experimental Mechanics*, 8 (10), pp. 35N–38N.

JOHNES, S.W., KIRBY, P.A., and NETHERCOT, D.A. (1983), The analysis of frames with semi-rigid connections – a state-of-the-art report., *J Construct Steel Research*, 3 (2), pp. 2–13.

JOHNSTON, B.G. and MOUNT, E.H. (1942), Analysis of building frames with semi-rigid connections, *Engineering News–Record*, 125 (15), pp. 484–487.

K

KAWASHIMA, S. and FUJIMOTO, T. (1984), Vibration analysis of frames with semi-rigid connections, *Computers & Structures*, 19 (1), pp. 85–92.

KEIL, M. (2009), Das historische Dachtragwerk über dem Thronsaal der staatlichen Eremitage Sankt Petersburgs, Diplomarbeit, Brandenburgische Technische Universität Cottbus, Deutschland.

KENNEDY, J. and EBERHART, R. (1995), Particle swarm optimization, *Proceedings of the IEEE International Conference on Neural Networks*.

KIM, B.H. and PARK, T. (2007), Estimation of cable tension force using the frequency-based system identification method, *Journal of Sound and Vibration*, 304, pp. 660–676.

KLEIN, B. (1957), Determination of Effective End Fixity of Columns with Unequal Rotational End Restraints by Means of Vibration Test Data, *The Journal of the Royal Aeronautical Society*, 61 (554), pp. 131–132.

KRENK, S. and HØGSBERG, J. (2013), Truss Structures, in *Statics and Mechanics of Structures*, Springer Netherlands, Dordrecht. pp. 39–89.

KURRER, K.–E. (2008), *The History of the Theory of Structures: From Arch Analysis to Computational Mechanics*, Ernst & Sohn, ISBN: 978–3–433–01838–5.

KYSKA, R., KOUTNY, V., ROSKO, P. (1991), Tension measurement in cable of cable-stayed bridges and in free cables, In: *Proceedings of the Second Conference on Traffic Effects on Structures and Environment*, Zilina, Slovakia, pp. 190–194.

L

LAGOMARSINO, S. and CALDERINI, C. (2005), The dynamical identification of the tensile force in ancient tie-rods, *Engineering Structures*, 27, pp. 846–856.

LAMMENS, S., HEYLEN, W., SAS, P., and BROWN, D. (1993), Modal updating and perturbed boundary condition testing, 11th International Modal Analysis Conference: Kissimmee, Florida, pp. 449–455.

LI, S., REYNDERS, E., MAES, K., and DE ROECK, G. (2012), Vibration-based estimation of axial force for a beam member with uncertain boundary conditions, *Journal of Sound and Vibration*, 332 (4), pp. 795–806.

LIEW, J.Y.R., YU, C.H., NG, Y.H., and SHANMUGAM, N.E. (1997), Testing of semi-rigid unbraced frames for calibration of second-order inelastic analysis, *Journal of Constructional Steel Research*, 41 (2), pp. 159–195.

LINK, M. and WEILAND, M. (2009), Damage identification by multi-model updating in the modal and in the time domain, *Mechanical Systems and Signal Processing*, 23 (6), pp. 1734–1746.

LIVINGSTON, T., BÉLIVEAU, J.G., and HUSTON, D.R. (1995), Estimation of axial load in prismatic members using flexural vibrations, *Journal of Sound and Vibration*, 179, pp. 899–908.

- LORENZ, W. (1990), Die Entwicklung des Dreigelenksystems im 19. Jahrhundert, *Stahlbau* 59 (1990), H.1, S.1–10. ISSN 0038–9145.
- LORENZ, W. (2001), Building with Iron in Nineteenth Century Bavaria: The Valhalla Roof Truss and its Architect Leo von Klenze, *Construction History Journal*, 17, pp. 55–74, ISSN 0267–7768.
- LORENZ, W. (2005), Archäologie des Konstruierens – Eremitage, Walhalla, Neues Museum Berlin. Bundesingenieurkammer (Hrsg.): *Ingenieurbaukunst in Deutschland – Jahrbuch 2005/2006.*, Hamburg, Junius Verlag GmbH, 2005, S. 172– 181. ISBN 3–88506–563–0. 172– 181.
- LORENZ, W. and HERES, B. (2006), Archäologie des Konstruierens – Untersuchungen zur Entstehung von Konstruktionsprachen an den Eisentragwerken der Eremitage St. Petersburg, In: *Forum der Forschung* 10 (2006), H.19, S.163–170.
- LORENZ, W. (2010), Современные музеи в мировом культурном наследии – конструктивные особенности и конструктивные решения. (Modern Museums in World Heritage Monuments – Structural challenges, structural solutions), In: *Proceedings of the 1st International Conference “Museums of the 21st century – restoration, reconstruction, renovation”*, 20.–22. 10. 2008, St. Petersburg, The State Hermitage Publishers, pp. 28–36, ISBN 978–5–93572–392–7.
- LORENZ, W. (2011), *Stahlbau unter Denkmalschutz (Einführung als Herausgeber)*, *Stahlbau*, 80 (6), pp. 377–378. ISSN: 0038–9145.
- LORENZ, W. (2012), From Cast Iron to Steel. Materials., 2nd European Summer School on Construction History (CH.ESS), “The Birth of Modern Engineering – Iron, Steel and Reinforced Concrete”, Vrije Universiteit Brussels.
- LORENZ, W. and HERES, B. (2015), The Demidov Ironworks In Nevyansk (Ural Mountains) – Iron Structures In Building From The First Half Of The 18th Century, *Proceedings of the 5th International Congress on Construction History. Chicago, June 3–7, 2015, Chicago: Construction History Society of America, 2015 vol.2*, pp.505–517. ISBN 978–1–329–15030–0.
- LUI, E.M. and LOPES, A. (1997), Dynamic analysis and response of semirigid frames, *Engineering Structures*, 19 (8), pp. 644–654.
- LUONG, H.T.M. (2010), Identification of the tensile force in tie–rod using modal analysis tests, M.Sc. Thesis, University of Minho, Portugal.
- LUONG, H.T.M., RAMOS, L.F., and AGUILAR, R. (2011), Identification of the Tensile Force in Tie–rods of Historical Constructions, in *Civil Engineering Topics, Volume 4: Proceedings of the 29th IMAC, A Conference on Structural Dynamics, 2011*, T. Proulx (Ed.), Springer New York, pp. 71–81.
- LUONG, H.T.M. (2012), Experimentelle und numerische Untersuchung der Normalkraft in historischen Stahl–Zugankern mit Hilfe von dynamischen Methoden, *Forum Altbausanierung* 7:23. Hanseatische Sanierungstage vom 1. bis 3. November 2012 im Ostseebad Heringsdorf/ Usedom, Beuth Verlag GmbH und Fraunhofer IRB Verlag.
- LUONG, H.T.M. (2012), Dynamical Approach to Identify the State of Stress in Historical Truss Structures, 2nd European Summer School on Construction History (CH.ESS), “The Birth of Modern Engineering – Iron, Steel and Reinforced Concrete”, Vrije Universiteit Brussels.
- LUONG, H.T.M. (2012), Development of Standard Charts to Determine the Tensile Stress in Historic Metallic Tie–bars, In: *Joint International Symposium on Experimental Mechanics and Society for Experimental Mechanics Fall Conference (ISEM’12–Taipei)*, Taipei, Taiwan.
- LUONG, H.T.M., ZABEL, V., LORENZ, W., and ROHRMANN, R.G. (2016), Vibration–based Model Updating and Identification of Multiple Axial Forces in Truss Structures, 6th Asia Pacific Workshop on Structural Health Monitoring, 7–9 December 2016, Hobart, Australia, In: *Procedia Engineering*, vol. 188, 2017, pp. 385–392, ISSN 1877–7058, DOI: <https://doi.org/10.1016/j.proeng.2017.04.499>.
- LUONG, H.T.M., ZABEL, V., LORENZ, W., and ROHRMANN, R.G. (2017), Non–destructive Assessment of the Axial Stress State in Iron and Steel Truss Structures by Dynamic Measurements, *Procedia Engineering*, vol. 199, pp. 3380–3385, ISSN 1877–7058, DOI: <https://doi.org/10.1016/j.proeng.2017.09.447>.

LUONG, H.T.M., LORENZ, W., ROHRMANN, R.G., ZABEL, V., and SAID, S. (2017), Finite Element Model Calibration of a Historic Wiegmann–Polonceau Truss Based on Experimental Modal Parameters, In: Conte J., Astroza R., Benzoni G., Feltrin G., Loh K., Moaveni B. (eds), *Experimental Vibration Analysis for Civil Structures, EVACES 2017, Lecture Notes in Civil Engineering*, vol. 5. Springer, Cham, DOI: https://doi.org/10.1007/978-3-319-67443-8_18.

LURIE, H. (1951), Effective end restraint of columns by frequency measurements, *Journal of the Aeronautical Sciences*, 19, pp. 21–22.

M

MAES, K., PEETERS, J., REYNDERS, E., LOMBAERT, G., and DE ROECK, G. (2013), Identification of axial forces in beam members by local vibration measurements, *Journal of Sound and Vibration*, 332 (21), pp. 5417–5432.

MAIA, N.M.M. and SILVA, J.M.M. (1997), *Theoretical and experimental modal analysis*, Research Studies Press, Taunton.

MANDERLA, H. (1880), Die Berechnung der Sekundärspannungen, welche im einfachen Fachwerk in Folge starrer Knotenverbindungen auftreten, *Allgemeine Bauzeitung* 45: 27 – 43.

MARWALA, T. (2010), *Finite Element Model Updating Using Computational Intelligence Techniques: Applications to Structural Dynamics*, Heidelberg: Springer. pp. 1–247. ISBN 978-1-84996-322-0.

MEHRABI, A.B. and TABATABAI, H. (1998), Unified finite difference formulation for free vibration of cables, *Journal of Structural Engineering*, 124, pp. 1313–1322.

MEHRABI, A.B. (2006), In–Service Evaluation of Cable–Stayed Bridges, *Overview of Available Methods and Findings*, *Journal of Bridge Engineering*, 11 (6), pp. 716–724.

MOHR, O. (1892/93), Die Berechnung der Fachwerke mit starren Knotenverbindungen, *Zivilingenieur*, Vol. 38 (1892), pp. 577 – 594, Vol. 39 (1893), pp. 67 – 78.

MONCARZ, P.D. and GERSTLE, K.H. (1981), Steel frames with nonlinear connections, *Journal of the Structural Division, Proceedings of the ASCE*, 107 (ST8), pp. 1427–41.

MONFORTON, G.R. and WU, T.S. (1963), Matrix analysis of semi–rigidly connected frames, *J. Struct. Div., ASCE*, 89 (6), pp. 13–39.

MOTTERSHEAD, J.E. and FRISWELL, M.I. (1993), Model Updating In Structural Dynamics: A Survey, *Journal of Sound and Vibration*, 167 (2), pp. 347–375.

MUSILEK, P., KRÖMER, P., and BARTOŇ, T. (2015), Review of nature–inspired methods for wake–up scheduling in wireless sensor networks, *Swarm and Evolutionary Computation*, 25, pp. 100–118.

N

NADER, M.N. and ASTANEH, A. (1991), Dynamic behavior of flexible, semirigid and rigid steel frames, *Journal of Constructional Steel Research*, 18 (3), pp. 179–192.

NALITOLELA, N.G., PENNY, J.E.T., and FRISWELL, M.I. (1990), Updating structural parameters of a finite element model by adding mass or stiffness to the system, 8th International Modal Analysis Conference: Kissimmee, Florida, pp. 836–842.

NALITOLELA, N.G., PENNY, J.E.T., and FRISWELL, M.I. (1992), A mass or stiffness addition technique for structural parameter updating, *International Journal of Analytical and Experimental Modal Analysis*, 7 (3), pp. 157–168.

NATKE, H.G. (1998), Problems of Model Updating Procedures: A Perspective Resumption, *Mechanical Systems and Signal Processing*, 12 (1), pp. 65–74.

NGUYEN, P.–C. and KIM, S.–E. (2013), Nonlinear elastic dynamic analysis of space steel frames with semi–rigid connections, *Journal of Constructional Steel Research*, 84, pp. 72–81.

NIEUWMEIJER, G.G. (2001), Polonceau–spanten., *Monumenten*, 11, pp. 20–23.

NOCEDAL, J. and WRIGHT, S.J. (1999), *Numerical optimization*, Springer Series in Operations Research, Springer–Verlag New York, Inc. Glynn, Peter; Robinson, Stephen M. (Ed.).

O

O'SULLIVAN, M. and SWAILES, T. (2008), A study of historical test data for better informed assessment of wrought-iron structures, *Structural Analysis of Historic Construction – D'Ayala & Fodde (eds)*, Taylor & Francis Group, London, ISBN 978-0-415-46872-5.

OHLSSON, S. (1988), *Structural Information via Modal Testing*, 13th International Association for Bridge and Structural Engineering (IABSE) Congress. Helsinki.

P

PARK, S., CHOI, S., OH, S.-T., STUBBS, N., and SONG, H.-C. (2006), Identification of the tensile force in high-tension bars using modal sensitivities, *International Journal of Solids and Structures*, 43 (10), pp. 3185–3196.

PEETERS, B. and DE ROECK, G. (1999), Reference-based stochastic subspace identification for output-only modal analysis, *Mechanical Systems and Signal Processing*, 13 (6), pp. 855–878.

PEETERS, B. (2000), *System Identification and Damage Detection in Civil Engineering*, Ph.D. Thesis, KU Leuven, Belgium.

PETERSEN, C. (2000), *Dynamik der Baukonstruktion*, Ernst & Sohn, WILEY-VCH Verlag, doi. 10.1007/978-3-322-80314-6.

PLAUT, R.H. (1991), Stability and vibration of a column model with load-dependent support stiffness, *Dynamics and Stability of Systems*, 6 (1), pp. 79–88.

R

RAMIRES, F.B., ANDRADE, S.A.L.D., VELLASCO, P.C.G.D.S., and LIMA, L.R.O.D. (2012), Genetic algorithm optimization of composite and steel endplate semi-rigid joints, *Engineering Structures*, 45, pp. 177–191.

RAZAVI, M. and ABOLMAALI, A. (2014), Earthquake resistance frames with combination of rigid and semi-rigid connections, *Journal of Constructional Steel Research*, 98, pp. 1–11.

REBECCHI, G., TULLINI, N., and LAUDIERO, F. (2013), Estimate of the axial force in slender beams with unknown boundary conditions using one flexural mode shape, *Journal of Sound and Vibration*, 332 (18), pp. 4122–4135.

RECHENBERG, I. (1973), *Evolutionsstrategie: Optimierung technischer Systeme nach Prinzipien der biologischen Evolution*, Stuttgart, Frommann-Holzboog.

REN, W.-X., CHEN, G., and HU, W.-H. (2005), Empirical formulas to estimate cable tension by cable fundamental frequency, *Structural Engineering and Mechanics*, 20, pp. 363–380.

REN, W.-X. and CHEN, H.-B. (2010), Finite element model updating in structural dynamics by using the response surface method, *Engineering Structures*, 32, pp. 2455–65.

REYNDERS, E. and DE ROECK, G. (2008), Reference-based combined deterministic-stochastic subspace identification for experimental and operational modal analysis, *Mechanical Systems and Signal Processing*, 22 (3), pp. 617–637.

REYNDERS, E., SCHEVENELS, M., and DE ROECK, G. (2011), MACEC 3.2: a Matlab toolbox for experimental and operational modal analysis, Report BWM-2011-01, Department of Civil Engineering, KU Leuven, Belgium.

REYNDERS, E. (2012), System Identification Methods for (Operational) Modal Analysis: Review and Comparison, *Archives of Computational Methods in Engineering*, 19 (1), pp. 51–124.

RIAD, K.H. (2006), *Überwachung der Vorspannkraft Externer Spannglieder mit Hilfe der Modalanalyse*, Ph.D. Thesis, Universität Kassel.

RIBEIRO, D., CALÇADA, R., DELGADO, R., BREHM, M., and ZABEL, V. (2012), Finite element model updating of a bowstring-arch railway bridge based on experimental modal parameters, *Engineering Structures*, 40, pp. 413–435, ISSN 0141-0296.

RINKE, M. and KOTNIK, T. (2010), The changing concept of truss design caused by the influence of science, *Structures and Architecture – Cruz (Ed.)*, Taylor & Francis Group, London, ISBN 978-0-415-49249-2, pp. 1959–67.

- RINKE, M. and SCHWARTZ, J. (2010), The ambivalence of the revolution, in *Before steel: the introduction of structural iron and its consequences*, M. Rinke and J. Schwartz, Editors, Verlag Niggli AG, Sulgen, Zürich.
- ROMSTAD, K.M. and SUBRAMANIAN, C.V. (1970), Analysis of frame with partial connection rigidity, *Journal of the Structural Division, Proceedings of the ASCE*, 96 (ST11), pp. 2283–300.
- RUSSELL, J.C. and LARDNER, T.J. (1998), Experimental Determination of Frequencies and Tension for Elastic Cables, *Journal of Engineering Mechanics*, 124 (10), pp. 1067–1072.
- S**
- SCHÄDLICH, C. (2015), *Das Eisen in der Architektur des 19. Jahrhunderts*, Aachen/Berlin, Geymüller. 328, ISBN 978–3–943164–05–3.
- SCHEIBE and DEMELT (1998), SUSPA–Spannverfahren für externe Vorspannung, Externe Vorspannung und Segment Segmentbauweise, Vorträge anlässlich des Workshops Externe und verbundlose Vorspannung – Segmentbrücken, Karlsruhe, Verlag Ernst und Sohn, Berlin.
- SCHITTKOWSKI, K. (1985), A fortran subroutine solving constrained nonlinear programming problems, *Annals of Operations Research*, 5, pp. 485–500.
- SCHMITT and LANDSBERG (1897), *Dachstuhl–Konstruktionen und Dächer*, Leipzig, ISBN 3–8262–1211–8, Reprint–Verlag–Leipzig.
- SCHULTZ, H.C., SOBEK, W., and HABERMAN, K.J. (2001), *Stahlbau Atlas*, Birkhäuser Verlag für Architektur, 1. unveränderte Auflage 2001.
- SCHWEDLER, J. W. (1851), Theorie der Brückenbalkensysteme, *Zeitschrift für Bauwesen* 1, Col. 114 – 123, 162 – 173 & 265 – 278.
- SEGALL, A. and BARUCH, M. (1980), A nondestructive dynamic method for the determination of the critical load of elastic columns, *Experimental Mechanics*, 20 (8), pp. 285–288.
- SEKULOVIC, M. and SALATIC, R. (2001), Nonlinear analysis of frames with flexible connections, *Computers & Structures*, 79 (11), pp. 1097–1107.
- SEKULOVIC, M., SALATIC, R., and NEFOVSKA, M. (2002), Dynamic analysis of steel frames with flexible connections, *Computers & Structures*, 80 (11), pp. 935–955.
- SHINKE, T., HIRONAKA, K., ZUI, H., and NISHIMURA, H. (1980), Practical formulas for estimation of cable tension by vibration methods, *Proceedings of JSCE*, pp. 25–34.
- SIEGERT, DIENG, BREVET, and TOUTLEMONDE (2005), Parameter identification of a hanger or stay–cable model based on measured resonant frequencies, *Proceedings of the International Conference on Experimental Vibration Analysis for Civil Engineering Structures (EVACES 2005)*, Bordeaux, France, October 2005.
- SIGEL, P., DÄHMLow, S., SEEHAUSEN, F., and ELMENHORST, L. (2006), *Architekturführer Potsdam*, Dietrich Reimer Verlag, Berlin 2006, ISBN 3–496–01325–7.
- SIVAKUMARAN, K.S. (1988), Seismic response of multi–storey steel buildings with flexible connections, *Engineering Structures*, 10 (4), pp. 239–248.
- SKRINAR, M. (2002), One lastic beams parameter identification using eigenfrequencies changes and the method of added mass, *Computational Materials Science*, 25 (1–2), pp. 207–217.
- SORACE, S. (1996), Parameter models for estimating in–situ tensile force in tie–rods, *Journal of Engineering Mechanics*, 122, pp. 818–825.
- STEPHENS, B.C. (1936), Natural vibration frequencies of structural members as an indication of end fixity and magnitude of stress, *Journal of the Aeronautical Sciences*, 4, pp. 54–56.
- STUTZKI, C. (1982), *Traglastberechnung raumlicher Stabwerke unter Berücksichtigung verformbarer Anschlüsse*, Dotoral dissertation, University of Aachen, West Germany.
- SUTHERLAND, R.J.M. (1963–64), The introduction of structural wrought iron, *Transactions of the Newcomen Society*. 36 (67–84).
- SUTHERLAND, R.J.M. (1997), *Structural Iron, 1750–1850*, Aldershot et al.: Ashgate (XIII–XLI).

T

- TEUGHEL, A. (2003), Inverse modelling of civil engineering structures based on operational modal data, Ph.D. Thesis, KU Leuven, Belgium.
- TIMOSHENKO, S., YOUNG, D.H., and WEAVER, W. (1974), *Vibration problems in engineering*, 4th ed., New York: Wiley.
- TULLINI, N. and LAUDIERO, F. (2008), Dynamic identification of beam axial loads using one flexural mode shape, *Journal of Sound and Vibration*, 318 (1–2), pp. 131–147.
- TULLINI, N. (2013), Bending tests to estimate the axial force in slender beams with unknown boundary conditions, *Mechanics Research Communications*, 53 (0), pp. 15–23.
- TURKER, T. (2008), Structural parameter identification of fixed end beams by inverse method using measured natural frequencies, *Shock and Vibration*, 15 (5), pp. 505–515.
- TÜRKER, T., KARTAL, M.E., BAYRAKTAR, A., and MUVAFIK, M. (2009), Assessment of semi-rigid connections in steel structures by modal testing, *Journal of Constructional Steel Research*, 65 (7), pp. 1538–1547.

V

- VAN OVERSCHEE, P. and DE MOOR, B. (1991), Subspace Algorithms for the Stochastic Identification Problem, 30th Conference on Decision and Control, Brighton. England.

W

- WANG, T., WU, Z., and MAO, J. (2007), PSO-based hybrid algorithm for multi-objective TDMA scheduling in wireless sensor networks, *Second International Conference on Communications and Networking in China, CHINACOM'07*, IEEE: Shanghai, pp. 850–854.
- WERNER, F. and SEIDEL, J. (1992), *Der Eisenbau– vom Werdegang einer Bauweise*, Verlag für das Bauwesen, Berlin 1992, ISBN 3–345–00466–6.
- WICHMANN, H.–J., BUDELMANN, H., HOLST, A., and LAUBE, M. (2013), Bestimmung der Vorspannkraft und Detektion von Schädigungen an Stahlzuggliedern mit Spulensensoren, 5. Symposium "Experimentelle Untersuchung von Baukonstruktionen".
- WINKLER, E. (1880), Die Lage der Stützlinie im Gewölbe, *Deutsche Bauzeitung*, 13.
- WINKLER, E. (1881), Die Sekundär-Spannungen in Eisenkonstruktionen, *Deutsche Bauzeitung* 14: 110 – 111, 129 – 130 & 135 – 136.
- WONG, C.W., MAK, W.H., and KO, J.M. (1995), System and parametric identification of flexible connections in steel framed structures, *Engineering Structures*, 17 (8), pp. 581–595.
- WOUTERS, I., DE GRAEVE, I., VAN DE VELDE, D., DE BOUW, M., and COLLETTE, Q. (2011), Towards a non-destructive methodology to distinguish wrought iron from mild steel in 19th century structures, *Structural Repairs and Maintenance of Heritage Architecture XII, WIT Transactions on The Built Environment*, Vol 118, pp. 285–293.
- WOUTERS, I. and COOMANS, T. (2015), Iron roofs in 19th century churches, *Correspondence, Gesellschaft für Bautechnikgeschichte*.

Y

- YANG, X.–S. (2014), *Nature-Inspired Optimization Algorithms* Oxford, Elsevier.
- YEOMANS, D. (1992), *The Trussed Roof: its history and development*, Aldershot: Scolar Press, England.
- YOUNG, T. (1845), *Course of Lectures on Natural Philosophy and the Mechanical Arts*, London: Taylor and Walton.
- YU, C.H. and SHANMUGAM, N.E. (1986), Stability of frames with semirigid joints, *Computers & Structures*, 23 (5), pp. 639–648.
- YU, X. and GEN, M. (2010), *Introduction to evolutionary algorithms*, London (UK): Springer.

Z

- ZABEL, V. (2003), Applications of Wavelet Analysis in System Identification, Ph.D. Thesis, Bauhaus-Universität Weimar.
- ZABEL, V. and BREHM, M. (2008), Dynamic testing and numerical modelling of a typical short span high-speed railway bridge, Proceedings of the Fourth International Conference on Bridge Maintenance, Safety, and Management (IABMAS). July 13–17, Seoul, Korea.
- ZABEL, V. and BREHM, M. (2009), System identification of high-speed railway bridges, In: Dynardo GmbH (Ed.), Weimar Optimization and Stochastic Days, November 20–21, 2009, Weimar.
- ZABEL, V. and BREHM, M. (2009), Model updating methods – a comparative study, Proceedings of the IMAC-XXVII, February 9–12, 2009 Orlando, Florida USA.
- ZÁRATE, B.A. and CAICEDO, J.M. (2008), Finite element model updating: Multiple alternatives, Engineering Structures, 30 (12), pp. 3724–3730.
- ZHU, K., AL-BERMANI, F.G.A., KITIPORNCHAI, S., and LI, B. (1995), Dynamic response of flexibly jointed frames, Engineering Structures, 17 (8), pp. 575–580.
- ZOETEMEIJER, P. (1983), Summary of the research on bolted beam-to-column connections (period 1978–1983). Technical Report 6–85–M, Steven Laboratory, Delft.
- ZUI, H., SHINKE, T., and NAMITA, Y. (1996), Practical formulas for estimation of cable tension by vibration method, Journal of Structural Engineering, ASCE, 122, pp. 651–656.

Codes of Practice

- DIN EN 1991–1–1 (2010), Eurocode 1 – Actions on structures – Part 1–1: General actions – Densities, self-weight, imposed loads for buildings (Einwirkungen auf Tragwerke – Teil 1–1: Allgemeine Einwirkungen auf Tragwerke – Wichten, Eigengewicht und Nutzlasten im Hochbau).
- DIN EN 1993–1–1 (2010), Eurocode 3: Design of steel structures – Part 1–1: General rules and rules for buildings (Bemessung und Konstruktion von Stahlbauten – Teil 1–1: Allgemeine Bemessungsregeln und Regeln für den Hochbau).
- DIN EN 1993–1–8 (2005), Eurocode 3: Design of steel structures – Part 1–8: Design of joints (Bemessung und Konstruktion von Stahlbauten – Teil 1–8: Bemessung von Anschlüssen).
- DIN EN ISO 6892–1 (2009), Metallische Werkstoffe – Zugversuch – Teil 1: Prüfverfahren bei Raumtemperatur, Beuth Verlag, Berlin, Dezember 2009.

Programme

- ANSYS® (2012–2017), Academic Research, Release 13.0, Bundesanstalt für Materialforschung und –prüfung (BAM).
- MACCEC (2012–2017), developed by Section Structural Mechanics, Department of Civil Engineering, KU Leuven, License at Bundesanstalt für Materialforschung und –prüfung (BAM).
- MATLAB (2012–2017), User Manual, Release 7.2, Bundesanstalt für Materialforschung und –prüfung (BAM).
- OptiSLang® (2012–2017), Dynardo GmbH, Institut für Strukturmechanik (ISM), Bauhaus-Universität Weimar.

LIST OF FIGURES

Chapter 1

1.1 – Examples of historic iron roof trusses that exist in present–time.	6
1.2 – Development principle of Wiegmann–Polonceau truss [adapted from Kurrer (2008)].	8
1.3 – Example of historic iron Wiegmann–Polonceau trusses: Gare d’Austerlitz, Paris (1869), span length of approximately 51 m and height of about 28 m from the ground.	8
1.4 – Historic iron Wiegmann–Polonceau trusses at <i>Reithalle</i> Potsdam (1885–1891) with span length of approximately 18 m, height of approximately 6 m and several members with turnbuckles to adjust lengths and apply preload.	10
1.5 – Turnbuckle elements and optimally–shaped compressive struts of the historic iron Wiegmann–Polonceau trusses at <i>Reithalle</i> Potsdam (1885–1891).	10
1.6 – Iron trusses in the State Hermitage Museum, Saint Petersburg [BTU CS (2011)].	12
1.7 – Details of bearings and connections for the case–study of iron roof trusses in the State Hermitage Museum in Saint Petersburg [BTU CS (2011)].	12
1.8 – Outline of the thesis.	18

Chapter 2

2.1 – Rectangular beam in the laboratory tests by Li et al. (2012).	30
2.2 – Identified forces by different analytical–based methods using data sets from laboratory tests of Li et al. (2012) and numerical calculations.	32
2.3 – Graphical representation of the results of the identified and measured forces from the laboratory tests given in the work of Maes et al. (2013).	32
2.4 – Schematic diagram of the proposed methodology to identify the axial forces and estimate the joint stiffnesses of truss structures.	46
2.5 – Flowchart of the optimization process of the proposed methodology.	49

Chapter 3

3.1 – Single bar model.	52
3.2 – Numerical natural frequencies of the first six modes of the pinned vs. rigid single bar system B4 without and with the effects of stress stiffening in the numerical study.	55
3.3 – Numerical modal parameters of the first six modes of six target systems of single bar B1 in the numerical study.	56
3.4 – The numerical natural frequencies of the first mode of single bar B4 at varying constraint conditions and stress stiffening.	57
3.5 – Numerical natural frequencies of the first two modes of single bar B4 at varying stress stiffening and constraint conditions.	58
3.6 – Different arrangements of sensors on single bar system B1 in the numerical study.	59
3.7 – Identified axial forces using analytical–based methods in the numerical study of bar B1.	60

3.8 – Spearman correlation matrix between the parameters and responses of the numerical model of the single bar target system B1_S1_CS1.....	62
3.9 – Spearman correlation matrix between the parameters and responses of the numerical model of the single bar target system B1_S3_CS5.....	63
3.10 – Results of all identified axial forces of four optimization runs with different initial parameter sets using three different optimization techniques in the numerical study of the single-bar systems.....	65
3.11 – Convergence of optimization by different optimization techniques in the numerical study of the target system B1_S1_CS3.....	66
3.12 – Convergence of optimization with different initial parameter sets by the PSO in the numerical study of the target system B1_S1_CS3.....	67
3.13 – Single bar model with an added mass.....	69
3.14 – Symmetric two-bar system for global and local analyses.....	72
3.15 – Numerical natural frequencies and mode shapes of first sixteen modes of pinned system at zero-applied load in the numerical study of symmetric two-bar structure.....	73
3.16 – Numerical natural frequencies of the first twelve modes of pinned vs. rigid system with and without stress stiffening in the numerical study of symmetric two-bar structure.....	74
3.17 – Spearman correlation matrix between the parameters and responses of the numerical model of the first target system in the numerical study of symmetric two-bar structure.....	75
3.18 – Two types of asymmetric two-bar systems to examine the estimation of different joint stiffnesses at symmetric locations of the structure.....	78
3.19 – Examples of numerical natural frequencies and mode shapes of the asymmetric two-bar systems assuming pinned connections at zero-applied load showing different vibration behaviour of the two members.....	79
3.20 – Numerical global model of the five-bar truss system.....	82
3.21 – Numerical natural frequencies of the modes in the frequency range up to 120 Hz of the two-bar and five-bar systems assuming nearly rigid joints.....	82
3.22 – Numerical natural frequencies and mode shapes of first sixteen modes of a semi-rigid five-bar truss ($\gamma_{kr} = 0.75$) at zero-applied force.....	84
3.23 – Pairing of the simulated experimental and numerical frequencies by the MAC and EMAC in the numerical study for the second target system of the five-bar truss.....	85
3.24 – Numerically calculated natural frequencies and mode shapes of twelve modes of the second target system as simulated experimental modes in the numerical study of the five-bar truss.....	86
3.25 – Spearman correlation matrix between the parameters and responses using simulated experimental data of the third target system in the numerical study of the five-bar truss.....	88
 Chapter 4	
4.1 – Overview of the laboratory test for the bar B1.....	94
4.2 – Equipment in the laboratory tests of the single bars.....	95
4.3 – Stabilization diagram in the laboratory experiment of the bar B1 at one load step.....	96
4.4 – Experimentally identified and analytically/numerically calculated natural frequencies at different stress states in the laboratory experiment of single bar B1.....	97

4.5	– Results of the identified axial forces and natural frequencies of the first four modes in the laboratory experiment of the single–bar systems.	98
4.6	– Overview of the laboratory experiment of the symmetric two–bar system.....	100
4.7	– Details of the laboratory test on the asymmetric systems <i>UnsymM</i> and <i>UnsymL</i>	100
4.8	– Overview of the laboratory experiment of the asymmetric two–bar system <i>UnsymL</i>	100
4.9	– Measured applied load of the hydraulic actuator by load cell and calculated axial forces in the two members from the measured strains during the measurements in the laboratory experiments of the two–bar systems.	102
4.10	– Stress–strain curve from the tensile tests for the specimens of the solid circular steel tension members of the two–bar system in the laboratory experiments.	103
4.11	– Experimentally identified modal parameters of the first six modes at the first load step in laboratory experiments of the symmetric two–bar system and asymmetric system <i>UnsymM</i>	105
4.12	– Results of the identified axial forces and natural frequencies of the first five modes in the laboratory experiment of the symmetric two–bar structure.	106
4.13	– Results of the identified fixity factors $\gamma_{krIII.link}^{id}$ at different load steps in the laboratory experiment of the symmetric two–bar structure.....	107
4.14	– Comparison of measured applied loads of the hydraulic actuator and calculated axial forces from the measured strains in the laboratory experiment of the five–bar truss.....	110
4.15	– Overview of the laboratory experiment of the five–bar truss structure.	111
4.16	– Boundary conditions, joint connections and attached accelerometers on a tension truss member in the laboratory experiment of the five–bar system.	111
4.17	– Experimentally identified mode shapes of the first six modes at the eighth load step in the laboratory experiment of five–bar truss system.	113
4.18	– Results of the identified axial forces and natural frequencies of the first four modes in the laboratory experiment of the five–bar truss.	115

Chapter 5

5.1	– In–situ experiments on a historic Wiegman–Polonceau truss.	118
5.2	– Detailed view of one single truss system at <i>Reithalle</i> in Potsdam and selected joints.	119
5.3	– Characteristics of selected members of the historic truss in the in–situ experiment.....	120
5.4	– Numerical model of the historic truss with numbering scheme.....	121
5.5	– Different finite element models of the truss to examine meaningful simplifications of the numerical models.	121
5.6	– The cross–section showing the components of the loads on the truss.	122
5.7	– Plan of a unit roof containing three trusses for the calculation of point loads of the roof.	122
5.8	– Global finite element model of the truss with assumed applied roof loads.	122
5.9	– Static analysis for the axial force distribution of global finite element model of the truss.	123
5.10	– Numerical natural frequencies and mode shapes of the first twenty–one modes of a semi–rigid system ($\gamma_{kr} = 0.15$) at zero applied force in the in–situ experiment of the historic truss.	124
5.11	– Local measurement and analysis of a single bar as member of a global truss structure.	125

5.12 – Setting up of the equipment and performance of the in–situ experiment.	126
5.13 – Experimentally identified modal parameters from local measurement of the second truss member.	127
5.14 – Numerical mode shapes of the truss model based on the pairing of the experimentally identified and numerically computed modes of the second truss member.	131
5.15 – Recommended scheme for in–situ testing on existing truss structures.	132
5.16 – Recommended positions of instrumented sensors on selected truss members.	136
5.17 – Example of different setups in case of limited sensors on selected truss members.	136
5.18 – Suggestion of a possible sensor setup for in–situ tests on a truss system.	136

Appendix

B.1 – Individual effects of selected parameters on the first natural frequency of single bar.	169
B.2 – Combined effects of selected parameters on the first natural frequency of single bar.	169
C.1 – Static analyses of the normal stress and bending stress distribution of the finite element models with stress stiffening assuming rigid joint conditions of the investigated systems in the numerical study and laboratory experiments.	170
D.1 – Location of the historic truss in Potsdam for the exemplary in–situ experiment.	171
D.2 – Architectural illustration of the building <i>Reithalle</i> after renovation for residential apartments [Berner Group GmbH (2010)].	171
E.1 – Static analysis of the axial force, normal stress and bending stress distribution of the finite element model assuming the manually calculated roof loads and rigid joint conditions of the historic truss in the in–situ experiment.	172

LIST OF TABLES

Chapter 1

- 1.1 – Key properties of the alloys of iron [adapted from Addis (2012)]. 4
- 1.2 – Overview of axial force identification methods (from 1936 onwards). 16

Chapter 2

- 2.1 – Comparison of identified forces between different analytical-based methods using data sets from laboratory tests of Li et al. (2012) and numerical calculations. 32
- 2.2 – Brief overview of the work relating to semi-rigid connections of steel frames. 35

Chapter 3

- 3.1 – Geometrical and material properties of single bars in the numerical study. 52
- 3.2 – Load cases of single-bar systems in the numerical study. 53
- 3.3 – Case studies of connection rigidity of single-bar systems in the numerical study. 53
- 3.4 – Parameters of target systems for the numerical study of the single bars. 54
- 3.5 – Numerical natural frequencies of the first six modes of the single bar B4 without and with stress stiffening based on different static analyses for the stress stiffening. 54
- 3.6 – Numerical natural frequencies of the first six modes of the six target systems compared to the pinned system at zero-load of the single bar B1 in the numerical study. 55
- 3.7 – Characterization of the parameters of the numerical models for the sensitivity analysis. 61
- 3.8 – Results of the identified axial forces and corresponding stresses, as well as the identified rotational spring stiffness and fixity factors, in the numerical study of single-bar systems. 64
- 3.9 – Assumptions of different initial starting values of the design parameters of the axial force and rigidity factor in numerical study of single-bar systems. 65
- 3.10 – Numerical error analysis of the single-bar systems. 67
- 3.11 – Results of the identified axial forces and stresses as well as the identified fixity factors in the numerical error analysis of the single-bar systems. 68
- 3.12 – Parameters of target systems for the numerical study of the bar B4 with added mass. 70
- 3.13 – Results of the identified axial forces and corresponding stresses in the numerical study of the single bar B4 with added mass. 70
- 3.14 – Results of the rotational spring stiffness and fixity factors in the numerical study of single bar B4 with added mass. 71
- 3.15 – Numerical natural frequencies of the first twelve modes the pinned and rigid symmetric two-bar structure without and with stress stiffening. 72
- 3.16 – Parameters of the target systems in the numerical study of symmetric two-bar structure. 76
- 3.17 – Results of the identified axial forces and stresses in the numerical study of symmetric two-bar structure. 76

3.18 – Results of the identified rotational spring stiffness and fixity factors in the numerical study of the symmetric two–bar structure.....	77
3.19 – Results of the identified axial forces and stresses in the numerical error analysis of the symmetric two–bar structure.	78
3.20 – Parameters of the axial forces and corresponding stresses of the target systems in the numerical study of the asymmetric two–bar structures.	79
3.21 – Parameters of the rotational spring stiffness and fixity factors of the target systems in the numerical study of the asymmetric two–bar structures.	79
3.22 – Results of the identified axial forces and stresses in the numerical study of the asymmetric two–bar structures <i>UnsymM</i> and <i>UnsymL</i>	80
3.23 – Results of the identified rotational spring stiffness and fixity factors in the numerical study of the asymmetric two–bar structures <i>UnsymM</i> and <i>UnsymL</i>	80
3.24 – Geometrical and mechanical properties of the five–bar truss in the numerical study.	81
3.25 – Numerically calculated axial forces and normal stresses of the five–bar truss at different applied loads.....	83
3.26 – Parameters of the axial forces and stresses of the target systems in the numerical study of the five–bar structure.....	83
3.27 – Parameters of the rotational spring stiffness and fixity factors of the target systems in the numerical study of the five–bar structure.....	83
3.28 – Relative modal strain energy (MSE) of members of the five–bar truss in the numerical study of the second target system.....	87
3.29 – Selection of identified axial member forces based on analytical–based method using the relative MSE in the numerical study of the second target system of the five–bar truss.	87
3.30 – Results of the identified axial forces and stresses in the numerical study of five–bar truss.....	89
3.31 – Results of the identified rotational spring stiffness and fixity factors in the numerical study of the five–bar truss.....	90

Chapter 4

4.1 – Summary of single–bar systems in the performed laboratory tests.....	95
4.2 – Values of applied forces and corresponding stresses from the measured strains in the laboratory experiments of the single bars.....	95
4.3 – Experimentally identified natural frequencies in the laboratory experiments of single bars B1, B2 and B3.....	96
4.4 – Results of the identified axial forces and corresponding stresses as well as the rotational spring stiffness and fixity factors in the laboratory experiment of single bar B1.	98
4.5 – Comparison of measured applied load of the hydraulic actuator by load cell and calculated member axial forces from the measured strains in the laboratory experiment of the symmetric two–bar system.....	99
4.6 – Comparison of measured applied load of the hydraulic actuator by load cell and calculated member axial forces from the measured strains in the laboratory experiment of the asymmetric two–bar system <i>UnsymM</i>	101
4.7 – Comparison of measured applied load of the hydraulic actuator by load cell and calculated axial forces in the two members from the measured strains in the laboratory experiment for the asymmetric two–bar system <i>UnsymL</i>	101
4.8 – Characteristics of the tensile specimens of the two–bar structure for material tests [DIN EN 6892–1 (2009)].	103

4.9 – Results of the tensile tests for the specimens of the solid circular steel tension members of the two–bar system in the laboratory experiments.	103
4.10 – Experimentally identified natural frequencies of the first six modes in the laboratory experiments of the symmetric and asymmetric two–bar structures.	104
4.11 – Results of the identified axial forces and stresses in the laboratory experiment of the symmetric two–bar system.	105
4.12 – Results of the identified rotational spring stiffness and fixity factors in the laboratory experiment of the symmetric two–bar system.	106
4.13 – Results of the identified axial forces and stresses in the laboratory experiment of the asymmetric two–bar system <i>UnsymM</i>	107
4.14 – Results of the identified rotational spring stiffness and fixity factors in the laboratory experiment of the asymmetric two–bar system <i>UnsymM</i>	108
4.15 – Results of the identified axial forces and stresses in the laboratory experiment of the asymmetric two–bar system <i>UnsymL</i>	108
4.16 – Results of the identified rotational spring stiffness and fixity factors in the laboratory experiment of the asymmetric two–bar system <i>UnsymL</i>	109
4.17 – Measured applied forces of the hydraulic actuator and calculated member axial forces from the measured strains in the laboratory experiment of the five–bar truss.	112
4.18 – Experimentally identified natural frequencies of the first six modes in the laboratory experiment of the five–bar system.	112
4.19 – Identified axial forces in the first tension member by applying the analytical–based algorithm for the first six modes in the laboratory experiment of the five–bar system.	113
4.20 – Results of the identified loads, axial forces and axial stresses of the first to second tension members in the laboratory experiment of the five–bar truss.	114
4.21 – Results of the identified rotational spring stiffness and fixity factors in the laboratory experiments of five–bar system.	116

Chapter 5

5.1 – Assumed variations for the parameters of the finite element model of a truss member as single beam.	127
5.2 – Numerically calculated natural frequencies based on the finite element model of the second truss member.	128
5.3 – Identified member axial forces and stresses based on analytical–based algorithm using experimentally identified natural frequencies and different sets of mode shape displacements for the first two modes.	129
5.4 – Assumed values and variations of the parameters using an analytical–based algorithm.	130
5.5 – Identified member axial forces and stresses based on an analytical–based algorithm for the mode at 20.19 Hz using experimental mode shape displacements and an assumed additional mode shape displacement based on polynomial interpolation of the measurement data.	130

Appendix

A.1 – Highlights of development of iron and steel production, theory formation and selected examples of iron roof truss constructions from approximately 1709 until 1893.	167
B.1 – Characteristics of the parameters in the numerical parametric study of single–bar systems.	169

APPENDIX

A Study Context of Historic Truss Structures

Table A.1 – Highlights of development of iron and steel production, theory formation and selected examples of iron roof truss constructions from approximately 1709 until 1893.

Year	Development	Reference
1709	First production of pig iron in a coke blast furnace by Abraham Darby at Coalbrookdale	LORENZ (2012)
1722	Begin construction of Leaning Tower of Nevyansk and its porch including a roof truss built entirely of wrought iron flat bars with a span of about 9 m and height of about 7.5 m	LORENZ and HERES (2015)
1784	Patenting of the puddling process by Henry Cort for the production of puddle iron or weld iron	LORENZ (2012)
1786–1790	Wrought iron roof truss at Théâtre Français by Victor Louis with a span of approximately 28 m	ADDIS (2012)
1789	Wrought iron roof truss at the Salon Carré du Louvre, Paris	LORENZ and HERES (2015)
1790	First calibre mill for further processing of puddle iron by Cort and Panel in England (flat rectangle cross sections)	HELMERICH (2005)
1807	Introduction of modulus of elasticity by Thomas Young	YOUNG (1845)
1808	Theory of elastic line of bending of beams <i>Handbuch der Statik fester Körper</i> by Johann Albert Eytelwein (1764–1848)	HOLZER (2012)
1823–1825	Iron roof at the Court and National Theatre, Munich with a span of more than 10 m	LORENZ (2001)
1824	First puddle plant in Rasselstein near Neuwied, Germany by owner family Rémy, friends of John Cockerill (1790–1840)	ERLER and SCHMIEDEL (1988)
1826	Theory of the bending of beams and analysis of simple structures by Claude Louis Marie Henri Navier (1785–1836)	HOLZER (2012)
1828–1832	Wrought and cast iron roof and ceiling structures at the Aleksandrinskij Theatre, Saint Petersburg by engineer Matthew Clark (1776–1846) and classicist Carlo Rossi	LORENZ (2001)
1830	First railway rails, T-profile, Z-iron in England manufactured by Stephenson, i.e. mold or façon iron	WERNER and SEIDEL (1992)
1836	Iron roof truss of the Chartres Cathedral, Paris with a span of about 14 m and height of 10 m	LORENZ (2012)
1836	Realisation of three interconnected pin-jointed plates of bars also forming a plate by Rudolf Wiegmann	KURRER (2008)
1838	Reconstruction of the building complex of the State Hermitage Museum, Saint Petersburg with iron structures with great variety of prototypes for roofs and floors (see Chapter 1)	LORENZ (2005, 2010); LORENZ and HERES (2006), HERES (2006)
1839–1840	Theory of three pin-jointed truss by Rudolf Wiegmann and Camille Polonceau; invention of Wiegmann–Polonceau truss structures	KURRER (2008); HOLZER (2006); SCHÄDLICH (2015)
1840	Iron roof trusses with a span of about 11.7 m and height of 2.5 m over the main hall of Valhalla, Donaustauf	LORENZ (2001)
1843–1850	Wrought iron roof trusses of the Bibliotheque Sainte Geneviève, Paris	LORENZ (2012)
1851	Statically determinate truss theories by Karl Culmann (1821–1881) and Johann Wilhelm Schwedler (1823–1894)	KURRER (2008)

Table A.1 – Highlights of development of iron and steel production, theory formation and selected examples of iron roof truss constructions from approximately 1709 until 1893 (continued).

Year	Development	Reference
1851	Crystal Palace with iron framework of cast iron columns and cast and wrought iron trusses by engineers William Barlow and Charles Fox	ADDIS (2006)
1851–1853	Wiegmann–Polonceau iron roof trusses at <i>Schrannenhalle</i> , Munich; the hall is approximately 430 m long	HOLZER (2006)
1852	Iron riveted roof trusses at Gare Saint–Lazare, Paris by Alfred Armand and Eugène Flachet spanning about 40 m	HOLZER (2012)
1853	Riveted wrought iron roof trusses of the Gare de l’Ouest, Paris, France by Eugène Flachet (1802–1873)	KURRER (2008)
1854	Assessment of the continuity effect of the rafters in Wiegmann–Polonceau truss by Gustav Adolf Breymann	KURRER (2008)
1855	<i>Bessemer converter</i> , acid lining, production of low–carbon iron by Bessemer (1813–1898)	LORENZ (2012)
1858	Truss theory <i>Manual of applied mechanics</i> by William John Macquorn Rankine (1820–1872)	HOLZER (2012)
1861	Description of the three–hinged frame theoretically by Claus Köpcke	LORENZ (1990)
1863	Static calculation of shells as circular roofs by Schwedler	KURRER (2008)
1864	Theory of general hyperstatic systems on the calculation of the equilibrium and stiffness of frames by James Maxwell	HOLZER (2012)
1864–1865	<i>Siemens–Martin process</i> , stove freshener process by Wilhelm Siemens, Pierre and Emilé Martin	LORENZ (2012)
1864–1866	Graphical statics by Karl Culmann	KURRER (2008)
1864	Theory of general hyperstatic systems on the calculation of the equilibrium and stiffness of frames by James Maxwell	HOLZER (2012)
1865	The first three–hinged frame for the <i>Bochumer Dampfhammer</i> by Schwedler	LORENZ (1990)
1868	Statics of two– and three–hinged arches by Winkler	WINKLER (1880)
1869	Iron roof truss at Gare d’Austerlitz, Paris with a span length of approximately 52 m	SCHULTZ et al. (2001)
1869	Iron roof over the council chamber in new City Hall Berlin by Schwedler; rafters of the Wiegmann–Polonceau truss are parabolic simply supported beams with pinned joints	KURRER (2008)
1878	<i>Thomas converter</i> , basic lining by Sidney G. Thomas with Percy C. Gilchrist	LORENZ (2012)
1878	Wiegmann–Polonceau iron roof trusses at Military Riding Hall, Dresden composed of timber rafters, optimal shaped cast iron struts and wrought iron ties with turnbuckles	HOLZER (2012)
1879	Approximation method for determining the secondary stresses in trussed frameworks by Engesser	ENGESSER (1879)
1880	Theory of secondary stresses in trussed frameworks with rigid joints by Manderla	MANDERLA (1880)
1881	Theory of secondary stresses with the difference between end tangents and member chord angles of rotation at the joint as well as eccentric truss joints by Winkler	WINKLER (1881)
1885–1891	Wiegmann–Polonceau iron roof trusses at <i>Reithalle</i> , Potsdam (see Chapter 5)	SIGEL et al. (2006)
1892–1893	Theory of secondary stresses with clear differentiation between the joint angles of rotation and member angles of rotation for the determination of the deformed state of trussed frameworks with rigid joints	MOHR (1892/93)

B Numerical Parametric Study

Table B.1 – Characteristics of the parameters in the numerical parametric study of single-bar systems.

Parameter	Designation	Range (lower/upper)	Base value	Unit
σ	Axial tensile stress	0 / 200	0	N/mm ²
$k_{r1} = k_{r2}$	Rotational spring stiffness at supports	0 / 200	0	kNm/rad
\emptyset	Diameter of solid circular cross-section	20 / 30	20	mm
E	Modulus of elasticity	150 000 / 220 000	210 000	N/mm ²
ρ	Mass density	7065 / 8635	7850	kg/m ³
L	Length	1500 / 3000	1750	mm

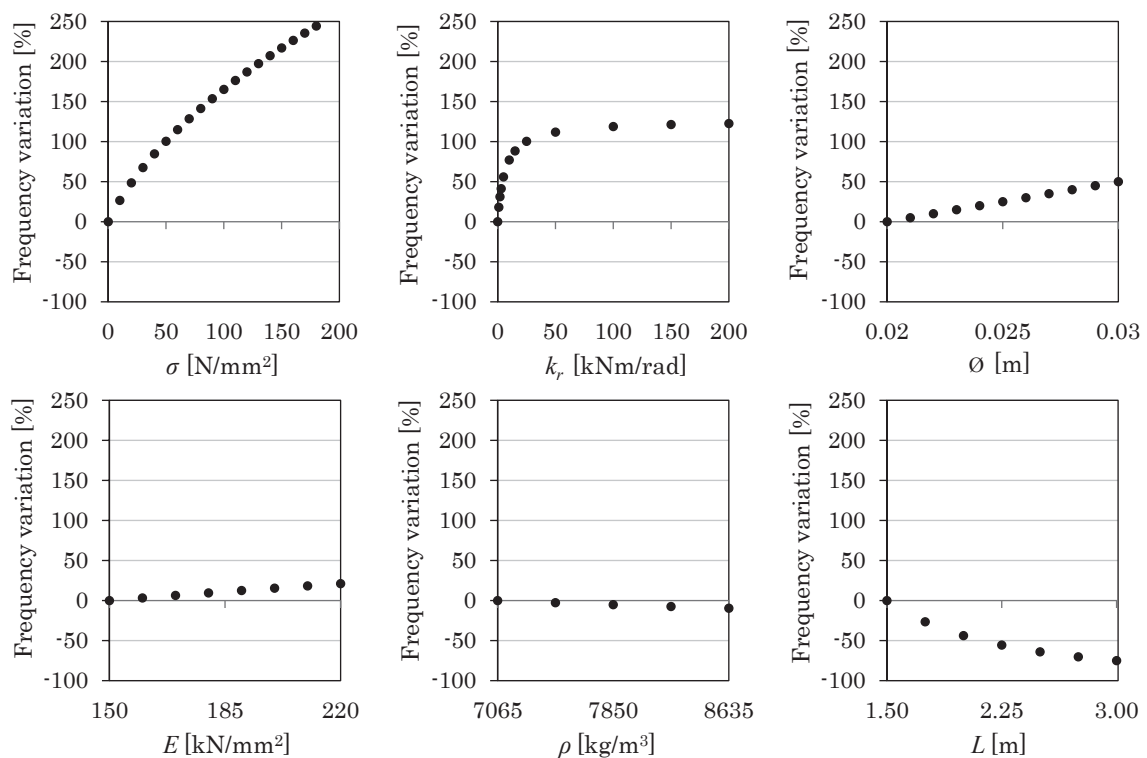


Figure B.1 – Individual effects of selected parameters on the first natural frequency of single bar.

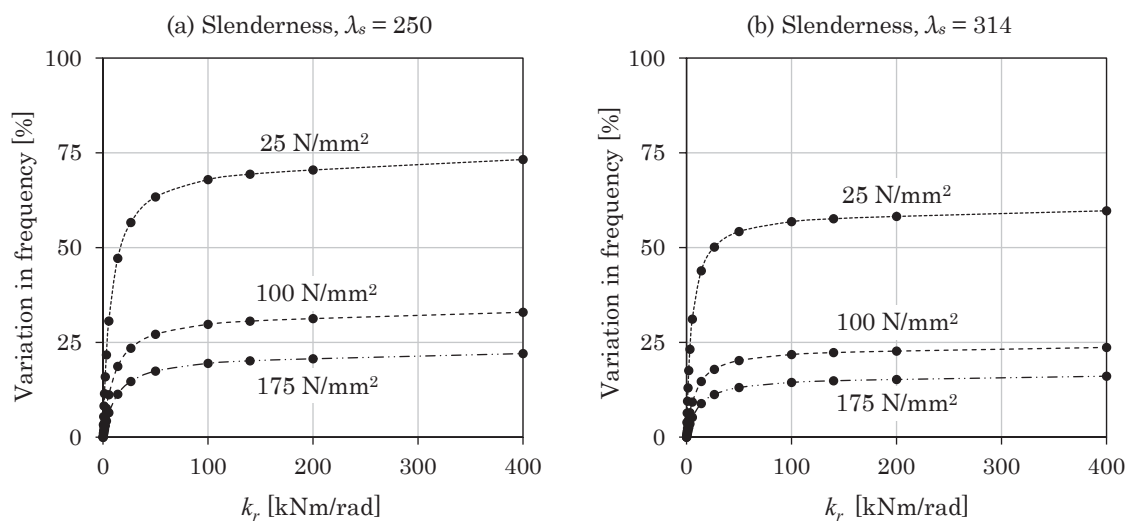
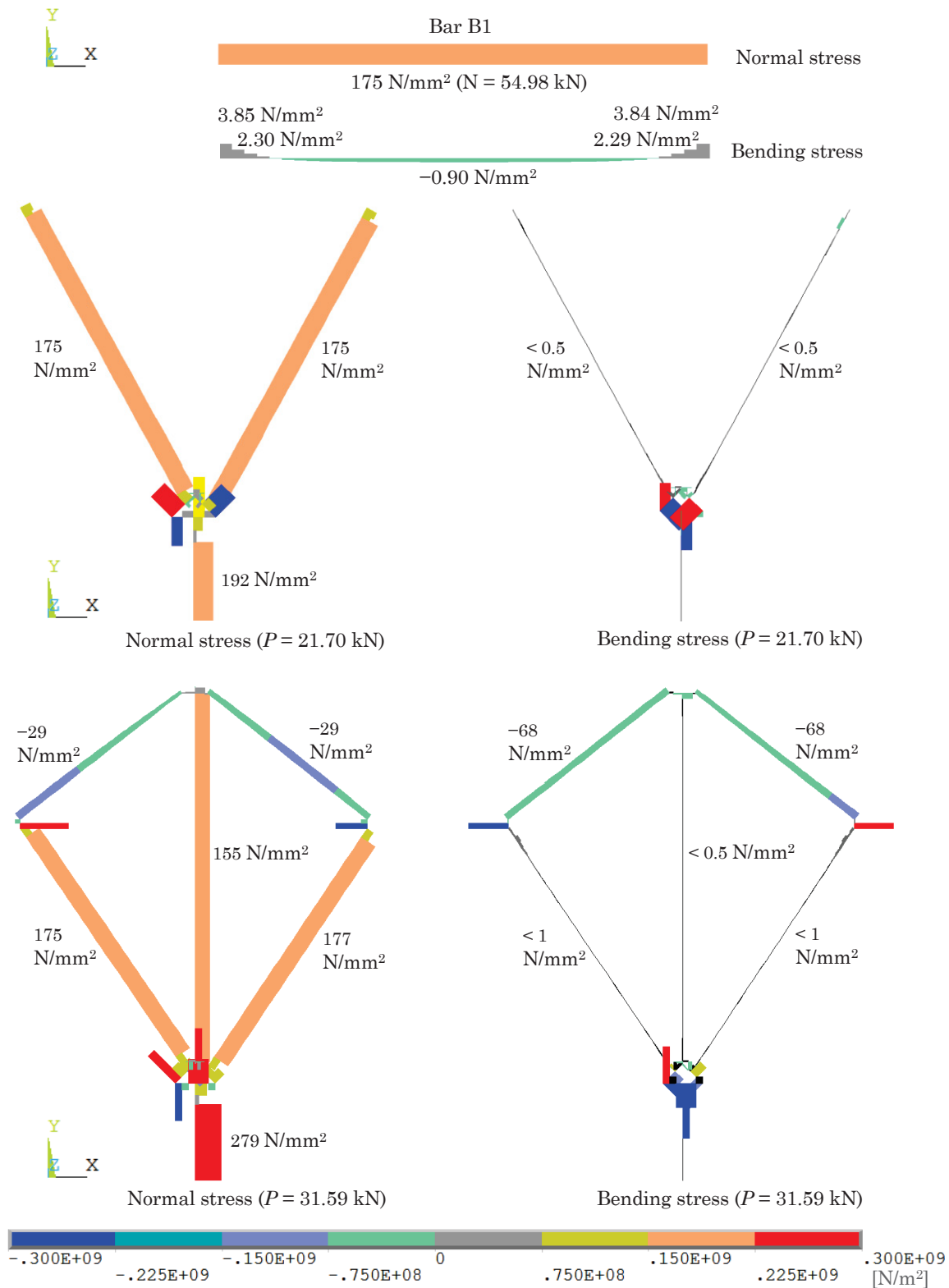


Figure B.2 – Combined effects of selected parameters on the first natural frequency of single bar.

C Numerical Static Analysis of Systems in Numerical Study and Laboratory Experiments



*Geometric nonlinear static analyses were performed by the finite element programme ANSYS.

Figure C.1 – Static analyses of the normal stress and bending stress distribution of the finite element models with stress stiffening assuming rigid joint conditions of the investigated systems in the numerical study and laboratory experiments.

D In-Situ Experiment – Location and Measurement Equipment

The historic roof truss systems are located in a building called *Reithalle* at Pappelallee 22–24 in the city of Potsdam. It is recognized as a heritage protected building. In 2012, the building was under renovation for residential apartments.

About the measurement equipment, the data acquisition system SCADAS II was integrated in a mobile measuring vehicle of BAM. The equipment included 72 amplifiers having measurement range of 1 mV to 10 V; 72 analogue filters measuring 20 Hz to 20 kHz; AD-converter of 16-bit resolution; variable scan rate (2000 Hz in the in-situ experiment), variable block size and automatic filter adjustment of 1/3 of scan frequency. Considering vibration velocity sensor, geophones HS1 by Geospace were used having a weight of approximately 0.3 kg each and natural frequency of 4.5 Hz. For excitation force, an impact hammer PCB/086D20 was used that has a weight of about 1.1 kg and is able to measure a pulse up to 22.2 kN with sensitivity of 0.23 mV/N.

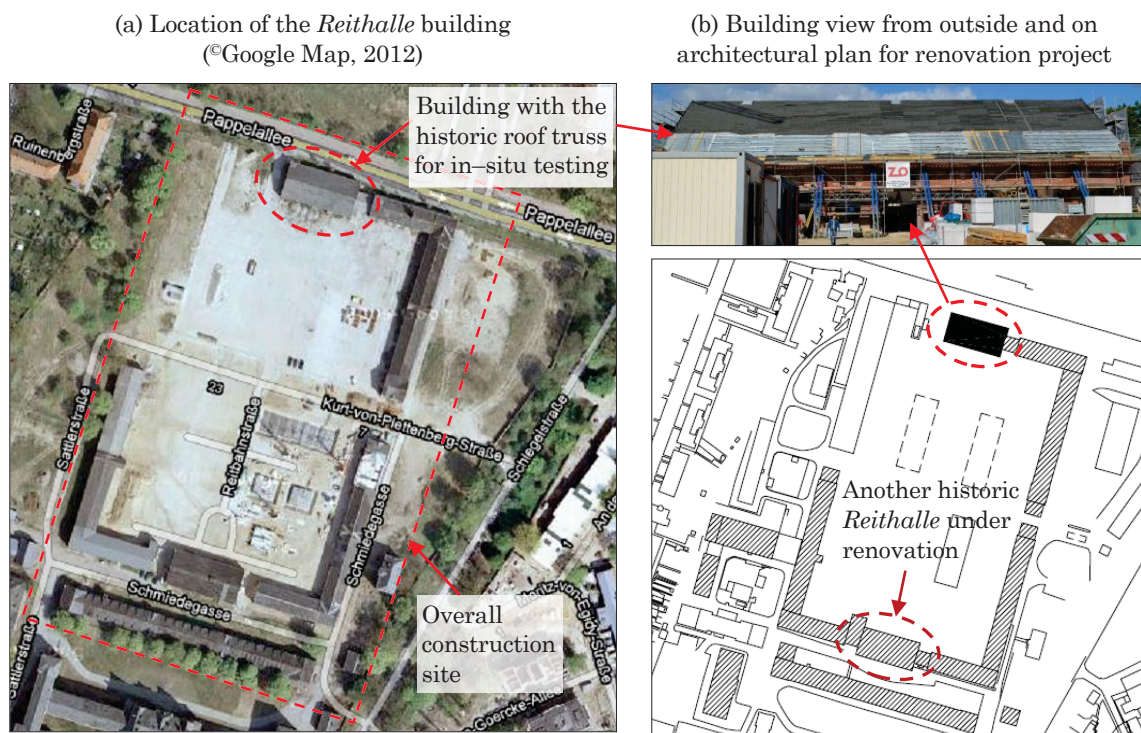
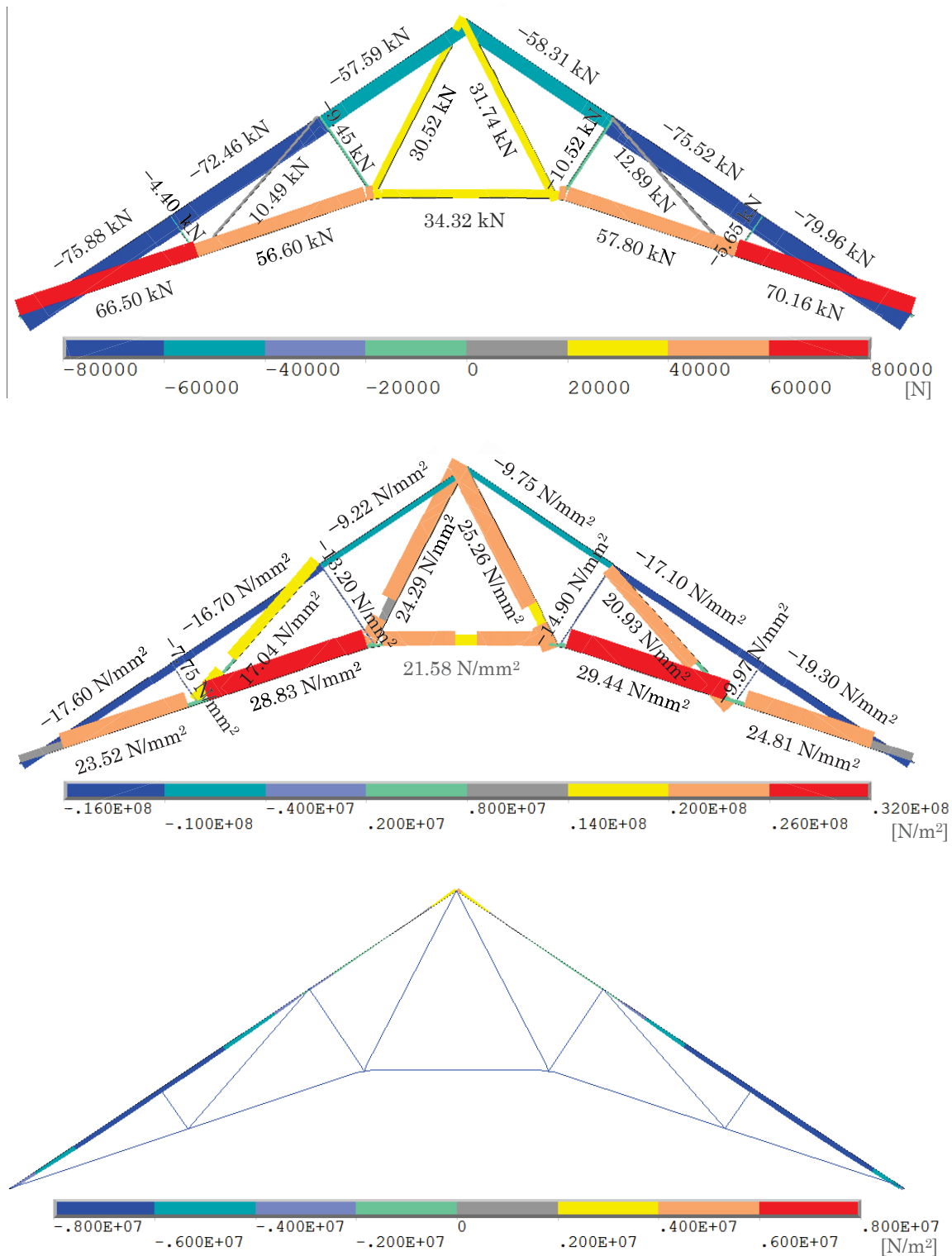


Figure D.1 – Location of the historic truss in Potsdam for the exemplary in-situ experiment.



Figure D.2 – Architectural illustration of the building *Reithalle* after renovation for residential apartments [Berner Group GmbH (2010)].

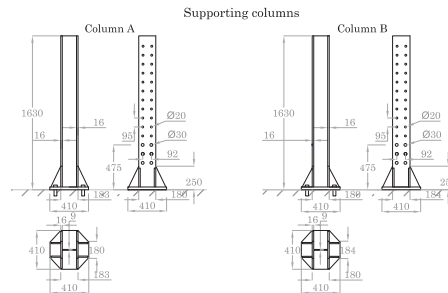
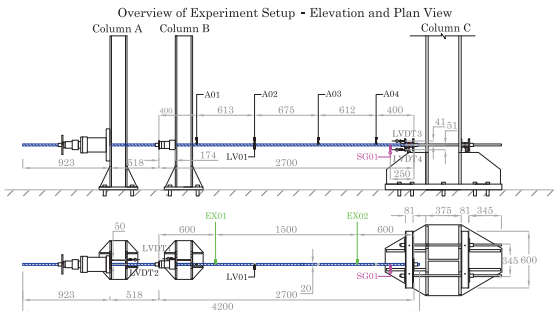
E Numerical Static Analysis of the Truss System in In-Situ Experiment



*Geometric nonlinear static analyses were performed by the finite element programme ANSYS.

Figure E.1 – Static analysis of the axial force, normal stress and bending stress distribution of the finite element model assuming the manually calculated roof loads and rigid joint conditions of the historic truss in the in-situ experiment.

Laboratory Experiments on Bar B1 [1:40]



Legend

- Ai indicates accelerometers
- SGi indicates strain gauge
- LVj indicates laser vibrometer
- EXi indicates excitation points
- Tie-bar
- Supporting frame
- Dimension

All dimensions are in millimeters. Geometrical measurements were carried out with calipers and rulers.



Overview of test setup for Bar B1 (2700 mm)



Hydraulic cylinder



Applying load



Impact hammer



Accelerometer

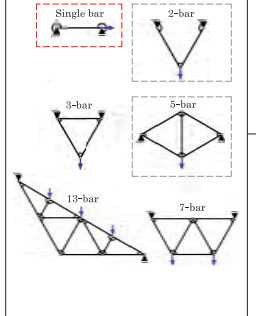


Laser vibrometer



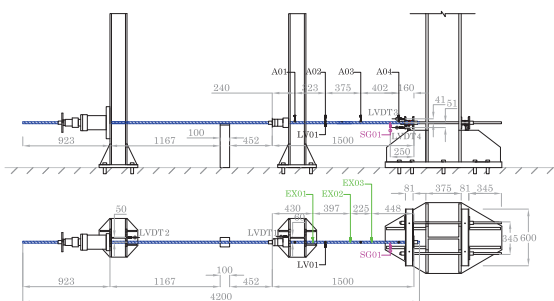
Labview DAQ

Overview Laboratory Experiment Campaigns



Laboratory Experiments on Bar B2 [1:40]

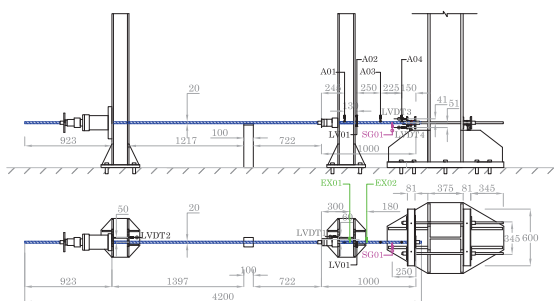
Overview of Experiment Setup - Elevation and Plan View



Overview of test setup for Bar B2 (1500 mm)

Laboratory Experiments on Bar B3 [1:40]

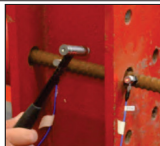
Overview of Experiment Setup - Elevation and Plan View



Overview of test setup for Bar B3 (1000 mm)



Overview of test setup for Bar B2 (1500 mm)



Hammer excitation



Overview of test setup for Bar B3 (1000 mm)

1st Laboratory Experimental Campaign
Laboratory Experiments on Single Bar Systems

Plan Name: LE - 01
Scale: 1:40
Paper: A3
Location of Experiments: VTE, Bauhaus-Universität Weimar
Experiments planned and performed by: Luong (2013 - 2015)
Drawing by: Luong

Identification of the State of Stress in Iron and Steel Truss Structures by Vibration-based Experimental Investigations



